Doctorate Program in Molecular Oncology and Endocrinology
Doctorate School in Molecular Medicine

XXV cycle - 2009–2012
Coordinator: Prof. Massimo Santoro

"PARP inhibition as new approach to increase the oncolytic activity of the adenoviral mutant *dl*922-947 against Anaplastic Thyroid Carcinoma"

Carmela Passaro

Università degli Studi di Napoli Federico II
Dipartimento di Medicina Molecolare e Biotecnologie Mediche

Administrative Location

Università degli Studi di Napoli Federico II
Dipartimento di Medicina Molecolare e Biotecnologie Mediche

Partner Institutions

Italian Institutions
Università degli Studi di Napoli "Federico II", Naples, Italy
Istituto di Endocrinologia ed Oncologia Sperimentale "G. Salvatore", CNR, Naples, Italy
Seconda Università di Napoli, Naples, Italy
Università degli Studi di Napoli "Parthenope", Naples, Italy
Università degli Studi del Sannio, Benevento, Italy
Università degli Studi di Genova, Genova, Italy
Università degli Studi di Padova, Padova, Italy
Università degli Studi "Magna Graecia", Catanzaro, Italy
Università degli Studi di Udine, Udine, Italy

Foreign Institutions
Université Libre de Bruxelles, Bruxelles, Belgium
Universidade Federal de Sao Paulo, Brazil
University of Turku, Turku, Finland
Université Paris Sud XI, Paris, France
University of Madras, Chennai, India
University Pavol Jozef Šafàrik, Kosice, Slovakia
Universidad Autonoma de Madrid, Centro de Investigaciones Oncologicas (CNIO), Spain
Johns Hopkins School of Medicine, Baltimore, MD, USA
Johns Hopkins Krieger School of Arts and Sciences, Baltimore, MD, USA
National Institutes of Health, Bethesda, MD, USA
Ohio State University, Columbus, OH, USA
Albert Einstein College of Medicine of Yeshiwa University, N.Y., USA

Supporting Institutions
Dipartimento di Biologia e Patologia Cellulare e Molecolare "L. Califano", Università degli Studi di Napoli "Federico II", Naples, Italy
Istituto di Endocrinologia ed Oncologia Sperimentale "G. Salvatore", CNR, Naples, Italy
Istituto Superiore di Oncologia, Italy

Italian Faculty

Salvatore Maria Aloj
Francesco Saverio Ambesi Impiombato
Francesco Beguinot
Maria Teresa Berlingieri
Bernadette Biondi
Francesca Carlomagno
Gabriella Castoria
Maria Domenica Castellone
Angela Celetti
Lorenzo Chiariotti
Annamaria Cirafici
Annamaria Colao
Sabino De Placido
Gabriella De Vita
Monica Fedele
Pietro Formisano
Alfredo Fusco
Domenico Grieco
Michele Grieco
Maddalena Illario
Paolo Laccetti
Antonio Leonardi
Paolo Emidio Macchia
Barbara Majello
Rosa Marina Melillo
Claudia Miele
Nunzia Montuori
Roberto Pacelli
Giuseppe Palumbo
Maria Giovanna Pierantoni
Rosario Pivonello
Giuseppe Portella
Maria Fiammetta Romano
Giuliana Salvatore
Massimo Santoro
Giampaolo Tortora
Donatella Tramontano
Giancarlo Troncone
Giancarlo Vecchio,
Giuseppe Viglietto
Mario Vitale

"IL CORPO FACCIA QUELLO CHE VUOLE,
IO NON SONO IL CORPO, IO SONO LA MENTE"
Rita Levi Montalcini

To my father and my mother
which taught me to never give up.
To Niko, always by my side.

“PARP inhibition as new approach to increase the oncolytic activity of the adenoviral mutant *dl*922-947 against Anaplastic Thyroid Carcinoma”

TABLE OF CONTENTS

LIST OF PUBLICATIONS

This dissertation is based upon the following publications:

1. **Passaro C**, Libertini S, Volpe M, Botta G, Gillespie D, and Portella G. The PARP inhibitor AZD2281 increase the oncolytic activity of the adenoviral mutant *dl*922-947 against Anaplastic Thyroid Carcinoma *in vitro* and *in vivo.* Manuscript in preparation. (Main body of the dissertation).

2. **Passaro C**, Abagnale A, Libertini S, Volpe M, Botta G, Cella L, Pacelli R, Halldèn G, Gillespie D, and Portella G. Ionizing radiation enhances *dl*922-947-mediated cell death of Anaplastic Thyroid Carcinoma cells. Endocrine-Related Cancer, major revision. (Attached at the end of the dissertation).

3. Botta G, **Passaro C**, Libertini S, Abagnale A, Barbato S, Hallden G, Beguinot F, Formisano P, Portella G. Inhibition of autophagy enhances the effects of E1A defective oncolytic adenovirus dl922-947 against glioma cells *in vitro* and *in vivo.* Human gene therapy 2012; 23:1–12. (Attached at the end of the dissertation).

4. Portella G, **Passaro C**, Chieffi P. Aurora B: a new prognostic marker and therapeutic target in cancer. Curr Med Chem 2011;18(4):482-96.

5. Libertini S, Abagnale A, **Passaro C**, Botta G, Chieffi P, Portella G. AZD1152 negatively affects the growth of anaplastic thyroid carcinoma cells and enhances the effects of oncolytic virus *dl*922-947. Endocr Relat Cancer 2011;18(1):129-41. (Attached at the end of the dissertation).

6. Libertini S, Abagnale A, **Passaro C**, Botta G, Portella G. Aurora B inhibitors as novel agents for cancer therapy. Recent Pat Anticancer Drug Discov 2010;5(3):219-41.

LIST OF ABBREVIATIONS

53BP1 p53 Binding Protein 1
5-FU 5-Fluorouracil
AMPK AMP-activated protein Kinase
APE1 DNA AP endonuclease
ATC Anaplastic Thyroid Carcinoma
ATM Ataxia Telangiectasia Mutated
ATR Ataxia Telangiectasia and Rad-3 related
ATRIP ATR Interacting Protein
BER Base Excision Repair
BRCA1 BReast CAncer 1
BRCT BRCA1 C-Terminus repeat
CAK Cdk-Activating Kinase
CAR Coxsackie and adenovirus receptor
CETN2 Centrin, EF hand protein 2
CSB Cockayne Syndrome B
DDR DNA damage response
DNA-PK DNA dependent Protein Kinase
DSB Double Strand Break
dsDNA double stranded DNA
ERCC1 Excision Repair Cross-Complementing rodent repair deficiency, complementation group 1
FEN1 Flap structure specific ENdonuclease 1
FACS Fluorescence-Activated Cell Sorting
GGR Global Genome Repair
HMGN1 High Motility Group Nucleosome binding domain 1
HR Homologous Recombination
hTERT human Telomerase Reverse Transcriptase
MDC1 Mediator of DNA damage Checkpoint 1
MGMT O^6-Methylguanine-DNA-Methyltransferase
MMR MisMatch Repair
NBS1 Nijmegen Breakage Syndrome 1
NER Nucleotide Excision Repair
NHEJ Non-Homologous End Joining
ORF Open Reading Frame
OV Oncolytic Virus
PARG Poly(ADP-Ribose) Glycohydrolase
PARP-1 Poly(ADP-Ribose) Polymerase 1
PBM PAR binding motif
PBZF PAR binding zinc finger
PCNA Proliferating Cell Nuclear Antigen
PML Promielocyte Leukaemia
PSA Prostate Specific Antigen
pTP pre-Terminal Protein
RFC Replication Factor C
RPA Replication Protein A
SCCHN Squamous Cell Carcinoma of the Head and Neck
SSB Single Strand Break
TCR Transcription-Coupled Repair
TNK Tankyrase
UV-DDB UV Damaged DNA Binding protein
VRC Viral Replication Center
XAB2 XPA Binding protein 2
XLF XRCC4 Like Factor
XPC Xeroderma Pigmentosum complementation group C
XRCC4 X-Ray cross-complementation group 4

ABSTRACT

Anaplastic Thyroid Carcinoma (ATC) is one of the most aggressive tumor characterized by an average survival time of 3-6 months after diagnosis. Multimodality therapy, which includes surgical debulking, external radiation therapy and chemotherapy, has failed to show any improvements in survival. Therefore, novel therapies with different mechanisms of action are required.

Oncolytic viruses (OVs) represent a novel therapeutic tool for the treatment of aggressive tumors. OVs as single agents have demonstrated limited efficacy in a clinical setting, thus highlighting the need of novel combinatorial therapies (i.e. OVs plus a rationally selected drug) with a potential great impact on clinical use. In this study, we showed that the oncolytic adenovirus *dl*922-947 induces massive S-phase entry in ATC cell lines, followed by an extensive DNA damage, quantified by γH2AX staining. Moreover, we demonstrated that *dl*922-947 triggered a DNA damage response, characterized by the activation of the checkpoint kinases ATM and Chk1, and at the same time impaired the ability of the DNA repair, by affecting MRN complex protein levels. The virus-induced single-strand DNA breaks (SSBs) activate the Poly-ADP-Ribose Polymerase (PARP) to signal SSBs to the enzymatic machinery involved in their repair.

Here, we demonstrate that the pharmacological inhibition of PARP increases *dl*922-947 cytotoxicity against Anaplastic Thyroid Carcinoma both *in vitro* and *in vivo*. We also show that PARP inhibitor AZD2281 synergizes with *dl*922-947 increasing viral replication and accelerating cell death pathways. Furthermore, we showed that the virus as single treatment induced an apoptotic-like cell death, as indicated by the presence of Caspase 3 activation, PARP cleavage, Annexin V positivity and Cytochrome C release from mitochondria, although lacking the morphological features of apoptosis.

In this regard we also proved that *dl*922-947 acts on the pathway involved in membrane blebbing by inhibiting Myosin Light Chain 2 (MLC2) phosphorylation. Using a pan caspase inhibitor, both caspase-dependent and -independent cell death pathways are found activated upon *dl*922-947 infection.

Our data clearly suggest that the combination of the oncolytic adenovirus *dl*922-947 with PARP inhibitor could represent a novel and effective therapeutic approach for the treatment of Anaplastic Thyroid Carcinoma.

1. INTRODUCTION

1.1 ANAPLASTIC THYROID CARCINOMA

Malignant tumors originated from thyroid follicular cell have traditionally been classified as well-differentiated thyroid carcinoma, that comprises papillary and follicular carcinoma, and Anaplastic Thyroid Carcinoma (ATC).

ATC is one of the most aggressive solid tumors that affect humans, with a median survival time of 3-6 months after diagnosis (Nagaiah et al. 2011). Even that ATC counts less than 1–3% of all thyroid cancers, it contributes up to 14–50% of the annual mortality associated with thyroid cancer (Patel and Shaha 2006, Nagaiah et al. 2011).

The mean age at ATC diagnosis is 55 to 65 years, for this reason it is considered a disease of the elderly. It is observed that ATC is more common in places with endemic goiter (Bakiri 1998). Although its pathogenesis is not completely understood, there are evidences suggesting its origin from a pre-existing well-differentiated thyroid carcinoma, prevalently papillary thyroid carcinoma (Patel and Shaha 2006). Macroscopically ATC appears as an unencapsulated, tan-white, fleshy tumors that infiltrate into the surrounding soft tissue of the neck, microscopically it is characterized by the presence of spindle, giant or squamoid cells. All these three types of cells do not have thyrotropin receptors, do not transport iodine, and do not produce thyroglobulin. Local symptoms of ATC most commonly begin with a rapidly evolving central neck mass followed by noticeable dysphagia, voice change or hoarseness, and stridor. At the disease presentation, in half of the patients metastases were found, with a prevalence in lungs; however also bone and brain were often affected (Nel et al. 1985).

ATC is usually resistant to standard chemotherapy; so far the treatment consist of surgery, when feasible, combined with radiation and chemotherapy.

However this multimodality treatment confers only a short term palliative and survival benefit.

In the last years targeted therapies are appearing in the clinic. There are two small-molecule tyrosine-kinase inhibitors in the midst of Phase II clinical trials including imatinib mesylate (Gleevac, Novartis) (Podtcheko et al. 2003, Podtcheko et al. 2006) and sorafenib (Nexavar, Onyx) (Kim et al. 2007). Other agents that have been reported to be effective in *in vitro* studies include replication-competent vaccinia virus (GLV-1h68) (Lin et al. 2007). Moreover several preclinical studies have demonstrated the effectiveness of virotherapy, alone or in combination with rational choosed drug, for the treatment of

anaplastic thyroid carcinoma (Libertini et al. 2007, Lin et al. 2008, Reddi et al. 2008, Libertini et al. 2011, Reddi et al. 2012).

1.2 ONCOLYTIC VIRUSES

Oncolytic viruses (OVs) are replication-selective viruses developed to be used as anticancer therapeutics. Nowadays they represent a promising and novel approach for the treatment of aggressive tumors both as single agents and both in combination with current clinical regimens (Parato et al. 2005, Liu et al. 2007) [Table 1].

OVs are viral mutants genetically engineered to specifically replicate and lyse tumor cells. The selectivity for tumor cells can be achieved using several strategies. Among these, the most common strategy is to eliminate viral function that are essential for the replication in normal cells, whereas the deregulated pathways in cancer cells complement the functions and enable viral propagation. Pathways that have frequently been targeted include cell cycle and apoptosis, function that are altered in almost all cancer cells (Bischoff et al. 1996, Heise et al. 2000, Sherr and McCormick 2002, White 2006).

Other approaches include the exchange of viral promoters for tissue/tumor-specific promoters, inhibition of replication in normal tissue by insertion of miRNA target sequences, tropism modifications for selective attachment to tumor antigens or a combination of these strategies (Small et al. 2006, Waehler et al. 2007, Cawood et al. 2009).

OVs have several potential benefits as anticancer therapeutics: tumor-selective replication with up to 10,000-fold amplification of the input dose, stimulation of antitumoral immune responses, enhancement of cell killing in combination with other cytotoxic agents, efficacy independent of resistance to current anticancer therapeutics, no generation of neoplastic cell clones or treatment resistance, higher efficacy in cancer stem cells compared to conventional therapies in experimental models (Jiang et al. 2007).

No or mild side effects result from their limited capacity to productively infect and spread in normal tissue; although low levels of replication in normal cells do not necessarily indicate clinical toxicity (Parato et al. 2005, Liu et al. 2007).

Table 1. Oncolytic viruses under active investigation

VIRUS	NAME	MODIFICATION	PHASE	TUMOR	COMBINATION	TRIAL IDENTIFIER
Adenovirus	Oncorine (H101)	E1B55K-, E3-	2	SCCHN	Cisplatin	PMID: 14693057
			3	SCCHN	Cisplatin	PMID: 15601557
	Onyx-015	E1B55K-, E3-	1	SCCHN		PMID: 10741699
			1	Sarcoma	Mitomycin-C, dox, cisplatin	PMID: 15647767
			1/2	PanCa	Gemzar	PMID: 12576418
			2	SCCHN	Cisplatin, 5-FU	PMID: 10932224
			2	CRC	5-FU/leucovorin	PMID: 15803147
	CV706	PSA control	1	Prostate cancer	RT	PMID: 11606381
	CG7870	Rat probasin-E1A, hPSA-E1B, E3+	1/2	Prostate cancer	Docetaxel	NCT00103428
	CG0070	E2F-1,GM-CSF	2/3	Bladder cancer		PMID: 16397056
	Telomelysin	hTERT	1	Solid tumors		PMID: 19935775
	Ad5-CD/TKrep	CD/TK	1	Prostate cancer	5-FC and GCV	PMID: 12208748
			2/3	Prostate cancer	IR	NCT00583492
	Ad5-Δ24-RGD	RGD, delta-24	1	Ovarian cancer		PMID: 20978148
			1/2	Glioma		Recruiting
	Ad5-SSTR/TK-RGD	SSTR, TK, RGD	1	Ovarian cancer	GCV	PMID: 16397056
	CGTG-102	Ad5/3, GM-CSF, Delta-24	1/2	Solid tumors		PMID: 20664527
Herpes Simplex Virus	Talimogene laherparepvec (OncoVEX)	GM-CSF, ICP34.5-, ICP47-, Us11↑	2	Melanoma		PMID: 19915919
			3	Melanoma		Active
			1/2	SCCHN	RT, cisplatin	PMID: 20670951
	G207	ICP34.5-, ICP6-	1/2	Glioma		PMID: 18957964
	G47Delta	From G207, ICP47-	1	Glioma		PMID: 11353831
	HSV 1716 (Seprehvir)	ICP34.5-	1	SCCHN		PMID: 18615711
			1	Glioma		PMID: 15334111
			1	Melanoma		PMID: 11229673
	HF10	HSV-1 HF strain	1	PanCa		PMID: 21102422
	NV1020		1	CRC liver mets		PMID: 19018254
Measles Virus (Edmonston)	MV-CEA	CEA	1	Ovarian cancer		PMID: 20103634
Newcastle disease virus	NDV-HUJ		1/2	Glioma		PMID: 16257582
	PV701		1	Solid tumors		PMID: 16638865
	MTH-68/H		2	Solid tumors		PMID: 8275514
	NV1020		1	Solid tumors		PMID: 11980996
Parvovirus	H-1PV		1/2	Glioma		PMID: 20299703
Poliovirus (Sabin)	PVS-RIPO	IRES	1	Glioma		PMID: 20299272
Reovirus (Dearing)	Reolysin		1/2	Glioma		PMID: 18253152
			3	SCCHN	PTX, CBDCA	Recruiting
Seneca Valley virus	NTX-010		2	Small cell lung cancer		PMID: 17971529
Retrovirus	Toca 511	CD	1/2	Glioma	5-FC	PMID: 16257382
Vaccinia (Wyeth strain)	JX-594	GM-CSF, TK-	1	HCC		PMID: 18495536
Vaccinia (Western Reserve)	wDD-CDSR	TK-, VGF-, LacZ, CD, Somatostatina R	1	Solid tumors		PMID: 15336655
Vaccinia (Lister)	GL-ONC1 (GLV-h68)	Renilla luciferase, GFP, β-gal, β-glucoronidase	1	Solid tumors		PMID: 21779374

A search was carried out on http://www.clinicaltrials.gov and the clinical trial database of the Journal of Gene Medicine (http://www.wiley.com/legacy/wileychi/genmed/clinical/).

5-FC: 5-fluorocytosine; 5-FU: 5-fluorouracil; β-gal: β-galactosidase; Ca: Cancer; CBDCA: Carboplatin; CD: Cytosine deaminase; CEA: Carcinoembryonic antigen; CRC: colorectal cancer; GCV: Ganciclovir; Gemzar: Gemcitabine; GFP: Green fluorescent protein; GM-CSF: Granulocyte-macrophage colony-stimulating factor; HCC: Hepatocellular carcinoma; HSV: Herpes simplex virus; hTERT: Human telomerase reverse transcriptase; ICP: infected cell protein; IRES: Internal ribosomal entry site; Mets: metastases; PanCa: Pancreatic cancer; PSA: Prostate specific antigen; PTX: Paclitaxel; RT: Radiation; SCCHN: Squamous cell carcinoma of the head and neck; Somatostatin R: Somatostatin Receptor; TK: Thymidine kinase; VGF: Vaccinia growth factor; Wt: Wild type.

Oncolytic mutants in clinical therapies

At the beginning of 20th century it was observed that tumor regression was achieved in two isolated cases of cervical carcinoma and Burkitt's lymphoma after inoculation with attenuated rabies virus (De Pace 1921) and measles virus (Bluming and Ziegler 1971) respectively.

Until the 1970s several preclinical and clinical studies were performed with various virus species such as rabies virus (Pack 1950), mumps virus (Asada 1974), West Nile virus (Southam and Moore 1952), Newcastle disease virus (Sinkovics and Horvath 2000) and Adenovirus serotype 4 (Southam et al. 1956). However the outcomes of these studies were disappointing with severe side effects or even deaths of treated patients.

In the late 1980s, the demonstrated feasibility of gene delivery with viral vector renewed the interest in OVs; moreover advancement of viral engineering, production, and purification technologies together with a better understanding of the molecular alterations in cancer cells further promoted the development of viral mutants selectively targeting tumor tissue.

Oncolytic mutants generated from other viral species rather than adenovirus have been or are currently being considered as anticancer agents.

Herper Simplex Virus HSV-1 mutant G207 was one of the first oncolityc virus to enter in clinical trials for the treatment of recurrent gliomas. This mutant was deleted in the ICP34.5 loci preventing neurovirulence and in the ICP6 gene inactivating ribonucletide reductase allowing selective replication in cancer cell (Markert et al. 2000) [Table 1].

Based on G207 backbone several HSV mutants have entered in clinical trials such as OncoVex GM-CSF (BioVex-Amgen, MA, USA) (Hu et al. 2006). Several clinical trials (shown in table 1) have demonstrated OncoVex GM-CSF effectiveness and safety with only limited flu-like side effects.

Attenuated vaccine strains of Vaccinia virus (Poxvirus family) have also been evaluated in the clinic. The most promising of these mutants is JX-594 (Jennerex Biotherapeutics, Inc., CA, USA) of the Wyeth strain, expressing GM-CSF and β-galactosidase (Park et al. 2008, Breitbach et al. 2011). JX-594 bears a deletion of the viral thymidine kinase gene that allow viral replication selectively in cancer cells harboring constitutively active epidermal growth factor receptor (EGFR)/Ras signalling and elevated nucleotide synthesis (Kim et al. 2006). Clinical trials performed with JX-594 [Table 1] showed no major toxicity and reported tumor necrosis and stimulation of the immune responses related to viral replication.

The Reovirus subtype Reolysin (Oncolytics Biotech) selectively targets neoplastic cells with activated Ras pathway (Coffey et al. 1998). Many clinical

trials with Reolysin in combination with cytotoxic drugs have been completed [Table 1] and a Phase III trial was approved targeting head and neck cancers (http://clinicaltrials.gov/NCT01166542).

It is worth to note that a first-in-class US approval is expected soon for OncoVex, which is being tested in a randomized phase 3 clinical trial for the treatment of melanoma that has recently completed accrual (http://clinicaltrials.gov/NCT00769704).

1.3 ONCOLYTIC ADENOVIRUSES

Adenoviruses

Among the different OVs, adenoviral mutants were considered better suited for therapy of epithelial malignancies, but they show activity also against hematological cancer.

Adenoviruses are non-enveloped icosahedral viruses. Their capsid comprises of the structural proteins hexon and penton that bind to Coxsackie and Adenovirus Receptor (CAR) and $\alpha_v\beta_{3,5}$ integrins respectively for virus internalization. Furthermore adenovirus have a double-stranded DNA (dsDNA) of approximately 36 Kb.

The adenovirus life-cycle includes the following steps: (1) virus entry into the cell following CAR and integrin binding, (2) release from the endosome and subsequent entry into the nucleus, (3) expression of early region gene products, (4) cell entry into S phase, (5) prevention of p53-dependent and -independent apoptosis, (6) shut-off of host cell protein synthesis, (7) viral DNA replication, (8) viral structural protein synthesis, (9) virion assembly in the nucleus, (10) cell death and (11) virus release [Figure 1].

Fig 1

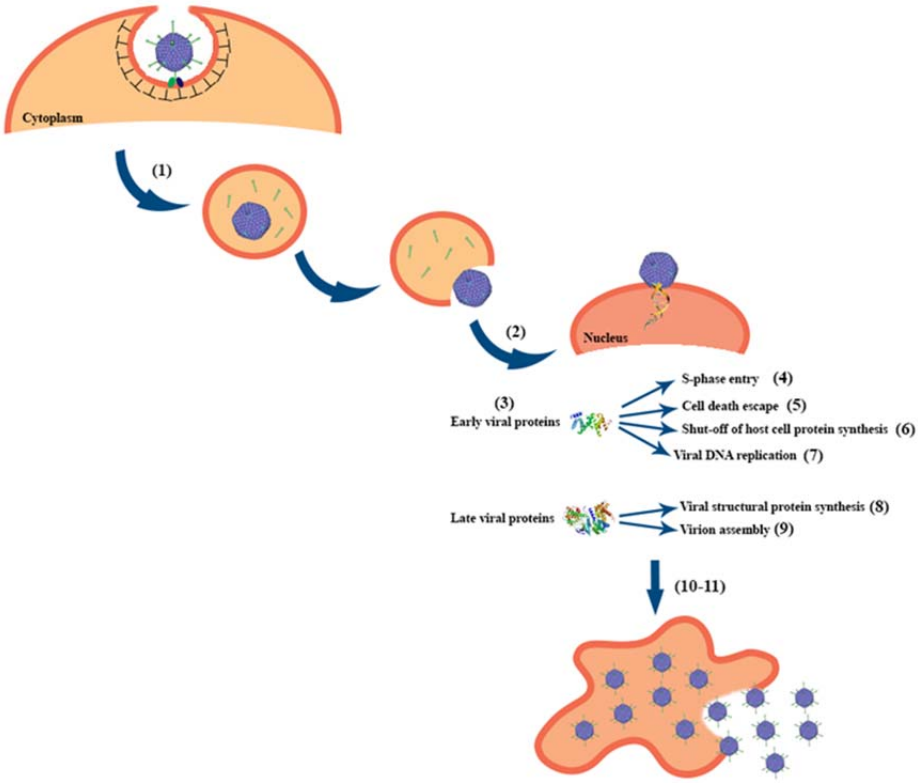

Figure 1. Adenovirus life-cycle
The adenovirus life-cycle includes the several steps: (1) virus entry into the cell following CAR and integrin binding, (2) release from the endosome and subsequent entry into the nucleus, (3) expression of early region gene products, (4) cell entry into S phase, (5) prevention of p53-dependent and -independent apoptosis, (6) shut-off of host cell protein synthesis, (7) viral DNA replication, (8) viral structural protein synthesis, (9) virion assembly in the nucleus, (10) cell death and (11) virus release

Adenoviral replication is divided into early and late phase. Soon after infection, Early 1A (E1A) is the first gene to be transcribed.

The most important E1A function is the induction of S-phase in infected cells through the binding of E1A Conserved Region 2 (CR2) and 1 (CR1) to pRb and p300/CBP. This binding displaces the transcriptional repressor pRb from E2F transcription factors resulting in the auto-stimulation of E1A expression and in the activation of the downstream viral expression units E1B, E2, E3 and E4 as well as promoting cellular gene expression (Shenk 1996).

To antagonized E1A-induced apoptosis, adenoviruses have evolved two proteins E1B-19K and E1B-55K both encoded by E1B gene. In particular E1B-19K is an homologue of Bcl2 protein and inhibits apoptosis heterodimerizing with Bax and Bak pro-apoptotic proteins (White 2001), whereas E1B-55K binds to and inhibits p53 as a transactivator protein (Yew and Berk 1992).

Early E3 protein it is involved in counteracting immune response elicited by the host cell against the virus, indeed this protein can block the transport of MHC class I heavy chain to cell surface (gp19K) and inhibit TNFα and Fas ligand-induced cell death by degradating their receptors (Horwitz 2001).

E2 region encodes for proteins directly involved in adenoviral replication such as preTerminal Protein (pTP), DNA Polymerase (AdPol) and single stranded DNA binding protein (DBP) (Liu et al. 2003). Since replicated viral DNA tends to form concatamers that are too large to be packed into the virion, the protein complex E1B55K/E4orf6 induces the degradation of protein involved in concatamers formation (see next paragraphs) (Stracker et al. 2002). E4orf6 is one of the six protein, termed as open reading frame proteins (E4orf1-6/7), encoded by E4 region. These protein have been shown to be regulators of viral and cellular transcription (E4orf4, E4orf6, E4orf6/7), viral pre-mRNA splicing (E4orf3, E4orf4, E4orf6), viral and cellular mRNA transport (E4orf6), cellular protein degradation (E4orf6), nuclear structure organization (E4orf3), and the aforementioned concatamerization (E4orf3, E4orf6) (Tauber and Dobner 2001, Stracker et al. 2002).

Late viral gene encodes for protein involved in encapsidation and maturation of the virus particle.

Oncolytic virotherapy using adenoviruses

In oncolytic virotherapy, among different viral species, adenoviruses have shown several advantages. First of all they have a well characterized small linear DNA genome that result easy to manipulate; they do not integrate into host genome; they require a simple technology for production to GMP (Good Manufacturing Practice) standards; they have a natural tropism for epithelial cell and adenocarcinoma. Moreover species C adenoviruses can cause only mild flu-like side effect or asymptomatic infections.

While recent reports demonstrate that serotype 11, 3 and 35 of species B might have better efficacy in certain preclinical models (Kim et al. 2011), serotype 5 (Ad5) of species C is the most widely used for generation of oncolytic mutants. This difference in efficacy could be related to viral uptake in tumor cells, indeed species B mutants bind to the ubiquitously expressed CD46 receptors (Sirena et al. 2004), while species C binds to CAR that is downregulated in some cancers. Furthermore, while most humans have neutralizing antibodies towards serotype 5, pre-existing antibodies to other serotype are less prevalent (Kueberuwa et al. 2010). Exploiting different advantages of various serotype, chimeric mutants have been generated resulting in Ad5/3 chimeras that are directed to CD46 receptor, highly

expressed on tumor cells, thereby improving antitumor efficacy (Ranki and Hemminki 2010).

The main disadvantage of the use of adenovirus is that intravenous administration is less feasible because of the high viral binding affinity for complement and other blood factors. This binding is followed by rapid elimination by hepatic Kupffer cells (Baker et al. 2007b, Kueberuwa et al. 2010). However several groups overcame these obstacles coating mutants with various polymers followed by retargeting to tumors (Fisher and Seymour 2010).

Two broad approaches are currently being used to engineer tumor-selective adenovirus replication. One is the use of tumor- and/or tissue-specific promoters; the second approach is to delete gene functions that are critical for efficient viral replication in normal cells but are expendable in tumor cells. The latest approach is based on the observation that many of the same critical regulatory proteins, that are inactivated by viral gene products during adenovirus replication, are also inactivated during carcinogenesis (Bischoff et al. 1996, Heise et al. 2000, Sherr and McCormick 2002).

To the first group belong, for example, the mutant CG7870, in which the expression of the viral E1A gene is under the control of the rat probasin promoter, and E1B expression is under the control of the human Prostate-Specific Antigen (PSA) promoter (Dilley et al. 2005), and OBP-301 in which the human TElomerase Reverse Transcriptase (hTERT) promoter drives E1 gene expression (Hashimoto et al. 2012).

However the most extensively clinically evaluated replication-selective oncolytic viruses to date are engineered using the second approach. In particular the first replication-competent adenoviral mutant, *dl*1520 (Onyx-015 and H101), is based on chimeric adenoviruses serotype 5 and 2 (Ad5/Ad2) and contains a deletion of E1B55K, which normally inhibits p53 to prevent premature cellular apoptosis (Heise et al. 1997). In the great majority of cancer cells, E1B55K deletion is complemented by functional inactivation of p53 and alteration in mRNA nuclear export mechanisms. The E1B55K-deleted H101 (Shanghai Sunway Biotech) was the world's first oncolytic virus approved in China for cancer treatment. In its phase III clinical trial it is reported a 79% response rate for H101 plus chemotherapy, compared with 40% for chemotherapy alone in patients with head and neck cancer (Yu and Fang 2007).

Although the toxicity profile of *dl*1520 in over 200 patients treated in phase I/II trials was promising, with little dose-limiting toxicity, durable responses to single-agent *dl*1520 were rare; moreover in *in vitro* studies it has been

demonstrated that this mutant can also lyse cancer cells with normal p53 status raising questions to its mechanism of action (Kirn 2001). These observations have encouraged the search for more effective replicating adenoviral agents.

A second generation adenoviral mutant, *dl*922-947, has been engineered deleting 24bp in the E1A-CR2 domain. This mutant can replicate only in cells with deregulated growth control such as the majority of cancer cells with altered G1/S checkpoint and pRb/Ras signaling pathway.

*dl*922-947 has superior oncolytic potency both *in vitro* and *in vivo* in human pancreatic (Bhattacharyya et al. 2011), glioma (Yong et al. 2009, Botta et al. 2012), thyroid (Libertini et al. 2008, Libertini et al. 2011) and ovarian cancer cells (Lockley et al. 2006).

In contrast, in quiescent normal cells, *dl*922-947-driven replication was significantly less than with Ad5wt (Heise et al. 2000). A similar adenovirus, Δ24, with the same deletion in E1A-CR2, has shown activity in preclinical models of glioma (Fueyo et al. 2000).

Ad5ΔCR2, another E1A-CR2-deleted mutant, has been retargeted to integrins inserting an RGD sequence (Ad5ΔCR2RGD). This mutant has been evaluated in phase I trial for recurrent ovarian cancer showing safe and with potential antitumor responses (Kimball et al. 2010); moreover it is currently investigated in a second Phase I trial targeting recurrent gliomas (http://clinicaltrials.gov/NTC00805376).

A variant of Ad5ΔCR2RGD armed with the immunostimulatory Granulocyte-Macrophage Colony-Stimulating Factor (GMCSF) administered to patients with advanced refractory disease prevented tumor progression in three out of six patients and stable disease was reported in two additional patients (Pesonen et al. 2012).

AdΔΔ is a mutant double deleted in the E1A-CR2 region and in E1B19K. The lack of E1B19K expression prevents viral spread in normal host cell by TNF-induced apoptosis, but not in cancer cells due to the frequently inactivated apoptotic pathway in these cells (White 2006). AdΔΔ oncolytic potency it has been already demonstrated in *in vitro* and *in vivo* models of pancreatic (Cherubini et al. 2011) and prostate (Oberg et al. 2010) cancer.

Oncolytic Adenoviruses: combinatorial therapies

In the last ten years several preclinical and clinical studies have been performed to assess the safety and efficacy of oncolytic adenoviruses alone or in combination with cytotoxic drugs or radiotherapy [Table 1].

These studies have demonstrated the higher efficacy of drug/radiotherapy and adenovirus combination compared to single-agent treatment highlighting the

evidence that adenoviruses, both wild type and oncolytic mutants, can operate in synergy with chemotherapeutic drugs to kill cancer cells.

Different approaches have been exploited to enhance the effects of oncolytic adenoviruses. These approaches include agents able to increase viral entry, viral replication or viral diffusion; able to modulate the immune response; able to interfere with cell proliferation; or again able to induce a DNA damage and the subsequent cell death.

In the latter approaches are included drugs such as cisplatin, doxorubicin, mitomycin-C and ionizing radiation that are already used in the clinic for the treatment of several type of cancer.

In two completed phase II and phase III clinical trials, the oncolytic mutant H101 (E1B55k-deleted) has been combined to cisplatin to treat Squamous Cell Carcinoma of the Head and Neck (SCCHN). Both studies clearly demonstrate the superior efficacy of cisplatin treatment if combined with H101 mutant (Xu et al. 2003, Xia et al. 2004).

Another mutant called Onyx-015 (E1B55k- and E3-deleted) has been combined with MAP chemotherapy (Mitomycin-C, Doxorubicin and Cisplatin) in a phase I/II trial in patients with advanced sarcoma (Galanis et al. 2005). This study showed that ONYX-015 in combination with MAP chemotherapy is well tolerated with no significant toxicity; moreover there was evidence of antitumor activity in one out of six patients (Galanis et al. 2005).

The oncolytic adenovirus CV706 (Prostatic-Specific Antigen-regulated expression of E1A gene) has been used in combination with radiotherapy in patients with prostate cancer in a phase I trial. The intraprostatic delivery of CV706 has proved to be safe, even at high doses, and the data also suggest that CV706 possesses enough clinical activity, as reflected by changes in serum PSA (DeWeese et al. 2001).

Due to the intrinsic ability of viruses to interfere with cell proliferation, agents modulating these cellular steps have been selected to increase the efficacy of oncolytic adenoviruses.

The nucleoside analogue Gemcitabine (marketed as Gemzar) has been combined with Onyx-015 in a phase I/II trial for the treatment of pancreatic cancer. After combination therapy, 2 patients had partial regressions of the injected tumor, 2 had minor responses, 6 had stable disease and 11 had progressive disease or had to go off study because of treatment toxicity (Hecht et al. 2003).

5-FluoroUracil (5-FU) is a pyrimidine analog which is used in the treatment of cancer. It works through irreversible inhibition of thymidylate synthase impeding DNA replication. In a phase II clinical trial have been evaluated the

effects of Onyx-015 among metastatic colorectal cancer patients that have failed prior treatment with 5-FU/leucovorin. Onyx-015 hepatic artery infusion prolonged the median survival to 19 months compared to patients to those patients only received 5-FU/leucovorin that was 10.7 months (Reid et al. 2005).

In another phase II clinical trial Onyx-015 has been used in combination both with a cytostatic agent, 5-FU, both with a cytotoxic agent, cisplatin in patients with SCCHN. This combinatorial regimen demonstrate substantial objective responses, including a high proportion of complete responses. Moreover, by 6 months, none of the responding tumors had progressed, whereas all non-injected tumors treated with chemotherapy alone had progressed (Khuri et al. 2000).

The adenoviral mutant CV787 have the viral gene E1B under the control of human PSA promoter. This mutant has been used in combination with docetaxel in phase I/II trial for the treatment of prostate cancer (http://clinicaltrials.gov/NCT00103428). This study is terminated; however results are not yet available.

The history of OVs field suggests that immunosuppressed patients generally respond better to oncolytic virus therapy than those with an intact immune system. It follows that combining virotherapy with immunosuppressive drugs could be useful for enhancing their antitumor activity. Among the different immunosuppressive drugs, cyclophosphamide is currently the most favored because it has several advantages: is potently toxic both against T and B lymphocyte, has direct antitumor activity, has been widely used since 1949 and is reasonably priced. A phase I clinical trial to investigate the safety and the recommended dose for later use of an oncolytic adenovirus CGTG-102 in combination with cyclophosphamide is currently in a recruiting stage (http://clinicaltrials.gov/NCT01598129); however several preclinical studies have shown that cyclophosphamide can retard immune clearance of OVs, enhancing the persistence of virus infection and prolonging therapeutic efficacy (Chiocca 2008).

In addition to combining OVs with drugs, another strategy is to engineer prodrug-converting enzyme, such as Cytosine Deaminase (CD) or Thymidine Kinase (TK), into the viral genome. Subsequently the selective conversion of non-toxic prodrugs to toxic drugs will occur only in tumor cells infected by the oncolytic mutant, resulting in greatly reduced systemic drug toxicity. In this regard very promising results were reported in a phase I clinical trial for the treatment of prostate cancer; indeed the results demonstrate that intraprostatic administration of the replication-competent Ad5-CD/TKrep virus followed by

2 weeks of 5-FluoroCytosine (5-FC) and ganciclovir prodrug therapy can be safely applied to humans and is showing signs of biological activity (Freytag et al. 2002). Moreover a modified improved version of this mutant, Ad5CD/TKrepADP, has now been approved for phase III trials in combination with 5-FC, ganciclovir and radiotherapy (http://clinicaltrials.gov/NCT00583492).

All these extensive studies have demonstrated that adenoviruses are less efficacious when administered alone, especially in the treatment of aggressive tumors, and that synergistic cell killing occurs when adenoviral mutants are combined with other drugs. To improve these combinations or to develop more powerful clinical therapies, it is necessary to better understand the interplay between oncolytic adenoviruses and the host cell during infection.

1.4 DNA DAMAGE REPAIR PATHWAYS

Organisms are permanently exposed to endogenous and exogenous agents that damage DNA. If not repaired, such damage can result in mutations, diseases and cell death.

The DNA repair mechanisms have an important role in the innate intracellular defense against foreign invaders. For example viral infection and replication produce a large amounts of exogenous genetic material, much of which with an unusual DNA secondary structure that represent targets for cellular proteins involved in the response to abnormal and damaged DNA.

There are various forms of DNA damage, such as base modifications, single strand breaks (SSB), double strand breaks (DSB), crosslinks and mismatches.

To reply to these different DNA damage, cells have evolved numerous DNA repair pathways. The major DNA repair pathways include direct repair (O^6-MethylGuanine-DNA-MethylTransferase, MGMT), Base Excision Repair (BER), Nucleotide Excision Repair (NER), MisMatch Repair (MMR), Homologous Recombination (HR) and Non-Homologous End-Joining (NHEJ) repair.

DNA damage recognition

The first step in DNA repair is the damage recognition. The DNA damage response (DDR) is a signal transduction pathway that senses DNA damage and replication stress [Figure 2]. It involves several proteins that are grouped into four categories based on their activity: sensors, mediators, transducers and effectors.

Fig 2

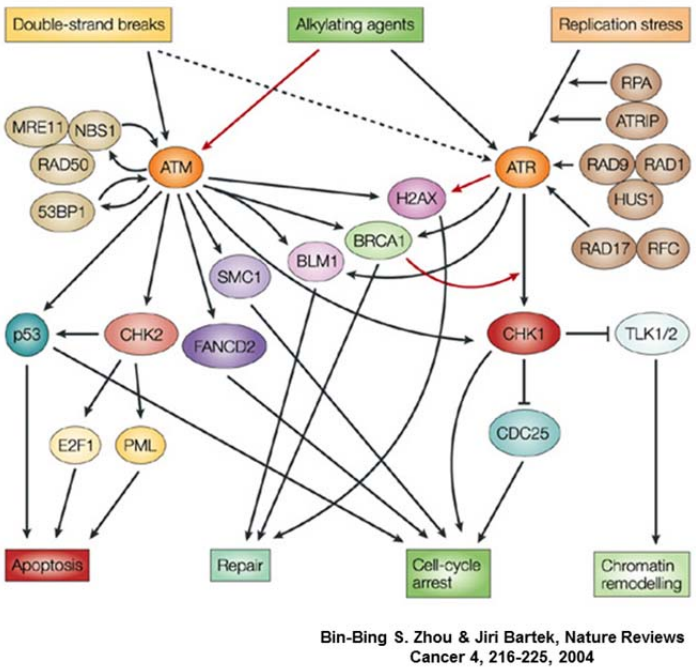

Figure 2: DNA-damage-response signal-transduction network.
The DNA-damage-response network consists of two parallel pathways that respond to different types of DNA damage. The ATM pathway responds to the presence of double-strand breaks (DSBs). It can activate many of the downstream components of the ATR pathway, which also responds to DSBs, but more slowly than ATM. In addition, the ATR pathway can respond to agents that interfere with the function of DNA replication forks, such as ultraviolet light and hydroxyurea. DNA alkylating agents might activate both pathways, although these types of DNA damage impose stress on progressing replication forks, they clearly also could elicit strand breaks under some circumstances. The single-stranded DNA-binding protein replication protein A (RPA) is required for the recruitment of ATR and its partner protein ATRIP to sites of DNA damage and for ATR-mediated CHK1 activation. Full activation of the damage-response pathway also requires the RAD9–RAD1–HUS1 and RAD17–RFC complexes. Sensors MRE11–RAD50–NBS1 complex binds to ATM and DNA. CHK1 and CHK2 lie downstream of ATM and ATR. The effectors include proteins that are involved in DNA repair, transcription regulation, replication, cell-cycle control and apoptosis, such as BRCA1, FANCD2, NBS1, H2AX, BLM1, 53BP1, CDC25 and p53.Dashed lines represent less strong interactions. Red lines represent interactions that are supported by only limited data.

The 9-1-1 heterotrimeric complex (composed by Rad9, Rad1 and Hus1) acts as a sensor complex, indeed once DNA is damaged, the 9-1-1 complex is recruited to the damage site under the regulation of Rad17 complex (Melo et al. 2001). The chromatin-bound 9-1-1 complex then facilitates phosphorylation mediated by transducer proteins Ataxia Telangiectasia and Rad-3-related (ATR) and Ataxia Telangiectasia Mutated (ATM).

In mammals, there are four mediator-type proteins that contain BRCA1 C-terminus repeat (BRCT) domains that are involved in protein–phosphoprotein interaction (Manke et al. 2003). Mediator of DNA Damage Checkpoint 1

(MDC1) functions as a molecular bridge between histone H2AX phosphorylated on serine 139 (called γH2AX) and Nijmegen Breakage Syndrome 1 (NBS1) in the MRN complex (MRE11–Rad50–NBS1). Unlike sensor proteins that accumulate at the sites of DNA damage in an ATM-independent manner, recruitment of these mediator proteins depends on the phosphorylation of γH2AX by ATM (Niida and Nakanishi 2006). γH2AX formation has normally been associated with the induction DSBs after exposure to IR or other DNA-damaging agents and marks chromatin regions spanning megadaltons of DNA flanking each DSB (Rogakou et al. 1998). However, a number of reports have shown phosphorylation of H2AX after DNA replication stress (Ward and Chen 2001, Furuta et al. 2003, Ewald et al. 2007).

Signals initiated by the sensors are very rapidly transduced to ATM and ATR kinases, which are both extremely large proteins that phosphorylate a great number of substrates. ATM is activated by DNA-damaging agents (e.g., ionizing radiation and genotoxins) that create DSBs, whereas ATR is activated following recruitment to RPA-coated ssDNA regions generated at stalled replication forks by agents interfering with the function of DNA replication forks, such as UltraViolet (UV) light and hydroxyurea (Smith et al. 2010).

Under unstressed conditions ATM exists as a homodimer in which the kinase domain is physically blocked by tight intermolecular binding to a protein domain at around Ser1981. DSBs cause a conformational change in the ATM protein that stimulates the kinase to phosphorylate Ser1981 by intermolecular autophosphorylation, resulting in dissociation of the homodimer. ATM is also regulated by recruitment to the substrate sites by binding to MRE11. Activated ATM phosphorylates many proteins, including BReast CAncer 1 (BRCA1) (Cortez et al. 1999), NBS1 (Lim et al. 2000), Chk2 and p53 (Banin et al. 1998), as well as itself (Bakkenist and Kastan 2003). In particular, in response to a DNA damage, ATM phosphorylates Chk2 on threonine 68. Even if biochemical analyses revealed that activated Chk2 phosphorylates Cdc25A at Ser123, Cdc25C on Ser216, BRCA1 at Ser988 and p53 at several sites, including Ser20, the examination of Chk2-deficient mice and cells revealed that this enzyme functions mainly in p53-dependent apoptosis but not in G2/M arrest upon DNA damage (Takai et al. 2002).

Another important DNA damage signal transducer is ATR. In human cells, ATR exists in a stable complex with ATR interacting protein (ATRIP), a potential regulatory partner. ATR–ATRIP complex is recruited at sites of DNA damage by the binding of ATRIP to RPA and it is implicated in monitoring the progression of DNA replication. Once activated, ATR phosphorylate in serine

317/345 and activate its main target Chk1. In turn Chk1 has been shown to phosphorylate a series of effector proteins such as Cdc25-A, Cdc25-B and Cdc25-C, downregulating their phosphatase activity. These phosphatases dephosphorylate the Cdks that regulate cell cycle transitions. Therefore Chk1 seems to be indispensable for the cell-cycle arrest in response to genotoxic stresses (Niida and Nakanishi 2006).

Among the effector proteins, in addition to the already mentioned phosphatases and Cdks, the tumor suppressor protein p53 plays a central role in the decision of a cell to undergo either cell-cycle arrest or apoptosis after DNA damage (Prives and Hall 1999). Moreover, p53 can directly activates repair pathways such as NER through regulation of the NER factors XPC and DDB2 and induces dNTP synthesis (Niida and Nakanishi 2006). During DDR both ATM and ATR phosphorylate p53 at Ser15. This phosphorylation inhibits the interaction of p53 with Mdm2, resulting in p53 stabilization. Moreover ATM is also able to phosphorylate Mdm2 reducing its capability to promote nucleo–cytoplasmic shuttling and the subsequent degradation of p53 (Maya et al. 2001).

ATM and ATR are required for the activation of NHEJ, HR, and NER, as well as replication fork stability during unperturbed DNA replication and in response to replication blocks.

Double strand breaks repair: nonhomologous end joining and homologous recombination

DSBs are the most dangerous of all types of DNA damage and arise in cells from endogenous (reactive oxygen species) as well as from exogenous (Ionizing Radiation, IR, and UV light) attacks on the DNA backbone. When unrepaired, DSBs can be lethal and trigger apoptosis. DSB repair occurs primarily by two pathways: NonHomologous End Joining (NHEJ) and Homologous Recombination (HR).

NHEJ repair is the result of the direct ligation of the free ends of the DNA DSB, whereas HR uses strand invasion of the homologous chromatid to synthesize DNA across the DSB using this homologous chromatid sequence as a template. Thus, HR can take place only after DNA replication, in S/G2/M cell-cycle phases, whereas NHEJ is preferred in G0/G1. Because HR uses a homologous template to repair a DSB, it is quite accurate, whereas NHEJ may require end trimming that makes it less accurate. Both NHEJ and HR have 2 subpathways. In NHEJ the choice between classic and alternate pathways is regulated by p53 Binding Protein 1 (53BP1), which promotes classic NHEJ, and Poly (ADP-ribose) polymerase 1 (PARP-1), which promotes alternative

NHEJ. Alternative NHEJ involves more resection of the free DNA ends to find microhomologies than classic NHEJ, which directly ligates the free ends. Therefore alternative NHEJ is less accurate and can result in large deletions or translocations.

Classic NHEJ is a relatively simple DSB repair pathway. Both ends of the break are first bound by the Ku70/Ku80 heterodimer, which then recruits the catalytic subunit of the DNA dependent Protein Kinase (DNA-PKcs). If necessary, the ends can be trimmed by nucleases (such as Artemis) or filled in by DNA polymerases (such as Polμ or Polλ) to create compatible ends. Finally, the ligation complex, consisting of DNA ligase IV, X-ray cross-complementation group 4 (XRCC4) and Xrcc4 like factor (XLF), also known as Cernunnos, ligates the ends [Figure 3] (Lieber 2010).

Fig 3

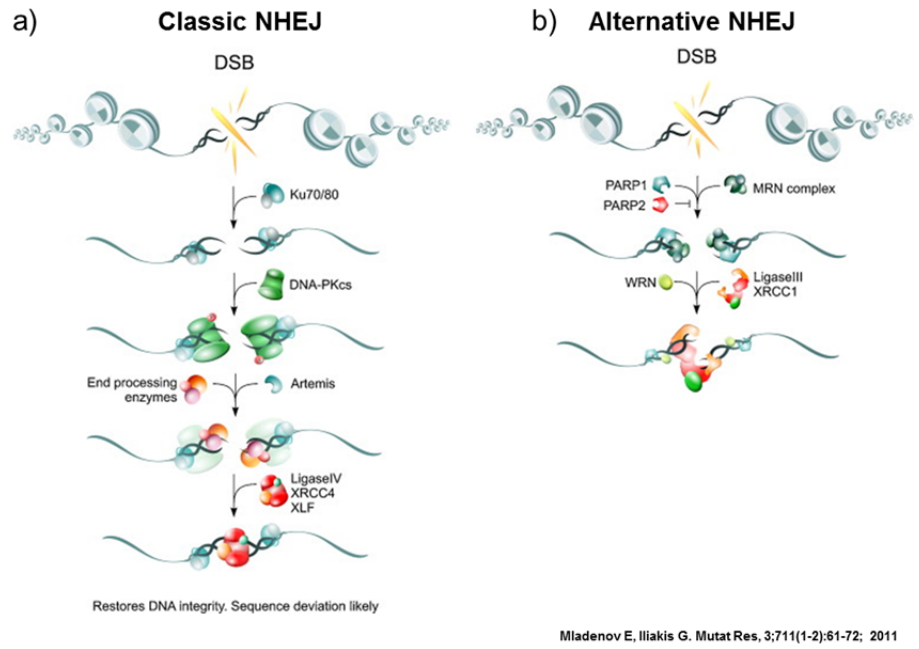

Figure 3: Outline of the main players and of the key steps of NonHomologous End Joining (NHEJ).
a) Classic NHEJ pathway efficiently restores genomic integrity without ensuring sequence restoration. Association of Ku to DNA ends facilitates the recruitment of DNA-PKcs, a major kinase activated by DNA ends and contributing to the efficiency of this repair pathway. DNA-PKcs promotes end-processing by the Artemis nuclease and subsequent rejoining of broken DNA ends by the LigIV/XRCC4/XLF complex; b) The enzymatic activities implicated in alternative NHEJ pathway are shown together with their possible contributions in the process.

Alternative NHEJ pathway requires single-strand end-resection by the MRE11/RAD50/NBS1 (MRN) complex, and the CtIP tumor-suppressor. This

resection exposes microhomologies that promote pairing of broken ends, which are then ligated by Ligase III/XRCC1 [Figure 3] (Shaheen et al. 2011).

HR also includes accurate and inaccurate subpathways, both of which require extensive single-strand end-resection to allow for invasion by the remaining strand of the homologous template (sister chromatids, homologous chromosomes or linked or unlinked repeated sequences). End resection occurs in 2 phases, with limited resection initiated by MRN/CtIP and extensive resection mediated by the BLM helicase and the EXO1 and DNA2 exonucleases (Shaheen et al. 2011).

In the accurate HR pathway, homologous DNA sequences are used as templates to copy genetic information for repair. After resection, accurate HR involves binding of RPA to single strands, and BRCA2-mediated replacement of RPA with RAD51 to form a RAD51 nucleoprotein filament, which searches for and invades the homologous template. The invading strand is extended by synthesis of new DNA. The newly synthesized strand can then anneal with the other resected end, and additional synthesis and ligation completes high-fidelity repair [Figure 4] (Brandsma and Gent 2012).

Inaccurate HR is termed Single-Strand Annealing (SSA), in which extensive resection exposes complementary sequences in linked direct repeats, which anneal in a reaction promoted by RAD52. SSA is always inaccurate because it deletes one of the repeats and the intervening sequence, or it results in translocations when 2 DSBs occur within or near repeats on different chromosomes [Figure 4] (Shaheen et al. 2011).

Fig 4

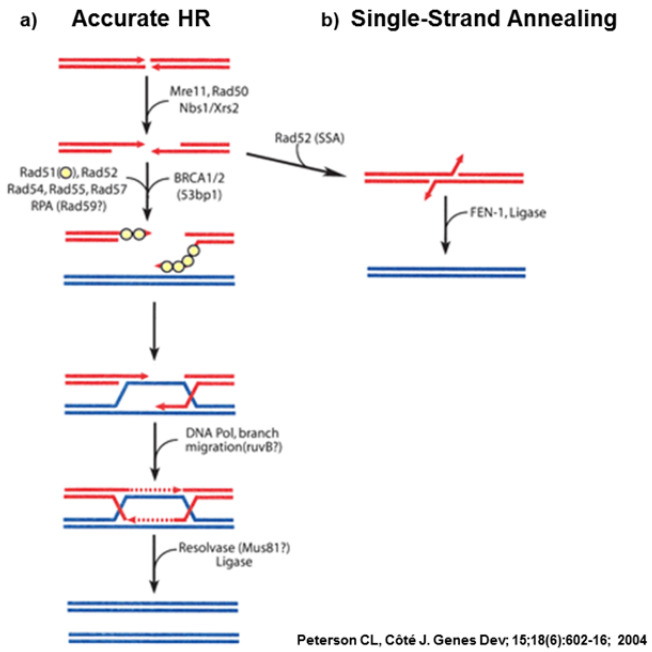

Figure 4: Homologous Recombination (HR) subpathways.
a) After detection of the DSB, the 5′ strands are resected, producing long 3′ single-stranded DNA tails that then serve as a substrate for assembly of a Rad51 nucleoprotein filament. This presynaptic complex also contains Rad52, Rad54, Rad55, and Rad57. This complex searches the genome for DNA sequence homology that is then used for subsequent strand invasion. Branch migration of this joint DNA molecule, DNA synthesis, ligation, and resolution of Holliday junctions restores the DNA templates. b) An alternative HR repair pathway (single-strand annealing) uses Rad52 to search for homologous sequences on the resected 3′ ends. The FEN-1 endonuclease removes the "flap" DNA ends and ligation occurs. This pathway leads to DNA sequence deletions.

The remaining mentioned repair pathways operate on nucleotide lesions occurring on single strands.

Single strand breaks repair: direct repair

MGMT plays an important biological role in directly repairing O^6-methylguanine in DNA formed by alkylating agents, indeed MGMT removes methyl adducts from O^6 position of guanine (formed by temozolomide, streptozotocin, procarbazine and dacarbazine), as well as O^4-methyl thymine, O^6-ethylguanine (formed by ethylnitrosourea and diethylnitrosamine and related compounds) and O^6-chloroethylguanine adducts [formed by bis-(2-cholorethyl)-nitrosourea (BCNU) and 1-(2-chloroethyl)-3-cyclohexyl-1-nitrosourea; CCNU]. Then MGMT transfers the alkyl group from the target base to a cysteine residue within its active site and thereby inactivates itself in the process [Figure 5] (Madhusudan and Hickson 2005).

Fig 5

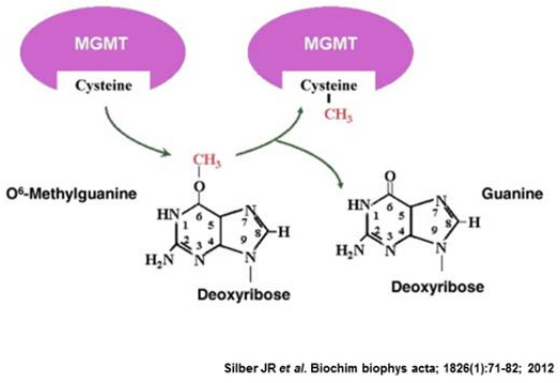

Figure 5: Repair of O^6-alkylguanine adducts by MGMT.
MGMT mediates a stoichiometric reaction in which methyl and other alkyl groups bound to the O^6 position of guanine in DNA via a thioester linkage to a cysteine residue in the active site. Alkylation of MGMT leads to rapid degradation of the protein.

Single strand breaks repair: nucleotide excision repair

For bulky helix-distorting damage, such as lesions induced by UV light, the principal repair mechanism is the evolutionarily conserved NER pathway. Essentially it consists of several sequential steps: lesion sensing, opening of a denaturation bubble, incision of the damaged strand, displacement of the lesion-containing oligonucleotide, gap filling, and ligation. However NER recognizes and removes helical distortions in two different modes: throughout the genome (global genome repair, GGR), or selectively from the transcribed strand of active genes (transcription-coupled repair, TCR) (Kamileri et al. 2012). In GGR, the DNA is surveyed by two proteic complexes that sense and bind the DNA lesion: the xeroderma pigmentosum complementation group C (XPC)-RAD23-centrin, EFhand protein, 2 (CETN2) complex, and the UV damaged DNA-binding protein (UV-DDB) complex (DDB1-DDB2-containing E3-ubiquitin ligase complex). The opening of a denaturation bubble around a lesion and the stabilization of the single-stranded DNA require transcription factor IIH (TFIIH), a complex containing XPB, p62, p52, p44, p34, p8, XPD in addition to the Cdk-activating-kinase (CAK) complex and XPG. Unwinding of the DNA mainly relies on the ATPase activity of XPB to form a 27-nucleotide bubble that asymmetrically flank the damage. Then damaged DNA is stabilized for incision by Replication Protein A (RPA) acting in complex with XPA, XPB and XPD. RPA activates XPG and excision repair cross-complementing rodent repair deficiency, complementation group 1 (ERCC1)-XPF, structure-specific endonucleases that cleave the 30 and 50 side of the 24–32-nucleotide fragment containing the damaged DNA. The single-strand gap is then filled by the replicative DNA polymerases δ and ε or the translesion DNA polymerase κ;

their polymerase activity is stimulated and coordinated by Proliferating Cell Nuclear Antigen (PCNA) loaded onto the DNA by Replication Factors C (RFC) and A. The nascent DNA fragment is finally sealed by DNA ligase III-XRCC1 and DNA ligase I [Figure 6] (Kamileri et al. 2012).

Fig 6

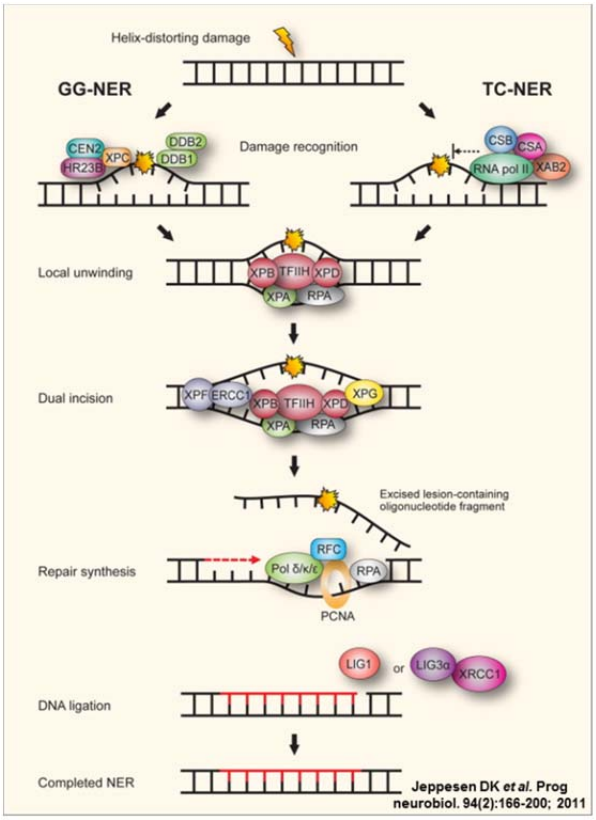

Figure 6: The two subpathways of mammalian nucleotide excision repair (NER).
In global genome nucleotide excision repair (GG-NER) helix-distorting DNA damage anywhere in the genome is recognized by the XPC–HR23B–CEN2 complex. The DDB complex, consisting of the two subunits DDB1 and DDB2 (XPE), can facilitate recognition of lesions that by themselves cause little distortion of the helix. In transcription-coupled nucleotide excision repair (TC-NER) recognition is by the stalling of RNA pol II at DNA lesions on the transcribed strand of active genes, facilitated by CSB, CSA and XAB2. Either XPC in GG-NER or CSB and CSA in TC-NER recruit TFIIH to the repair site followed by converging of the subpathways. The XPB and XPD subunits of TFIIH are DNA helicases that unwind the DNA in the immediate vicinity of the lesion. RPA and XPA bind to keep the DNA strands apart. For the dual incision, XPA recruits the XPF–ERCC1 endonuclease to incise the damaged DNA strand 5′ to the lesion while XPG incises 3′ to it. The lesion is thus excised in an oligonucleotide fragment leaving behind a single-strand gap. Repair synthesis is performed by DNA polymerase δ and κ, or ε (Pol δ/κ/ε) with the help of the accessory proteins RFC, PCNA and RPA. The remaining nick in the DNA backbone is sealed with ligation by either LIG1 or LIG3α–XRCC1.

GGR and TCR differ only in how helix-distorting DNA lesions are recognized. Following damage detection, the two sub-pathways merge into a

common mechanism to unwind the DNA around the lesion, to stabilize and excise the DNA fragment containing the damage, and to fill in and ligate the single strand gap. TCR damage recognition requires RNA polymerase II (RNAPII). Stalled RNAPII colocalizes with Cockayne syndrome B (CSB), a DNA-dependent ATPase and CSA, a protein that is part of an E3-ubiquitin ligase complex. In particular, CSB binds stalled RNAPII and triggers the assembly of the remaining NER factors and histone acetyltransferase p300. In turn, CSA recruits (together with CSB) the High Mobility Group Nucleosome binding domain 1 protein (HMGN1), XPA binding protein 2 (XAB2) and TFIIS. Once chromatin is accessible for TCR, the lesion is removed by the core NER reaction (Kamileri et al. 2012).

Single strand breaks repair: DNA mismatch repair

DNA mismatch repair (MMR) is an evolutionarily conserved process that corrects mismatches generated during DNA replication and escape proofreading. Repair is initiated when complexes of MutS homologs, either MSH2-MSH6 (MutSα) or MSH2-MSH3 (MutSβ), bind to a mismatch. The MutSα is involved primarily in the repair of base substitutions and small mismatched loops, whereas MutSβ repairs both small loops as well as large loop mismatches (~10 nucleotide loops). MutS heterodimer initially binds double-stranded DNA at the site of a mismatch and then recruits MutL. The MutL heterodimer is present in a number of forms, including the MutLα complex (composed by MLH1 and PMS2), the MutLβ heterodimer (MLH1 and PMS1), and MutLγ (MLH1 and MLH3). The primary MutL activity for mismatch correction is MutLα, with MutLβ apparently providing a minor role, whereas MutLγ plays a role in meiosis (Kunkel and Erie 2005).

As the function of postreplicative MMR is to reverse errors of replication (i.e., replication errors that are found in newly synthesized DNA), the MMR machinery must be able to distinguish parental DNA from daughter DNA and then remove and replace the (presumably aberrant) daughter DNA sequence. It is thought that intermittent gaps in DNA in between Okazaki fragments on lagging strand DNA could represent a signal that distinguishes parental from daughter strand in mammalian MMR. However, the discriminatory signal on leading-strand DNA in mammalian cells is still unclear (Martin et al. 2010).

The DNA exonuclease EXO1, guided by the MutS/MutL, starts removing daughter-strand DNA towards and then beyond the site of the mismatch. Once the mismatch is removed, the activity of EXO1 is suppressed by MutL, thus terminating DNA excision. At the completion of this process, a DNA polymerase synthesizes DNA in place of the excised sequence. Finally a DNA

ligase joins any remaining gaps in the DNA sequence [Figure 7] (Martin et al. 2010).

Fig 7

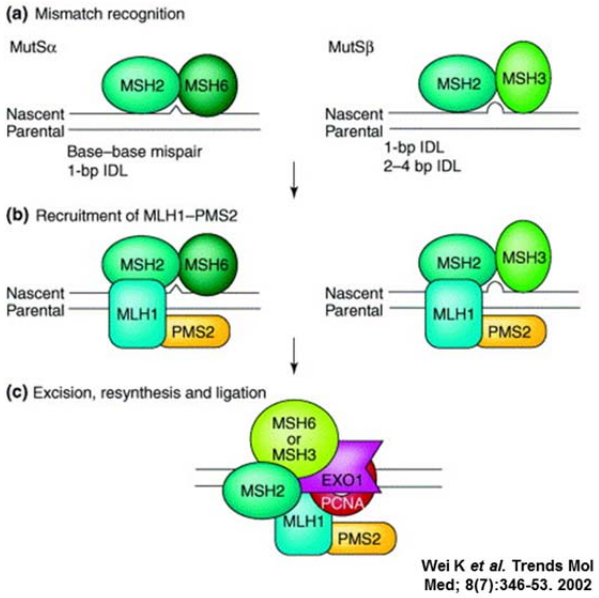

Figure 7: model for mammalian DNA mismatch repair (MMR).
a) The MSH2–MSH6 (MutSα) complex recognizes base–base mismatches and 1-bp insertion/deletion loops (IDLs), and the MSH2–MSH3 (MutSβ) complex recognizes 1-bp IDLs as well as 2–4-bp IDLs. b) and c) The interaction of MLH1–PMS2 (MutLα) activates downstream repair events that facilitate the excision of the DNA strand carrying the mutant base as well as its resynthesis and ligation. Several proteins have been identified by virtue of their interaction with either MSH2 or MLH1. EXO1, is a 5′→3′ exonuclease that was shown to bind to MSH2, MSH3 and MLH. Another protein known to be capable of interacting with MSH3, MSH6 and MLH1 is the proliferating cellular nuclear antigen (PCNA). The role of EXO1 and PCNA in these processes is indicated.

Single strand breaks repair: base excision repair

About 10 000 spontaneous SSBs occur in each cell every day (Lindahl 1993). The BER pathway is the main repair mechanism of these lesions; moreover it is involved in correcting base lesions that arise from oxidative, alkylation, deamination, and depurination/depyrimidination damage. BER facilitates the repair of damaged DNA via two general pathways: short-patch and long-patch. The short-patch BER pathway leads to a repair tract of a single nucleotide, whereas the long-patch BER pathway produces a repair tract of at least two nucleotides.

A currently accepted model for the core BER pathway reveals five distinct enzymatic steps for the repair of damaged bases. The first step in BER is the recognition of a damaged base by a DNA glycosylase. After recognition the

glycosylase catalyzes the cleavage of an N-glycosidic bond, effectively removing the damaged base and creating an apurinic or apyrmidinic site (AP site). However the DNA backbone is cleaved by either a DNA AP Endonuclease (APE 1) or a DNA AP lyase, an activity present in some glycosylases. The newly created nick is processed by APE1, creating a single-nucleotide gap in the DNA (Robertson et al. 2009).

In short-patch BER, XRCC1 is one of the first proteins recruited to the nick generated by the action of a glycosylase and/or AP endonuclease and function as scaffold interacting with DNA polymerase beta (Polβ). Polβ fills in the gap with the correct nucleotide; then a DNA ligase III completes the repair process and restores the integrity of the helix by sealing the nick [Figure 8] (Robertson et al. 2009).

In long-patch BER, APEX1 catalyzes the formation of a nick 5' to the AP site. This action recruits Polβ or DNA polymerase delta (Polδ), PCNA, Flap structure-specific ENdonuclease 1 (FEN1), and probably the replicative DNA ligase I. In particular a PCNA-dependent manner Polβ displaces and polymerizes tracts of DNA longer than one base. The strand displacement activity of Polβ produces a flapped substrate that is refractory to ligation. FEN1 is involved in the removal of the flap generated by Polβ [Figure 8] (Robertson et al. 2009).

Fig 8

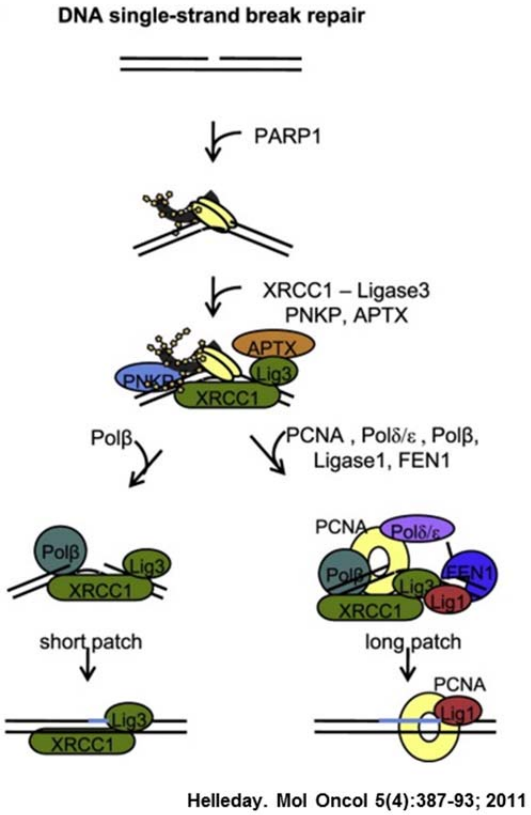

Figure 8: Short- and long-patch base-excision repair pathways.
Short-patch repair, occurring after excision of a damaged base (indirect breaks), involves recruitment of poly(ADP-ribose) polymerase 1 (PARP1), or PARP2, which then recruits the scaffold protein XRCC1 and DNA polymerase β (Polβ) to replace the damaged nucleotide. Finally, DNA ligase III (Lig3) is recruited to ligate the nick, and intact DNA is restored. Long-patch repair, occurring after direct DNA breaks (for example, after ionizing radiation damage), involves recruitment of PARP1 followed by XRCC1, which then recruits polynucleotide kinase (PNK) to convert the damaged ends to 5'-phosphate and 3'-hydroxyl moieties. Proliferating cell nuclear antigen (PCNA) and DNA polymerase δ/ε (Polδ/ε) extend and fill the gap by 2–15 nucleotides, and flap endonuclease 1 (FEN1) cleaves the resulting flap. The nick is subsequently ligated by DNA ligase I (Lig1).

The switch from short-patch to long-patch BER depends on the relative ATP concentration near the AP site, which is apparently modulated by DNA ligase III and XRCC1 (Petermann et al. 2003). It was shown that long-patch BER occurred more frequently at low ATP concentrations, whereas short-patch BER appeared to be the preferred mechanism with elevated concentrations of ATP.

During BER pathway, Poly(ADP-Ribose) Polymerase 1 and 2 (PARP-1 and PARP-2) have a crucial role, indeed they interact with BER factors such as XRCC1, DNA polymerase β and DNA ligase III recruiting them at damaged sites (Schreiber et al. 2002, El-Khamisy et al. 2003). Moreover, recently, Khodyreva et al. (2010) have demonstrated a new role for PARP-1 in the

regulation of the BER process through its interaction at the AP site. PARP-1 interaction at the AP site could protect the site until APE1 becomes available to initiate strands incision and BER (Khodyreva et al. 2010).

1.5 ADENOVIRUSES AND DNA DAMAGE RESPONSE

Within first few hours of adenovirus infection, the host cell responds to the virus, perhaps in recognition of viral DNA or cellular stress, by activating a classical damage response. Indeed it is likely that double-stranded DNA termini of the adenovirus genome could be perceived by the host cell as a double strand break.

In the case of adenovirus harboring deletion of the open reading frame (ORF) within the E4 region, a much more pronounced cellular response can be observed, with increased phosphorylation of DDR substrates and concatenation of viral DNA (Weiden and Ginsberg 1994, Stracker et al. 2002). Importantly, after infection with wild-type (WT) group A and group C viruses, a number of cellular proteins such as p53, MRE11, DNA ligase IV and BLM are degraded (Querido et al. 1997, Stracker et al. 2002, Baker et al. 2007a, Carson et al. 2009) ensuring that the HR and NHEJ pathways are incapacitated. Substrates amongst the DDR proteins vary with different adenovirus serotypes. Thus p53, BLM and MRE11 are not degraded by the group B and group D viruses (Forrester et al. 2011) and TOPBP1 appears to be degraded by only the group A viruses (Blackford et al. 2010, Forrester et al. 2011).

It is possible that adenoviruses can inhibit the DDR independently of protein degradation. Ad5E4orf6 and Ad5E4orf3 have been shown to bind directly to DNA-PK, although they did not appear to inhibit its kinase activity against heterologous substrates (Boyer et al. 1999). However, autophosphorylation of DNA-PKcs (at Threonine 2609) was reduced during DSB repair (Hart et al. 2005). Ad5E4orf6 also enhances the DDR by inhibiting protein phosphatase 2A (PP2A), which leads to prolonged phosphorylation of H2AX, activation of PARP and apoptosis (Hart et al. 2007).

Although adenoviruses inhibit the DDR by promoting the rapid degradation of key components, they are also able to affect the localization of various DDR proteins. During infection, a number of DDR proteins are recruited to viral replication centers (VRCs) (Turnell and Grand 2012). RPA32 is recruited to these sites after infection with both WT and mutant viruses (Stracker et al. 2005). Other DDR proteins recruited to VRCs after WT infection include ATR, ATRIP, Rad9, TOPBP1, Rad17 and hnRNPUL1 (Carson et al. 2003, Blackford et al. 2008, Carson et al. 2009). As well as initiating protein degradation and localization to VRCs, adenoviruses can also promote relocalization to other

sites. Promielocytic leukaemia (PML) bodies play a role in sensing DNA damage, and a number of DDR proteins localize to them (Lombard and Guarente 2000). Following Ad infection, PML bodies are disrupted and the PML protein is relocalized into 'track-like' structures; this is dependent on the activity of the AdE4orf3 protein [Figure 9] (Carvalho et al. 1995, Doucas et al. 1996, Leppard and Everett 1999).

Fig 9

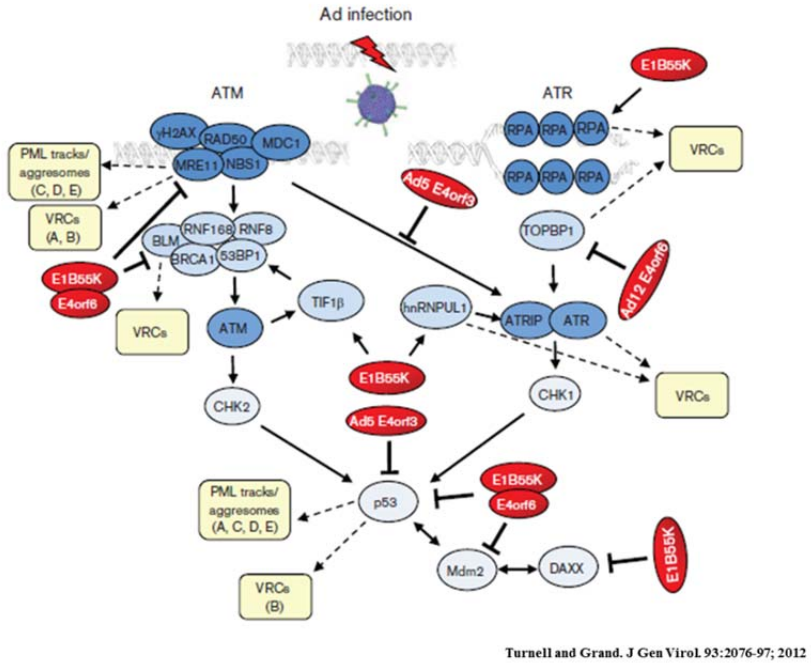

Figure 9: Regulation of ATM and ATR signalling pathways by adenovirus.
E1B55K–E4orf6 complexes recruit cellular ubiquitin ligases to promote the degradation of p53, BLM and MRE11, whilst Ad12 E4orf6 recruits an E3 ligase to promote TOPBP1 degradation and E1B55K recruits an E3 ligase to promote the degradation of DAXX. Ad5 E4orf3 sequesters MRN to aggresomes to inhibit the MRN-dependent activation of ATR, and inhibits p53 epigenetically. Components of the ATM and ATR pathways are recruited to VRCs or PML-containing nuclear tracks and aggresomes during infection. MRE11 and p53 are regulated differentially by different Ad types (shown in parentheses). E1B-55K also associates with TIF1b, hnRNPUL1 and the RPA complex, although the significance of these observations awaits clarification. Viral proteins are shown in red; cellular proteins are shown in blue. Broken arrows show cellular proteins that are recruited to PMLtracks, aggresomes or VRCs. Viral inactivation of cellular proteins is depicted by 'T'. Arrows linking viral proteins to cellular proteins indicate protein–protein interactions whose significance has yet to be fully established.

It has been suggested that, during Ad5 infection, the MRN complex is initially localized to 'nuclear tracks' by Ad5E4orf3, where it binds to the E1B55K protein. Protein complexes containing Ad5E1B55K, Ad5E4orf3, Ad5E4orf6 and MRN are then transported to the aggresomes, where MRE11 undergoes rapid degradation (Evans and Hearing 2005, Liu et al. 2005).

It is clear that different virus species adopt very different strategies to modulate the damage response. In the case of adenoviruses, degradation of cellular DDR components is a priority and, presumably, this has the effect of disabling the cellular response.

Understanding the relationship between the DNA damage response machinery and adenovirus infections will provide insights into viral pathology and persistence, but it may also guide the effective design of new oncolytic adenoviral mutant for cancer therapy, or may suggest new molecular targets to potentiate the cytotoxicity of already existing oncolytic adenoviral mutants.

1.6 POLY(ADP-RIBOSE) POLYMERASE (PARP)

Poly(ADP-ribosyl)ation is a ubiquitous protein modification involved in the regulation of transcription, cell proliferation, differentiation, DNA methylation and apoptosis which modulates protein function by regulating either enzymatic activities or macromolecular interactions between proteins, DNA or RNA (Hakme et al. 2008). This modification is carried out by the Poly(ADP-Ribose) Polymerases (PARPs), also known as ADP-ribosyltransferases (ADPRTs) or poly(ADP-ribose) synthetases.

PARP members are a family of highly conserved enzymes found in plants and animals, first described more than 40 years ago (Chambon et al. 1963). PARP-1 was the first of this enzyme family to be described. Afterwards, based on sequence similarity with PARP-1 catalytic domain, 16 structurally-related proteins have been identified (Ame et al. 2004). In addition to the catalytic domain, these proteins typically contain one or more additional motifs or domains, including zinc fingers, ‘‘BRCA1 C-Terminus-like’’ (BRCT) motifs, ankyrin repeats, macro domains and WWE domains (involved in DNA or RNA binding, protein–protein interaction or cell signaling), conferring unique properties on each PARP protein (Ame et al. 2004).

Among PARP members only six of these protein may actually be considered poly(ADP-ribose) polymerases, whereas the reminder are probably mono-ADP-ribosyltransferases. These six “true” PARP are subdivided in three groups, with PARP-1, PARP-2 and PARP-3 in the first group, PARP-4 (also known as vault PARP) in the second, and tankyrase 1 (TNKS1) and TNKS2 in the third (Rouleau et al. 2010).

PARP-1 and PARP-2 are the only ones reported until now to be highly stimulated by DNA damage; however PARP-2 is thought to be responsible for no more than 15% of the total poly(ADP-ribose) (PAR) synthesis stimulated by DNA strand breaks (Shieh et al. 1998).

PARP-1 is a 116-kDa protein comprising an N-terminal DNA-binding domain, which contain three zinc-binding domain, a central automodification domain, which contain several glutamate, aspartate, and lysine residues as putative acceptors for auto(ADP-ribosyl)ation, a leucine zipper motif that mediates homodimerization or heterodimerization, a BRCT phosphopetide-binding motif and a C-terminal catalytic domain that contains three crucial residues (an histidine and a tyrosine that are important for NAD^+ binding and a glutamic acid that is essential for polymerase activity) [Figure 10] (Rouleau et al. 2010).

Fig 10

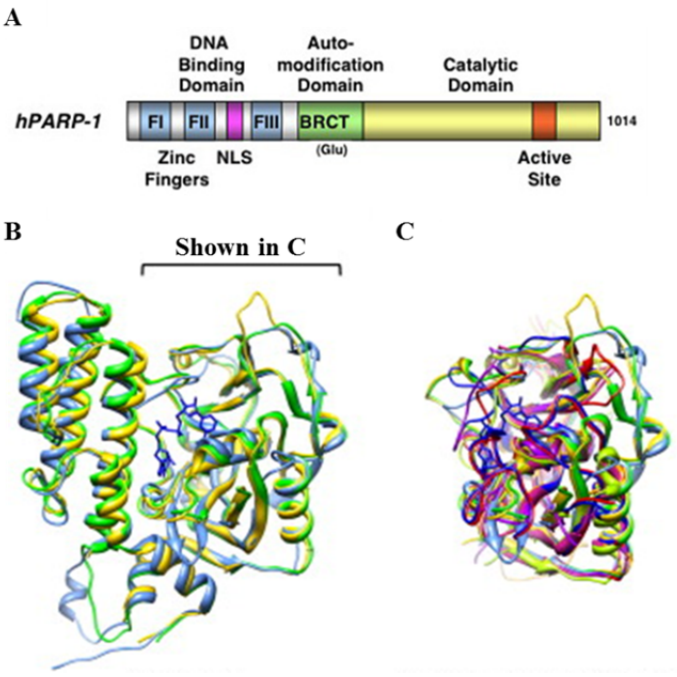

Figure 10: Structural and functional organizations of PARP-1
a) PARP-1 has a highly conserved structural and functional organization including an N-terminal DNA-binding domain with two Cys-Cys-His-Cys zinc finger motifs (FI and FII), a nuclear localization signal (NLS), a central automodification domain containing a BRCT protein-protein interaction motif, and a C-terminal catalytic domain with a contiguous 50-amino-acid sequence, the "PARP signature" motif, that forms the active site; b and c) PARP-1 three-dimensional representation.

Once activated, PARP-1 rapidly catalyzes the transfer of ADP-ribose moieties from NAD^+ to the acceptor protein, including histones, DNA repair proteins, transcription factors and chromatin modulators, resulting in the attachment of linear or branched polymers of ADP-ribose. PARP-1 itself is the primary target for poly(ADP-ribos)ylation in vivo, with more than 90% of PAR being found on PARP-1 (D'Amours et al. 1999). The modifications are heterogeneous with respect to length (from a few to 200 ADP-ribose units) and

extent of branching (one branch per 20–50 ADP-ribose units). Poly(ADP-ribosyl)ation is a dynamic process consuming substantial amounts of NAD^+. The in vivo half-life of the polymer is less than 1 min with the steady-state levels of PAR being regulated by the catalytic reactions of poly(ADP-ribose) glycohydrolase (PARG) and possibly the ADP-ribose hydrolase (ARH3). The degradation of PAR may begin immediately after the initiation of PAR synthesis and can be completed within minutes after the cessation of PAR synthesis has occurred (D'Amours et al. 1999). This generates large amounts of AMP that in turn activates the bioenergetics sensor AMP-activated protein kinase (AMPK). Free or protein-bound PAR polymers work as signal transducers by binding other proteins through their conserved PAR recognition modules, including PAR-binding motifs (PBMs), PAR-binding zinc finger (PBZF) domains, and macrodomains (Kraus 2009). PAR, which is a negatively charged polymer, alters the biochemical properties of modified or interacting proteins, modulating their structure, function, and localization (Schreiber et al. 2006).

As discussed above PARP-1 is a molecular sensor of DNA strand breaks and through its ribosylating activity plays a key role in the spatial and temporal organization of their repair. Through its own poly(ADP-ribosyl)ation and that of histones, PARP-1 loosens the chromatin allowing access to DNA strand breaks and is also involved in the recruitment of the components of the BER/SSBR pathways (El-Khamisy et al. 2003). The automodification of PARP-1 itself promotes its interaction with XRCC1 through its BRCT domain. This leads to the recruitment of DNA polymerase β and DNA ligase III thus completing the repair of the single-strand break. PARP-1 has also been shown to be involved in FEN-1-dependent strand displacement during DNA synthesis by DNA polymerase β (Prasad et al. 2001). In addition to its role in BER, PARP-1 is involved in several other DNA damage repair processes, including the repair of DNA DSBs. For instance, the recruitment of MRE11, NBS1, and ATM to DSBs has been reported to depend on PARP-1 activity and PARP-1 is a component of an alternative pathway of NHEJ. When essential components of the classical pathway of NHEJ are absent, PARP-1 is recruited for DSB repair with the ligase III and probably with histone H1. The presence of poly(ADP-ribose) chains at the site of DNA damage also acts as an anti-recombinogenic factor, preventing the inappropriate recombination of homologous DNA (Megnin-Chanet et al. 2010). It has been shown that PARP-1 function also as a transcriptional activator of NF-kB, the transcription factor that regulates immune and inflammatory response genes (Hassa and Hottiger 2002).

PARP inhibitors

Despite the important role of the PARP-1 in DNA damage repair, PARP-1 deficiency does not seem to be such a problem for nonmalignant cells. As a matter of fact, mice engineered to lack PARP-1 enzyme (PARP-$1^{-/-}$) are both viable and fertile (de Murcia et al. 1997, D'Amours et al. 1999). These PARP-$1^{-/-}$ mice do not seem to develop early onset tumors (Conde et al. 2001). However the simultaneous absence in other genes involved in HR pathway (such as BRCA1 and BRCA2) confers sensitivity to PARP deficiency or inhibition (McCabe et al. 2006). The acquired sensitivity could be explained by the concept of synthetic lethality, first described in 1946 by Dobzhansky (Dobzhansky 1946), that is a situation when a mutation in one of two genes individually has no effect but combining the mutations leads to cell death.
Indeed cells exposed to a PARP inhibitor are flooded with SSBs that are converted into DSBs at replication forks. Normally the repair of DSBs is able mainly through HR activity. The HR-deficiency unable to utilize the HR pathway. Instead, DSBs are repaired via NHEJ or the SSA sub-pathway of HR with large numbers of chromatid aberrations leading to cell lethality.

These findings raise the possibility that PARP inhibitors may play a role in a broad range of tumors with dysfunction of HR or identified as "BRCAness". The use of a PARP inhibitor in a BRCA-deficient cancer is probably the first example of the clinical application of the concept of synthetic lethality (Farmer et al. 2005).

Most of the PARP inhibitors in development mimic the nicotinamide moiety of NAD^+ (Jagtap and Szabo 2005, Peralta-Leal et al. 2009). These molecules block the binding of the NAD^+ to the enzyme, inhibiting PARP activity. First-generation inhibitors were developed 30 years ago: nicotinamide, benzamide, and substituted benzamide, in particular 3-aminobenzamide (3-AB), were shown to be competitive inhibitors of PARP. Benzamides lack specificity and potency; moreover they affect cell viability, glucose metabolism and DNA synthesis (Milam and Cleaver 1984). A second generation of very potent PARP inhibitors was developed in 1990s, producing 170 specific inhibitors. All these inhibitors may be classified as analogs of benzamide. A third generation of inhibitors, benzamidazoles, not only had potency, but also allowed the elucidation of the PARP inhibitor structure-activity relationship. Some of 3rd generation agents have entered clinical trials, including AZD2281 (KuDos/Astra Zeneca) (also known as Olaparib or KU-0059436), AG014699 (Pfizer), INO-1001 (Inotek/Genentech), ABT-888 (Abbott) and BSI-201 (BiPar/Sanofi-Aventis). However PARP inhibitors under clinical investigation do not discriminate between PARP-1 and 2.

Based on the demonstration of the role of BRCA selectivity, it has been proposed the use of PARP inhibitors for cancer therapy after selecting for BRCA mutations or BRCAness either as single agents or in combination with chemotherapy. In this regard, recently, the effect of AZD2281 was demonstrated in $BRCA2^{-/-}$ mammary tumors arising spontaneously in a mouse model, which is a relevant preclinical model with important advantages over the xenograft models (Hay et al. 2009).

In addition, the synergy of AZD2281 in combination with platinum drugs has been demonstrated in vivo with both $BRCA1^{-/-}$ $p53^{-/-}$ mammary tumors transplanted into wild-type mice (Rottenberg et al. 2008). Moreover, *in vitro* there is a synergy between AZD2281 and cisplatin in BRCA2-deficient cell lines (Evers et al. 2008).

Before a role for PARP inhibitors was suspected in BRCA-deficient tumors, these molecules were developed as chemosensitisers. Experimental data have shown a synergistic effect between PARP inhibitors and specific cytotoxic agents (Huang et al. 2008, Daniel et al. 2009). Furthermore, several *in vitro* (Calabrese et al. 2004, Dungey et al. 2008) and *in vivo* (Calabrese et al. 2004, Russo et al. 2009) models demonstrate that PARP inhibitors are synergistic with radiotherapy. This synergistic effect is supported by the idea that radiotherapy damages cells by causing DNA breaks, and PARP inhibitors disrupt DNA repair mechanisms leading to cell death.

It is worth to note that a number of clinical studies have been initiated in glioma using PARP inhibitors in combination with temozolomide. This was supported by knowledge that DNA repair mechanisms may play an important role in the response of glioblastoma to temozolomide. Indeed translational studies suggest that epigenetic silencing of the MGMT DNA repair enzyme by methylation of its promoter inhibits DNA repair and may lead to enhanced response to alkylating agents such as temozolomide and to longer survival in patients with glioblastoma, whereas glioblastomas with MGMT intact are resistant to alkylating agents (Esteller et al. 2000, Hegi et al. 2005).

The most important clinical trials with PARP inhibitors have been summarized in table 2.

Table 2. PARP inhibitor in clinical trials

AGENT	PHASE	TUMOR	COMBINATION	TRIAL IDENTIFIER
Olaparib, AZD2281, KU0059436 (Astra Zeneca/KuDOS Pharm)	II	BRCA-mutated ovarian cancer or recurrent high-grade ovarian cancer or triple-negative breast cancer/failed standard chemotherapy		NCT00679783
	II	Platinum-sensitive ovarian cancer		NCT00753545
	II	BRCA-mutated breast cancer		NCT00494234
	II	Ovarian cancer		NCT00494442
	II	BRCA-positive ovarian cancer		NCT00628251
	II	Metastatic colorectal cancer		NCT00912743
	I	Triple-negative breast cancer/neoadjuvante	Cisplatin	NCT007822574
	I	Metastatic triple-negative breast cancer	Paclitaxel	NCT00707707
	I	Metastatic solid tumors	Carboplatin or paclitaxel or carboplatin/paclitaxel	NCT00516724
	I	Pancreas cancer	Gemcitabine	NCT00515866
	I	Solid tumors	Topotecan	NCT00516438
	I	Colorectal cancer	Irinitecan	NCT00535353
	I	Melanoma	Decarbazine	NCT00516802
	I	Solid tumors	Bevacizumab	NCT00710268
	II	Gastric cancer	Paclitaxel	NCT01063517
Iniparib, BSI-201 (BiPar Sciences/Sanofi-Aventis)	II	BRCA1- or BRCA2-associated primary peritoneal cancers, advanced epithelial ovarian cancer		NCT00677079
	III	Triple-negative breast cancer	Gemcitabine/carboplatin	NCT00938652
	I/II	Glioma	Temozolomide	NCT00687765
	Ib/II	Metastatic breast cancer	Irinotecan	NCT00298675
	II	Platinum-sensitive recurrent ovarian cancer	Carboplatin/gemcitabine	NCT01033123
AG014699, PF-01367338 (Pfizer)	II	BRCA-mutated breast or ovarian cancer		NCT00664781
	I	BRCA-mutated, hereditary breast, ovarian cancer	Carboplatin/paclitaxel	NCT00535119
	II	Colorectal cancer	Temozolomide	NCT01051596
	I	Solid tumors and lymphoma	Cyclophosphamide	NCT00810966
	I	Solid tumors with brain metastasis	Whole-brain radiation	NCT00649207
	II	Melanoma	Decarbazine	NCT00804908
	I	Lymphoma	Irinotecan	NCT00576654
	II	Metastatic breast cancer	Temozolomide	NCT01009788
	I	Metastatic or unresectable solid tumors or non-Hodgkin lymphoma	Cyclophosphamide/Doxorubicin	NCT00740805
MK-4827 (Merck)	I	BRCA-mutated cancer		NCT00749502
CEP-9722 (Cephalon)	I	Advanced solid tumors	Temozolomide	NCT00920595

A search was carried out on http://www.clinicaltrials.gov

Clinical trials to date have shown that PARP inhibitors in combination with chemotherapeutic agents have manageable side effects. However enhanced mutation frequency by blocking a DNA repair pathway remains a major concern. In addition, early evidence suggests that tumor cells can become resistant to PARP inhibition by developing mutations that restore HR.

2. AIMS OF THE STUDY

Current therapies for the treatment of anaplastic thyroid carcinoma confer only a short term palliative and survival benefit. Overall, a comprehensive understanding of the molecular basis for the development of novel therapeutic approaches is still incomplete and urgently required.

Accordingly, in the present study, the specific aims are as follows:

- To exploit the potential of the inhibition of Poly(ADP-ribose) polymerases (PARP) as a strategy to improve the efficacy of the oncolytic adenovirus *dl*922-947 against ATC cells
- To investigate in detail study the cell death pathways activated by *dl*922-947, in order to identify novel therapeutic targets, which can be assessed for their "druggability".

In addition, I have been involved in several projects aimed to identify new combinatorial therapy (*dl*922-947 plus rational chosen drug) for the treatment of aggressive tumors such as Anaplastic Thyroid Carcinoma and Glioblastoma Multiforme. The resulting publications are attached at the end of the dissertation.

3. MATERIALS AND METHODS

CELLS, ADENOVIRUSES AND DRUGS

Human thyroid anaplastic carcinoma cell lines BHT101-5 and FRO have been described and authenticated as shown elsewhere (Schweppe et al. 2008). *dl*922-947 and AdGFP viral stocks were expanded in the human embryonic kidney cell line HEK-293, purified and stored as previously reported (Libertini et al. 2007). Viral stocks were expanded, purified, stored and quantified as previously reported (Botta et al. 2012). Both cell lines were cultured in DMEM medium, supplemented with 10% fetal bovine serum and 1% penicillin/streptomycin and incubated in standard culture conditions (95% air and 5% CO_2 at 37 °C). All cell culture reagents were purchased from Invitrogen Gibco, unless otherwise stated.

For *in vitro* experiments AZD2281 (Selleck) was dissolved in DMSO to a final concentration of 10 mM and stored at -20°C. For *in vivo* study AZD2281 was solubilized in DMSO and diluted to 5 mg/mL with PBS containing 10% 2-hydroxy-propyl-betacyclodextrin (Sigma).

zVAD-fmk (Tocris bioscence) was dissolved in DMSO to a final concentration of 10 mM and stored at -20°C.

BrdU (Sigma) was dissolved in PBS to a final concentration of 10 mM and stored at -20°C.

Digitonin (Sigma) was dissolved in absolute ethanol to a final concentration of 2 mg/mL and stored at -20°C.

FLUORESCENCE-ACTIVATED CELL SORTING ANALYSIS

For all FACS experiments FRO and BHT101-5 cells were seeded in 100 mm cell culture dish at densities of $4x10^5$ cells/dish and treated as indicated.

BrdU staining: FRO and BHT101-5 cells were infected with *dl*922-947 for 24h. Thirty minutes before harvesting cells were labeled with 10 μM BrdU (Sigma). Cells were fixed over-night in ice-cold 70% ethanol (in PBS) at -20°C. Then cells were washed once with PBS and incubated with 2N HCl to denature DNA for 15 minutes at room temperature. Cells were washed with PBT (0.5% BSA, 0.1% Tween20 in PBS) and resuspended in PBT containing anti-BrdU antibody (Dako, M0744, 1:40). After 30 minutes cells were washed twice with PBT, and then resuspended in PBT containing Alexa488 anti-mouse (Invitrogen #A11001, 1:100) at dark for 30'. Cells were washed twice with PBS, resuspended in PI 0.015 M in PBS for 20' and analyzed for the emission in FL1 and FL3 channels. To remove artifacts—doublets and aggregates—

from the analysis, an electronic doublet discrimination was performed using the area and width of the fluorescence (FL3) pulse.

γH2AX/PI staining*:* FRO and BHT101-5 cells were detached and fixed over-night in ice-cold 70% ethanol at -20°C. Pellet was washed with PBT (0.5% BSA, 0.1% Tween20 in PBS) and resuspended in PBT containing anti-γH2AX antibody (Millipore #05-636, 1:100). After 1 h incubation at room temperature, samples were washed in PBT and then resuspended in PBT containing Alexa488 anti-mouse (Invitrogen #A11001, 1:100) at dark. After further 30 minutes, cells were washed with PBT, resuspended in PI 0.015 M in PBS for 20' and analyzed for the emission in FL1 and FL3 channels. To remove artifacts—doublets and aggregates—from the analysis, an electronic doublet discrimination was performed using the area and width of the fluorescence (FL3) pulse.

AdGFP infection*:* FRO and BHT101-5 cells were infected with AdGFP (25 pfu/cell) and harvested 48 hours later. Pellet was resuspended in PBS and emission in the FL1 channel analyzed.

Cell cycle: attached and detached FRO and BHT101-5 cells were collected and fixed over-night in ice-cold 70% ethanol at -20°C. Washed pellets were resuspended in PBS containing RNaseA 0.4 U (Roche) and propidium iodide 0.015 M in PBS (Sigma), incubated for 20' at room temperature, and analyzed for emission in the FL3 channel. To remove artifacts—doublets and aggregates—from the analysis, an electronic doublet discrimination was performed using the area and width of the fluorescence (FL3) pulse.

Annexin V/PI staining*:* attached and detached FRO and BHT101-5 cells were collected and washed with Annexin V binding buffer (Biolegend). Pellet was resuspended in Annexin V binding buffer containing FITC-conjugated Annexin V (Biolegend #640906, 1:40). After 15' incubation at room temperature, 250µl of propidium iodide solution 0.0015 M in PBS was added to each sample just before analysis.

Cytochrome C release from mitochondria*:* attached and detached FRO and BHT101-5 cells were harvested and treated with digitonin (50µg/mL in PBS containing 150mM KCl and 1 mM EDTA) for 10' on ice. The selective permeabilization of the plasma membrane with digitonin allows virtually all of the cytoplasmic cytochrome C to diffuse out of the cell. Permeabilized cells were fixed in paraformaldehyde (4% in PBS) for 20 minutes on ice, washed three times in PBS and incubated in blocking buffer (0.5% saponin, 1% BSA in

PBS) for 20’ at room temperature. Cells were then incubated for 2h at room temperature with anti-Cytochrome C antibody (BD Pharmigen, #556432, 1:200) in blocking buffer, washed three times and incubated for 30’ at room temperature with Alexa488 anti-mouse (Invitrogen #A11001, 1:100) in blocking buffer at dark. Stained cells were washed twice with PBS, resuspended in PBS and analyzed by flow cytometry detecting Alexa488 fluorescencein FL-1 channel.

All samples were acquired by a BD LSRFortessa (BD Biosciences, San Jose, CA, USA) and analyzed using BD FACSDiva Software.

PROTEIN EXTRACTION AND WESTERN BLOT ANALYSIS

After the indicated treatments, attached and detached cells were harvested and lysates prepared as already described (Botta et al. 2012). 50 μg of lysate proteins were probed with the following antibodies: caspase 3 (Abcam #Ab13585, 1:500), p-ATM s1981 (Cell Signaling, #4526, 1:1000), p-chk1 s345 (Cell Signaling, #2348, 1:1000), chk1 (Cell Signaling, #2345, 1:1000), MRE11 (SantaCruz, #sc-5859, 1:1000), NBS1 (Novus Biologicals, NB100-143, 1:1000), p-H2AX s139 (Millipore, #05-636, 1:1000), H2AX (Cell Signaling, #2095, 1:1000), PAR (Trevigen, #4336-BPC-100, 1:1000), PARP (Cell Signaling, #9542, 1:1000), ROCK1 (BD Biosciences, #611137, 1:1000), p-MLC2 thr18/ser19 (Cell Signaling, #3674, 1:1000), α-tubulin (SIGMA #T9026, 1:5000).

VIRAL REPLICATION

FRO and BHT101-5 cells were infected with *dl*922-947, media collected 48 hpi (hours post infection) and viral DNA extracted using the High pure viral nucleic acid kit (Roche Diagnostics). Specific primers for the viral hexon gene (from 99 to 242 bp) were used to measure viral replication by Real-Time PCR: 5’-GCC ACC GAG ACG TAC TTC AGC CTG-3’ (upstream primer) and 5’TTG TAC GAG TAC GCG GTA TCC TCC GCG GTC-3’ (downstream primer). A standard curve was constructed by assaying serial dilutions of *dl*922-947.

IMMUNOFLUORESCENCE STAINING

To analyze p-chk1 (s345) and p-H2AX (s139) localization FRO cells were seeded on cover slips in 24-well dishes and infected with 5 pfu/cell of *dl*922-947. After 24h cells were fixed with 4% paraformaldehyde for 15 min at room temperature, washed and permeabilized with 0.1% Triton X-100 in PBS. Cells

were then blocked with bovine serum albumin (BSA) blotting buffer (0.5% BSA in PBS) for 30 min and then incubated with BSA blotting buffer plus primary antibody overnight at 4°C (p-H2AX s139, Millipore #05-636, 1:250; p-chk1 s345, Abcam Ab47318, 1:200). After washing three times with 0.1% Triton X-100 in PBS, cells were incubated with Alexa-488 anti-mouse and Alexa-594 anti-rabbit (Invitrogen #A11001 and #A11012 respectively, 1:100). Fixed and stained cells were mounted using Vectashield-mounting medium with DAPI (Vector Laboratories, H-1200). Images were acquired with a Nikon A1R confocal microscope (Nikon), using a 60x oil objective and processed with NIS element software (Nikon).

To analyze nuclear morphology of infected cells, FRO cells were grown on cover slips in 24-well dishes and infected with 5 pfu/cell of *dl*922-947 for 24h or incubated over night with 0.5 μM staurosporine (as positive control for apoptosis). After treatment cells were fixed with 4% paraformaldehyde for 15 minutes at room temperature and then mounted using Vectashield-mounting medium with DAPI (Vector Laboratories, H-1200). Images were acquired with a Leica DMLB microscope and processed with Adobe Photoshope CS software (Adobe Systems Incorporated).

VIABILITY ASSAY AND ANALYSIS OF THE COMBINED DRUG EFFECT

FRO and BHT101-5 cells were seeded in 96-well plates at densities of 500 cells/well and allowed to attach for 24h. Cells were exposed to graded concentrations (six replicates) of AZD2281 or *dl*922-947 either alone or in combination for 6 days. At the end of the treatment, cells were fixed with 50% TCA and stained with 0.4% sulforhodamine B in 1% acetic acid as already described (Vichai and Kirtikara 2006, Libertini et al. 2008). The percentages of surviving cells after treatment were calculated by assuming that the number of surviving untreated cells is 100%. The concentration of each agent or of the combined treatment required to kill 50% of cells (median lethal dose, LD_{50}) was determined by a dose-response curve using GraphPad prism (GraphPad Software).

Drug synergy was determined by the isobologram and combination-index methods as previously described (Tallarida 2001). Data obtained from the viability assays were used to perform these analyses. The isobologram method is a graphical representation of the pharmacologic interaction and is formed by selecting a desired fractional cell kill (LD_{50}) and plotting the individual drug doses required to generate that LD_{50} on their respective x- and y-axes. A straight line is then drawn to connect the points. The observed dose

combination of the two agents that achieved that particular LD_{50} is then plotted on the isobologram. Combination data points that fall on the line represent an additive drug-drug interaction, whereas data points that fall below or above the line represent synergism or antagonism, respectively. The combination-index (CI) method is a mathematical and quantitative representation of a two-drug pharmacologic interaction. Using data from the growth inhibitory experiments and computerized software, CI values were generated. A CI of 1 indicates an additive effect between two agents, whereas a CI<1 or CI>1 indicates synergism or antagonism, respectively.

GROWTH CURVE

FRO and BHT101-5 cells were seeded in 12-well culture plates at density of $1x10^4$ cells/well and allowed to attach for 24h. Cells were then treated with zVAD-fmk and *dl*922–947 alone or in combination as indicated. After 24h, 48h and 72h attached cells were harvested and a cell count performed using a Bürker chamber.

TUMORIGENICITY ASSAY

FRO cells in exponential phase were prepared at a concentration of $4x10^7$ cells/ml in DMEM medium. CD-I athymic mice were obtained from Charles River and all experiments were carried out with 6-week-old females. To initiate tumor xenografts, 0.2 ml of cell suspension was injected into the right flank of 60 animals. Tumor diameters were measured with calipers and tumor volume (V) was calculated by the formula for a rotational ellipsoid: $V=A \cdot B^2/2$ (A, axial diameter; B, rotational diameter). Mice weights were monitored daily.

Twenty days post-injection mice with similar tumor size were randomized into four groups (15 animals/group): untreated, treated with AZD2281, treated with *dl*922–947, or treated with both. AZD2281 (50 mg/kg) was administered intraperitoneally three consecutive day a week. A low viral dose ($2x10^6$ pfu/cell) was administered two times a week (the day before and the day after AZD2281 administration) by intratumoral injection to avoid any first-pass effect (Libertini et al. 2007, Libertini et al. 2008, Libertini et al. 2011). AZD2281 vehicle was administered to the control groups. Statistical analysis were done by ANOVA (analysis of variance) and the Bonferroni post hoc test, using commercial software (Prism 4; GraphPad Software). Differences in the rate of tumor growth in mice were assessed for each time point of the observation period.

Mice were maintained at the Dipartimento di Biologia e Patologia Cellulare e Molecolare Animal Facility. All animal experiments were conducted in

accordance with accepted standards of animal care and in accordance with the Italian regulations for the welfare of animals used in studies of experimental neoplasia. Study was approved by our institutional committee on animal care.

4. RESULTS

dl922-947 increases the percentage of cells in S-phase

To investigate the effect of *dl*922-947 on S-phase in ATC cells, I evaluated BrdU incorporation in two different ATC cell lines, FRO and BHT101-5, 24 hours after infection (hpi). BrdU is an analogue of thymidine that is incorporated into the newly synthesized DNA of replicating cells (during the S phase of the cell cycle).

Fig. 11

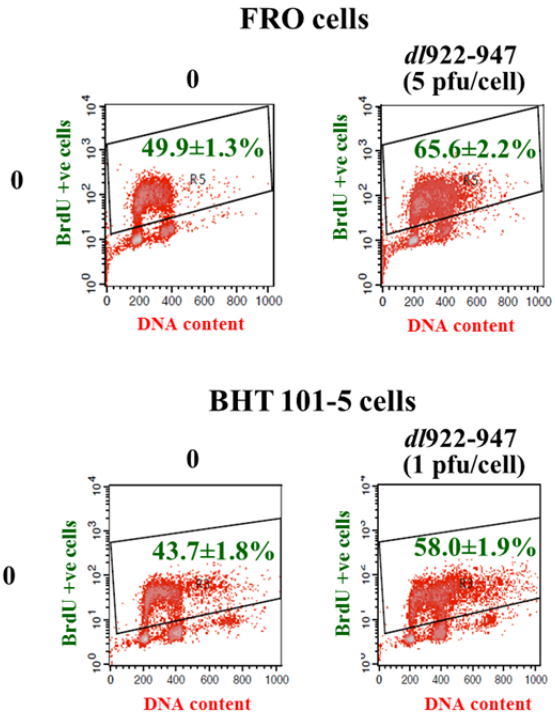

Figure 11. Effects of *dl*922-947 infection on host cell S-phase entry.
FRO (upper panel) and BHT 101-5 (lower panel) were infected with *dl*922-947 (5 or 1 pfu/cell, respectively) for 24h. Then, cells were pulse labelled with BrdU for 30 minutes. Once harvested, cells were stained with a primary antibody anti-BrdU, followed by incubation with a secondary antibody (anti-mouse-FITC conjugate) for determination of DNA synthesis, and with propidium iodide (PI) for determination of total DNA content. The dot plot represents BrdU incorporation (y-axis) vs DNA content, as determined by PI staining (x-axis). DNA synthesis (S-phase) was determined by quantifying cells positive for BrdU staining in the dot plots. Green numbers represent the percentage of BrdU-positive cells and the standard deviation of three independent experiments.

As shown in figure 11, *dl*922-947 infection increased the percentage of cells in S-phase from ~50% to ~66% in FRO cells, and from ~44% to 58% in BHT101-5 cells.

dl922-947 induces the accumulation of DNA damage

Induction of DNA damage has been previously reported in response to adenovirus infection (Prakash et al. 2012). Therefore, I tested the effect of the adenoviral mutant *dl*922-947 on DNA damage. To this aim, I performed a Fluorescence-Activated Cell Sorting (FACS) analysis to assess the positivity of infected cells for γH2AX (namely, histone H2AX phosphorylated on serine 139), which marks the spots where foci containing DNA repair enzymes will localize.

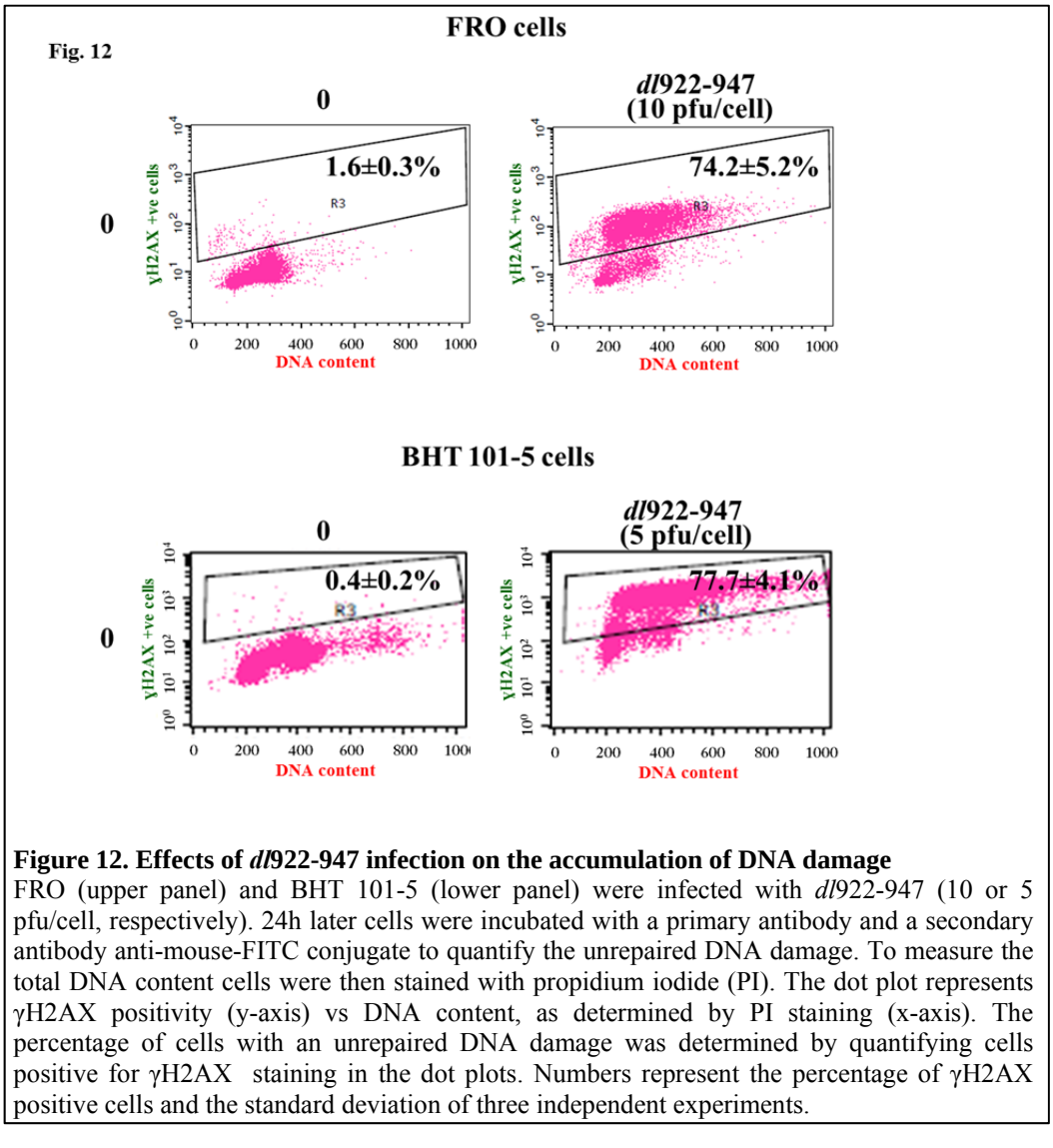

Figure 12. Effects of *dl*922-947 infection on the accumulation of DNA damage
FRO (upper panel) and BHT 101-5 (lower panel) were infected with *dl*922-947 (10 or 5 pfu/cell, respectively). 24h later cells were incubated with a primary antibody and a secondary antibody anti-mouse-FITC conjugate to quantify the unrepaired DNA damage. To measure the total DNA content cells were then stained with propidium iodide (PI). The dot plot represents γH2AX positivity (y-axis) vs DNA content, as determined by PI staining (x-axis). The percentage of cells with an unrepaired DNA damage was determined by quantifying cells positive for γH2AX staining in the dot plots. Numbers represent the percentage of γH2AX positive cells and the standard deviation of three independent experiments.

A robust increase in the percentage of γH2AX positive cells was found in both FRO and BHT101-5 cells 24h after *dl*922-947 infection [Figure 12], suggestive of accumulation of an unrepaired DNA damage.

dl922-947 impairs Double Strand Breaks (DSBs) repair pathway

γH2AX is the main marker of double strand breaks (DSB) (Rogakou et al. 1998). As *dl*922-947 replication lead to H2AX phosphorylation, I decided to deepen the analysis of DSB repair pathway, by monitoring the activation of some of its crucial mediators. To this aim, I assessed ATM and Chk1 phosphorylation on serine 1981 and 345 respectively, indicative of their activation, and I analyzed the levels of NBS1 and Mre11, in FRO cells, at different time point from *dl*922-947 infection (1, 3, 6 and 24h) .

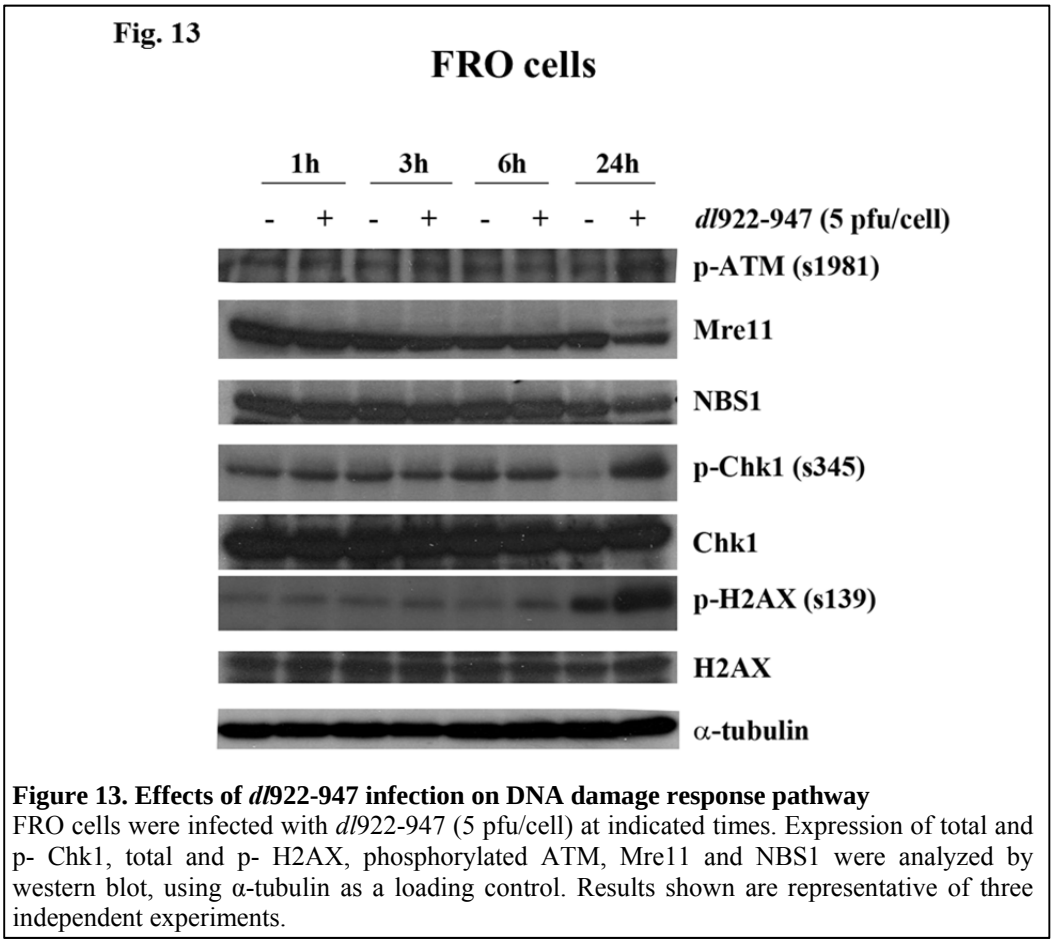

Figure 13. Effects of *dl*922-947 infection on DNA damage response pathway
FRO cells were infected with *dl*922-947 (5 pfu/cell) at indicated times. Expression of total and p- Chk1, total and p- H2AX, phosphorylated ATM, Mre11 and NBS1 were analyzed by western blot, using α-tubulin as a loading control. Results shown are representative of three independent experiments.

As shown in figure 13, phosphorylation of both ATM and Chk1 is clearly induced 24h after the infection, suggestive of activation of DSB repair pathway. However, this effect is paralleled by the degradation of the proteins of the MRN complex NBS1 and Mre11, suggesting that *dl*922-947 may hamper the execution of DSB repair.

To further confirm γH2AX accumulation and Chk1 activation, I performed an immunofluorescence experiment in FRO cells infected with *dl*922-947 for

24h [Figure 14].

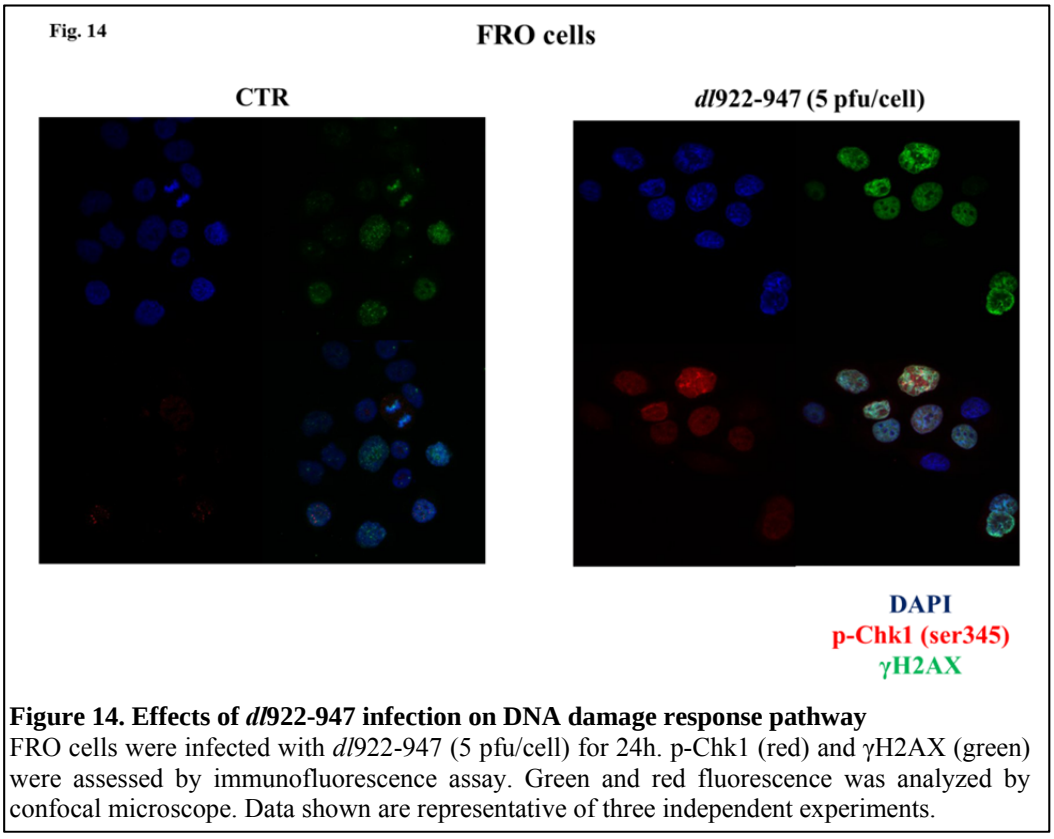

Figure 14. Effects of *dl*922-947 infection on DNA damage response pathway
FRO cells were infected with *dl*922-947 (5 pfu/cell) for 24h. p-Chk1 (red) and γH2AX (green) were assessed by immunofluorescence assay. Green and red fluorescence was analyzed by confocal microscope. Data shown are representative of three independent experiments.

dl922-947 induces PARP activation

It has been reported that an unscheduled DNA synthesis -such as the one induced by viral infection- can cause the accumulation of replication-associated DNA lesions, namely single strand break (SSB) (Connell et al. 2011). SSBs are repaired by the SSB repair machinery, which requires PARP (Poly-ADP Ribose Polymerase) activity.

During DNA damage response, PARP is mainly responsible for the addition of PAR (poly-ADP ribose) residues on the target proteins, including histones, DNA repair proteins, transcription factors and chromatin modulators, to facilitate the recognition and their access to the site of the damage.

To investigate the presence of replication-associated DNA lesions, upon *dl*922-947 infection, I evaluated PARP activation in infected cells. To this aim, the levels of PARylated proteins in FRO and BHT101-5 cells were analyzed by western blot 24h after *dl*922-947 infection [Figure 15].

Fig. 15

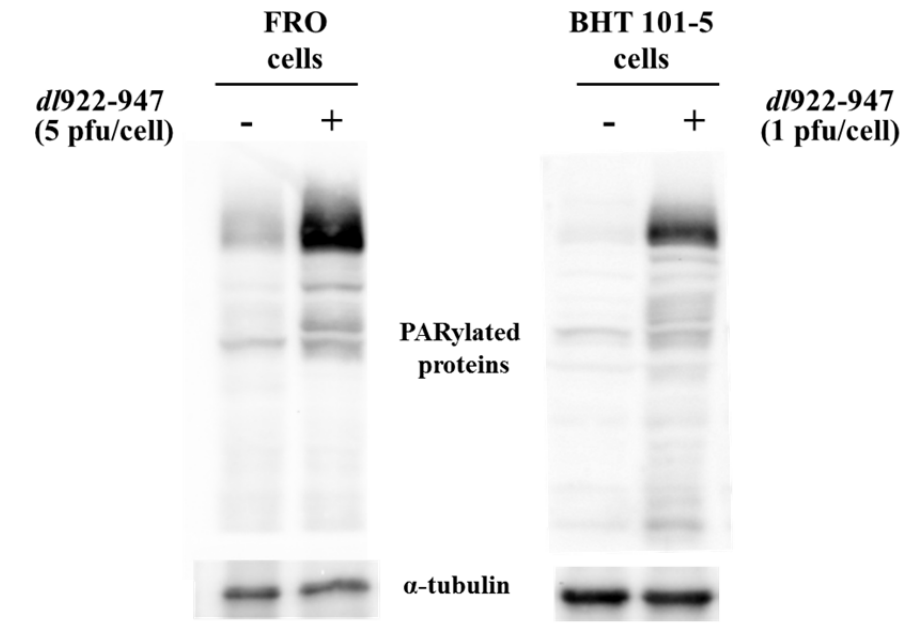

Figure 15. Effects of *dl*922-947 infection on PARP activity
FRO and BHT101-5 cells were infected with *dl*922-947 for 24h at indicated pfu/cell. Expression of PARylated proteins was analyzed by Western blot using an anti-PAR antibody. α-tubulin was used as a loading control. Results shown are representative of three independent experiments.

Interestingly, a robust increase of PARylated proteins levels was observed in infected cells compared to uninfected. These data indicate that the virus strongly induces PARP activation, thus leading to the activation of SSB repair machinery.

PARP inhibition increases the percentage of γH2AX-positive cells induced by dl922-947

To inhibit PARP activity, I used AZD2281, a competitive inhibitor of NAD^+ in the PARP catalytic site (Peralta-Leal et al. 2009). I confirmed the effective inhibition of PARP activity by AZD2281, at concentrations used in the literature (Senra et al. 2011, Hirai et al. 2012). To this aim, I treated ATC cells with both single or combined treatment AZD2281/*dl*922-947, and evaluated PARylated protein levels by western blot 24h after infection.

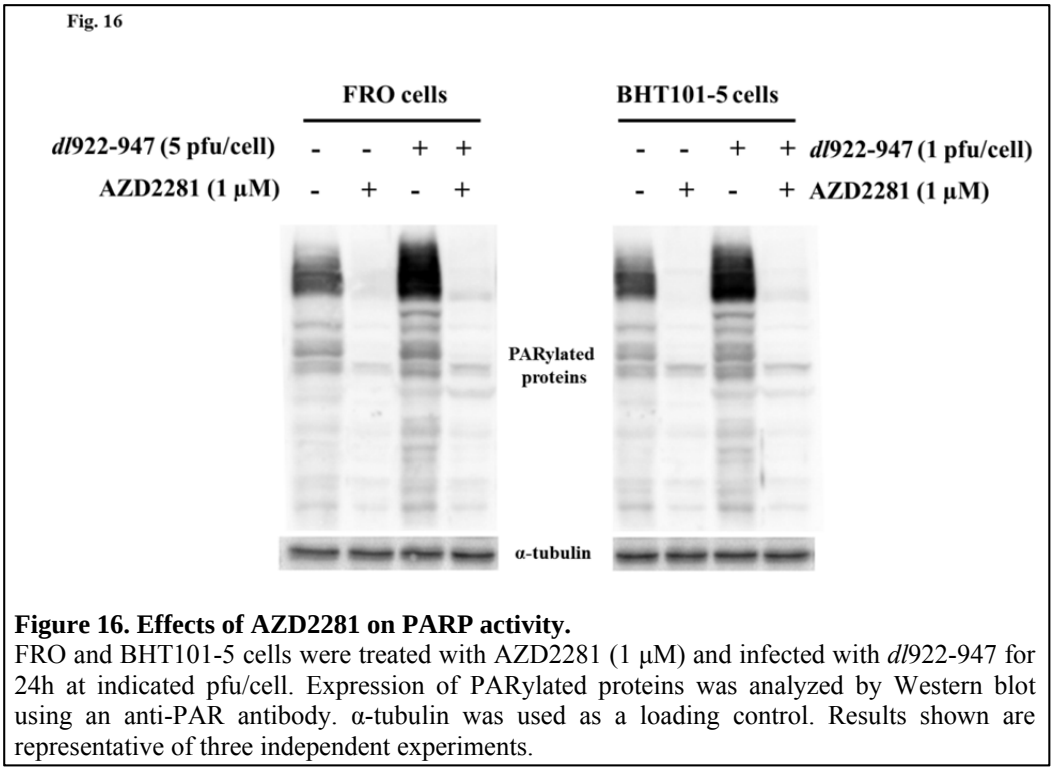

Figure 16. Effects of AZD2281 on PARP activity.
FRO and BHT101-5 cells were treated with AZD2281 (1 µM) and infected with *dl*922-947 for 24h at indicated pfu/cell. Expression of PARylated proteins was analyzed by Western blot using an anti-PAR antibody. α-tubulin was used as a loading control. Results shown are representative of three independent experiments.

As shown in figure 16, in both FRO and BHT101-5 cells, AZD2281 treatment at 1 µM is sufficient to completely revert the increase in PARP activity mediated by *dl*922-947 infection.

Given these results, I hypothesize that the combined inhibition of SSB repair, using the PARP inhibitor AZD2281, and the DSB repair, mediated by *dl*922-947, could induce the accumulation of an unrepaired DNA damage, leading to an increase in cell death. To test this hypothesis, I analyzed γH2AX levels by FACS analysis in cells undergoing the combined treatment AZD2281/*dl*922-947.

Fig. 17

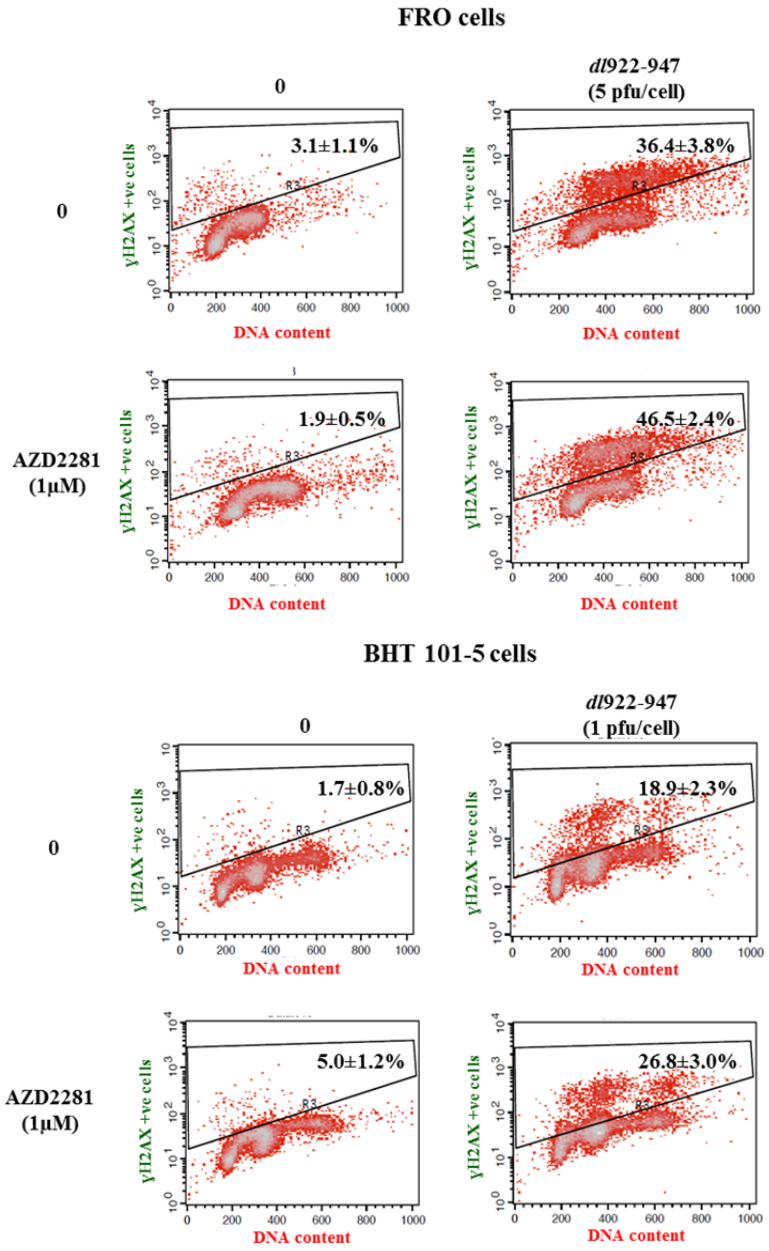

Figure 17. Effects of the combined treatment *dl*922-947/AZD2281 on the accumulation of a DNA damage

FRO (upper panel) and BHT 101-5 (lower panel) were infected with *dl*922-947 (5 or 1 pfu/cell, respectively) in the presence or not of AZD2281. After 24h cells were stained with a primary anti-γH2AX antibody and a secondary anti-mouse-FITC conjugate antibody for determination of unrepaired DNA damage. To measure the total DNA content, cells were also stained with propidium iodide (PI). The dot plot represents γH2AX positivity (y-axis) vs DNA content, as determined by PI staining (x-axis). The positivity for γH2AX staining is indicative of the percentage of cells with an unrepaired DNA damage. Numbers represent the percentage of γH2AX positive cells and the standard deviation of three independent experiments.

An increase in the percentage of γH2AX-positive cells is observed in cells infected with *dl*922-947, but not in those treated with AZD2281 [Figure 17]. Importantly, the combined treatment led to a much greater increase in the percentage of γH2AX-positive cells than in the single *dl*922-947 treatment, (36.4% vs 46.5% and 18.9% vs 26.8% in FRO and BHT101-5 cells, respectively) [Figure 17].

PARP inhibition has a synergistic effect on dl922-947 cytotoxicity

To explore the effect of the PARP inhibitor AZD2281 on the oncolytic activity of the mutant adenovirus *dl*922-947, FRO and BHT101-5 were infected and treated with AZD2281 at the same time.

Fig. 18

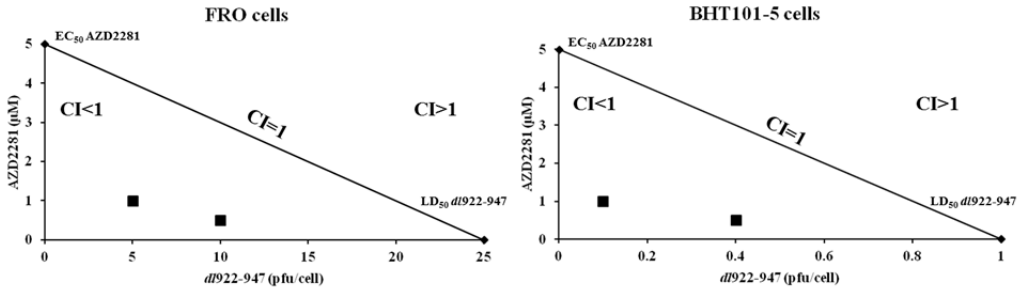

Ratio [(pfu/cell)/(nM)]	LD_{50} dl922-947 (pfu/cell)	EC_{50} AZD2281 (nM)	CI
AZD2281 alone	0	5000	
*dl*922-947 alone	10	0	
1:100	5	500	0.6
1:1000	1	1000	0.3

Ratio [(pfu/cell)/(nM)]	LD_{50} *dl*922-947 (pfu/cell)	EC_{50} AZD2281 (nM)	CI
AZD2281 alone	0	5000	
*dl*922-947 alone	1	0	
1:1250	0.4	500	0.5
1:10000	0.1	1000	0.3

Figure 18. Effects of AZD2281 on *dl*922-947 cytotoxicity
FRO and BHT101-5 cells were treated with two combination of *dl*922-947 and AZD2281, and cell viability was determined 7 days post infection by sulforhodamine B assay. Dose–response curve and LD_{50} or EC_{50} values were generated and used to construct isobolograms and calculate combination indexes (CI) for each ratio. The shown line connects the LD_{50} values of the virus and EC_{50} of the drug, both as a single agent. A ratio producing a CI<1 is considered synergistic, CI=1 additive, CI>1 antagonistic. A synergistic effect was observed in all used combination (CI<1).

Combination index, calculated by isobologram analysis, showed a potent, statistically significant synergy of cell killing in both cell lines, at all combinations, after one week treatment [Figure 18].

dl922-947 viral replication, but not viral entry, is affected by PARP inhibition

To verify whether the enhanced oncolytic activity in presence of AZD2281

was due to an increased viral entry into target cells, I evaluated the infection efficiency of ATC cells in presence or not of AZD2281. FRO and BHT101-5 were treated with 1 μM of AZD2281 and infected with a non-replicating reporter adenovirus transducing GFP (AdGFP, 25 pfu/cell). After 48h from infection, GFP emission, indicative of viral entry, was evaluated by cytofluorimetric analysis.

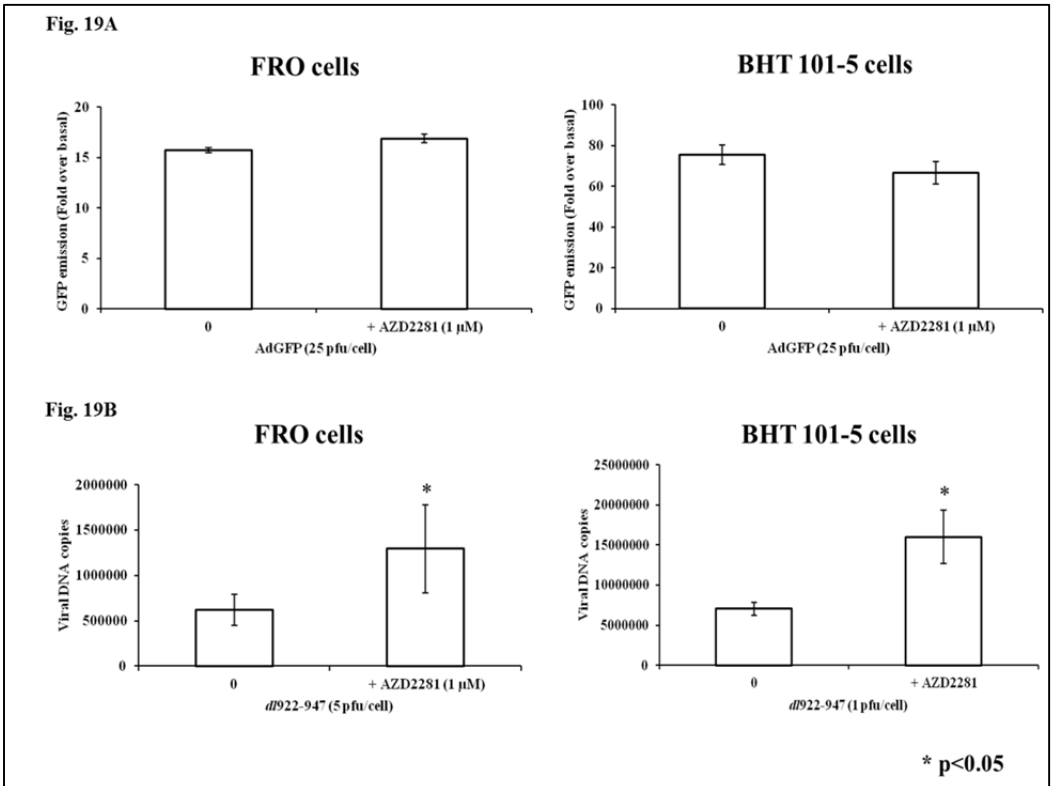

Figure 19. Effects of AZD2281 on *dl*922-947 viral entry and viral replication
A) FRO and BHTH101-5 were treated with AZD2281 (1μM) and infected with 25 pfu/cell of AdGFP. The histograms show the fold change GFP emission compared to uninfected cells. GFP emission in unchanged in presence of AZD2281. The data shown represent the mean of three different experiments.
B) Real Time PCR genome equivalent analysis. FRO and BHTH101-5 cells were infected with *dl*922-947 (5 or 1 pfu/cell, respectively) in presence or not of AZD2281 (1μM).
Significant (*$p<0.05$) differences in viral replication levels were observed in AZD2281 treated cells compared to untreated. The data represent the mean of three different experiments.

Treatment with AZD2281 did not affect viral entry, as indicated by an unchanged average of green emission of individual infected cells, in both cell lines [Figure 19A].

Next, the expression of viral hexon gene was quantified by Real-Time PCR assay to evaluate viral replication. FRO and BHT101-5 cells were infected with *dl*922-947 (5 and 1 pfu/cell for FRO and BHT101-5 cells, respectively), and

treated or not with AZD2281 (1 μM). 48h later, viral genome copies were evaluated by Real Time PCR. This analysis revealed that treatment with AZD2281 induced a significant (* $p<0.05$) increase of viral replication in both cell lines [Figure 19B].

PARP inhibition increases the percentage of cells in sub-G1 phase and the percentage of polyploid cells induced by dl922-947

It has been reported that forcing cells with damaged DNA into mitosis causes severe chromosome segregation defects aborting cytokinesis; therefore cells enter S phase and become polyploids (Chow and Poon 2010). Since I demonstrated that the combined treatment AZD2281/*dl*922-947 induces the accumulation of DNA damage, I evaluated cell cycle profile by FACS analysis. FRO and BHT101-5 cell were treated with 1 μM of AZD2281 and infected with *dl*922-947 (5 or 1 pfu/cell, respectively). 72h later cells were stained with Propidium Iodide (PI) and cell cycle profile analysed by FACS analysis.

Fig. 20

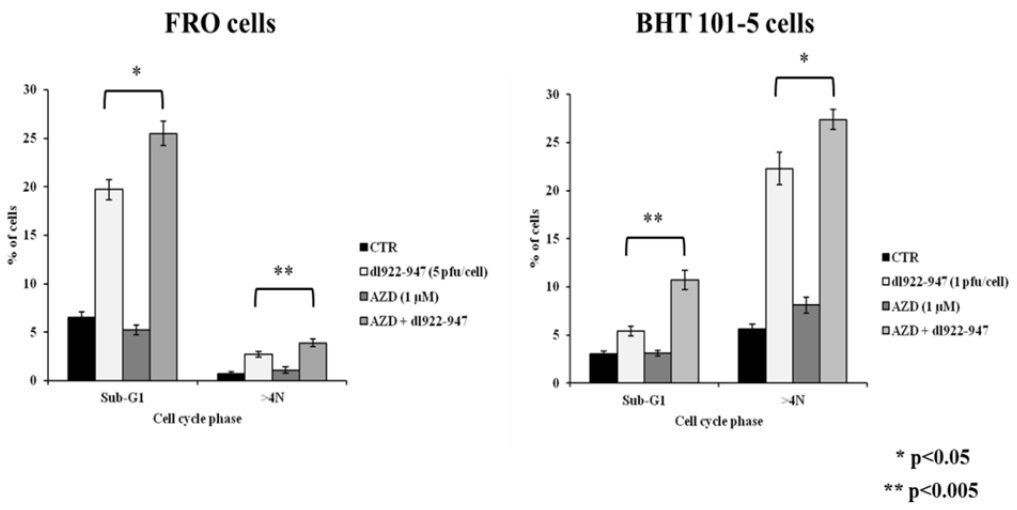

Figure 20. Effects of AZD2281 on *dl*922-947 viral entry and replication
FRO (left panel) and BHT 101-5 (right panel) were infected with *dl*922-947 (5 or 1 pfu/cell respectively) for 72h in the presence or not of AZD2281. Sub-G1 and polyploidy are represented by histograms. The percentage of cells in sub-G1 phase and polyploid cells was significantly (*$p<0.05$) or highly significantly (**$p<0.005$) increased by the combined treatment compared to the single infection treatment.
The data are the mean of three different experiments.

A highly significant accumulation of polyploidy cells was observed in FRO cells undergoing the combined treatment compared to those only receiving the infection [Figure 20]. In addition, this effect is paralleled by a significant

increase in the percentage of cells in sub-G1 phase [Figure 20]. Although similar results were obtained using BHT101-5 cells [Figure 20] these cells displayed a higher percentage of polyploidy cells and a lower percentage of cells in sub-G1 phase than FRO cells. In accordance with the hypothesis that polyploidy can result from mitotic defects leading to cell death, the differences between FRO and BHT101-5 cells could be explained by a different timing in the escape from mitotic block and, subsequently, in cell death activation.

PARP inhibition increases apoptosis-like cell death induced by dl922-947

Accumulation of cells in sub-G1 phase is indicative of DNA fragmentation and cell death, either by necrosis or apoptosis. I decided to investigate both these cell death modalities in infected ATC cells in presence or not of AZD2281. To discriminate between necrosis and apoptosis, unfixed cells were stained with propidium iodide (PI) and Annexin V. PI can penetrate only in non-vital cells, whereas Annexin V binds to living cells with exposed phospholipid phosphatidylserine. The exposure of phosphatidylserine is due to the loss of membrane asymmetry and is considered to be an early marker of apoptosis (Fadok et al. 2001). Necrotic cells are positive for PI, whereas apoptotic cells are positive for Annexin V or double positive for Annexin V and PI.

At 72 hpi, an increase in annexin V staining, indicative of apoptosis, was observed in the combined treatment with respect to single treatments, in both cell lines [Figure 21]. To further investigate the involvement of apoptosis, we also analyzed levels of pro- and cleaved caspase 3 by western blot in FRO and BHT101-5 cells treated as described above. In parallel, I also evaluated the levels of PARP, both full length and cleaved protein.

Fig. 21

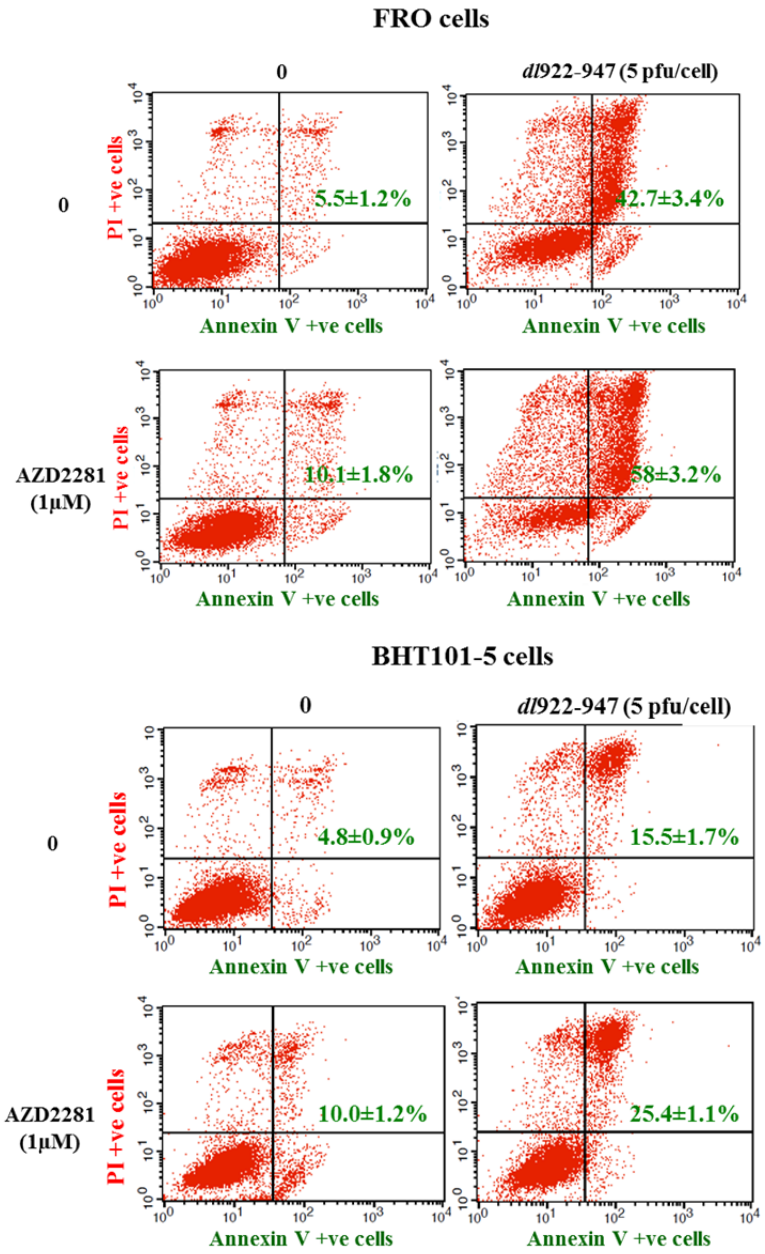

Figure 21. Effects of the combined treatment *dl*922-947/AZD2281 on phosphatydilserine exposition on plasma membrane

FRO (upper panel) and BHT 101-5 (lower panel) were infected with *dl*922-947 at indicated pfu/cell for 72h in the presence or not of AZD2281. Annexin V binds to living cells with exposed phospholipid phosphatidylserine. The exposure of phosphatidylserine is due to the loss of membrane asymmetry and is considered to be an early marker of apoptosis. Apoptotic cells are positive for Annexin V or double positive for Annexin V and PI (Right quadrants). The combined treatment increased the percentage of apoptotic cells with respect to single treatments. Green numbers represent the percentage of annexin V positive cells and the standard deviation of three independent experiments.

Fig. 22

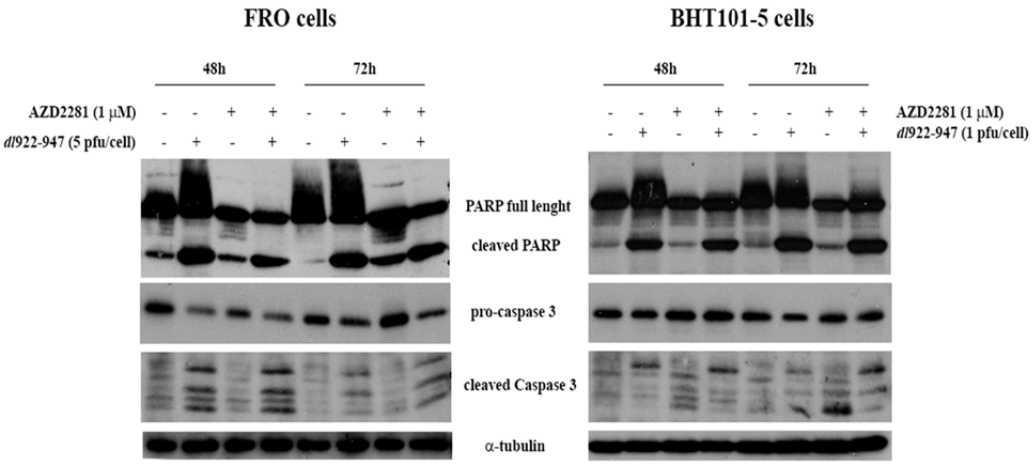

Figure 22. Effects of the combined treatment *dl*922-947/AZD2281 on cell death pathway
FRO and BHT101-5 cells were infected with *dl*922-947 at indicated pfu/cell in the presence or not of AZD2281 (1μM). After 48 and 72h, PARP and caspase 3 cleavage was analyzed by Western blot, using α-tubulin as a loading control.

A decrease of pro-caspase 3, paralleled by a concomitant slight increase of the cleaved form, strongly suggested the activation of caspase 3 in cells undergoing the combined treatment compared to single treatments, in both FRO and BHT101-5 cell lines [Figure 22].

Next, I investigated the presence of another well-known marker of apoptosis, mitochondrial permeabilization (Martinou and Green 2001, Waterhouse et al. 2002). Selective permeabilization of the mitochondrial outer membrane is an integral event in apoptosis induced by several stimuli. As a result several pro-apoptotic proteins, including cytochrome C, are released from the mitochondrial intermembrane space to the cytoplasm. To evaluate this phenomena, the percentage of cells releasing cytochrome C from mitochondria was quantified by FACS analysis in cells undergoing the combined treatment.

As shown in figure 23, the single treatment with *dl*922-947, but not with AZD2281, increased the percentage of cytochrome C negative cells 72hpi, in both FRO and BHT101-5 cells, indicating the presence of mitochondrial permeabilization upon infection. This viral effect is further increased by the combination with AZD2281 (16.9% vs 24.7 in FRO cells; 24.4 vs 53.8 in BHT101-5).

Overall, the presence of mitochondrial permeabilization, together with the cleavage of caspase-3 and the annexin V positivity, clearly indicate a more active apoptotic pathway in cells undergoing the combined treatment compared with those only infected with *dl*922-947.

Fig. 23

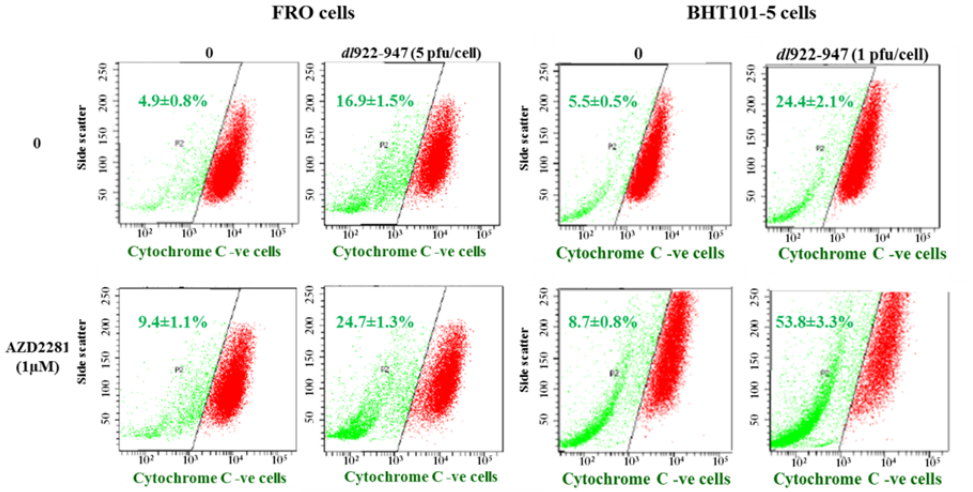

Figure 23. Effects of the combined treatment *dl*922-947/AZD2281 on cytochrome C release from mitochondria

FRO and BHT101-5 cells were infected with *dl*922-947 at indicated pfu/cell in the presence or not of AZD2281 (1μM). After 72h citochrome C release from mitochondria was assessed by FACS analysis. Cells with intact mitochondria result positive to the staining for cytochrome C, while a lower fluorescence is indicative of cells with higher release of cytochrome C from mitochondria (cytochrome C negative cells). The combined treatment increases the percentage of cytochrome C negative cells compared to only infected cells. Green numbers represent the percentage of cytochrome C negative cells and the standard deviation of three independent experiments.

PARP inhibitor AZD2281 increases dl922-947 oncolytic activity in vivo

To evaluate the therapeutic potential of synergism between *dl*922-947 and the PARP inhibitor AZD2281, I analyzed the effects of the combined treatment on ATC tumor xenografts.

Athymic mice were inoculated subcutaneously with FRO cells. Mice were then randomized into four groups (15 animals/group) with similar average tumor size (> 100mm^3). In accordance to previous reports (Kortmann et al. 2011, Senra et al. 2011), animals were injected *i.p.* with AZD2281 at the dose of 50mg/kg three consecutive day/week. *dl*922-947 (2x10^6 pfu) was administered two times per week (the day before and the day after AZD2281 treatment) by intratumoral injection. The control group was injected with AZD2281 vehicle. *dl*922-947 was administered by intratumoral injection to avoid first pass effect, and the low viral dose (2x10^6 pfu) was chosen to enable a better visualization of the effects of the combined treatment versus *dl*922-947 infection alone.

Tumor diameters were measured every third day to monitor the growth.

Fig. 24

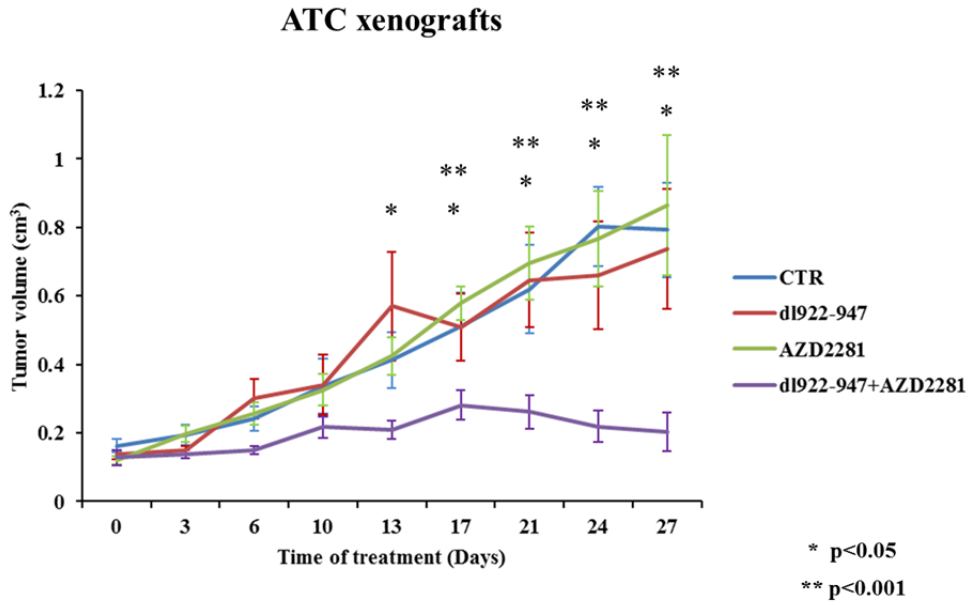

Figure 24. Effects of the combined treatment *dl*922-947/AZD2281 on tumor growth
Animals were injected *i.p.* with AZD2281 three consecutive days per week; *dl*922-947 was administered two times per week (the day before and the day after AZD2281 treatment) by intratumoral injection. The difference between animals receiving the combined treatment and single treatment groups and control group becomes statistically significant (**p<0.05*) from day 13. By day 17 growth inhibition was highly significant (***p<0.001*) compared to control group and AZD2281 group.

As shown in figure 24, a significant reduction of tumor growth was achieved in the combined treatment group compared to those receiving both the single treatments and the untreated one. At day 13, The growth inhibition difference of the combined treatment group started to be statistically significant ($p<0.05$) compared to single treatments and control group, and became highly significant ($p<0.001$) from day 17 compared to control group and AZD2281 group. Treated animals did not show any weight loss or dehydration.

Caspase inhibition attenuates dl922-947-induced cell death

Cell death mechanisms activated by the host cells represent a well-known obstacle for viral infection. Accordingly, during their evolution, adenoviruses have developed two proteins, E1B-19K and E1B-55K, able to antagonize E1A-induced apoptosis (Yew and Berk 1992, White 2001). In this study, I hypothesized that a deeper mechanistic understanding of the cell death mechanism induced by the oncolytic mutant *dl*922-947 in ATC cell lines may allow for novel discovered mediators to be therapeutically exploited, ultimately enabling the development of new combinatorial strategies with

oncolytic adenoviruses. Given the involvement of several apoptotic markers (described above) in *dl*922-947 infection, I decided to verify whether apoptosis is necessary for *dl*922-947-driven cell death. To this aim, I used zVAD-fmk a pan caspase inhibitor.

ATC cells were infected with *dl*922-947 in presence or not of zVAD-fmk, and caspase 3 cleavage was assessed by western blot 72h later.

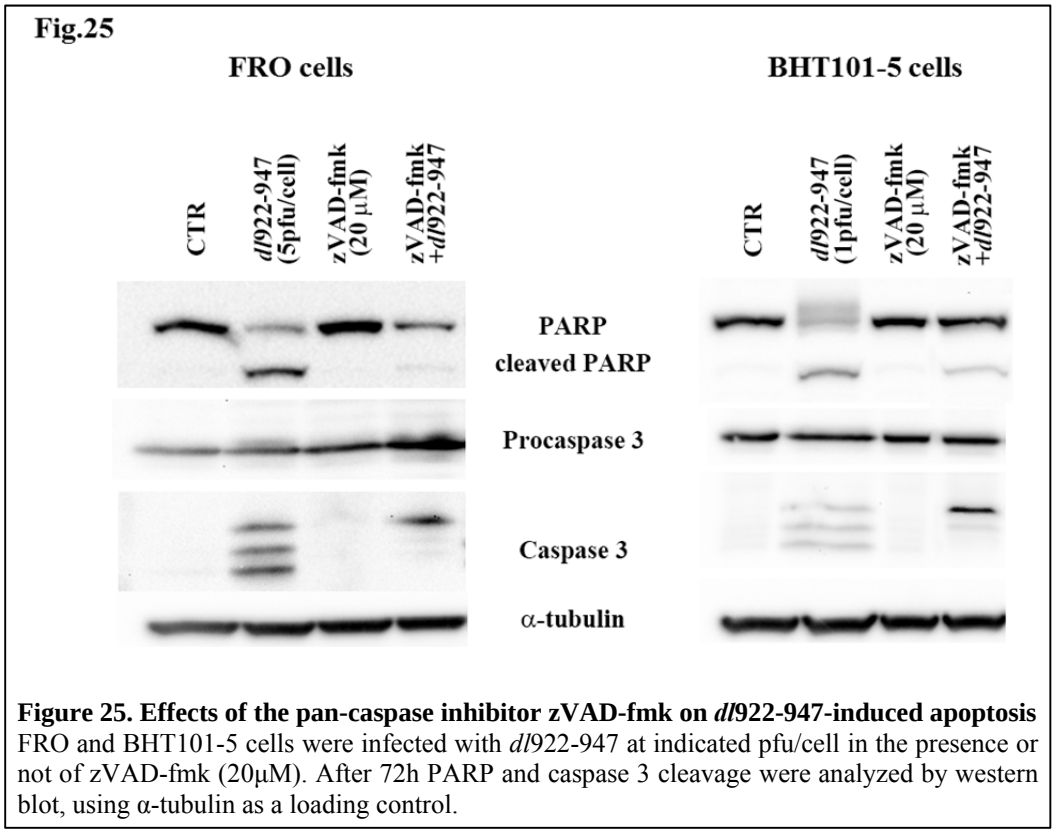

Figure 25. Effects of the pan-caspase inhibitor zVAD-fmk on *dl*922-947-induced apoptosis
FRO and BHT101-5 cells were infected with *dl*922-947 at indicated pfu/cell in the presence or not of zVAD-fmk (20μM). After 72h PARP and caspase 3 cleavage were analyzed by western blot, using α-tubulin as a loading control.

As shown in figure 25, zVAD-fmk, at 20 μM concentration, effectively reverted *dl*922-947-mediated caspase-3 cleavage in FRO and BHT101-5 cells, as indicated by an increase of the procaspase-3 and a reduction of the cleaved form. Indeed, it is worth to note that the presence of the upper band of the cleaved caspase 3, still detected in presence of zVAD-fmk, is not an active form of cleaved caspase 3 and therefore not suggestive of its activation (Johnson et al. 2000). Similar results were obtained for PARP cleavage [Figure 25].

Next, we evaluated the cell growth of FRO and BHT101-5 cells infected with *dl*922-947 (5 and 1 pfu/cell, respectively), in presence or not of the caspase inhibitor zVAD-fmk (20 μM), for 24, 48 and 72h.

Fig. 26

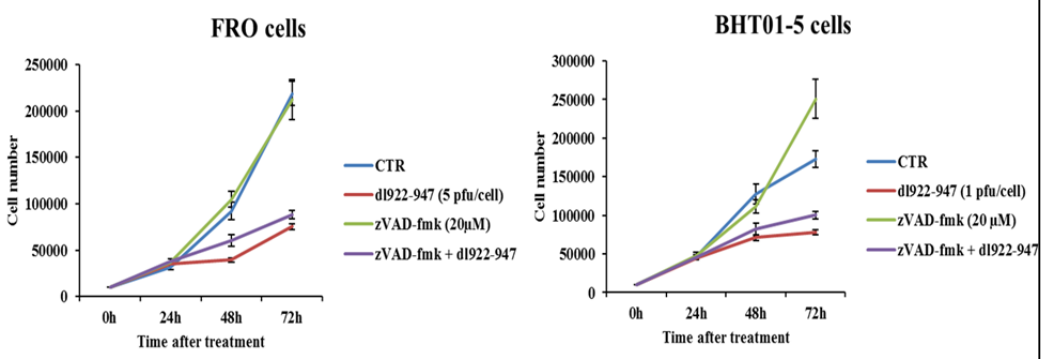

Figure 26. Effects of the pan caspase inhibitor zVAD-fmk on *dl*922-947 oncolytic activity
FRO and BHT101-5 cells were plated in 12-well plates and infected with *dl*922-947 in the presence or not of zVAD-fmk at indicated time points and concentration. Caspase inhibition increased cell viability in presence of the virus compared to only infected cell. The data represent the mean of three independent experiments.

The growth of FRO cells in presence of zVAD-fmk was unchanged compared to untreated cells, whereas the drug induced a slight increase of BHT101-5 cell growth at 72h [Figure 26].

Caspase inhibitor treatment in combination with *dl*922-947 was able to attenuate *dl*922-947-induced cell death at 48 and 72hpi, in both cell lines [Figure 26]. However, the lack of a complete rescue from virus-induced cell death in presence of the drug, suggested that the virus may leverage additional cell death mechanisms to kill the cells.

To further characterize the reduction of virus-induced cell death in presence of a caspase inhibitor, I have also analyzed other apoptotic markers, such as Annexin V [Figure 27] and cytochrome C release [Figure 28] by FACS analysis, as described above, after 72h of infection.

Fig. 27

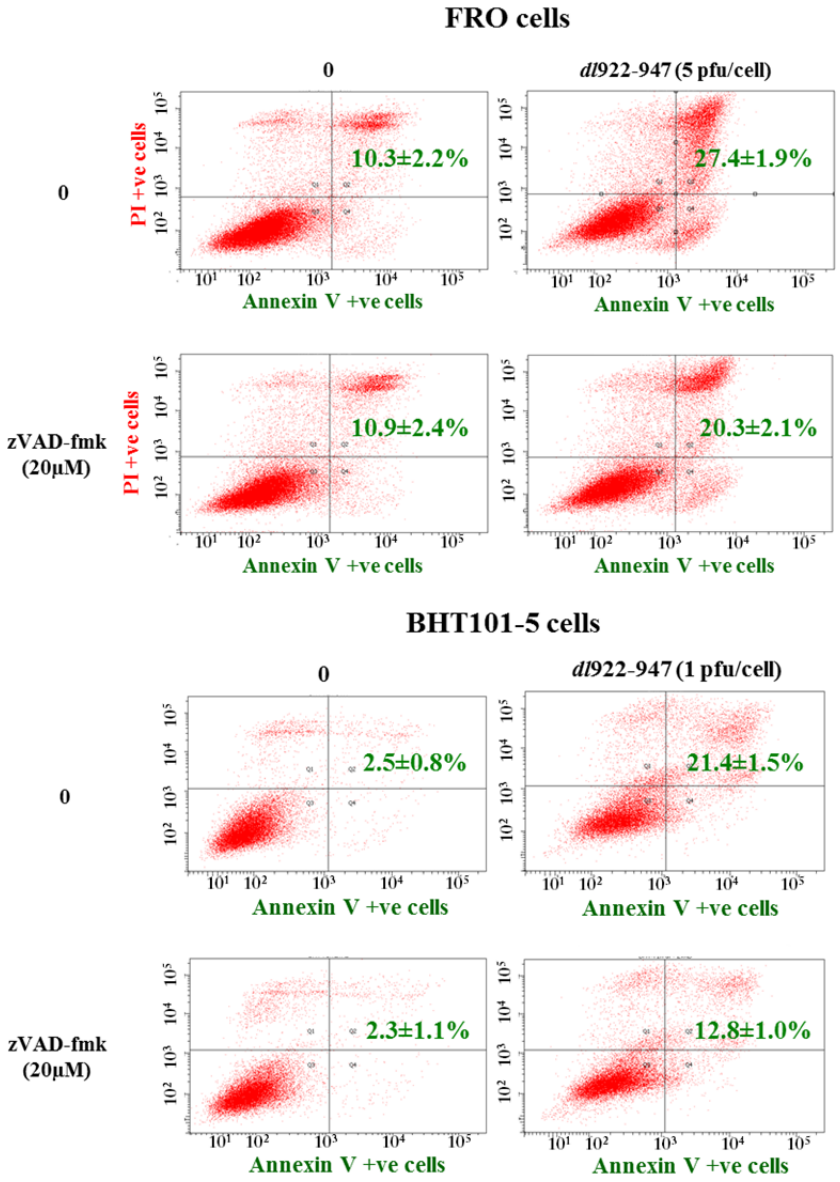

Figure 27. Effects of zVAD-fmk on *dl*922-947-induced phosphatydilserine exposition on plasma membrane

FRO (upper panel) and BHT 101-5 (lower panel) were infected with *dl*922-947 at indicated pfu/cell for 72h in the presence or not of zVAD-fmk (20 µM). Annexin V binds to living cells with exposed phospholipid phosphatidylserine. Caspase inhibition reduced the percentage of apoptotic cells with respect to single treatments. Green numbers represent the percentage of annexin V positive cells and the standard deviation of three independent experiments.

The annexin V staining showed that the treatment with zVAD-fmk (20 µM) is able to reduce *dl*922-947-induced annexin V positivity from 27.4 to 20.3 in

FRO cells, and from 21.4 to 12.8 in BHT101-5 cells, indicating that caspase inhibition attenuates *dl*922-947-induced cell death.

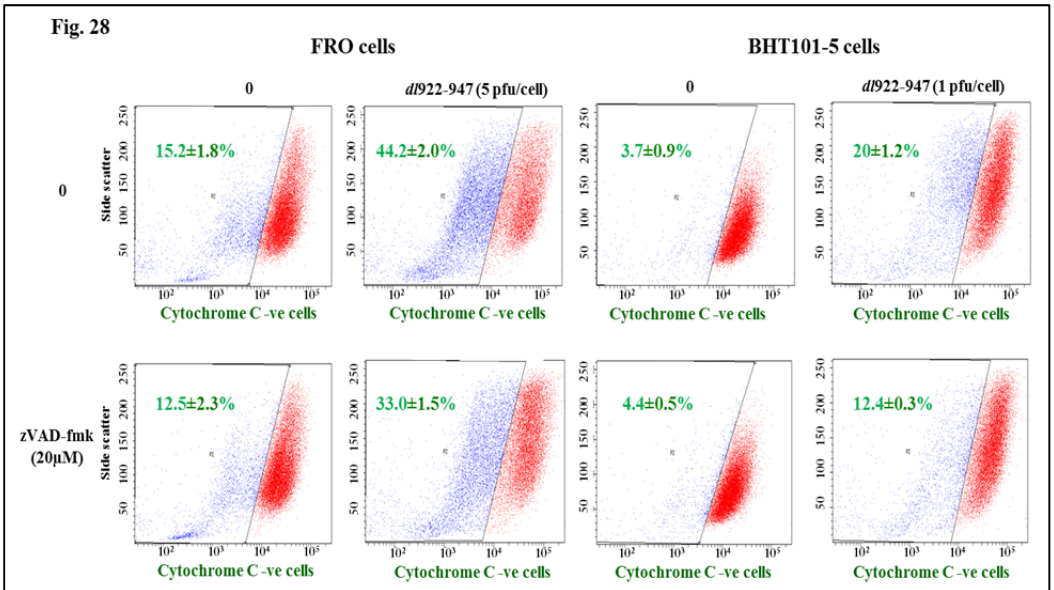

Figure 28. Effects of zVAD-fmk on *dl*922-947-induced cytochrome C release from mitochondria.
FRO and BHT101-5 cells were infected with *dl*922-947 at indicated pfu/cell in the presence or not of AZD2281 (1μM). After 72h, cytochrome C release from mitochondria was assessed by FACS analysis. Cells with intact mitochondria result positive to the staining for cytochrome C, while a lower fluorescence is indicative of cells with higher release of cytochrome C from mitochondria (cytochrome C negative cells). Caspase inhibition reduced the percentage of cytochrome C negative cells compared to only infected cells. Green numbers represent the percentage of cytochrome C negative cells and the standard deviation of three independent experiments.

Accordingly, quantification of cytochrome C release from mitochondria also revealed that cytochrome C release induced by *dl*922-947, and consequently the mitochondrial permeabilization, is reduced when apoptosis is inhibited by zVAD-fmk (20 μM) (from 44.2 to 33.0 in FRO cells, and from 20.0 to 12.4 in BHT101-5 cells [Figure 28].

dl922-947 induces an apoptotic-like cell death mechanism lacking the peculiar apoptotic morphology

Apoptosis is morphologically characterized by membrane blebbing. Blebs formation is driven by modulation of actin-myosin activity, that create hydrodynamic forces during contraction to induce, collapse at points of structural weakness within the cell (Street and Bryan 2011).

Fig. 29

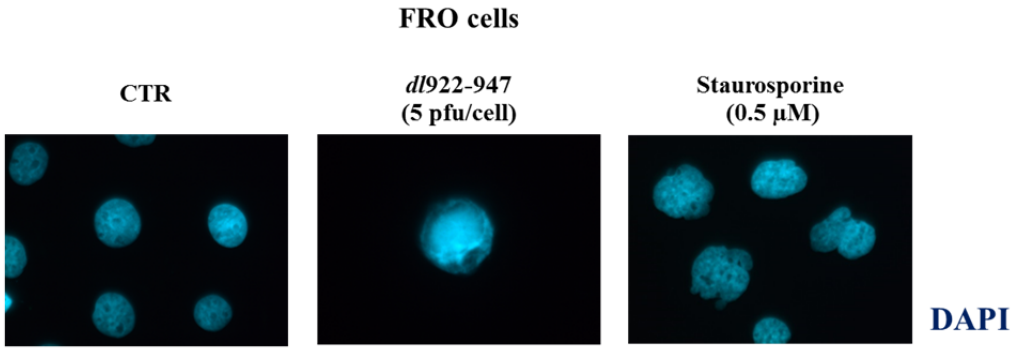

Figure 29. Effects of *dl*922-947 on apoptosis morphology
FRO cells infected with *dl*922-947 (5 pfu/cell) for 24h or incubated over night with 0.5 µM staurosporine (as positive control for apoptosis). After staining with DAPI, nuclei were visualized by fluorescence microscope. *dl*922-947 infected cells showed a different nuclear morphology (cells round up and nucleus remain intact) compared to staurosporine treated cells (nuclear fragmentation).
Data shown are representative of three independent experiments.

As programmed cell death progresses blebs may become packed with cellular organelles and condensed chromatin to form the basis of fragmentary membrane-clad apoptotic bodies (Wickman et al. 2012). Therefore, I investigated the presence of membrane blebbing, as morphological apoptotic feature, in infected cells, by immunofluorescence experiment for condensed/fragmented chromatin staining cells with DAPI.

Despite *dl*922-947 infected cells displayed several apoptotic markers, such as caspase 3 and PARP cleavage, Annexin V positivity and cytochrome C release, no signs of blebbing formation were found, as indicated by the round shape displayed by cell after infection and by the presence of nucleus still intact. As positive control for apoptotic blebbing, I treated FRO cells with the well-known apoptotic inducer staurosporine (Couldwell et al. 1994, Antonsson and Persson 2009).

ROCK proteins are essential for multiple aspects of apoptotic processes, including regulation of cytoskeletal-mediated cell contraction and membrane blebbing, nuclear membrane disintegration, modulation of Bcl2-family member, caspase expression/activation and phagocytosis of the fragmented apoptotic bodies. ROCK proteins are direct targets of caspases that cleave the ROCK autoinhibitory C terminal domain (Wickman et al. 2012). This results in constitutive kinase activity of ROCK and its subsequent regulation of actin-myosin cellular contraction. In blebbing cells, an higher ROCK cleavage by caspases results in increased phosphorylation of Myosin Light Chain 2 (MLC2), thus leading to contraction of cortical actin within the cell (Wickman

et al. 2012).

To evaluate molecular mechanisms involved in cellular blebbing, I have analyzed caspase-mediated ROCK cleavage and MLC2 phosphorylation, by western blot analysis, in FRO cells infected with *dl*922-947 (5 pfu/cell) for 48h. Cells treated with staurosporine (0.5 μM) were used as positive control of ROCK1 cleavage [Figure 30].

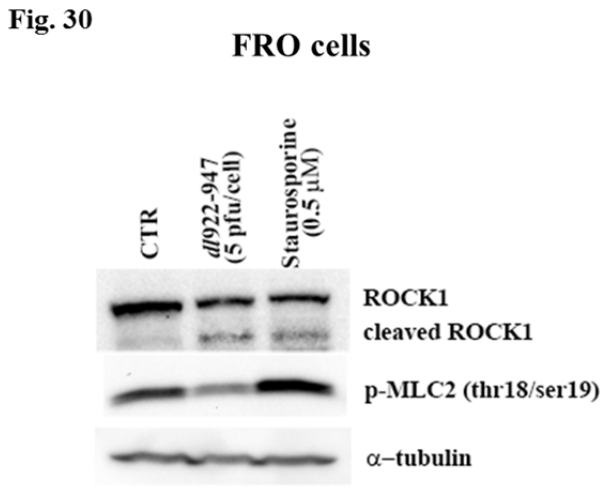

Figure 30. Effects of *dl*922-947 on blebbing pathway
FRO cells were infected with *dl*922-947 at 5 pfu/cell or incubated over night with 0.5 μM staurosporine (as positive control for apoptosis). After 48h, ROCK1 cleavage and MLC2 phosphorylation were analyzed by western blot, using α-tubulin as a loading control.

As demonstrated in figure 30 *dl*922-947 infection induced the formation of ROCK1 active form. Surprisingly, phosphorylation levels of ROCK1 target MLC2 resulted lower than untreated cells, highlighting the possibility that the virus may contrast the blebbing formation.

5. DISCUSSION

Anaplastic Thyroid Carcinoma is one of the most aggressive human neoplasia with an average survival time of six months after diagnosis. ATC is usually resistant to currently available treatments. So far, the treatment consist of surgery, when feasible, combined with radiation and chemotherapy. However, this multimodality treatment confers only a short term palliative and survival benefit.

ATC is characterized by a local growth, difficult to control and rapidly leading to trachea obstruction, asphyxia and death. Clinical studies have proven tumor selective replicating adenoviruses as an effective treatment against localized lesions (Russell et al. 2012), highlighting their potential use as strategy to improve the therapeutic outcome of ATC

Replication selective Oncolytic Viruses (OVs) are a rapidly expanding therapeutic platform for cancer treatment. As they are replication competent viral mutants, OVs are able to complete their life cycle exclusively in tumor cells. With respect to classical anti-cancer drugs, OVs present several advantages: tumor-selective replication with amplification of the input dose, stimulation of anti-tumoral immune responses, and relatively few mild side effects when administered to human patients. The development of cross resistance is unlikely, since the mechanism of action of OVs is independent from conventional anti-cancer therapeutics (Eager and Nemunaitis 2011) (Hallden and Portella 2012). Oncolytic viruses have been tested in clinical trials confirming their safety and showing varying degrees of success. *dl*1520 has been evaluated in phase I and II clinical trials and a related virus, H101, has been recently licensed in China for the treatment of head and neck carcinoma (Garber 2006). Reovirus and herpes simplex virus are in late phase testing. Other viruses, including measles virus and vaccinia virus, have completed phase I testing, showing promising results. A first-in-class US approval is expected soon for OncoVex, which is being tested in a randomized phase 3 clinical trial for the treatment of melanoma that has recently completed accrual (http://clinicaltrials.gov/NCT00769704).

In the last decade, several preclinical studies have demonstrated the effectiveness of virotherapy, alone or in combination with rational chosen drugs, for the treatment of ATC (Libertini et al. 2007, Lin et al. 2008, Reddi et al. 2008, Libertini et al. 2011, Reddi et al. 2012). In this regard, we have already demonstrated that the oncolytic adenovirus *dl*1520 is active against ATC cells and tumor xenografts (Portella et al. 2002, Portella et al. 2003, Libertini et al. 2007). Moreover, we have also proven that the most effective

second generation oncolytic adenovirus *dl*922-947 exerted a great antitumor effect against ATC cells and tumor xenografts (Libertini et al. 2008).

Although the great antineoplastic potential of oncolytic viruses has been confirmed in preclinical and clinical studies, the lack of full efficacy still represents a medical challenge. We have already exploited different approaches to use in combination with oncolytic adenoviruses, including drugs able to ameliorate the vascularization of tumors (anti VEGF antibody), to increase the replicative potential of the virus (AZD1152), or able to affect complementary cell death pathways (Libertini et al. 2008, Libertini et al. 2011, Botta et al. 2012).

Understanding how the neoplastic cells react and counterbalance the infection to extend their survival might uncover new insights in the field of virotherapy, allowing for novel effectors to be discovered and targeted to increase the efficacy of OVs.

The linear adenovirus genome has double-stranded DNA termini that could be targeted by cellular double strand break (DSB) repair pathways. It has been observed that the activation of the DSB repair pathway leads to formation of viral genome concatamers that impedes viral packaging into virions and the consequent viral replication (Lakdawala et al. 2008). To overcome this barrier, adenoviruses have evolved different strategies to modulate the DNA damage response (Turnell and Grand 2012). For example, the E4 region encodes viral factors that prevent concatamer formation through inhibition of the DSB repair; indeed, infection with adenoviruses harboring deletions of E4orf3 and E4orf6 results in concatenation of viral DNA, and prevention of replication and packaging (Weiden and Ginsberg 1994).

Recently, we have shown that *dl*922-947 infection triggers a DNA Damage Response (DDR) in ATC cells (Passaro et al, peding revision). We speculate that the DDR system may act as cellular protective mechanism to hinder viral infection and/or replication, and that its inhibition could be tested as strategy to enhance *dl*922-947 cytotoxicity. Accordingly, we have demonstrated that the ATM inhibitor KU55933 increased the oncolytic activity of *dl*922-947 and its replication (Passaro et al*.,* pending revision). Moreover Connell and colleagues (2011) showed that ATR and Chk1 inhibition is able to increase the *dl*922-947 cytotoxicity in ovarian cancer cells (Connell et al. 2011).

All these data further support the hypothesis that the DNA damage system could be a target exploitable to increase the efficacy of oncolytic adenoviruses.

Poly(ADP-ribose) polymerase (PARP) is a nuclear enzyme playing a critical role in DNA damage response processes (El-Khamisy et al. 2003). Targeting DNA repair using PARP inhibitors has great potential as anticancer therapeutic

strategy, either in conjunction with other DNA-damaging agents, or as a single agent. In particular, as a single agent, PARP inhibitors could be used in tumors with pre-existing homologous recombination pathway defects such a in BRCA-deficient cancers (Sandhu et al. 2010). This strategy is in the line with the concept of synthetic lethality that is a situation when a mutation in one of two genes that individually has no effect but combining the mutations leads to cell death. Indeed, PARP inhibition leads to the persistence of the SSBs, converted to a DSBs at the replication fork. In normal replicating cells, DSBs are efficiently repaired by the error free homologous recombination pathway. Whereas, cells homozygous for a defect in homologous recombination are highly sensitive to PARP inhibition due to persistent multiple unrepaired DSBs, a potent stimulus for cell death (Underhill et al. 2011).

In this work, I induced a synthetic lethality-like effect by combining *dl*922-947 with the PARP inhibitor, namely AZD2281, in ATC. Indeed, it is well known that an unscheduled DNA synthesis, such as that one induced by viral replication, causes the accumulation of single strand break (SSB) as replication-associated DNA lesions (Machida and Dutta 2005, Connell et al. 2011). SSBs accumulation leads to PARP activation, protein PARylation and SSB repair. PARP inhibition should prevent the repair of SSBs, which are then converted in DSBs at the replication fork. Although ATC cells do not show any mutation in DSB repair proteins, I hypothesized that *dl*922-947 can impair DSB repair, causing a persistence of multiple unrepaired DSBs and leading to cell death.

In this work, I demonstrated that the oncolytic adenovirus mutant *dl*922-947 is effectively able to push two different ATC cell lines (FRO and BHT101-5) to entry in S-phase. This effect is also paralleled by the accumulation of an unrepaired DNA damage, demonstrated by an high percentage of γH2AX-positive cells. Although γH2AX formation has historically been associated with the induction DSBs, a number of reports have shown H2AX phosphorylation after DNA replication stress (Ward and Chen 2001, Ewald et al. 2007). In addition *dl*922-947 infection induced PARP hyperactivation, suggesting SSB formation that should be repaired by BER pathway.

I have also demonstrated that *dl*922-947 elicits DSB repair pathway activation in the host cell, as suggested by ATM and Chk1 phosphorylation; however, the virus also hampers the execution of DSB repair downregulating MRN complex protein, probably through protein degradation. In this scenario, I combined a PARP inhibitor, AZD2281, with *dl*922-947, showing that, in both ATC cell lines FRO and BHT101-5, the combined treatment further increased

the accumulation of an unrepaired DNA damage. As expected, PARP inhibitor alone had no effect on DNA damage accumulation.

Then, I evaluated the effect of AZD2281 treatment on *dl*922-947 cytotoxicity. By performing an isobologram analysis, I showed that effect of such combined treatment is synergistic, at all used concentration.

To deepen our understanding of how AZD2281 is able to enhance oncolytic activity, we first monitored viral entry upon drug treatment. Our data show that AZD2281 does not affect viral entry. On the contrary, we observed a significant increase in viral replication in ATC cells also treated with AZD2281.

These results led me to hypothesize that the inhibition of DNA damage repair pathways, mediated by both AZD2281 and the virus itself, may accelerate cell cycle, thus enhancing viral replication, given the lack of repair of replication-associated DNA lesions by host cells.

However, the increased viral replication may not suffice to entirely explain the enhanced cell killing. In this regard, several studied have demonstrated an enhancement in viral cytotoxicity without an increase in viral replication (Libertini et al. 2011, Botta et al. 2012). Therefore, I evaluated cell death mechanisms induced by virus, and how these were affected by the drug.

First, I analyzed cell cycle profile to quantify the percentage of cell in sub-G1 phase. Sub-G1 phase is a generic marker of cell death, since it only indicate the presence of DNA fragmentation, that can occur either during necrosis or apoptosis.

The combination between the drug and the virus significantly increased the percentage of cells in sub-G1 fraction compared with infected cells. AZD2281 alone did not induce any effect.

It has been shown that forcing cells with damaged DNA into mitosis causes severe chromosome segregation defects leading to polyploidy. Cell cycle profile analysis confirmed a significant increase in polyploidy induced by the combined treatment. The polyploidy observed in ATC cells infected with *dl*922-947 or undergoing the combined treatment could be ascribed to a more robust entry into mitosis in presence of an unrepaired DNA damage. I also hypothesize that dying cells in sub-G1 fraction may arise from polyploid cells.

I even explored the involvement of apoptotic mechanism in the cell death induced in treated/infected cells, by evaluating some apoptotic markers, such as Annexin V positivity, PARP and caspase 3 cleavage, and cytochrome C release from mitochondria. The association with AZD2281 increased the percentage of Annexin V positive cells, as well as the percentage of Cytochrome C negative

cells. Accordingly, caspase 3 was found to be more active in cell receiving the combined treatment.

The results clearly indicate that AZD2281 enhances the cytotoxic effects of oncolytic viruses either by potentiating the virus-induced cell death mechanisms and by increasing viral replication.

To validate the potential therapeutic use of AZD2281 in association with *dl*922-947, I analyzed the effects of the combined treatment on ATC xenograft tumors, by injecting FRO cells in athymic mice. Starting from day 13, I observed that the combined treatment AZD2281/*dl*922-947 significantly reduced tumor growth compared to single treatment group and control group. Overall, these data clearly demonstrate the efficacy of AZD2281/*dl*922-947 combination in ATC both *in vitro* and *in vivo*.

In accordance to Baird and colleagues (Baird et al. 2008), we previously observed that infection of ATC cells with *dl*922-947 led to programmed cell death lacking the morphological features of classical apoptosis, but showing some apoptotic markers, such as sub-G1 accumulation and caspase-3 activation (Libertini et al. 2011). Here, I demonstrate that in ATC cell the virus induces the activation of an apoptotic-like cell death, characterized by Annexin V positivity, PARP and caspase 3 cleavage, and cytochrome C release from mitochondria. However, classical morphological signs of apoptosis, including cell shrinkage, membrane blebbing, cellular disintegration, and chromosome condensation are missing. It should be noted that apoptotic blebbing is not a universal feature of programmed cell death, some cell types do not appear to generate membrane blebs nor undergo fragmentation (Wickman et al. 2012). To demonstrated that FRO cell are neither resistant to form membrane blebs nor undergo fragmentation, we compared cells infected with *dl*922-947 to cells treated with staurosporine, a well-known apoptosis inducer (Couldwell et al. 1994, Antonsson and Persson 2009), observing a different nuclear morphology. Indeed infected cells rounded up and nucleus remain intact, whereas staurosporine treated cells showed a clear nuclear fragmentation.

Membrane blebbing is a crucial step for apoptotic bodies clearance by monocytes and macrophages. Since this phenomena was lacking in *dl*922-947-infected cells, I hypothesized that *dl*922-947 could prevent membrane blebbing and apoptotic bodies formation, thus causing a not apoptotic-like morphology. To demonstrate my hypothesis, I analyzed the molecular pathway involved in membrane blebbing. In blebbing cells, an higher ROCK cleavage by caspases results in increased phosphorylation of Myosin Light Chain 2 (MLC2), thus leading to contraction of cortical actin within the cell (Wickman et al. 2012). In FRO cells, *dl*922-947 infection induced the formation of ROCK1 active form.

Surprisingly, phosphorylation levels of ROCK1 target MLC2 resulted lower than untreated cells, highlighting the possibility that the virus may contrast the blebbing formation.

In addition, analysis of cell growth curve showed that the cell death induced by *dl*922-947 is partially reverted by the addition of a pan caspase inhibitor, zVAD-fmk. In the presence of the inhibitor, an higher number of living cells was observed compared to only infected cells. This result is further supported by the observation that zVAD-fmk reduced the percentage of apoptotic cells (Annexin V positive and Cytochrome C negative), although cell death processes are still partially active in presence of the inhibitor.

These data suggest us that *dl*922-947 infection may concomitantly leverage different cell death mechanisms in ATC cells. Future experiments are required to clarify these data. Apoptotic process is an established obstacle to viral infection, and viruses have evolved genes inhibiting the host cell apoptosis. In this scenario, host cells need to activate an alternative cell death mechanism to circumvent inhibition of apoptosis in order to curtail viral infection. It is conceivable that elucidating the exact death mechanisms activated by the host cell after infection might allow the identification of new therapeutic targets, able to potentiate oncolytic adenoviral cytotoxicity.

6. CONCLUSION

Anaplastic Thyroid Carcinoma (ATC) is one of the most aggressive human malignancies. Multimodality therapy, which includes surgical debulking, external radiation therapy and chemotherapy, has failed to show improvements in median survival. The development and the validation of novel and more effective treatment strategies still represent a medical challenge.

Oncolytic viruses are replication competent viral mutants able to complete their life cycle exclusively in tumor cells. In the present study, I have demonstrated that the oncolytic adenovirus *dl*922-947 induces the accumulation of an unrepaired DNA damage with the concomitant activation of Poly(ADP-ribose) Polymerase (PARP), and impairs the pathway implicated in the double strand break repair. Exploiting the concept of synthetic lethality I combined *dl*922-947 with the PARP inhibitor AZD2281, proving this drug as effective in enhancing the oncolytic activity of *dl*922-947 in two ATC cell lines. Indeed, I have also shown that this effect is paralleled by an increased cell death and an increased viral replication.

Importantly, I successfully validated the therapeutic combination AZD2281/*dl*922-947 against ATC *in vivo*, demonstrating that AZD2281 significantly enhances the *dl*922-947 oncolytic effect in ATC tumor xenograft. Basing on these findings, I strongly suggest that AZD2281 could be therapeutically used in combination with the oncolytic virus *dl*922-947 for the treatment of ATC.

Finally, I have also demonstrated that *dl*922-947 is able to impede the apoptotic membrane blebbing activated by cells in response to the infection, acting on ROCK 1/Myosin Light Chain 2 pathway.

Since membrane blebbing is a crucial step for apoptotic bodies clearance by monocytes and macrophages and the apoptotic process is an obstacle to viral infection, I suggest that ROCK 1 could be an additional therapeutic target to be potentially used in combination with oncolytic viruses against anaplastic thyroid carcinoma.

Thus, this project has enabled us to identify novel mechanisms implicated in the infection of ATC cells with oncolytic adenoviruses. In future studies, additional regulators or downstream effectors of the identified pathways will be assessed for their “druggability” in *in vitro* and *in vivo* models of ATC. This new knowledge will allow the development of new therapeutic strategies to test in combination with oncolytic adenoviruses, potentially capable of driving benefits for the treatment of ATC, which is still a formidable medical challenge.

7. AKNOWLEDGEMENTS

I am very glad to say thank you:

To my tutor, Professor Portella, who made me scientifically grow up and always supported me.

To Professor Beguinot and Professor Formisano, who significantly contributed to my scientific growth.

To Professor Gillespie, who gave me the opportunity to attend his lab at the Beatson Institute for Cancer Research, and to people from R11 lab, that greeted me warmly in a cold Glasgow.

To Dr Libertini and Dr Botta who always took care of me. All that I am today I owe to you. I really hope I made you proud of me!

To Giuseppe, Michele, Rossella, Sara and Viviana. I spend more time with you than with my family. You always were by my side, even in times of trouble for this I wish you well!

To Antonella, who not only physically shared with me the lab, but also shared with me the good and bad times of a lab's life.

To all my students: Max, Liberato, Eloise. This thesis is also the result of your work (especially Max's work).

To Serena, with whom I started and I am finishing this "adventure", with the hope we can start together many other successes.

To all the people from Beguinot's and Formisano's lab who supported me during my PhD.

To my roommates that, very patiently, tolerated my disorder.

To my friend Luana, who always showed me her sincere friendship.

To my family and Niko. There are not enough words to say thank you. I can only share with you this success saying that without you nothing would make sense!

8. REFERENCES

Ame JC, Spenlehauer C and de Murcia G. The PARP superfamily. Bioessays 2004; 26(8): 882-93.

Antonsson A and Persson JL. Induction of apoptosis by staurosporine involves the inhibition of expression of the major cell cycle proteins at the G(2)/m checkpoint accompanied by alterations in Erk and Akt kinase activities. Anticancer Res 2009; 29(8): 2893-8.

Asada T. Treatment of human cancer with mumps virus. Cancer 1974; 34(6): 1907-28.

Baird SK, Aerts JL, Eddaoudi A, Lockley M, Lemoine NR and McNeish IA. Oncolytic adenoviral mutants induce a novel mode of programmed cell death in ovarian cancer. Oncogene 2008; 27(22): 3081-90.

Baker A, Rohleder KJ, Hanakahi LA and Ketner G. Adenovirus E4 34k and E1b 55k oncoproteins target host DNA ligase IV for proteasomal degradation. J Virol 2007a; 81(13): 7034-40.

Baker AH, McVey JH, Waddington SN, Di Paolo NC and Shayakhmetov DM. The influence of blood on in vivo adenovirus bio-distribution and transduction. Mol Ther 2007b; 15(8): 1410-6.

Bakiri FD, F.K.; Mokrane L.A.; Djidel F.K. The relative roles of endemic goiter and socioeconomic development status in the prognosis of thyroid carcinoma. Cancer 1998; 82: 1146-53.

Bakkenist CJ and Kastan MB. DNA damage activates ATM through intermolecular autophosphorylation and dimer dissociation. Nature 2003; 421(6922): 499-506.

Banin S, Moyal L, Shieh S, Taya Y, Anderson CW, Chessa L, Smorodinsky NI, Prives C, Reiss Y, Shiloh Y and Ziv Y. Enhanced phosphorylation of p53 by ATM in response to DNA damage. Science 1998; 281(5383): 1674-7.

Bhattacharyya M, Francis J, Eddouadi A, Lemoine NR and Hallden G. An oncolytic adenovirus defective in pRb-binding (dl922-947) can efficiently eliminate pancreatic cancer cells and tumors in vivo in combination with 5-FU or gemcitabine. Cancer Gene Ther 2011; 18(10): 734-43.

Bischoff JR, Kirn DH, Williams A, Heise C, Horn S, Muna M, Ng L, Nye JA, Sampson-Johannes A, Fattaey A and McCormick F. An adenovirus mutant that replicates selectively in p53-deficient human tumor cells. Science 1996; 274(5286): 373-6.

Blackford AN, Bruton RK, Dirlik O, Stewart GS, Taylor AM, Dobner T, Grand RJ and Turnell AS. A role for E1B-AP5 in ATR signaling pathways during adenovirus infection. J Virol 2008; 82(15): 7640-52.

Blackford AN, Patel RN, Forrester NA, Theil K, Groitl P, Stewart GS, Taylor AM, Morgan IM, Dobner T, Grand RJ and Turnell AS. Adenovirus 12 E4orf6 inhibits ATR activation by promoting TOPBP1 degradation. Proc Natl Acad Sci U S A 2010; 107(27): 12251-6.

Bluming AZ and Ziegler JL. Regression of Burkitt's lymphoma in association with measles infection. Lancet 1971; 2(7715): 105-6.

Botta G, Passaro C, Libertini S, Abagnale A, Barbato S, Maione AS, Hallden G, Beguinot F, Formisano P and Portella G. Inhibition of autophagy enhances the effects of E1A-defective oncolytic adenovirus dl922-947 against glioma cells in vitro and in vivo. Hum Gene Ther 2012; 23(6): 623-34.

Boyer J, Rohleder K and Ketner G. Adenovirus E4 34k and E4 11k inhibit double strand break repair and are physically associated with the cellular DNA-dependent protein kinase. Virology 1999; 263(2): 307-12.

Brandsma I and Gent DC. Pathway choice in DNA double strand break repair: observations of a balancing act. Genome Integr 2012; 3(1): 9.

Breitbach CJ, Burke J, Jonker D, Stephenson J, Haas AR, Chow LQ, Nieva J, Hwang TH, Moon A, Patt R, Pelusio A, Le Boeuf F, Burns J, Evgin L, De Silva N, Cvancic S, Robertson T, Je JE, Lee YS, Parato K, Diallo JS, Fenster A, Daneshmand M, Bell JC and Kirn DH. Intravenous delivery of a multi-mechanistic cancer-targeted oncolytic poxvirus in humans. Nature 2011; 477(7362): 99-102.

Calabrese CR, Almassy R, Barton S, Batey MA, Calvert AH, Canan-Koch S, Durkacz BW, Hostomsky Z, Kumpf RA, Kyle S, Li J, Maegley K, Newell DR, Notarianni E, Stratford IJ, Skalitzky D, Thomas HD, Wang LZ, Webber SE, Williams KJ and Curtin NJ. Anticancer chemosensitization and radiosensitization by the novel poly(ADP-ribose) polymerase-1 inhibitor AG14361. J Natl Cancer Inst 2004; 96(1): 56-67.

Carson CT, Orazio NI, Lee DV, Suh J, Bekker-Jensen S, Araujo FD, Lakdawala SS, Lilley CE, Bartek J, Lukas J and Weitzman MD. Mislocalization of the MRN complex prevents ATR signaling during adenovirus infection. EMBO J 2009; 28(6): 652-62.

Carson CT, Schwartz RA, Stracker TH, Lilley CE, Lee DV and Weitzman MD. The Mre11 complex is required for ATM activation and the G2/M checkpoint. EMBO J 2003; 22(24): 6610-20.

Carvalho T, Seeler JS, Ohman K, Jordan P, Pettersson U, Akusjarvi G, Carmo-Fonseca M and Dejean A. Targeting of adenovirus E1A and E4-ORF3 proteins to nuclear matrix-associated PML bodies. J Cell Biol 1995; 131(1): 45-56.

Cawood R, Chen HH, Carroll F, Bazan-Peregrino M, van Rooijen N and Seymour LW. Use of tissue-specific microRNA to control pathology of wild-type adenovirus without attenuation of its ability to kill cancer cells. PLoS Pathog 2009; 5(5): e1000440.

Chambon P, Weil J and Mandel P. Nicotinamide mononucleotide activation of a newDNA-dependent polyadenylic acid synthesizing nuclear enzyme. Biochem Biophys Res Commun 1963; 11(1): 39-43.

Cherubini G, Kallin C, Mozetic A, Hammaren-Busch K, Muller H, Lemoine NR and Hallden G. The oncolytic adenovirus AdDeltaDelta enhances selective cancer cell killing in combination with DNA-damaging drugs in pancreatic cancer models. Gene Ther 2011; 18(12): 1157-65.

Chiocca EA. The host response to cancer virotherapy. Curr Opin Mol Ther 2008; 10(1): 38-45.

Chow J and Poon RY. DNA damage and polyploidization. Adv Exp Med Biol 2010; 676: 57-71.

Coffey MC, Strong JE, Forsyth PA and Lee PW. Reovirus therapy of tumors with activated Ras pathway. Science 1998; 282(5392): 1332-4.

Conde C, Mark M, Oliver FJ, Huber A, de Murcia G and Menissier-de Murcia J. Loss of poly(ADP-ribose) polymerase-1 causes increased tumour latency in p53-deficient mice. EMBO J 2001; 20(13): 3535-43.

Connell CM, Shibata A, Tookman LA, Archibald KM, Flak MB, Pirlo KJ, Lockley M, Wheatley SP and McNeish IA. Genomic DNA damage and ATR-Chk1 signaling determine oncolytic adenoviral efficacy in human ovarian cancer cells. J Clin Invest 2011; 121(4): 1283-97.

Cortez D, Wang Y, Qin J and Elledge SJ. Requirement of ATM-dependent phosphorylation of brca1 in the DNA damage response to double-strand breaks. Science 1999; 286(5442): 1162-6.

Couldwell WT, Hinton DR, He S, Chen TC, Sebat I, Weiss MH and Law RE. Protein kinase C inhibitors induce apoptosis in human malignant glioma cell lines. FEBS Lett 1994; 345(1): 43-6.

D'Amours D, Desnoyers S, D'Silva I and Poirier GG. Poly(ADP-ribosyl)ation reactions in the regulation of nuclear functions. Biochem J 1999; 342 (Pt 2): 249-68.

Daniel RA, Rozanska AL, Thomas HD, Mulligan EA, Drew Y, Castelbuono DJ, Hostomsky Z, Plummer ER, Boddy AV, Tweddle DA, Curtin NJ and Clifford SC. Inhibition of poly(ADP-ribose) polymerase-1 enhances temozolomide and topotecan activity against childhood neuroblastoma. Clin Cancer Res 2009; 15(4): 1241-9.

de Murcia JM, Niedergang C, Trucco C, Ricoul M, Dutrillaux B, Mark M, Oliver FJ, Masson M, Dierich A, LeMeur M, Walztinger C, Chambon P and de Murcia G. Requirement of poly(ADP-ribose) polymerase in recovery from DNA damage in mice and in cells. Proc Natl Acad Sci U S A 1997; 94(14): 7303-7.

De Pace N. Sulla scomparsa di un enorme cancro vegetante del collo dell'utero senza cura chirurgica. Ginecologia 1921; 9: 82-9.

DeWeese TL, van der Poel H, Li S, Mikhak B, Drew R, Goemann M, Hamper U, DeJong R, Detorie N, Rodriguez R, Haulk T, DeMarzo AM, Piantadosi S, Yu DC, Chen Y, Henderson DR, Carducci MA, Nelson WG and Simons JW. A phase I trial of CV706, a replication-competent, PSA selective oncolytic adenovirus, for the treatment of locally recurrent prostate cancer following radiation therapy. Cancer Res 2001; 61(20): 7464-72.

Dilley J, Reddy S, Ko D, Nguyen N, Rojas G, Working P and Yu DC. Oncolytic adenovirus CG7870 in combination with radiation demonstrates synergistic enhancements of antitumor efficacy without loss of specificity. Cancer Gene Ther 2005; 12(8): 715-22.

Dobzhansky T. Genetics of Natural Populations. Xiii. Recombination and Variability in Populations of Drosophila Pseudoobscura. Genetics 1946; 31(3): 269-90.

Doucas V, Ishov AM, Romo A, Juguilon H, Weitzman MD, Evans RM and Maul GG. Adenovirus replication is coupled with the dynamic properties of the PML nuclear structure. Genes Dev 1996; 10(2): 196-207.

Dungey FA, Loser DA and Chalmers AJ. Replication-dependent radiosensitization of human glioma cells by inhibition of poly(ADP-Ribose)

polymerase: mechanisms and therapeutic potential. Int J Radiat Oncol Biol Phys 2008; 72(4): 1188-97.

Eager RM and Nemunaitis J. Clinical development directions in oncolytic viral therapy. Cancer Gene Ther 2011; 18(5): 305-17.

El-Khamisy SF, Masutani M, Suzuki H and Caldecott KW. A requirement for PARP-1 for the assembly or stability of XRCC1 nuclear foci at sites of oxidative DNA damage. Nucleic Acids Res 2003; 31(19): 5526-33.

Esteller M, Garcia-Foncillas J, Andion E, Goodman SN, Hidalgo OF, Vanaclocha V, Baylin SB and Herman JG. Inactivation of the DNA-repair gene MGMT and the clinical response of gliomas to alkylating agents. N Engl J Med 2000; 343(19): 1350-4.

Evans JD and Hearing P. Relocalization of the Mre11-Rad50-Nbs1 complex by the adenovirus E4 ORF3 protein is required for viral replication. J Virol 2005; 79(10): 6207-15.

Evers B, Drost R, Schut E, de Bruin M, van der Burg E, Derksen PW, Holstege H, Liu X, van Drunen E, Beverloo HB, Smith GC, Martin NM, Lau A, O'Connor MJ and Jonkers J. Selective inhibition of BRCA2-deficient mammary tumor cell growth by AZD2281 and cisplatin. Clin Cancer Res 2008; 14(12): 3916-25.

Ewald B, Sampath D and Plunkett W. H2AX phosphorylation marks gemcitabine-induced stalled replication forks and their collapse upon S-phase checkpoint abrogation. Mol Cancer Ther 2007; 6(4): 1239-48.

Fadok VA, de Cathelineau A, Daleke DL, Henson PM and Bratton DL. Loss of phospholipid asymmetry and surface exposure of phosphatidylserine is required for phagocytosis of apoptotic cells by macrophages and fibroblasts. J Biol Chem 2001; 276(2): 1071-7.

Farmer H, McCabe N, Lord CJ, Tutt AN, Johnson DA, Richardson TB, Santarosa M, Dillon KJ, Hickson I, Knights C, Martin NM, Jackson SP, Smith GC and Ashworth A. Targeting the DNA repair defect in BRCA mutant cells as a therapeutic strategy. Nature 2005; 434(7035): 917-21.

Fisher KD and Seymour LW. HPMA copolymers for masking and retargeting of therapeutic viruses. Adv Drug Deliv Rev 2010; 62(2): 240-5.

Forrester NA, Sedgwick GG, Thomas A, Blackford AN, Speiseder T, Dobner T, Byrd PJ, Stewart GS, Turnell AS and Grand RJ. Serotype-specific inactivation of the cellular DNA damage response during adenovirus infection. J Virol 2011; 85(5): 2201-11.

Freytag SO, Khil M, Stricker H, Peabody J, Menon M, DePeralta-Venturina M, Nafziger D, Pegg J, Paielli D, Brown S, Barton K, Lu M, Aguilar-Cordova E and Kim JH. Phase I study of replication-competent adenovirus-mediated double suicide gene therapy for the treatment of locally recurrent prostate cancer. Cancer Res 2002; 62(17): 4968-76.

Fueyo J, Gomez-Manzano C, Alemany R, Lee PS, McDonnell TJ, Mitlianga P, Shi YX, Levin VA, Yung WK and Kyritsis AP. A mutant oncolytic adenovirus targeting the Rb pathway produces anti-glioma effect in vivo. Oncogene 2000; 19(1): 2-12.

Furuta T, Takemura H, Liao ZY, Aune GJ, Redon C, Sedelnikova OA, Pilch DR, Rogakou EP, Celeste A, Chen HT, Nussenzweig A, Aladjem MI, Bonner WM and Pommier Y. Phosphorylation of histone H2AX and activation of Mre11, Rad50, and Nbs1 in response to replication-dependent DNA double-strand breaks induced by mammalian DNA topoisomerase I cleavage complexes. J Biol Chem 2003; 278(22): 20303-12.

Galanis E, Okuno SH, Nascimento AG, Lewis BD, Lee RA, Oliveira AM, Sloan JA, Atherton P, Edmonson JH, Erlichman C, Randlev B, Wang Q, Freeman S and Rubin J. Phase I-II trial of ONYX-015 in combination with MAP chemotherapy in patients with advanced sarcomas. Gene Ther 2005; 12(5): 437-45.

Garber K. China approves world's first oncolytic virus therapy for cancer treatment. J Natl Cancer Inst 2006; 98(5): 298-300.

Hakme A, Wong HK, Dantzer F and Schreiber V. The expanding field of poly(ADP-ribosyl)ation reactions. 'Protein Modifications: Beyond the Usual Suspects' Review Series. EMBO Rep 2008; 9(11): 1094-100.

Hallden G and Portella G. Oncolytic virotherapy with modified adenoviruses and novel therapeutic targets. Expert Opin Ther Targets 2012; 16(10): 945-58.

Hart LS, Ornelles D and Koumenis C. The adenoviral E4orf6 protein induces atypical apoptosis in response to DNA damage. J Biol Chem 2007; 282(9): 6061-7.

Hart LS, Yannone SM, Naczki C, Orlando JS, Waters SB, Akman SA, Chen DJ, Ornelles D and Koumenis C. The adenovirus E4orf6 protein inhibits DNA double strand break repair and radiosensitizes human tumor cells in an E1B-55K-independent manner. J Biol Chem 2005; 280(2): 1474-81.

Hashimoto Y, Tazawa H, Teraishi F, Kojima T, Watanabe Y, Uno F, Yano S, Urata Y, Kagawa S and Fujiwara T. The hTERT promoter enhances the antitumor activity of an oncolytic adenovirus under a hypoxic microenvironment. PLoS One 2012; 7(6): e39292.

Hassa PO and Hottiger MO. The functional role of poly(ADP-ribose)polymerase 1 as novel coactivator of NF-kappaB in inflammatory disorders. Cell Mol Life Sci 2002; 59(9): 1534-53.

Hay T, Matthews JR, Pietzka L, Lau A, Cranston A, Nygren AO, Douglas-Jones A, Smith GC, Martin NM, O'Connor M and Clarke AR. Poly(ADP-ribose) polymerase-1 inhibitor treatment regresses autochthonous Brca2/p53-mutant mammary tumors in vivo and delays tumor relapse in combination with carboplatin. Cancer Res 2009; 69(9): 3850-5.

Hecht JR, Bedford R, Abbruzzese JL, Lahoti S, Reid TR, Soetikno RM, Kirn DH and Freeman SM. A phase I/II trial of intratumoral endoscopic ultrasound injection of ONYX-015 with intravenous gemcitabine in unresectable pancreatic carcinoma. Clin Cancer Res 2003; 9(2): 555-61.

Hegi ME, Diserens AC, Gorlia T, Hamou MF, de Tribolet N, Weller M, Kros JM, Hainfellner JA, Mason W, Mariani L, Bromberg JE, Hau P, Mirimanoff RO, Cairncross JG, Janzer RC and Stupp R. MGMT gene silencing and benefit from temozolomide in glioblastoma. N Engl J Med 2005; 352(10): 997-1003.

Heise C, Hermiston T, Johnson L, Brooks G, Sampson-Johannes A, Williams A, Hawkins L and Kirn D. An adenovirus E1A mutant that demonstrates potent and selective systemic anti-tumoral efficacy. Nat Med 2000; 6(10): 1134-9.

Heise C, Sampson-Johannes A, Williams A, McCormick F, Von Hoff DD and Kirn DH. ONYX-015, an E1B gene-attenuated adenovirus, causes tumor-specific cytolysis and antitumoral efficacy that can be augmented by standard chemotherapeutic agents. Nat Med 1997; 3(6): 639-45.

Hirai T, Shirai H, Fujimori H, Okayasu R, Sasai K and Masutani M. Radiosensitization effect of poly(ADP-ribose) polymerase inhibition in cells exposed to low and high liner energy transfer radiation. Cancer Sci 2012; 103(6): 1045-50.

Horwitz MS. Adenovirus immunoregulatory genes and their cellular targets. Virology 2001; 279(1): 1-8.

Hu JC, Coffin RS, Davis CJ, Graham NJ, Groves N, Guest PJ, Harrington KJ, James ND, Love CA, McNeish I, Medley LC, Michael A, Nutting CM, Pandha HS, Shorrock CA, Simpson J, Steiner J, Steven NM, Wright D and Coombes RC. A phase I study of OncoVEXGM-CSF, a second-generation oncolytic herpes simplex virus expressing granulocyte macrophage colony-stimulating factor. Clin Cancer Res 2006; 12(22): 6737-47.

Huang SH, Xiong M, Chen XP, Xiao ZY, Zhao YF and Huang ZY. PJ34, an inhibitor of PARP-1, suppresses cell growth and enhances the suppressive effects of cisplatin in liver cancer cells. Oncol Rep 2008; 20(3): 567-72.

Jagtap P and Szabo C. Poly(ADP-ribose) polymerase and the therapeutic effects of its inhibitors. Nat Rev Drug Discov 2005; 4(5): 421-40.

Jiang H, Gomez-Manzano C, Aoki H, Alonso MM, Kondo S, McCormick F, Xu J, Kondo Y, Bekele BN, Colman H, Lang FF and Fueyo J. Examination of the therapeutic potential of Delta-24-RGD in brain tumor stem cells: role of autophagic cell death. J Natl Cancer Inst 2007; 99(18): 1410-4.

Johnson VL, Ko SC, Holmstrom TH, Eriksson JE and Chow SC. Effector caspases are dispensable for the early nuclear morphological changes during chemical-induced apoptosis. J Cell Sci 2000; 113 (Pt 17): 2941-53.

Kamileri I, Karakasilioti I and Garinis GA. Nucleotide excision repair: new tricks with old bricks. Trends Genet 2012; 28(11): 566-73.

Khodyreva SN, Prasad R, Ilina ES, Sukhanova MV, Kutuzov MM, Liu Y, Hou EW, Wilson SH and Lavrik OI. Apurinic/apyrimidinic (AP) site recognition by the 5'-dRP/AP lyase in poly(ADP-ribose) polymerase-1 (PARP-1). Proc Natl Acad Sci U S A 2010; 107(51): 22090-5.

Khuri FR, Nemunaitis J, Ganly I, Arseneau J, Tannock IF, Romel L, Gore M, Ironside J, MacDougall RH, Heise C, Randlev B, Gillenwater AM, Bruso P, Kaye SB, Hong WK and Kirn DH. a controlled trial of intratumoral ONYX-015, a selectively-replicating adenovirus, in combination with cisplatin and 5-fluorouracil in patients with recurrent head and neck cancer. Nat Med 2000; 6(8): 879-85.

Kim JH, Oh JY, Park BH, Lee DE, Kim JS, Park HE, Roh MS, Je JE, Yoon JH, Thorne SH, Kirn D and Hwang TH. Systemic armed oncolytic and immunologic therapy for cancer with JX-594, a targeted poxvirus expressing GM-CSF. Mol Ther 2006; 14(3): 361-70.

Kim KH, Ryan MJ, Estep JE, Miniard BM, Rudge TL, Peggins JO, Broadt TL, Wang M, Preuss MA, Siegal GP, Hemminki A, Harris RD, Aurigemma R,

Curiel DT and Alvarez RD. A new generation of serotype chimeric infectivity-enhanced conditionally replicative adenovirals: the safety profile of ad5/3-Delta24 in advance of a phase I clinical trial in ovarian cancer patients. Hum Gene Ther 2011; 22(7): 821-8.

Kim S, Yazici YD, Calzada G, Wang ZY, Younes MN, Jasser SA, El-Naggar AK and Myers JN. Sorafenib inhibits the angiogenesis and growth of orthotopic anaplastic thyroid carcinoma xenografts in nude mice. Mol Cancer Ther 2007; 6(6): 1785-92.

Kimball KJ, Preuss MA, Barnes MN, Wang M, Siegal GP, Wan W, Kuo H, Saddekni S, Stockard CR, Grizzle WE, Harris RD, Aurigemma R, Curiel DT and Alvarez RD. A phase I study of a tropism-modified conditionally replicative adenovirus for recurrent malignant gynecologic diseases. Clin Cancer Res 2010; 16(21): 5277-87.

Kirn D. Clinical research results with dl1520 (Onyx-015), a replication-selective adenovirus for the treatment of cancer: what have we learned? Gene Ther 2001; 8(2): 89-98.

Kortmann U, McAlpine JN, Xue H, Guan J, Ha G, Tully S, Shafait S, Lau A, Cranston AN, O'Connor MJ, Huntsman DG, Wang Y and Gilks CB. Tumor growth inhibition by olaparib in BRCA2 germline-mutated patient-derived ovarian cancer tissue xenografts. Clin Cancer Res 2011; 17(4): 783-91.

Kraus WL. New functions for an ancient domain. Nat Struct Mol Biol 2009; 16(9): 904-7.

Kueberuwa G, Cawood R and Seymour LW. Blood compatibility of enveloped viruses. Curr Opin Mol Ther 2010; 12(4): 412-20.

Kunkel TA and Erie DA. DNA mismatch repair. Annu Rev Biochem 2005; 74: 681-710.

Lakdawala SS, Schwartz RA, Ferenchak K, Carson CT, McSharry BP, Wilkinson GW and Weitzman MD. Differential requirements of the C terminus of Nbs1 in suppressing adenovirus DNA replication and promoting concatemer formation. J Virol 2008; 82(17): 8362-72.

Leppard KN and Everett RD. The adenovirus type 5 E1b 55K and E4 Orf3 proteins associate in infected cells and affect ND10 components. J Gen Virol 1999; 80 (Pt 4): 997-1008.

Libertini S, Abagnale A, Passaro C, Botta G, Barbato S, Chieffi P and Portella G. AZD1152 negatively affects the growth of anaplastic thyroid carcinoma

cells and enhances the effects of oncolytic virus dl922-947. Endocr Relat Cancer 2011; 18(1): 129-41.

Libertini S, Iacuzzo I, Ferraro A, Vitale M, Bifulco M, Fusco A and Portella G. Lovastatin enhances the replication of the oncolytic adenovirus dl1520 and its antineoplastic activity against anaplastic thyroid carcinoma cells. Endocrinology 2007; 148(11): 5186-94.

Libertini S, Iacuzzo I, Perruolo G, Scala S, Ierano C, Franco R, Hallden G and Portella G. Bevacizumab increases viral distribution in human anaplastic thyroid carcinoma xenografts and enhances the effects of E1A-defective adenovirus dl922-947. Clin Cancer Res 2008; 14(20): 6505-14.

Lieber MR. The mechanism of double-strand DNA break repair by the nonhomologous DNA end-joining pathway. Annu Rev Biochem 2010; 79: 181-211.

Lim DS, Kim ST, Xu B, Maser RS, Lin J, Petrini JH and Kastan MB. ATM phosphorylates p95/nbs1 in an S-phase checkpoint pathway. Nature 2000; 404(6778): 613-7.

Lin SF, Gao SP, Price DL, Li S, Chou TC, Singh P, Huang YY, Fong Y and Wong RJ. Synergy of a herpes oncolytic virus and paclitaxel for anaplastic thyroid cancer. Clin Cancer Res 2008; 14(5): 1519-28.

Lin SF, Yu Z, Riedl C, Woo Y, Zhang Q, Yu YA, Timiryasova T, Chen N, Shah JP, Szalay AA, Fong Y and Wong RJ. Treatment of anaplastic thyroid carcinoma in vitro with a mutant vaccinia virus. Surgery 2007; 142(6): 976-83; discussion 76-83.

Lindahl T. Instability and decay of the primary structure of DNA. Nature 1993; 362(6422): 709-15.

Liu H, Naismith JH and Hay RT. Adenovirus DNA replication. Curr Top Microbiol Immunol 2003; 272: 131-64.

Liu TC, Galanis E and Kirn D. Clinical trial results with oncolytic virotherapy: a century of promise, a decade of progress. Nat Clin Pract Oncol 2007; 4(2): 101-17.

Liu Y, Shevchenko A, Shevchenko A and Berk AJ. Adenovirus exploits the cellular aggresome response to accelerate inactivation of the MRN complex. J Virol 2005; 79(22): 14004-16.

Lockley M, Fernandez M, Wang Y, Li NF, Conroy S, Lemoine N and McNeish I. Activity of the adenoviral E1A deletion mutant dl922-947 in

ovarian cancer: comparison with E1A wild-type viruses, bioluminescence monitoring, and intraperitoneal delivery in icodextrin. Cancer Res 2006; 66(2): 989-98.

Lombard DB and Guarente L. Nijmegen breakage syndrome disease protein and MRE11 at PML nuclear bodies and meiotic telomeres. Cancer Res 2000; 60(9): 2331-4.

Machida YJ and Dutta A. Cellular checkpoint mechanisms monitoring proper initiation of DNA replication. J Biol Chem 2005; 280(8): 6253-6.

Madhusudan S and Hickson ID. DNA repair inhibition: a selective tumour targeting strategy. Trends Mol Med 2005; 11(11): 503-11.

Manke IA, Lowery DM, Nguyen A and Yaffe MB. BRCT repeats as phosphopeptide-binding modules involved in protein targeting. Science 2003; 302(5645): 636-9.

Markert JM, Medlock MD, Rabkin SD, Gillespie GY, Todo T, Hunter WD, Palmer CA, Feigenbaum F, Tornatore C, Tufaro F and Martuza RL. Conditionally replicating herpes simplex virus mutant, G207 for the treatment of malignant glioma: results of a phase I trial. Gene Ther 2000; 7(10): 867-74.

Martin SA, Lord CJ and Ashworth A. Therapeutic targeting of the DNA mismatch repair pathway. Clin Cancer Res 2010; 16(21): 5107-13.

Martinou JC and Green DR. Breaking the mitochondrial barrier. Nat Rev Mol Cell Biol 2001; 2(1): 63-7.

Maya R, Balass M, Kim ST, Shkedy D, Leal JF, Shifman O, Moas M, Buschmann T, Ronai Z, Shiloh Y, Kastan MB, Katzir E and Oren M. ATM-dependent phosphorylation of Mdm2 on serine 395: role in p53 activation by DNA damage. Genes Dev 2001; 15(9): 1067-77.

McCabe N, Turner NC, Lord CJ, Kluzek K, Bialkowska A, Swift S, Giavara S, O'Connor MJ, Tutt AN, Zdzienicka MZ, Smith GC and Ashworth A. Deficiency in the repair of DNA damage by homologous recombination and sensitivity to poly(ADP-ribose) polymerase inhibition. Cancer Res 2006; 66(16): 8109-15.

Megnin-Chanet F, Bollet MA and Hall J. Targeting poly(ADP-ribose) polymerase activity for cancer therapy. Cell Mol Life Sci 2010; 67(21): 3649-62.

Melo JA, Cohen J and Toczyski DP. Two checkpoint complexes are independently recruited to sites of DNA damage in vivo. Genes Dev 2001; 15(21): 2809-21.

Milam KM and Cleaver JE. Inhibitors of poly(adenosine diphosphate-ribose) synthesis: effect on other metabolic processes. Science 1984; 223(4636): 589-91.

Nagaiah G, Hossain A, Mooney CJ, Parmentier J and Remick SC. Anaplastic thyroid cancer: a review of epidemiology, pathogenesis, and treatment. J Oncol 2011; 2011: 542358.

Nel CJ, van Heerden JA, Goellner JR, Gharib H, McConahey WM, Taylor WF and Grant CS. Anaplastic carcinoma of the thyroid: a clinicopathologic study of 82 cases. Mayo Clin Proc 1985; 60(1): 51-8.

Niida H and Nakanishi M. DNA damage checkpoints in mammals. Mutagenesis 2006; 21(1): 3-9.

Oberg D, Yanover E, Adam V, Sweeney K, Costas C, Lemoine NR and Hallden G. Improved potency and selectivity of an oncolytic E1ACR2 and E1B19K deleted adenoviral mutant in prostate and pancreatic cancers. Clin Cancer Res 2010; 16(2): 541-53.

Pack GT. Note on the experimental use of rabies vaccine for melanomatosis. AMA Arch Derm Syphilol 1950; 62: 694-5.

Parato KA, Senger D, Forsyth PA and Bell JC. Recent progress in the battle between oncolytic viruses and tumours. Nat Rev Cancer 2005; 5(12): 965-76.

Park BH, Hwang T, Liu TC, Sze DY, Kim JS, Kwon HC, Oh SY, Han SY, Yoon JH, Hong SH, Moon A, Speth K, Park C, Ahn YJ, Daneshmand M, Rhee BG, Pinedo HM, Bell JC and Kirn DH. Use of a targeted oncolytic poxvirus, JX-594, in patients with refractory primary or metastatic liver cancer: a phase I trial. Lancet Oncol 2008; 9(6): 533-42.

Patel KN and Shaha AR. Poorly differentiated and anaplastic thyroid cancer. Cancer Control 2006; 13(2): 119-28.

Peralta-Leal A, Rodriguez-Vargas JM, Aguilar-Quesada R, Rodriguez MI, Linares JL, de Almodovar MR and Oliver FJ. PARP inhibitors: new partners in the therapy of cancer and inflammatory diseases. Free Radic Biol Med 2009; 47(1): 13-26.

Pesonen S, Diaconu I, Cerullo V, Escutenaire S, Raki M, Kangasniemi L, Nokisalmi P, Dotti G, Guse K, Laasonen L, Partanen K, Karli E, Haavisto E, Oksanen M, Karioja-Kallio A, Hannuksela P, Holm SL, Kauppinen S, Joensuu T, Kanerva A and Hemminki A. Integrin targeted oncolytic adenoviruses Ad5-D24-RGD and Ad5-RGD-D24-GMCSF for treatment of patients with advanced chemotherapy refractory solid tumors. Int J Cancer 2012; 130(8): 1937-47.

Petermann E, Ziegler M and Oei SL. ATP-dependent selection between single nucleotide and long patch base excision repair. DNA Repair (Amst) 2003; 2(10): 1101-14.

Podtcheko A, Ohtsuru A, Namba H, Saenko V, Starenki D, Palona I, Sedliarou I, Rogounovitch T and Yamashita S. Inhibition of ABL tyrosine kinase potentiates radiation-induced terminal growth arrest in anaplastic thyroid cancer cells. Radiat Res 2006; 165(1): 35-42.

Podtcheko A, Ohtsuru A, Tsuda S, Namba H, Saenko V, Nakashima M, Mitsutake N, Kanda S, Kurebayashi J and Yamashita S. The selective tyrosine kinase inhibitor, STI571, inhibits growth of anaplastic thyroid cancer cells. J Clin Endocrinol Metab 2003; 88(4): 1889-96.

Portella G, Pacelli R, Libertini S, Cella L, Vecchio G, Salvatore M and Fusco A. ONYX-015 enhances radiation-induced death of human anaplastic thyroid carcinoma cells. J Clin Endocrinol Metab 2003; 88(10): 5027-32.

Portella G, Scala S, Vitagliano D, Vecchio G and Fusco A. ONYX-015, an E1B gene-defective adenovirus, induces cell death in human anaplastic thyroid carcinoma cell lines. J Clin Endocrinol Metab 2002; 87(6): 2525-31.

Prakash A, Jayaram S and Bridge E. Differential activation of cellular DNA damage responses by replication-defective and replication-competent adenovirus mutants. J Virol 2012; 86(24): 13324-33.

Prasad R, Lavrik OI, Kim SJ, Kedar P, Yang XP, Vande Berg BJ and Wilson SH. DNA polymerase beta -mediated long patch base excision repair. Poly(ADP-ribose)polymerase-1 stimulates strand displacement DNA synthesis. J Biol Chem 2001; 276(35): 32411-4.

Prives C and Hall PA. The p53 pathway. J Pathol 1999; 187(1): 112-26.

Querido E, Marcellus RC, Lai A, Charbonneau R, Teodoro JG, Ketner G and Branton PE. Regulation of p53 levels by the E1B 55-kilodalton protein and E4orf6 in adenovirus-infected cells. J Virol 1997; 71(5): 3788-98.

Ranki T and Hemminki A. Serotype chimeric human adenoviruses for cancer gene therapy. Viruses 2010; 2(10): 2196-212.

Reddi HV, Madde P, McDonough SJ, Trujillo MA, Morris JC, 3rd, Myers RM, Peng KW, Russell SJ, McIver B and Eberhardt NL. Preclinical efficacy of the oncolytic measles virus expressing the sodium iodide symporter in iodine non-avid anaplastic thyroid cancer: a novel therapeutic agent allowing noninvasive imaging and radioiodine therapy. Cancer Gene Ther 2012; 19(9): 659-65.

Reddi HV, Madde P, Reichert-Eberhardt AJ, Galanis EC, Copland JA, McIver B, Grebe SK and Eberhardt NL. ONYX-411, a conditionally replicative oncolytic adenovirus, induces cell death in anaplastic thyroid carcinoma cell lines and suppresses the growth of xenograft tumors in nude mice. Cancer Gene Ther 2008; 15(11): 750-7.

Reid TR, Freeman S, Post L, McCormick F and Sze DY. Effects of Onyx-015 among metastatic colorectal cancer patients that have failed prior treatment with 5-FU/leucovorin. Cancer Gene Ther 2005; 12(8): 673-81.

Robertson AB, Klungland A, Rognes T and Leiros I. DNA repair in mammalian cells: Base excision repair: the long and short of it. Cell Mol Life Sci 2009; 66(6): 981-93.

Rogakou EP, Pilch DR, Orr AH, Ivanova VS and Bonner WM. DNA double-stranded breaks induce histone H2AX phosphorylation on serine 139. J Biol Chem 1998; 273(10): 5858-68.

Rottenberg S, Jaspers JE, Kersbergen A, van der Burg E, Nygren AO, Zander SA, Derksen PW, de Bruin M, Zevenhoven J, Lau A, Boulter R, Cranston A, O'Connor MJ, Martin NM, Borst P and Jonkers J. High sensitivity of BRCA1-deficient mammary tumors to the PARP inhibitor AZD2281 alone and in combination with platinum drugs. Proc Natl Acad Sci U S A 2008; 105(44): 17079-84.

Rouleau M, Patel A, Hendzel MJ, Kaufmann SH and Poirier GG. PARP inhibition: PARP1 and beyond. Nat Rev Cancer 2010; 10(4): 293-301.

Russell SJ, Peng KW and Bell JC. Oncolytic virotherapy. Nat Biotechnol 2012; 30(7): 658-70.

Russo AL, Kwon HC, Burgan WE, Carter D, Beam K, Weizheng X, Zhang J, Slusher BS, Chakravarti A, Tofilon PJ and Camphausen K. In vitro and in vivo radiosensitization of glioblastoma cells by the poly (ADP-ribose) polymerase inhibitor E7016. Clin Cancer Res 2009; 15(2): 607-12.

Sandhu SK, Yap TA and de Bono JS. Poly(ADP-ribose) polymerase inhibitors in cancer treatment: a clinical perspective. Eur J Cancer 2010; 46(1): 9-20.

Schreiber V, Ame JC, Dolle P, Schultz I, Rinaldi B, Fraulob V, Menissier-de Murcia J and de Murcia G. Poly(ADP-ribose) polymerase-2 (PARP-2) is required for efficient base excision DNA repair in association with PARP-1 and XRCC1. J Biol Chem 2002; 277(25): 23028-36.

Schreiber V, Dantzer F, Ame JC and de Murcia G. Poly(ADP-ribose): novel functions for an old molecule. Nat Rev Mol Cell Biol 2006; 7(7): 517-28.

Schweppe RE, Klopper JP, Korch C, Pugazhenthi U, Benezra M, Knauf JA, Fagin JA, Marlow LA, Copland JA, Smallridge RC and Haugen BR. Deoxyribonucleic acid profiling analysis of 40 human thyroid cancer cell lines reveals cross-contamination resulting in cell line redundancy and misidentification. J Clin Endocrinol Metab 2008; 93(11): 4331-41.

Senra JM, Telfer BA, Cherry KE, McCrudden CM, Hirst DG, O'Connor MJ, Wedge SR and Stratford IJ. Inhibition of PARP-1 by olaparib (AZD2281) increases the radiosensitivity of a lung tumor xenograft. Mol Cancer Ther 2011; 10(10): 1949-58.

Shaheen M, Allen C, Nickoloff JA and Hromas R. Synthetic lethality: exploiting the addiction of cancer to DNA repair. Blood 2011; 117(23): 6074-82.

Shenk T. Adenoviridae: the viruses and their replication. Philadelphia: Lippincott-Raven; 1996.

Sherr CJ and McCormick F. The RB and p53 pathways in cancer. Cancer Cell 2002; 2(2): 103-12.

Shieh WM, Ame JC, Wilson MV, Wang ZQ, Koh DW, Jacobson MK and Jacobson EL. Poly(ADP-ribose) polymerase null mouse cells synthesize ADP-ribose polymers. J Biol Chem 1998; 273(46): 30069-72.

Sinkovics JG and Horvath JC. Newcastle disease virus (NDV): brief history of its oncolytic strains. J Clin Virol 2000; 16(1): 1-15.

Sirena D, Lilienfeld B, Eisenhut M, Kalin S, Boucke K, Beerli RR, Vogt L, Ruedl C, Bachmann MF, Greber UF and Hemmi S. The human membrane cofactor CD46 is a receptor for species B adenovirus serotype 3. J Virol 2004; 78(9): 4454-62.

Small EJ, Carducci MA, Burke JM, Rodriguez R, Fong L, van Ummersen L, Yu DC, Aimi J, Ando D, Working P, Kirn D and Wilding G. A phase I trial

of intravenous CG7870, a replication-selective, prostate-specific antigen-targeted oncolytic adenovirus, for the treatment of hormone-refractory, metastatic prostate cancer. Mol Ther 2006; 14(1): 107-17.

Smith J, Tho LM, Xu N and Gillespie DA. The ATM-Chk2 and ATR-Chk1 pathways in DNA damage signaling and cancer. Adv Cancer Res 2010; 108: 73-112.

Southam CM, Hilleman MR and Werner JH. Pathogenicity and oncolytic capacity of RI virus strain RI-67 in man. J Lab Clin Med 1956; 47(4): 573-82.

Southam CM and Moore AE. Clinical studies of viruses as antineoplastic agents with particular reference to Egypt 101 virus. Cancer 1952; 5(5): 1025-34.

Stracker TH, Carson CT and Weitzman MD. Adenovirus oncoproteins inactivate the Mre11-Rad50-NBS1 DNA repair complex. Nature 2002; 418(6895): 348-52.

Stracker TH, Lee DV, Carson CT, Araujo FD, Ornelles DA and Weitzman MD. Serotype-specific reorganization of the Mre11 complex by adenoviral E4orf3 proteins. J Virol 2005; 79(11): 6664-73.

Street CA and Bryan BA. Rho kinase proteins--pleiotropic modulators of cell survival and apoptosis. Anticancer Res 2011; 31(11): 3645-57.

Takai H, Naka K, Okada Y, Watanabe M, Harada N, Saito S, Anderson CW, Appella E, Nakanishi M, Suzuki H, Nagashima K, Sawa H, Ikeda K and Motoyama N. Chk2-deficient mice exhibit radioresistance and defective p53-mediated transcription. EMBO J 2002; 21(19): 5195-205.

Tallarida RJ. Drug synergism: its detection and applications. J Pharmacol Exp Ther 2001; 298(3): 865-72.

Tauber B and Dobner T. Adenovirus early E4 genes in viral oncogenesis. Oncogene 2001; 20(54): 7847-54.

Turnell AS and Grand RJ. DNA viruses and the cellular DNA-damage response. J Gen Virol 2012; 93(Pt 10): 2076-97.

Underhill C, Toulmonde M and Bonnefoi H. A review of PARP inhibitors: from bench to bedside. Ann Oncol 2011; 22(2): 268-79.

Vichai V and Kirtikara K. Sulforhodamine B colorimetric assay for cytotoxicity screening. Nat Protoc 2006; 1(3): 1112-6.

Waehler R, Russell SJ and Curiel DT. Engineering targeted viral vectors for gene therapy. Nat Rev Genet 2007; 8(8): 573-87.

Ward IM and Chen J. Histone H2AX is phosphorylated in an ATR-dependent manner in response to replicational stress. J Biol Chem 2001; 276(51): 47759-62.

Waterhouse NJ, Ricci JE and Green DR. And all of a sudden it's over: mitochondrial outer-membrane permeabilization in apoptosis. Biochimie 2002; 84(2-3): 113-21.

Weiden MD and Ginsberg HS. Deletion of the E4 region of the genome produces adenovirus DNA concatemers. Proc Natl Acad Sci U S A 1994; 91(1): 153-7.

White E. Mechanisms of apoptosis regulation by viral oncogenes in infection and tumorigenesis. Cell Death Differ 2006; 13(8): 1371-7.

White E. Regulation of the cell cycle and apoptosis by the oncogenes of adenovirus. Oncogene 2001; 20(54): 7836-46.

Wickman G, Julian L and Olson MF. How apoptotic cells aid in the removal of their own cold dead bodies. Cell Death Differ 2012; 19(5): 735-42.

Xia ZJ, Chang JH, Zhang L, Jiang WQ, Guan ZZ, Liu JW, Zhang Y, Hu XH, Wu GH, Wang HQ, Chen ZC, Chen JC, Zhou QH, Lu JW, Fan QX, Huang JJ and Zheng X. [Phase III randomized clinical trial of intratumoral injection of E1B gene-deleted adenovirus (H101) combined with cisplatin-based chemotherapy in treating squamous cell cancer of head and neck or esophagus]. Ai Zheng 2004; 23(12): 1666-70.

Xu RH, Yuan ZY, Guan ZZ, Cao Y, Wang HQ, Hu XH, Feng JF, Zhang Y, Li F, Chen ZT, Wang JJ, Huang JJ, Zhou QH and Song ST. [Phase II clinical study of intratumoral H101, an E1B deleted adenovirus, in combination with chemotherapy in patients with cancer]. Ai Zheng 2003; 22(12): 1307-10.

Yew PR and Berk AJ. Inhibition of p53 transactivation required for transformation by adenovirus early 1B protein. Nature 1992; 357(6373): 82-5.

Yong RL, Shinojima N, Fueyo J, Gumin J, Vecil GG, Marini FC, Bogler O, Andreeff M and Lang FF. Human bone marrow-derived mesenchymal stem cells for intravascular delivery of oncolytic adenovirus Delta24-RGD to human gliomas. Cancer Res 2009; 69(23): 8932-40.

Yu W and Fang H. Clinical trials with oncolytic adenovirus in China. Curr Cancer Drug Targets 2007; 7(2): 141-8.

Ionizing radiation enhances dl922-947-mediated cell death of Anaplastic Thyroid Carcinoma cells

Journal:	*Endocrine-Related Cancer*
Manuscript ID:	ERC-13-0001.R1
Manuscript Type:	Research Paper
Date Submitted by the Author:	n/a
Complete List of Authors:	Passaro, Carmela; Università degli Studi di Napoli "Federico II", Dipartimento di Biologia e Patologia Cellulare e Molecolare Abagnale, Antonella; Università degli Studi di Napoli "Federico II", Dipartimento di Biologia e Patologia Cellulare e Molecolare Libertini, Silvana; The Beatson Institute for Cancer Research, The Beatson Institute for Cancer Research Volpe, Massimiliano; Università degli Studi di Napoli "Federico II", Dipartimento di Biologia e Patologia Cellulare e Molecolare Botta, Ginevra; Università degli Studi di Napoli "Federico II", Dipartimento di Biologia e Patologia Cellulare e Molecolare Cella, Laura; Consiglio Nazionale delle Ricerche, Istituto di Biostrutture e Bioimmagini Pacelli, Roberto; Università degli Studi di Napoli "Federico II", Dipartimento di Diagnostica per Immagini e Radioterapia Halldèn, Gunnel; Queen Mary University of London, Centre for Molecular Oncology, Barts Cancer Institute Gillespie, David; The Beatson Institute for Cancer Research, The Beatson Institute for Cancer Research Portella, Giuseppe; Università di Napoli Ferdico II, Dipartimento di Biologia e Patologia Cellulare
Keywords:	Radiotherapy, Thyroid, Gene therapy

Ionizing radiation enhances *dl*922-947-mediated cell death of Anaplastic Thyroid Carcinoma cells

Carmela Passaro[1*], Antonella Abagnale[1*], Silvana Libertini[2], Massimiliano Volpe[1], Ginevra Botta[1#], Laura Cella[3], Roberto Pacelli[4], Gunnel Halldèn[5], David Gillespie[2], and Giuseppe Portella[1,§]

[1]Dipartimento di Biologia e Patologia Cellulare e Molecolare Università Federico II, Napoli, Italy.
[2]The Beatson Institute for Cancer Research, Switchback Road, Bearsden, Glasgow, G61 1BD, UK.
[3]Istituto di Biostrutture e Bioimmagini, Consiglio Nazionale delle Ricerche, Napoli, Italy
[4]Dipartimento di Diagnostica per Immagini e Radioterapia, Università Federico II, Napoli, Italy
[5]Centre for Molecular Oncology, Barts Cancer Institute, Queen Mary University of London, London, UK.

(*equal contribution)

Running Title: *dl922-947* and ionizing radiation

[#]present address: Department of Medical Oncology, Dana-Farber Cancer Institute, 450 Brookline Ave Boston, MA 02215, USA.

Key words: anaplastic thyroid carcinoma, oncolytic virus, irradiation, DNA damage

[§] Corresponding author: Giuseppe Portella,

Dipartimento di Biologia e Patologia Cellulare e Molecolare, Facoltà di Medicina e

Chirurgia, Università di Napoli Federico II,

via S. Pansini 5, 80131 Napoli, Italy.

Tel: ++39 081 7463056; Fax: 39 081 7463037; e-mail: portella@unina.it

Abstract

dl922-947 is an oncolytic adenovirus potentially suitable for the treatment of aggressive localized tumours, such as Anaplastic Thyroid Carcinoma (ATC).

In the present study, we have analyzed the effects of *dl*922-947 in combination with ionizing radiations, testing different schedules of administration and observing synergistic cell killing only when ATC cells were irradiated 24 hours prior to viral infection. Cell cycle analysis indicates that irradiation blocks ATC cells in a more permissive state (G2) for viral infection. Cells undergoing combined irradiation and infection treatment exhibit a marked increase in apoptotic cell death as quantified by annexinV staining and caspase 3 cleavage, indicating that enhanced apoptosis contributes to synergistic cell killing.

We also show that *dl922-947* triggers a DNA damage response, characterized by mobilization of the MRN complex, accumulation of γH2AX, and activation of the checkpoint kinases ATM and Chk1. Based on these observations we speculate that the DNA damage response acts as cellular protective mechanism to hinder viral infection and replication. To confirm this hypothesis, we demonstrate that the ATM inhibitor KU55933 increased the oncolytic activity of *dl922-947* and its replication.

Finally, we validate the potential therapeutic utility of this approach by showing that the combined treatment slows tumour xenograft growth more potently than either irradiation or infection alone *in vivo*.

Introduction

Anaplastic Thyroid Carcinoma (ATC) represents one of the most aggressive human malignancies. It arises from thyroid follicular cells showing morphological features of a malignant neoplasm, high proliferation rate and marked aneuploidy. The median survival of patients with ATC is ~6 months from diagnosis. Multimodality therapy, which includes surgical debulking, external radiation therapy and chemotherapy, has failed to show any improvements in survival and ATC still remains a formidable medical challenge (Ain 2000; Smallridge, et al. 2009). Therefore, novel therapies with different mechanisms of action are required.

Oncolytic viruses (OVs) are replication competent viral mutants able to complete their life cycle exclusively in tumour cells. With respect to classical anti-cancer drugs, OVs present several advantages: tumour-selective replication with amplification of the input dose, stimulation of anti-tumoural immune responses, and relatively few mild side effects when administered to human patients. Also, the development of cross resistance is unlikely since their mechanism of action is independent of conventional anti-cancer therapeutics (Eager and Nemunaitis 2011; Hallden and Portella 2012).

A number of oncolytic viruses, such as the vaccinia virus GLV-1h68 (Lin, et al. 2008b) and the oncolytic attenuated herpes virus G207 (Lin, et al. 2008a), have shown promising effects against ATC cells in preclinical studies.

We have previously demonstrated that the oncolytic adenoviruses *dl*1520 and *dl*922-947 could be useful for the therapy of ATC (Libertini, et al. 2011; Libertini, et al. 2007; Libertini, et al. 2008; Portella, et al. 2003; Portella, et al. 2002). *dl*1520, bearing a E1B 55K deletion, is the first mutant engineered for tumour specific cytolysis (Heise, et al. 1997). Since its replication is severely attenuated not only in normal cells but also in the majority of cancers (O'Shea, et al. 2004), *dl*1520 has shown limited utility as single agent. Hence, novel and more effective oncolytic viruses have been engineered. *dl*922-947 is a second generation adenoviral mutant bearing a 24-bp deletion in E1A-Conserved Region 2 (CR2) (Heise, et al. 2000a). This region binds to and inactivates the pRb tumour suppressor protein, dissociating the pRb-E2F complex and driving S-phase entry and viral replication. Because the mutant E1A protein encoded by *dl922-947* cannot bind pRb the virus is unable to trigger S-phase entry in normal cells and can therefore only replicate in cells with an aberrant G1-S checkpoint, a defect observed in over 90% human cancers (Sherr and McCormick 2002). Superior cell killing potency of *dl*922–947 with respect to *dl*1520 has been observed *in vitro* and *in vivo* in human cancer cells of different origin such as pancreas (Bhattacharyya, et al. 2011),

prostate (Radhakrishnan, et al. 2010), ovarian (Lockley, et al. 2006), thyroid (Libertini et al. 2008), and brain (Botta, et al. 2012; Botta, et al. 2010; Yong, et al. 2009). In addition other mutants with E1ACR2-region deletion have proved effective in experimental models (Jiang, et al. 2009; Oberg, et al. 2010).

Emerging evidences indicate that combining oncolytic viruses with standard chemotherapy and other types of anticancer treatments has the potential to increase the antitumor activity (Cheong, et al. 2008; Heise, et al. 2000b).

It has been clearly shown in preclinical and clinical studies that OVs and radiation therapy show additional or synergistic antitumour effects. Phase I and II/III clinical trials with replication competent oncolytic viruses have been completed (Immonen, et al. 2004; Touchefeu, et al. 2011). Despite the encouraging results obtained with such combined treatment modalities, relatively little is known about the mechanisms that result in enhanced tumour cell death. Understanding the mechanisms that underlie synergistic cell killing could enable further optimization of this strategy for future clinical development.

Ionising radiation is known to induce DNA damage and a subsequent block of the cell cycle progression with accumulation of cells either in G1 or G2, depending on the integrity of cell cycle checkpoints. After DNA repair, these cell cycle checkpoint arrests are released. It has been reported that drugs that block cells in G2/M or inhibit cytokinesis can enhance oncolytic viruses-mediated cell killing (Seidman, et al. 2001). For example, we recently demonstrated that the cytopathic effects of *dl*922-947 are enhanced by the Aurora B inhibitor AZD1152, which induces mitotic arrest, accumulation in G2/M phase and polyploidy (Libertini et al. 2011).

Here, we have evaluated the effect of *dl*922-947 in association with ionising radiation (IR) showing that the combination enhances the effect of *dl*922-947 against ATC cells *in vitro*. Comparing different schedules of treatment (virus administered before or after irradiation), we observed synergistic cell killing only when irradiation is administered prior to viral infection. The efficacy of the optimal combined treatment has been also confirmed in ATC tumour xenografts *in vivo*.

Material and Methods

Cells, adenoviruses and drugs

Human thyroid anaplastic carcinoma cell lines BHT101-5 and FRO have been described and authenticated as shown elsewhere (Schweppe, et al. 2008). *dl*922-947 and AdGFP viral stocks were expanded in the human embryonic kidney cell line HEK-293, purified and stored as previously reported (Libertini et al. 2007). Viral stocks were expanded, purified, stored and quantified as previously reported (Botta et al. 2010).

Cytotoxicity assay

Cytotoxicity was evaluated using the sulforhodamine B assay as previously described (Seidman et al. 2001). Dose–response curves were generated to calculate the concentration of each agent required to kill 50% of cells (median lethal dose, LD_{50}). Untreated cells or cells treated with single agents were used as a control.

Viral replication

FRO and BHT101-5 cells were infected with *dl*922-947, media collected 48 hpi (hours post infection) and viral DNA extracted using the High pure viral nucleic acid kit (Roche Diagnostics, Indianapolis, IN, USA). Specific primers for the viral hexon gene (from 99 to 242 bp) were used to measure viral replication by Real-Time PCR: 5'-GCC ACC GAG ACG TAC TTC AGC CTG-3' (upstream primer) and 5'TTG TAC GAG TAC GCG GTA TCC TCC GCG GTC-3' (downstream primer). A standard curve was constructed by assaying serial dilutions of *dl*922-947.

FACS analysis

Cell cycle: FRO and BHT101-5 cells treated as indicated were detached and fixed in 70% (v/v) ethanol for at least 1 hour at -20°C. Washed pellets were resuspended in PBS containing RNaseA (Roche, Indianapolis, IN, USA) (0.4 U) and propidium iodide (SIGMA, St. Louis, MO, USA) (0.015 mol l^{-1}), incubated for 20' at room temperature, and analyzed for emission in the FL3 channel. To remove artifacts—doublets and aggregates—from the analysis, an electronic doublet discrimination was performed using the area and width of the fluorescence (FL3) pulse.

AdGFP infection: FRO and BHT101-5 cells were infected with AdGFP (25 MOIs) and harvested 48 hours later. Pellet was resuspend in PBS and emission in the FL1 channel analysed.

Annexin V/PI staining: Attached and detached FRO and BHT101-5 cells were collected and washed with Annexin V binding buffer (Biolegend, San Diego, CA, USA). Pellet was resuspended in 50µl

of Annexin V binding buffer containing 2 µl of FITC-conjugated Annexin V (Biolegend #640906, San Diego, CA, USA). After 15' incubation at room temperature, 250µl of propidium iodide solution 0.0015 mol l^{-1} in PBS was added to each sample just before analysis.

γH2AX/PI staining: FRO cells were detached and fixed in 70% (v/v) ethanol for 2 hours at -20°C. Pellet was washed with PBT (0.5% w/v BSA, 0.1% v/v Tween20 in PBS) and resuspended in PBT containing γH2AX antibody (Millipore #05-636, 1:100, Billerica, MA, USA). After 1 h incubation at room temperature, samples were washed in PBT and then resuspended in PBT containing Alexa488 anti-mouse (Invitrogen #A11001, 1:100, Carlsbad, CA, USA) at dark. After further 30 minutes, cells were washed with PBT and resuspended in PI 0.015 mol l^{-1} for 20' and analyzed for the emission in FL1 and FL3 channels.

All samples were acquired with a BD LSRFortessa (BD Biosciences, San Jose, CA, USA) and analysed using BD FACSDiva Software.

Protein extraction and Western blot analysis

After the indicated treatments, attached and detached cells were harvested and lysates prepared as already described (Botta et al. 2010). 50 µg of lysate proteins were probed with the following antibodies: caspase 3 (Abcam #Ab13585, 1:500, Cambridge, UK), p-ATM s1981 (Cell Signaling, #4526, 1:1000, Boston, MA, USA), p-chk1 s345 (Cell Signaling, #2348, 1:1000, Boston, MA, USA), MRE11 (SantaCruz #sc-5859, 1:1000, Santa Cruz, CA, USA) and α-tubulin (SIGMA #T9026, 1:5000, St. Louis, MO, USA).

Tumorigenicity assay

FRO cells ($1x10^6$) were injected into the right flank of 80 athymic mice. After 30 days, tumour volume was evaluated and the animals were divided into four groups (20 animals/group) with similar average tumour size. At day 0, a single radiation dose of 10 Gy was administered on the tumour volume at a distance of 80 cm with a bolus interposition to avoid lower doses at the tumor external edge. *dl*922-947 ($2x10^6$ MOIs) was injected in the peritumoural area administered three times per week by intratumoural injection to avoid first pass effect in two groups. The control group was injected with saline solution.

Tumour diameters were measured with caliber and tumour volumes (V) were calculated by the formula of rotational ellipsoid: $V=AxB^2/2$ (A=axial diameter, B=rotational diameter).

Mice were maintained at the Dipartimento di Biologia e Patologia Cellulare e Molecolare Animal Facility. All animal experiments were conducted in accordance with accepted standards of animal

care and in accordance with the Italian regulations for the welfare of animals used in studies of experimental neoplasia. Study was approved by our institutional committee on animal care.

Statistical analysis

The analysis of the cytotoxic effect *in vitro* was made by isobolograms generated to calculate the combination index.

Comparisons among different treatment groups in the experiments *in vivo* were made by the ANOVA method and the Bonferroni post hoc test using commercial software (GraphPad Prism 4). Assessment of differences among rate of tumour growth in mice was made for each time point of the observation period.

Results

Effects of ionising radiation on dl922-947

To determine whether Ionizing Radiation (IR) could enhance the oncolytic activity of the mutant adenovirus *dl*922-947, anaplastic thyroid carcinoma cell lines FRO and BHT101-5 were infected and irradiated. To identify most appropriate treatment sequence, FRO and BHT101-5 cells were infected and then irradiated after 24 hours or *vice versa.* Cell survival was evaluated seven days after infection.

Combination index showed a potent, statistically significant synergy of cell killing in BHT101-5 cells at all combinations when cells were infected 24h after irradiation. In FRO cells using the same treatment schedule, a statistically significant synergy was observed in two combinations (2Gy plus 7.5 MOIs and 4 Gy plus 5 MOIs) whereas treating FRO cells with 8 Gy and 2 MOIs an additive effect was observed (Fig 1A upper panel).

In contrast, an antagonist effect was observed in FRO cells when infection was followed by irradiation, whereas in BHT101-5 cells only 4 Gy combined with 2.5 multiplicity of infection (MOIs) showed synergy with this schedule (Fig 1A lower panel). These data demonstrate that the cytotoxicity of *dl*922-947 is significantly enhanced when cells are irradiated 24h prior to infection.

Viral entry and viral replication analysis

It has been proposed that radiations could enhance oncolytic activity by increasing viral entry in target cells (Anders, et al. 2003). To monitor this step, FRO and BHT101-5 cells were irradiated and after 24h infected with a non-replicating reporter adenovirus transducing GFP (AdGFP). After additional 48h, GFP emission was evaluated by cytofluorimetric analysis. As shown in Fig.1B, irradiation neither increase the percentage of GFP positive cells nor the average green emission of individual cells, except for the 2Gy sample, where a slight, albeit significant positive shift in the GFP fluorescence was observed in both cell lines.

Next, a Real-Time PCR assay was performed to evaluate viral replication. FRO and BHT101-5 cells were irradiated (2-4-5 Gy) and after 24h infected with different MOIs (1-5-10) of *dl*922-947. After an additional 48h, viral genome copies were evaluated by Real Time PCR. This analysis revealed that IR induced a significant (* $p<0.05$) or highly significant(** $p<0.005$) dose dependent increase of viral replication (Fig 1C).

Analysis of cell cycle profile and cell death

It has been reported that drugs able to block cells in G2/M or inhibit cytokinesis can enhance the effects of oncolytic viruses (Libertini et al. 2011). Irradiation is known to induce a transitory block in G2 phase (Lisby, et al. 2004), therefore we analyzed cell cycle profiles to evaluate differences in cell cycle phases and timing of cell death. FRO and BHT101-5 cells were irradiated (8 Gy) and after 24h infected with 5 MOIs and 1 MOIs of *dl*922-947 respectively. Starting from 6 hpi (hours post infection), cells were collected, stained with propidium iodide and cell cycle analyzed.

In irradiated cells at 6 hours most of the cells were in G2/M phase, this checkpoint arrest facilitates DNA repair and can be observed up to 24h. G2/M accumulation was reversed at 48h after irradiation, when the cell cycle profile again resembled that of untreated cells. *dl*922-947-infected cells also accumulated in G2/M phase at 6 hpi. In contrast to the effect of irradiation alone, at 48hpi most of the cells were either still in G2/M phase or had become polyploid (Fig 2A).

Cells that were irradiated 24h prior to infection accumulated in G2/M phase at 6 hpi and, at 48 hpi the cell cycle profile was similar to infected rather than untreated cells (Fig 2A).

We also observed that cultures that had been irradiated prior to infection exhibited an increased percentage of cells in the subG1 fraction, which is indicative of DNA fragmentation and cell death either by necrosis or apoptosis. To discriminate between the two types of cell death, unfixed cells were stained with propidium iodide (PI) and Annexin V. PI can penetrate only in non-vital cells, whereas Annexin V binds to living cells with exposed phospholipid phosphatidylserine. The exposure of phosphatidylserine is due to the loss of membrane asymmetry and is considered to be an early marker of apoptosis. PI single positivity represents necrosis, single Annexin V staining early apoptosis, double positivity (annexin V and PI) indicates late apoptosis.

At 72 hpi, a strong reduction of the percentage of vital cells (to 19%) was observed in the cultures that had been irradiated prior to infection. 34% of cells remained alive in cultures that had been infected without irradiation, whereas the figure was 70% after irradiation alone, further confirming the efficacy of the combined treatment. An increase in annexin V staining, indicative of apoptosis, was observed in the combined treatment with respect to single treatments. Late stage cell death was also confirmed by double staining for Annexin V and PI or PI only (Fig 2B). Since the increase in annexin V positivity suggested the activation of the apoptotic pathway, we analysed Caspase-3 activation in FRO cells. A decrease of procaspase-3 and an increased activation of caspase 3 was observed in the combined treatment with respect to single treatments (Fig 2C).

DNA damage repair system and dl922-947 infection

IR induces DNA damage and, after its detection, cellular pathways are activated to halt cell cycle progression and repair the damage. Adenoviral replication also induces DNA damage (Touchefeu et al. 2011), therefore we analyzed in FRO cells the effects of viral infection, alone or in combination with radiation, on DNA damage repair system.

The MRN complex (composed by Mre11-Rad50-Nbs1) acts as a Double Strand Breaks (DSBs) sensor. It localizes to DNA breaks and activates the ATM dependent signaling pathway, which coordinates cell cycle arrest and DNA repair (Lavin 2007). Western blot analysis showed a strong reduction of Mre11 levels in infected cells, most probably due to protein degradation. The level of Mre11 was not altered in irradiated cells; however a similar decrease occurred when cells were subject to both irradiation and infection (Fig 3A). Cells treated with virus, alone or in combination with IR, also showed a strong activation of ATM at 24 hpi, whereas irradiated cells showed an earlier activation (1-3 hpi), reversed to basal levels by 24 hpi (Fig 3A).

Activation of the checkpoint kinase Chk1, as judged by phosphorylation on Serine 345 (S345) (Smith, et al. 2010), showed strong activation at early points (1-6 hours) that also declined to control levels by 24 after irradiation. In marked contrast infection with *dl*922-947 induced strong Chk1 S345 phosphorylation 24 hpi both with and without prior irradiation (Fig 3A).

Histone 2A is phosphorylated at serine 139 in response to DNA double-strand breaks, forming γH2AX. γH2AX marks sites of DNA damage recruits proteins involved in DNA repair and is widely accepted as a readout of ATM activation (Touchefeu et al. 2011). After DNA repair, histone H2AX is dephosphorylated. We therefore evaluated γH2AX levels by cytofluorimetric analysis to quantify both the percentage of positive cells (shown in green in Figure 3B) and the mean fluorescence value of the positive population (in red). After irradiation γH2AX levels reached a maximum after 3h and then progressively decline from 6h to 24h post irradiation, confirming that irradiation-induced DNA damage was repaired within this time frame. In infected cells, we observed an increase of γH2AX levels at 6 hpi and by 24 hpi most of the cells showed strong γH2AX positivity, indicating accumulation of DNA damage (Fig 3B). In cells subject to both irradiation and infection, a more rapid increase of γH2AX levels was observed at 6 hpi with respect to single treatments. However, at 24 hpi, γH2AX levels remained high as in cells infected with *dl*922-947 alone.

Pharmacological inhibition of ATM activation and dl922-947 infection

The reduction of Mre11 levels together with ATM phosphorylation suggests that viral genomes are recognized as DNA damage in infected cells and that viral function may target the MRN complex to prevent DNA repair processes interfering with viral replication.

To test whether activation of ATM signaling pathway hampers viral replication, infected cells were treated with a pharmacological inhibitor of ATM: KU55933. The specificity of KU55933 has been demonstrated by the ablation DNA damage-induced phosphorylation of a range of ATM substrates, including p53 and H2AX (Hickson, et al. 2004).

FRO and BHT101-5 cell lines were infected in combination with two different concentrations of the drug (5-10 μM). As shown in Figure 4A, KU55933 treatment potentiates the cytotoxic effects of *dl*922-947. KU55933 treatment alone did not show any cytotoxic effect on both cell lines, therefore combination index was not evaluated.

We also examined the effect of KU55933 on γH2AX formation after infection in FRO cells. As shown in Figure 4B, KU55933 almost completely inhibited the H2AX phosphorylation induced by the virus up to six hours; however after 24h H2AX phosphorylation levels were similar in infected cells with or without KU55933 treatment. This effect can be explained by a rapid drug catabolism, or to the activation of ATM-independent mechanism(s) of H2AX phosphorylation. Similar results were obtained with BHT101-5 cells (not shown).

Genome equivalent copies of *dl*922-947 in cells treated with KU55933 showed that the drug significantly enhanced viral replication in a dose dependent manner (Fig. 4C).

IR increases *dl922-947* oncolytic activity *in vivo*

To evaluate the therapeutic potential of synergism between *dl922-947* and ionising radiation, we analyzed the effects of the combined treatment on xenograft tumours.

Athymic mice were inoculated subcutaneously with FRO cells. Two groups were irradiated with a single radiation dose (10 Gy) on the tumor volume. A low viral dose ($2x10^6$ pfu) was used to better visualize the effects of the combined treatment versus *dl*922-947 infection alone. As shown in Fig. 5, the combined treatment group showed a significant reduction of tumour growth with respect to single treatments and to the untreated group. This difference was first evident by day 11, and by day 21 growth inhibition was highly statistically significant compared to control group (Fig.5).

Discussion

ATC represents one of the most aggressive human malignancies, with a poor prognosis, and its treatment still represents a major challenge (Ain 2000; Smallridge et al. 2009). Currently available treatments are considered palliative because of poor response rates and lack of demonstrable survival benefits, highlighting the need for more effective treatments (Ain 2000; Smallridge et al. 2009; Taccaliti, et al. 2012).

Oncolytic viruses represent a promising approach as anti-cancer therapeutics, however, preclinical and clinical studies have demonstrated limited efficacy of oncolytic viruses alone, prompting effort to combine them with other anti-cancer agents to improve their antitumor effects (Eager and Nemunaitis 2011; Hallden and Portella 2012). We have previously demonstrated that the oncolytic adenoviruses *dl1520* and *dl922-947* are active against ATC *in vitro* and *in vivo*(Libertini et al. 2007; Libertini et al. 2008).

Radiotherapy is frequently used for the treatment of ATC (Taccaliti et al. 2012) and we have also demonstrated that mutated adenovirus *dl*1520, despite its limited efficacy, enhances the effects of IR against ATC cells and xenograft tumours (Portella et al. 2003). Here, we have analyzed the effects of a more potent second generation oncolytic virus, *dl*922-947, in combination with IR. We show that both the cytopathic activity and replication of *dl*922-947 is significantly enhanced by IR.

The potentiating effect of irradiation on the cytopathic potential of oncolytic viruses, other than *dl*922-947, has already been demonstrated. However, optimal strategies for combining these therapeutic modalities still remain to be established as evidence suggests that they interact in complex ways that vary in a cell line- or virus-dependent fashion (Touchefeu et al. 2011). Here we have identified the most effective treatment sequence for ATC cells showing that irradiation prior to *dl*922-947 infection results in enhanced viral replication and synergistic cell killing. Irradiation after viral infection did not show synergistic or even additive effects.

It has been proposed that irradiation can increase viral uptake (Zhang, et al. 2003) either by enhancing CAR (coxsackie and adenovirus receptor) and integrins expression on cell membranes or by modulating the expression of Dynamin 2, an intracellular protein involved in adenoviral internalization (Qian, et al. 2005). In a study using a telomerase specific replication selective adenovirus (OBP-301), viral infection was shown to result in radiosensitivity in A459 small-cell lung cancer cells (Kuroda, et al. 2010). In the same study, a dose dependent increase of adenoviral uptake and coxsackie adenovirus receptor expression was also observed.

By infecting the cells with an AdGFP virus, we evaluated the effects of IR on viral uptake on ATC cells. In contrast to previous studies, we observed only very modest effects of IR on viral uptake. At 2 Gy a small increase was observed, whereas higher radiation doses do not significantly modify viral uptake. Moreover, CAR receptor levels were not modified by IR (data not shown). Differences in treatment sequence, virus and cell lines may explain the discrepancies with other studies.

Despite this, we did observe a significant increase in viral replication in irradiated cells. Existing data regarding the effect of radiation on viral replication are conflicting. Enhanced viral replication following IR has been reported in some studies (Advani, et al. 1998; Bieler, et al. 2008; Liu, et al. 2007), but not in others (Geoerger, et al. 2003; Lamfers, et al. 2002), suggesting that increased viral replication is not an absolute prerequisite for enhanced cell killing (Geoerger et al. 2003; Lamfers et al. 2002).

Subversion of the host cell cycle is an important feature of adenoviral infection. The expression of E1A gene products drives an unscheduled DNA synthesis followed by an abortive cytokinesis, thus inducing G2 accumulation (Davy and Doorbar 2007). The potential benefit of the G2 accumulation is represented by the pseudo S phase which maintains host cells in a replicative state (Davy and Doorbar 2007; Nichols, et al. 2009). It has been proposed that drugs blocking cells in G2 phase could enhance the effects of oncolytic viruses. Indeed, we have demonstrated that the inhibitor of the mitotic kinase Aurora B, AZD1152, enhances the effects of *dl*922-947 by inducing a G2 arrest (Libertini et al. 2011). Accordingly, the accumulation in G2 phase induced by radiation likely enhances the cytopathic effects of *dl*922-947. This hypothesis is further supported by the observation that infection followed by irradiation did not potentiate cell killing or viral replication (data not shown).

We have analyzed the effects of the different treatments, showing an increase of cells in sub G1 phase and a sharp reduction in the number of vital cells subject to irradiation followed by infection compared to either treatment alone. Double staining with Annexin V and propidium iodide confirmed that the combination treatment induces a cell death pathway with features of apoptosis. Irradiation and infection alone also triggered apoptosis, although with lesser efficiency. Activation of an apoptotic like cell death has been previously reported in cells infected by *dl*922-947 (Baird, et al. 2008; Libertini et al. 2011).

It is known that the cells respond to adenovirus infection by activating a classical DNA damage response (Lilley, et al. 2007; Nichols et al. 2009; Touchefeu et al. 2011). It has been proposed that the prolonged S-phase induced by the virus could resemble the cellular environment occurring in response to replication associated DNA damage. Since IR is also known to induce activation of the

DNA damage signaling pathway, we analyzed the effects of the combined treatment on key components of DSB repair signaling pathway.

ATM, ATR and DNA-PK (double strand DNA-activated protein kinase) are considered the initial responders to cellular DNA damage (Botta et al. 2012; Botta et al. 2010; Oberg et al. 2010; Yong et al. 2009), whilst the ultimate step is phosphorylation of histone H2AX leading to recruitment of multiple DNA processing and repair enzymes. In particular the MRN protein complex, composed of Mre11-Rad50-Nbs1, localizes to DNA breaks, contributing to DNA repair.

After the infection with *dl*922-947, a strong reduction of Mre11 protein levels were observed, likely due to degradation induced by viral proteins (Nichols et al. 2009). Infection led to an accumulation of γH2AX positive cells at 24 hpi, indicating the persistence of unrepaired DNA, in agreement with previous studies (Nichols et al. 2009; Touchefeu et al. 2011).

In cells subject to irradiation prior to infection, a similar pattern was observed, although a more rapid increase of γH2AX positive cells at 6 hpi was also seen, probably due to more rapid IR-induced DNA damage combined with that induced by viral infection at later times. Interestingly, it has been proposed that γH2AX could function as a determinant of repair/survival versus apoptotic responses to DNA damage and its increase can correlate with apoptosis in response to DNA damaging agents (Cook, et al. 2009).

ATM and Chk1 activation was observed in infected cells or undergoing the combined treatment. This observation is in contrast with other studies showing no activation of ATM after infection with telomerase driven adenovirus OBP301 (Kuroda et al. 2010). It is possible that *dl*922-947 is not able to fully suppress the early events in DNA damage signaling, as MRN complex degradation may not in itself be sufficient to preclude ATM and ATR kinase activation, as previously reported (Nichols et al. 2009).

It has been hypothesized that cellular DNA repair machinery can function as an obstacle to adenovirus infection. E4orf3 and E4orf6 interact with the adenovirus E1B55K protein forming complexes that degrade or delocalize the MRN complex and interfere with the DNA damage repair system. Therefore, we have hypothesized that a block of DNA damage signaling could enhance the replication and toxicity of *dl*922-947. Indeed, a pharmacological inhibitor of ATM, KU55933, significantly increased the replication and cytopathic potency of *dl*922-947 confirming that the DNA damage response restrains the cell killing of this oncolytic virus.

Finally, we confirmed the therapeutic potential of combining irradiation with *dl*922-947 infection using xenografts formed using ATC cells. Although the subcutaneous implant of neoplastic cells do not fully reproduce the stromal response and the pattern of spread of the neoplastic cells to lymph

nodes and other metastatic sites as in orthotopic models, the data obtained clearly demonstrate the efficacy of the combination therapy *in vivo*.

A majority of patients with ATC die from aggressive local regional disease, primarily from upper airway respiratory obstruction (Taccaliti et al. 2012). For this reason, radiotherapy has been used to control local growth, evolving from palliation on to preoperative or/and postoperative therapy to prolong survival.

Given the importance of radiotherapy in the control of ATC, our results suggest that *dl*922-947 could be combined with this modality in order to improve local control and offer the possibilities of new clinical trials for this intractable disease.

Declaration of interest

The authors declare that there is no conflict of interest that could be perceived as prejudicing the impartiality of the research reported

Funding

This study was supported by the Associazione Italiana per la Ricerca sul Cancro (AIRC). Silvana Libertini is a Marie Curie fellow.

Acknowledgments

We thank Salvatore Sequino for his excellent technical assistance.

References

Advani SJ, Sibley GS, Song PY, Hallahan DE, Kataoka Y, Roizman B & Weichselbaum RR 1998 Enhancement of replication of genetically engineered herpes simplex viruses by ionizing radiation: a new paradigm for destruction of therapeutically intractable tumors. *Gene Ther* **5** 160-165.

Ain KB 2000 Management of undifferentiated thyroid cancer. *Baillieres Best Pract Res Clin Endocrinol Metab* **14** 615-629.

Anders M, Christian C, McMahon M, McCormick F & Korn WM 2003 Inhibition of the Raf/MEK/ERK pathway up-regulates expression of the coxsackievirus and adenovirus receptor in cancer cells. *Cancer Res* **63** 2088-2095.

Baird SK, Aerts JL, Eddaoudi A, Lockley M, Lemoine NR & McNeish IA 2008 Oncolytic adenoviral mutants induce a novel mode of programmed cell death in ovarian cancer. *Oncogene* **27** 3081-3090.

Bhattacharyya M, Francis J, Eddouadi A, Lemoine NR & Hallden G 2011 An oncolytic adenovirus defective in pRb-binding (dl922-947) can efficiently eliminate pancreatic cancer cells and tumors in vivo in combination with 5-FU or gemcitabine. *Cancer Gene Ther* **18** 734-743.

Bieler A, Mantwill K, Holzmuller R, Jurchott K, Kaszubiak A, Stark S, Glockzin G, Lage H, Grosu AL, Gansbacher B, et al. 2008 Impact of radiation therapy on the oncolytic adenovirus dl520: implications on the treatment of glioblastoma. *Radiother Oncol* **86** 419-427.

Botta G, Passaro C, Libertini S, Abagnale A, Barbato S, Maione AS, Hallden G, Beguinot F, Formisano P & Portella G 2012 Inhibition of autophagy enhances the effects of E1A-defective oncolytic adenovirus dl922-947 against glioma cells in vitro and in vivo. *Hum Gene Ther* **23** 623-634.

Botta G, Perruolo G, Libertini S, Cassese A, Abagnale A, Beguinot F, Formisano P & Portella G 2010 PED/PEA-15 modulates coxsackievirus-adenovirus receptor expression and adenoviral infectivity via ERK-mediated signals in glioma cells. *Hum Gene Ther* **21** 1067-1076.

Cheong SC, Wang Y, Meng JH, Hill R, Sweeney K, Kirn D, Lemoine NR & Hallden G 2008 E1A-expressing adenoviral E3B mutants act synergistically with chemotherapeutics in immunocompetent tumor models. *Cancer Gene Ther* **15** 40-50.

Cook PJ, Ju BG, Telese F, Wang X, Glass CK & Rosenfeld MG 2009 Tyrosine dephosphorylation of H2AX modulates apoptosis and survival decisions. *Nature* **458** 591-596.

Davy C & Doorbar J 2007 G2/M cell cycle arrest in the life cycle of viruses. *Virology* **368** 219-226.

Eager RM & Nemunaitis J 2011 Clinical development directions in oncolytic viral therapy. *Cancer Gene Ther* **18** 305-317.

Geoerger B, Grill J, Opolon P, Morizet J, Aubert G, Lecluse Y, van Beusechem VW, Gerritsen WR, Kirn DH & Vassal G 2003 Potentiation of radiation therapy by the oncolytic adenovirus dl1520 (ONYX-015) in human malignant glioma xenografts. *Br J Cancer* **89** 577-584.

Hallden G & Portella G 2012 Oncolytic virotherapy with modified adenoviruses and novel therapeutic targets. *Expert Opin Ther Targets* **16** 945-958.

Heise C, Hermiston T, Johnson L, Brooks G, Sampson-Johannes A, Williams A, Hawkins L & Kirn D 2000a An adenovirus E1A mutant that demonstrates potent and selective systemic anti-tumoral efficacy. *Nat Med* **6** 1134-1139.

Heise C, Lemmon M & Kirn D 2000b Efficacy with a replication-selective adenovirus plus cisplatin-based chemotherapy: dependence on sequencing but not p53 functional status or route of administration. *Clin Cancer Res* **6** 4908-4914.

Heise C, Sampson-Johannes A, Williams A, McCormick F, Von Hoff DD & Kirn DH 1997 ONYX-015, an E1B gene-attenuated adenovirus, causes tumor-specific cytolysis and antitumoral efficacy that can be augmented by standard chemotherapeutic agents. *Nat Med* **3** 639-645.

Hickson I, Zhao Y, Richardson CJ, Green SJ, Martin NM, Orr AI, Reaper PM, Jackson SP, Curtin NJ & Smith GC 2004 Identification and characterization of a novel and specific inhibitor of the ataxia-telangiectasia mutated kinase ATM. *Cancer Res* **64** 9152-9159.

Immonen A, Vapalahti M, Tyynela K, Hurskainen H, Sandmair A, Vanninen R, Langford G, Murray N & Yla-Herttuala S 2004 AdvHSV-tk gene therapy with intravenous ganciclovir improves survival in human malignant glioma: a randomised, controlled study. *Mol Ther* **10** 967-972.

Jiang H, Gomez-Manzano C, Lang FF, Alemany R & Fueyo J 2009 Oncolytic adenovirus: preclinical and clinical studies in patients with human malignant gliomas. *Curr Gene Ther* **9** 422-427.

Kuroda S, Fujiwara T, Shirakawa Y, Yamasaki Y, Yano S, Uno F, Tazawa H, Hashimoto Y, Watanabe Y, Noma K, et al. 2010 Telomerase-dependent oncolytic adenovirus sensitizes human cancer cells to ionizing radiation via inhibition of DNA repair machinery. *Cancer Res* **70** 9339-9348.

Lamfers ML, Grill J, Dirven CM, Van Beusechem VW, Geoerger B, Van Den Berg J, Alemany R, Fueyo J, Curiel DT, Vassal G, et al. 2002 Potential of the conditionally replicative adenovirus Ad5-Delta24RGD in the treatment of malignant gliomas and its enhanced effect with radiotherapy. *Cancer Res* **62** 5736-5742.

Lavin MF 2007 ATM and the Mre11 complex combine to recognize and signal DNA double-strand breaks. *Oncogene* **26** 7749-7758.

Libertini S, Abagnale A, Passaro C, Botta G, Barbato S, Chieffi P & Portella G 2011 AZD1152 negatively affects the growth of anaplastic thyroid carcinoma cells and enhances the effects of oncolytic virus dl922-947. *Endocr Relat Cancer* **18** 129-141.

Libertini S, Iacuzzo I, Ferraro A, Vitale M, Bifulco M, Fusco A & Portella G 2007 Lovastatin enhances the replication of the oncolytic adenovirus dl1520 and its antineoplastic activity against anaplastic thyroid carcinoma cells. *Endocrinology* **148** 5186-5194.

Libertini S, Iacuzzo I, Perruolo G, Scala S, Ierano C, Franco R, Hallden G & Portella G 2008 Bevacizumab increases viral distribution in human anaplastic thyroid carcinoma xenografts and enhances the effects of E1A-defective adenovirus dl922-947. *Clin Cancer Res* **14** 6505-6514.

Lilley CE, Schwartz RA & Weitzman MD 2007 Using or abusing: viruses and the cellular DNA damage response. *Trends Microbiol* **15** 119-126.

Lin SF, Gao SP, Price DL, Li S, Chou TC, Singh P, Huang YY, Fong Y & Wong RJ 2008a Synergy of a herpes oncolytic virus and paclitaxel for anaplastic thyroid cancer. *Clin Cancer Res* **14** 1519-1528.

Lin SF, Price DL, Chen CH, Brader P, Li S, Gonzalez L, Zhang Q, Yu YA, Chen N, Szalay AA, et al. 2008b Oncolytic vaccinia virotherapy of anaplastic thyroid cancer in vivo. *J Clin Endocrinol Metab* **93** 4403-4407.

Lisby M, Barlow JH, Burgess RC & Rothstein R 2004 Choreography of the DNA damage response: spatiotemporal relationships among checkpoint and repair proteins. *Cell* **118** 699-713.

Liu C, Sarkaria JN, Petell CA, Paraskevakou G, Zollman PJ, Schroeder M, Carlson B, Decker PA, Wu W, James CD, et al. 2007 Combination of measles virus virotherapy and radiation therapy has synergistic activity in the treatment of glioblastoma multiforme. *Clin Cancer Res* **13** 7155-7165.

Lockley M, Fernandez M, Wang Y, Li NF, Conroy S, Lemoine N & McNeish I 2006 Activity of the adenoviral E1A deletion mutant dl922-947 in ovarian cancer: comparison with E1A wild-type

viruses, bioluminescence monitoring, and intraperitoneal delivery in icodextrin. *Cancer Res* **66** 989-998.

Nichols GJ, Schaack J & Ornelles DA 2009 Widespread phosphorylation of histone H2AX by species C adenovirus infection requires viral DNA replication. *J Virol* **83** 5987-5998.

O'Shea CC, Johnson L, Bagus B, Choi S, Nicholas C, Shen A, Boyle L, Pandey K, Soria C, Kunich J, et al. 2004 Late viral RNA export, rather than p53 inactivation, determines ONYX-015 tumor selectivity. *Cancer Cell* **6** 611-623.

Oberg D, Yanover E, Adam V, Sweeney K, Costas C, Lemoine NR & Hallden G 2010 Improved potency and selectivity of an oncolytic E1ACR2 and E1B19K deleted adenoviral mutant in prostate and pancreatic cancers. *Clin Cancer Res* **16** 541-553.

Portella G, Pacelli R, Libertini S, Cella L, Vecchio G, Salvatore M & Fusco A 2003 ONYX-015 enhances radiation-induced death of human anaplastic thyroid carcinoma cells. *J Clin Endocrinol Metab* **88** 5027-5032.

Portella G, Scala S, Vitagliano D, Vecchio G & Fusco A 2002 ONYX-015, an E1B gene-defective adenovirus, induces cell death in human anaplastic thyroid carcinoma cell lines. *J Clin Endocrinol Metab* **87** 2525-2531.

Qian J, Yang J, Dragovic AF, Abu-Isa E, Lawrence TS & Zhang M 2005 Ionizing radiation-induced adenovirus infection is mediated by Dynamin 2. *Cancer Res* **65** 5493-5497.

Radhakrishnan S, Miranda E, Ekblad M, Holford A, Pizarro MT, Lemoine NR & Hallden G 2010 Efficacy of oncolytic mutants targeting pRb and p53 pathways is synergistically enhanced when combined with cytotoxic drugs in prostate cancer cells and tumor xenografts. *Hum Gene Ther* **21** 1311-1325.

Schweppe RE, Klopper JP, Korch C, Pugazhenthi U, Benezra M, Knauf JA, Fagin JA, Marlow LA, Copland JA, Smallridge RC, et al. 2008 Deoxyribonucleic acid profiling analysis of 40 human thyroid cancer cell lines reveals cross-contamination resulting in cell line redundancy and misidentification. *J Clin Endocrinol Metab* **93** 4331-4341.

Seidman MA, Hogan SM, Wendland RL, Worgall S, Crystal RG & Leopold PL 2001 Variation in adenovirus receptor expression and adenovirus vector-mediated transgene expression at defined stages of the cell cycle. *Mol Ther* **4** 13-21.

Sherr CJ & McCormick F 2002 The RB and p53 pathways in cancer. *Cancer Cell* **2** 103-112.

Smallridge RC, Marlow LA & Copland JA 2009 Anaplastic thyroid cancer: molecular pathogenesis and emerging therapies. *Endocr Relat Cancer* **16** 17-44.

Smith J, Tho LM, Xu N & Gillespie DA 2010 The ATM-Chk2 and ATR-Chk1 pathways in DNA damage signaling and cancer. *Adv Cancer Res* **108** 73-112.

Taccaliti A, Silvetti F, Palmonella G & Boscaro M 2012 Anaplastic thyroid carcinoma. *Front Endocrinol (Lausanne)* **3** 84.

Touchefeu Y, Vassaux G & Harrington KJ 2011 Oncolytic viruses in radiation oncology. *Radiother Oncol* **99** 262-270.

Yong RL, Shinojima N, Fueyo J, Gumin J, Vecil GG, Marini FC, Bogler O, Andreeff M & Lang FF 2009 Human bone marrow-derived mesenchymal stem cells for intravascular delivery of oncolytic adenovirus Delta24-RGD to human gliomas. *Cancer Res* **69** 8932-8940.

Zhang M, Li S, Li J, Ensminger WD & Lawrence TS 2003 Ionizing radiation increases adenovirus uptake and improves transgene expression in intrahepatic colon cancer xenografts. *Mol Ther* **8** 21-28.

Figure legends

Figure 1

IR enhances the cytophatic effects of dl922-947

A. Combination index of FRO and BHT101-5 cells were irradiated and after 24h infected (upper panel) at different MOIs of *dl*922-947 or *vice versa* (lower panel). A synergistic effect was observed only in cells infected 24h after irradiation (CI<1).

B. FRO and BHTH101-5 were irradiated (2-4-8Gy) and after 24h infected with 25 MOIs of AdGFP. The histogram on the left shows the percentage of GFP positive cells; whereas on the right GFP emission is reported. The percentage of GFP positive cells and GFP emission, with the exception of 2 Gy, were not increased in irradiated cells. The data are the mean of three different experiments. (*p<0.01)

C. Real Time PCR genome equivalent analysis. FRO and BHTH101-5 cells were irradiated (2-4-5 Gy) and then infected with *dl*922-947, (1-5-10 MOIs). Irradiated cells showed significant or highly significant differences in viral replication levels with respect to non irradiated cells. The data are the mean of three different experiments. (*p<0.05; **p<0.005)

Figure 2

IR increases the cell death induced by dl922-947

A. Cell cycle analysis of FRO and BHT101-5 cells. SubG1, G2/M and polyploidy are represented by histograms. IR (8 Gy) induced an accumulation in G2 phase up to 24h post irradiation. At 48h the block is recovered. Infected cells (5MOIs) or cells undergoing the combined treatments show a G2 accumulation at 24 hpi. At 48 hpi, the block is not reversed and most of the cells show polyploidy. The percentage of cells in sub-G1 phase was increased by the combined treatment.
The data are the mean of three different experiments.

B. Annexin V-FITC/PI staining. FRO cells were irradiated with 8 Gy and after 24h infected with 5 MOIs of *dl*922-947 for 72h. Apoptotic cells are positive for Annexin V or double positive for Annexin V and PI (Right panels); Necrotic cells positive for PI only (upper left panel); vital cells (lower left panel). The combined treatment increases the percentage of apoptotic cells (44.2%) with respect to single treatments (32.6% infection alone; 12% irradiation alone).
Tables show the percentage of the different stained population after 24 and 48h of treatment.
Data are the representation of three different experiments.

C. Western blot analysis of procaspase 3 and caspase3 levels. Data are the representation of three different experiments.

Figure 3

dl922-947 infection activates the DNA damage signaling pathway and impairs DNA damage repair

A. Western blot analysis of pATM (Serine 1981), pChk1(serine 345), Mre11 levels .

B. Fixed cells stained with antibody for γH2AX and PI were analyzed using FACS. FRO cells were irradiated (8Gy) and infected with *dl*922-947 (5 MOIs) for 1-3-6-24h. IR increase *dl*922-947-induced γH2AX levels already at 1h after infection.

Figure 4

ATM inhibitor, KU55933, enhances the cytopatic effects of dl922-947

A. FRO and BHT101-5 cells were treated with KU55933 (5-10 μM) and infected at increasing MOIs (1-2.5-5-10 for FRO cells and 0.5-1-2.5-5 for BHT101-5 cells). Survival was evaluated after 7 days by sulforhodamine B method.

Data are the mean of three different experiments.

B. FRO cells were treated with KU55933 (5μM) and infected with *dl*922-947 (5 MOIs) for 3-6-24h. Fixed cells stained with antibody for γH2AX and PI were analyzed using FACS. Percentage of γH2AX positive cells (green) and median of FITC emission (red) are shown. Treatment with the ATM inhibitor reduces *dl*922-947-induced γH2AX levels, particularly as median of FITC emission.

Data are the representation of three different experiments.

C. Real Time PCR genome equivalent analysis. ATC cells were treated with KU55933(0.5-1-5 μM) and then infected with *dl*922-947 (5-10 MOIs). A highly significant difference in viral replication levels was observed with respect to cells not treated with KU55933, (*p<0.005; **p<0.0001).

The data are the mean of three different experiments.

Figure 5

The combined treatment (IR and dl922-947) reduces tumour growth

The difference between animals receiving the combined treatment and single treatment groups and control group becomes statistically significant (*$p<0.05$) from day 11. At day 21, a highly significant difference (**$p<0.005$) was observed.

Fig 1A

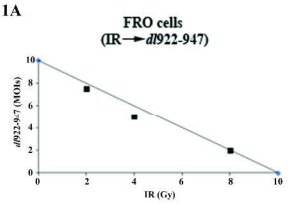

Ratio (Gy)/(MOIs)	EC_{50} IR (Gy)	EC_{50} dl922-947 (MOIs)	CI
IR alone	10	0	
dl922-947 alone	0	10	
1:3.75	2	7.5	0.95
1:1.25	4	5	0.9
4:1	8	2	1

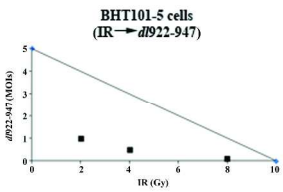

Ratio (Gy)/(MOIs)	EC_{50} IR (Gy)	EC_{50} dl922-947 (MOIs)	CI
IR alone	10	0	
dl922-947 alone	0	5	
2:1	2	1	0.4
8:1	4	0.5	0.5
80:1	8	0.1	0.82

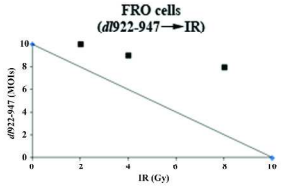

Ratio (Gy)/(MOIs)	EC_{50} IR (Gy)	EC_{50} dl922-947 (MOIs)	CI
IR alone	10	0	
dl922-947 alone	0	10	
1:5	2	10	1.2
1:2.25	4	9	1.3
1:1	8	8	1.6

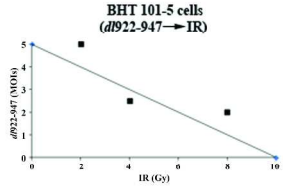

Ratio (Gy)/(MOIs)	EC_{50} IR (Gy)	EC_{50} dl922-947 (MOIs)	CI
IR alone	10	0	
dl922-947 alone	0	5	
1:2.5	2	5	1.2
1.6:1	4	2.5	0.9
4:1	8	2	1.2

Fig 1B

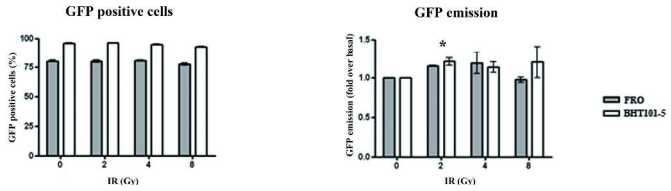

Fig 1C

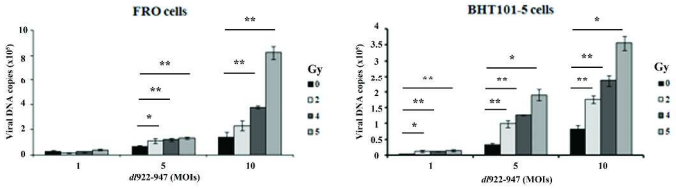

IR enhances the cytophatic effects of dl922-947

A. Combination index of FRO and BHT101-5 cells were irradiated and after 24h infected (upper panel) at different MOIs of dl922-947 or vice versa (lower panel). A synergistic effect was observed only in cells infected 24h after irradiation (CI<1).

B. FRO and BHTH101-5 were irradiated (2-4-8Gy) and after 24h infected with 25 MOIs of AdGFP. The histogram on the left shows the percentage of GFP positive cells; whereas on the right GFP emission is reported. The percentage of GFP positive cells and GFP emission, with the exception of 2 Gy, were not increased in irradiated cells. The data are the mean of three different experiments. (*p<0.01)

C. Real Time PCR genome equivalent analysis. FRO and BHTH101-5 cells were irradiated (2-4-5 Gy) and then infected with dl922-947, (1-5-10 MOIs). Irradiated cells showed significant or highly significant differences in viral replication levels with respect to non irradiated cells. The data are the mean of three different experiments. (*p<0.05; **p<0.005)

Fig 2A

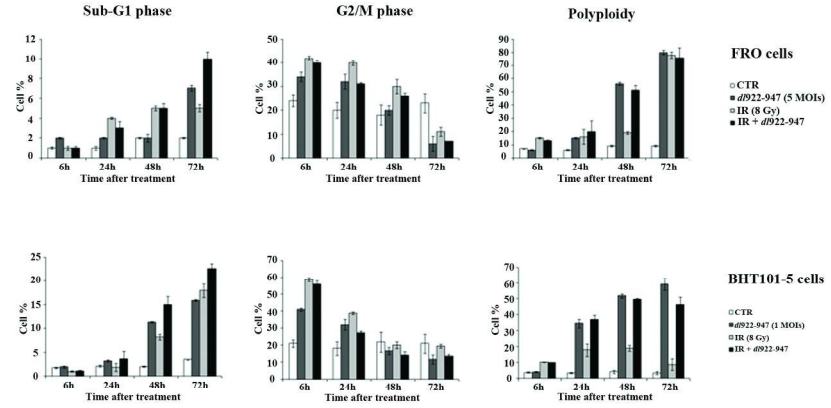

Fig 2B

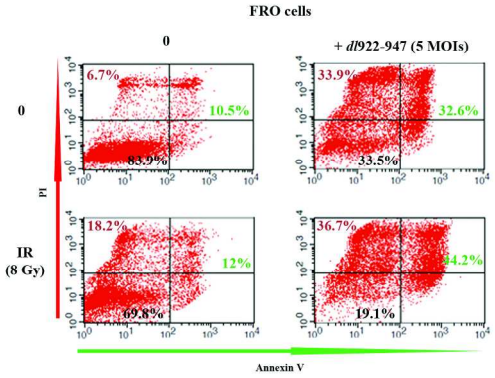

24h	Annexin V +ve cells	PI +ve cells	Living cells
CTR	16	5.8	78.2
*dl*922-947 (5 MOIs)	18.8	5.5	75.7
IR (8Gy)	16.2	5.6	78.2
IR+*dl*922-947	18.4	7.8	73.8

48h	Annexin V +ve cells	PI +ve cells	Living cells
CTR	12.8	12.8	74.4
*dl*922-947 (5 MOIs)	29.6	22.5	47.9
IR (8Gy)	14	11.4	74.6
IR+*dl*922-947	12.5	45.1	42.4

Fig 2C

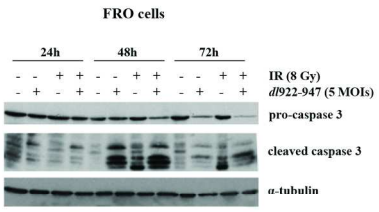

IR increases the cell death induced by dl922-947

A. Cell cycle analysis of FRO and BHT101-5 cells. SubG1, G2/M and polyploidy are represented by histograms. IR (8 Gy) induced an accumulation in G2 phase up to 24h post irradiation. At 48h the block is recovered. Infected cells (5MOIs) or cells undergoing the combined treatments show a G2 accumulation at 24 hpi. At 48 hpi, the block is not reversed and most of the cells show polyploidy. The percentage of cells in sub-G1 phase was increased by the combined treatment.

The data are the mean of three different experiments.

B. Annexin V-FITC/PI staining. FRO cells were irradiated with 8 Gy and after 24h infected with 5 MOIs of dl922-947 for 72h. Apoptotic cells are positive for Annexin V or double positive for Annexin V and PI (Right panels); Necrotic cells positive for PI only (upper left panel); vital cells (lower left panel). The combined treatment increases the percentage of apoptotic cells (44.2%) with respect to single treatments (32.6% infection alone; 12% irradiation alone).

Tables show the percentage of the different stained population after 24 and 48h of treatment.

Data are the representation of three different experiments.
C. Western blot analysis of procaspase 3 and caspase3 levels. Data are the representation of three different experiments.

171x228mm (300 x 300 DPI)

Fig 3A

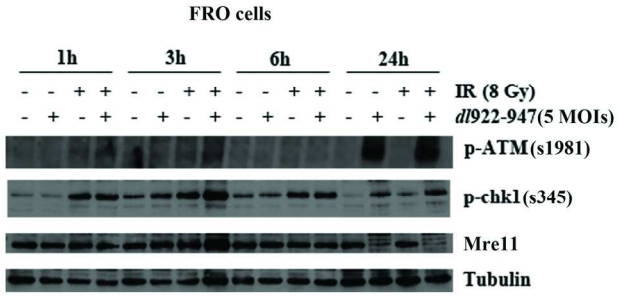

Fig 3B

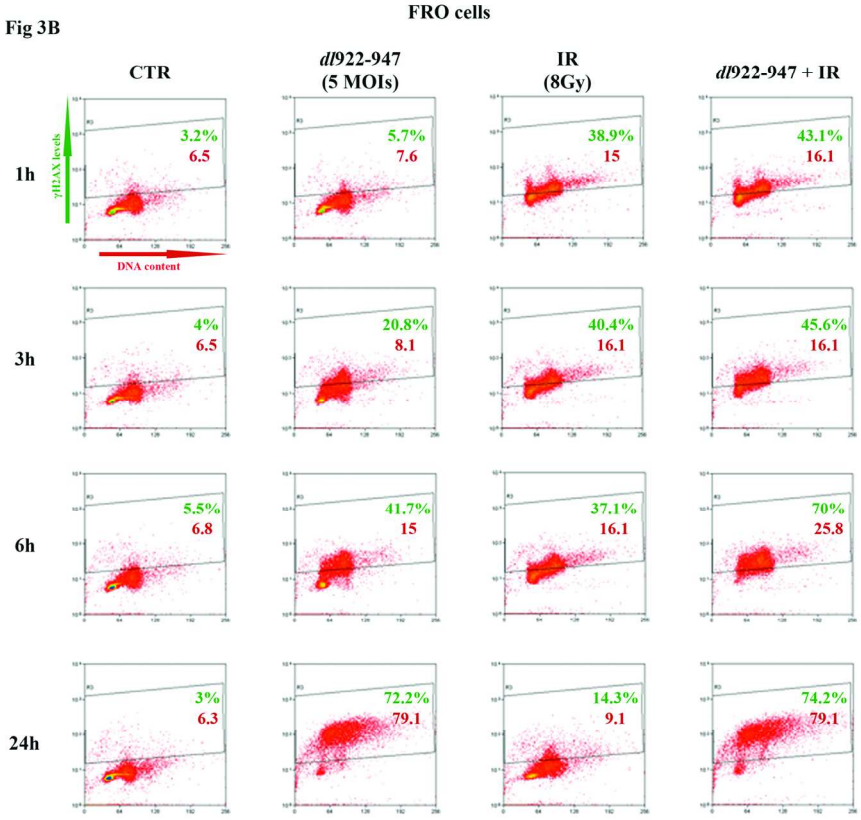

dl922-947 infection activates the DNA damage signaling pathway and impairs DNA damage repair
A. Western blot analysis of pATM (Serine 1981), pChk1(serine 345), Mre11 levels .
B. Fixed cells stained with antibody for γH2AX and PI were analyzed using FACS. FRO cells were irradiated (8Gy) and infected with dl922-947 (5 MOIs) for 1-3-6-24h. IR increase dl922-947-induced γH2AX levels already at 1h after infection.

184x225mm (300 x 300 DPI)

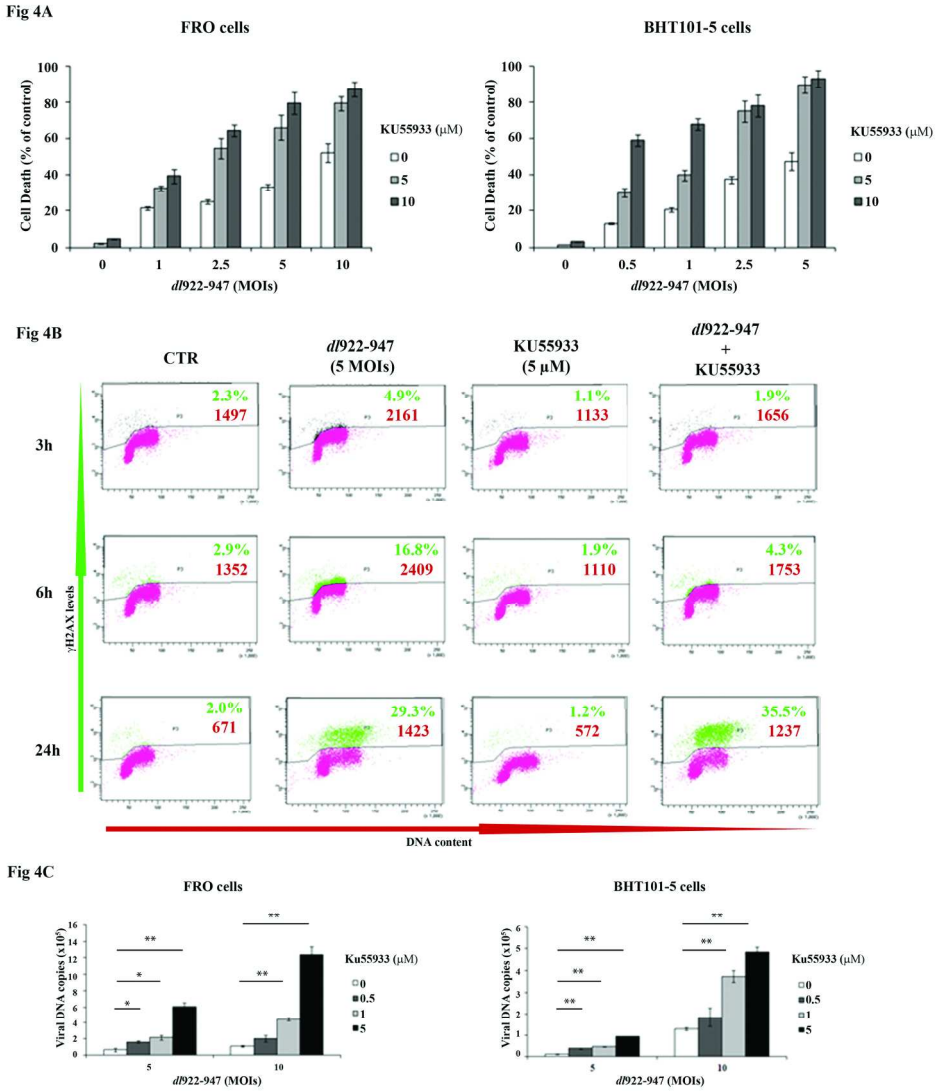

ATM inhibitor, KU55933, enhances the cytopatic effects of dl922-947

A. FRO and BHT101-5 cells were treated with KU55933 (5-10 μM) and infected at increasing MOIs (1-2.5-5-10 for FRO cells and 0.5-1-2.5-5 for BHT101-5 cells). Survival was evaluated after 7 days by sulforhodamine B method.

Data are the mean of three different experiments.

B. FRO cells were treated with KU55933 (5μM) and infected with dl922-947 (5 MOIs) for 3-6-24h. Fixed cells stained with antibody for γH2AX and PI were analyzed using FACS. Percentage of γH2AX positive cells (green) and median of FITC emission (red) are shown. Treatment with the ATM inhibitor reduces dl922-947-induced γH2AX levels, particularly as median of FITC emission.

Data are the representation of three different experiments.

C. Real Time PCR genome equivalent analysis. ATC cells were treated with KU55933(0.5-1-5 μM) and then infected with dl922-947 (5-10 MOIs). A highly significant difference in viral replication levels was observed with respect to cells not treated with KU55933, (*p<0.005; **p<0.0001).

The data are the mean of three different experiments.

184x208mm (300 x 300 DPI)

Fig 5

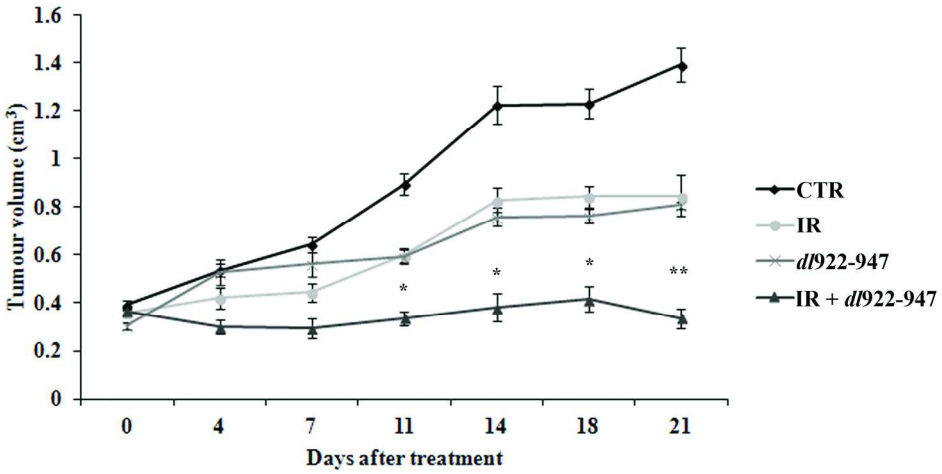

The combined treatment (IR and dl922-947) reduces tumour growth
The difference between animals receiving the combined treatment and single treatment groups and control group becomes statistically significant (*p<0.05) from day 11. At day 21, a highly significant difference (**p<0.005) was observed.

184x103mm (300 x 300 DPI)

HUMAN GENE THERAPY 23:1–12 (June 2012)

DOI: 10.1089/hum.2011.120

Inhibition of Autophagy Enhances the Effects of E1A-Defective Oncolytic Adenovirus *dl*922–947 Against Glioma Cells *In Vitro* and *In Vivo*

Ginevra Botta,[1] Carmela Passaro,[1] Silvana Libertini,[1,*] Antonella Abagnale,[1] Sara Barbato,[1] Angela Serena Maione,[1] Gunnel Hallden,[2] Francesco Beguinot,[1] Pietro Formisano,[1] and Giuseppe Portella[1]

Abstract

Oncolytic viruses represent a novel therapeutic approach for aggressive tumors, such as glioblastoma multiforme, which are resistant to available treatments. Autophagy has been observed in cells infected with oncolytic viruses; however, its role in cell death/survival is unclear. To elucidate the potential therapeutic use of autophagy modulators in association with viral therapy, we analyzed autophagy induction in human glioma cell lines U373MG and U87MG infected with the oncolytic adenovirus *dl*922–947. *dl*922–947 infection triggered an autophagic cellular response, as shown by the development of acidic vesicular organelles, LC3-I→LC3-II conversion, and reduction of p62 levels. However, on infection, the Akt/mTOR/p70s6k pathway, which negatively regulates autophagy, was activated, whereas the ERK1/2 pathway, a positive regulator of autophagy, was inhibited. Accordingly, MEK inhibition by PD98059 sensitized glioma cells to *dl*922–947 effects, whereas autophagy induction by rapamycin protected cells from *dl*922–947-induced death. Treatment with two inhibitors of autophagy, chloroquine and 3-methyladenine, increased the cytotoxic effects of *dl*922–947 *in vitro*. *In vivo*, the growth of U87MG-induced xenografts was further reduced by adding chloroquine to the *dl*922–947 treatment. In conclusion, autophagy acts as a survival response in glioma cells infected with *dl*922–947, thus suggesting autophagy inhibitors as adjuvant/neoadjuvant drugs in oncolytic virus-based treatments.

Introduction

Malignant glioma of astrocytic origin or glioblastoma multiforme (GBM) is one of the most aggressive human tumors (Furnari *et al*., 2007; Brandes *et al*., 2008), with a median survival time of about 12–15 months. The standard treatment protocol for newly diagnosed GBM includes surgical resection, radiotherapy, and chemotherapy (Furnari *et al*., 2007; Brandes *et al*., 2008). However, this therapeutic approach has achieved only a moderate increase in survival (Ahmadi *et al*., 2009), highlighting the need for the development of novel and more effective treatments.

Conditionally replicating oncolytic viruses (OVs) represent a promising approach for the treatment of cancer, and the feasibility and safety of this therapeutic strategy in glioblastoma patients have been demonstrated in previous studies (Haseley *et al*., 2009). *dl*922–947 is a replication-selective oncolytic adenoviral mutant, harboring a 24-bp deletion in E1A conserved region-2 (CR2), that is responsible for binding and inactivation of the retinoblastoma protein pRb (Heise *et al*., 2000), which regulates the G_1-to-S phase transition. Thus, *dl*922–947 virus is unable to induce G_1-to-S phase transition in normal cells, but can efficiently replicate in cells with an abnormal G_1–S checkpoint. Previous studies have confirmed the efficacy of E1A CR2-deleted adenoviruses, such as Δ24 (Fueyo *et al*., 2000; Jiang *et al*., 2007), for glioma cells, and we have demonstrated that *dl*922–947 exerts antineoplastic activity against the glioma cell lines U373MG and U343MG (Botta *et al*., 2010). A phase I clinical trial for the use of an E1A CR2-deleted mutant (Ad5-Δ24RGD) in recurrent malignant gliomas has been completed (http://clinicaltrialsfeeds.org/clinical-trials/show/NCT00805376).

Although the efficacy and safety of OVs have been clearly demonstrated in preclinical and clinical studies, most of the molecular and/or biochemical pathways activated in cancer cells, including the cell death mechanisms, are not fully understood. A better understanding of such mechanisms would be advantageous for future selection of novel drugs or

[1]Dipartimento di Biologia e Patologia Cellulare e Molecolare, Università Federico II, 80131, Naples, Italy.
[2]Centre for Molecular Oncology, Barts Cancer Institute, Queen Mary University of London, EC1M 6BQ, London, United Kingdom.
[*]Present address: Beatson Institute for Cancer Research, G61 1BD, Glasgow, United Kingdom.

treatments to further enhance the efficacy of oncolytic viruses. In various studies it has been shown that OVs activate the autophagic machinery in some cancer cells (Ito *et al*., 2006; Jiang *et al*., 2007; Baird *et al*., 2008; Tyler *et al*., 2009). Autophagy is a catabolic process whereby cytoplasm and cellular organelles are degraded through lysosomal machinery, allowing amino acid and energy recycling (Mizushima, 2007). It is well known that autophagy provides an alternative energy source, thus representing a temporary survival mechanism under stressful conditions. However, it has also been reported that autophagy plays an active role in cell death (Baehrecke, 2005; Loos and Engelbrecht, 2009).

Here we show that, on infection with the oncolytic virus *dl*922–947, formation of acidic vesicular organelles and the conversion of the cytosolic form of microtubule-associated protein-1 light chain-3 to the autophagosomal membrane-associated form (LC3-I→LC3-II) occur, indicative of a cellular autophagic response to viral infection.

Regulation of autophagy requires multiple signaling pathways (Meijer and Codogno, 2004). Akt/mTOR/p70s6k is the main pathway involved in the negative regulation of autophagy (Blommaart *et al*., 1995; Yang *et al*., 2005). Class I phosphatidylinositol-3-phosphate kinase (PI3K) is activated by ligand binding to growth factor receptors. PI3K activates the downstream target Akt, leading to activation of mammalian target of rapamycin (mTOR) (Díaz-Troya *et al*., 2008). TOR is a serine/threonine kinase that negatively affects the autophagic process, which is achieved by controlling translation and transcription or by either directly or indirectly affecting the Atg (autophagy-related genes) proteins (Díaz-Troya *et al*., 2008). p70 S6 kinase (p70s6k) is considered a candidate among the substrates of mTOR and in the control of autophagy downstream of mTOR (Blommaart *et al*., 1995). In the presence of amino acids, mTOR promotes phosphorylation of S6 through activation of p70s6k, thus facilitating the translation initiation of mRNAs (Díaz-Troya *et al*., 2008). On the other hand, the extracellular-signal regulated kinase-1/2 (ERK1/2) pathway has been described as a positive regulator pathway of autophagy (Pattingre *et al*., 2003).

Surprisingly, we found that, despite the autophagy activation in *dl*922–947-infected cells, viral infection activates the main negative regulator of autophagy—the Akt/mTOR/p70s6k pathway—and inhibits the positive regulator, the ERK1/2 pathway. In line with this, viral cytotoxicity is decreased by rapamycin (an mTOR inhibitor) and increased by ERK1/2 inhibitor PD98059, as well as by specific inhibitors of autophagy (3-methyladenine and chloroquine) or genetic tools such as Atg5 small hairpin RNA (shRNA). Although these data seem to contrast with previous results suggesting autophagy as a cell death mechanism induced by oncolytic viruses in glioma cells (Ito *et al*., 2006), our results led us to speculate that autophagy might play a survival/defensive role in glioma cells infected with *dl*922–947. Consistently, we demonstrated that chloroquine treatment of athymic mice bearing glioma tumor xenografts enhances the effects of *dl*922–947 in reducing tumor growth.

Materials and Methods

Cell lines and reagents

Human glioma cell lines U373MG and U87MG were purchased from the American Type Culture Collection (Manassas, VA) and grown as described (Botta *et al*., 2010).

Acridine orange, 3-methyladenine (3-MA), PD98059, and rapamycin were purchased from Sigma-Aldrich (St. Louis, MO). Chloroquine (CQ) was purchased from Fluka (Buchs, Switzerland).

Preparation of adenoviruses, infection, and viability assay

*dl*922–947 is a second-generation adenoviral mutant that has a 24-bp deletion in E1A conserved region-2 (CR2). AdGFP is a nonreplicating E1A-deleted adenovirus encoding green fluorescent protein. *dl*312 is a nonreplicating adenovirus (ΔE1A, ΔE3B) (Cheong *et al*., 2008). Viral stocks were expanded, purified, and stored as previously reported (Botta *et al*., 2010), and a plaque-forming units (PFU) assay was performed on HEK-293 cells to determine viral titer.

To evaluate the *dl*922–947 cytotoxic effect, 1×10^3 cells were seeded in 96-well plates. After 24 hr, the cells were treated with 3-MA (1 m*M*) or CQ (10 μM) for 2 hr and then infected. After 7 days, the cells were fixed with 10% trichloroacetic acid (TCA), stained with 0.4% sulforhodamine B in 1% acetic acid, and solubilized as previously reported (Libertini *et al*., 2011). Cell death rates, expressed as a percentage of treated cells, were calculated. Dose–response curves were generated to calculate the concentration of each agent required to kill 50% of cells (median lethal dose, LD_{50}); untreated cells or cells treated with single agents were used as a control.

Quantification of acidic vesicular organelles with acridine orange

The development of acidic vesicular organelles is a particular feature of autophagy. The cytoplasm and nucleoli of acridine orange-stained cells fluoresce bright green and dim red, respectively, whereas acidic compartments fluoresce bright red (Paglin *et al*., 2001). To assess autophagy in U373MG and U87MG cells, the acidic compartment was quantified by supravital acridine orange staining. Treated cells were trypsinized and stained with acridine orange (1.0 μg/ml) for 15 min at 37°C. Data were collected on a CyAn flow cytometer and analyzed using Summit software version 4.3 (both from Dako Cytomation, now Beckman Coulter, Miami, FL).

Generation of stable clones

To investigate autophagy induction, overexpression of GFP-tagged LC3 was induced in U373MG cells (Kabeya *et al*., 2000). The LC3 expression vector (pCAG-LC3) was kindly provided by N. Mizushima and T. Yoshimori (Osaka University, Suita, Japan). To obtain pGFP-LC3, LC3 cDNA was inserted into the *Bgl*II and *Eco*RI sites of pEGFP-C1, a GFP fusion protein expression vector (Clontech, Mountain View, CA) (Kabeya *et al*., 2000). Stable expression of GFP-LC3 cDNA in U373MG cells (U373 GFP-LC3) was accomplished by the Lipofectamine (Invitrogen, Carlsbad, CA) method, in accordance with the manufacturer's instructions. Cells were cultured in 60-mm dishes (Corning, Corning, NY) and incubated in serum-free Dulbecco's modified Eagle's medium (DMEM) supplemented with 5 μg of cDNA and

15 μl of Lipofectamine reagent. After 5 hr, DMEM supplemented with 20% fetal bovine serum was added and 1 day later was replaced with DMEM–10% serum. At 48 hr after the medium change, cells were selected in medium containing GIBCO G418 (400 mg/ml; Invitrogen) and G418-resistant clones were obtained. Expression of GFP-LC3 in the selected clones was evaluated by Western blot analysis using anti-GFP antibody.

To stably inhibit the expression of the Atg5 gene, APG5 shRNA (sc-41445-sh) and control shRNA (sc-108060) plasmids (Santa Cruz Biotechnology, Santa Cruz, CA) were transfected/selected in U373MG and U87MG cell lines as described previously.

Analysis of LC3 localization by immunofluorescence staining

U373 GFP-LC3 cells were seeded in 24-well dishes. After treatment, cells were fixed with 4% paraformaldehyde for 15 min at room temperature, washed three times with phosphate-buffered saline (PBS), permeabilized for 10 min with PBS containing 0.5% Triton X-100, and then washed three times with PBS. The cells were blocked with bovine serum albumin (BSA) blotting buffer (1% BSA in PBS) for 30 min and then incubated with BSA blotting buffer plus primary antibody overnight at 4°C (mouse monoclonal anti-hexon, diluted 1:50; US Biological, Swampscott, MA). After washing three times with PBS, cells were incubated with rhodamine-conjugated anti-mouse secondary antibody (Jackson ImmunoResearch, West Grove, PA). Images were acquired with an LSM510 inverted confocal microscope (Zeiss, Oberkochen, Germany), using a $\times 40$ oil objective and processed with LSM software (Zeiss).

Western blot analysis and antibodies

Protein extraction and tumor tissue homogenization were performed as previously described (Botta *et al.*, 2010; Oriente *et al.*, 2011).

Total homogenates were separated by sodium dodecyl sulfate–polyacrylamide gel electrophoresis (SDS–PAGE) under reducing conditions. Membranes were incubated overnight with the following primary antibodies: LC3-I/II (ab51520, diluted 1:3000) and caspase-3 (ab13585, diluted 1:500) from Abcam (Cambridge, UK); p62 (#5114, diluted 1:1000), p-ERK1/2 (#9101S, diluted 1:1000), p-Akt (#9271, diluted 1:1000), and p-p70s6k (#9205S, diluted 1:500), from Cell Signaling (Danvers, MA); Atg5 (sc-8666, diluted 1:500), ERK1/2 (sc-93-G, diluted 1:1000), and β-actin (sc-10731, diluted 1:2000) from Santa Cruz Biotechnology; and Akt (#28745, diluted 1:1000) from Upstate Biotechnology (Billerica, MA).

Quantitative real-time PCR of adenovirus

Twenty-four, 48, and 72 hr after infection, viral genomes were collected from the cell medium, using a QIAamp DNA mini kit (Qiagen, Valencia, CA), and then quantified by real-time PCR, using the following primers: 5′-GCC ACC GAG ACG TAC TTC AGC CTG-3′ (upstream primer) and 5′-TTG TAC GAG TAC GCG GTA TCC T-3′ (downstream primer) for the amplification of a 143-bp sequence of the viral hexon gene. Serial dilutions of *dl*922–947 were used to construct a standard curve for quantification.

In vivo *antitumor activity and statistical analysis*

CD-I athymic mice were obtained from Charles River (Wilmington, MA), and all experiments were carried out with 6-week-old females. Twenty days postinjection with U87MG cells (5×10^6), 80 mice with similar tumor size were randomized into four groups: untreated, treated with CQ, treated with *dl*922–947, or treated with both. CQ (45 mg/kg) was administered intraperitoneally every third day. A viral dose (2×10^6 PFU) was administered three times a week by intratumoral injection to avoid any first-pass effect (Libertini *et al.*, 2007, 2008, 2011). Saline solution was administered to the control groups. Tumor diameters were measured with calipers and tumor volume (V) was calculated by the formula for a rotational ellipsoid: $V = A \times B^2/2$ (A, axial diameter; B, rotational diameter). The experiment was terminated when tumors reached 1 cm^3 in volume and/or symptomatic tumor ulceration occurred. Statistical analysis were done by ANOVA (analysis of variance) and the Bonferroni post hoc test, using commercial software (Prism 4; GraphPad Software, San Diego, CA). Differences in the rate of tumor growth in mice were assessed for each time point of the observation period.

Results

Induction of autophagy in malignant glioma cells by dl922–947

First, we evaluated the cytotoxic effects of *dl*922–947 in U87MG and U373MG glioma cells, confirming its efficacy. The U373MG cell line is more sensitive to *dl*922–947, with an LD_{50} of 0.008 PFU/cell, compared with the U87MG LD_{50} at 0.09 PFU/cell (Fig. 1A).

Next, we evaluated the activation of autophagy in glioma cells infected with *dl*922–947. To this end, we analyzed the formation of acidic vesicular organelles (AVOs), a particular feature of autophagy, after infection with *dl*922–947. Quantification of AVOs in U373MG and U87MG cells was performed by acridine orange supravital cell staining. U373MG and U87MG cells were infected at 1, 5, and 10 multiplicities of infection (MOIs) with *dl*922–947 and acridine orange vital staining was performed 72 hr postinfection. FACS analysis showed an increase in bright red fluorescence in infected cells, in a MOI-dependent manner, up to 18% (U373MG) or up to 14% (U87MG). Untreated cells exhibited mainly green fluorescence (Fig. 1B) as the cells were infected with the nonreplicating control adenovirus, *dl*312 (data not shown). This indicates an accumulation of AVOs in glioma cells infected with *dl*922–947.

In amino acid starvation-induced autophagy, the microtubule-associated protein-1 light chain-3, LC3-I, is converted to LC3-II through some ubiquitination-like reactions. LC3-I is a cytosolic protein, whereas LC3-II is a protein membrane tightly attached to preautophagosomal (PAS) and autophagosomal membrane structures. The amount of LC3-II reflects the abundance of autophagosomes and variations in the ratio of LC3-II to LC3-I are indicative of autophagy induction (Kabeya *et al.*, 2000). LC3-I→LC3-II conversion was analyzed by Western blotting 72 hr after infection of U373MG and U87MG cells with *dl*922–947. An increase in LC3-II levels was observed in infected U373MG and U87MG cells, in an MOI-dependent manner (Fig. 1C).

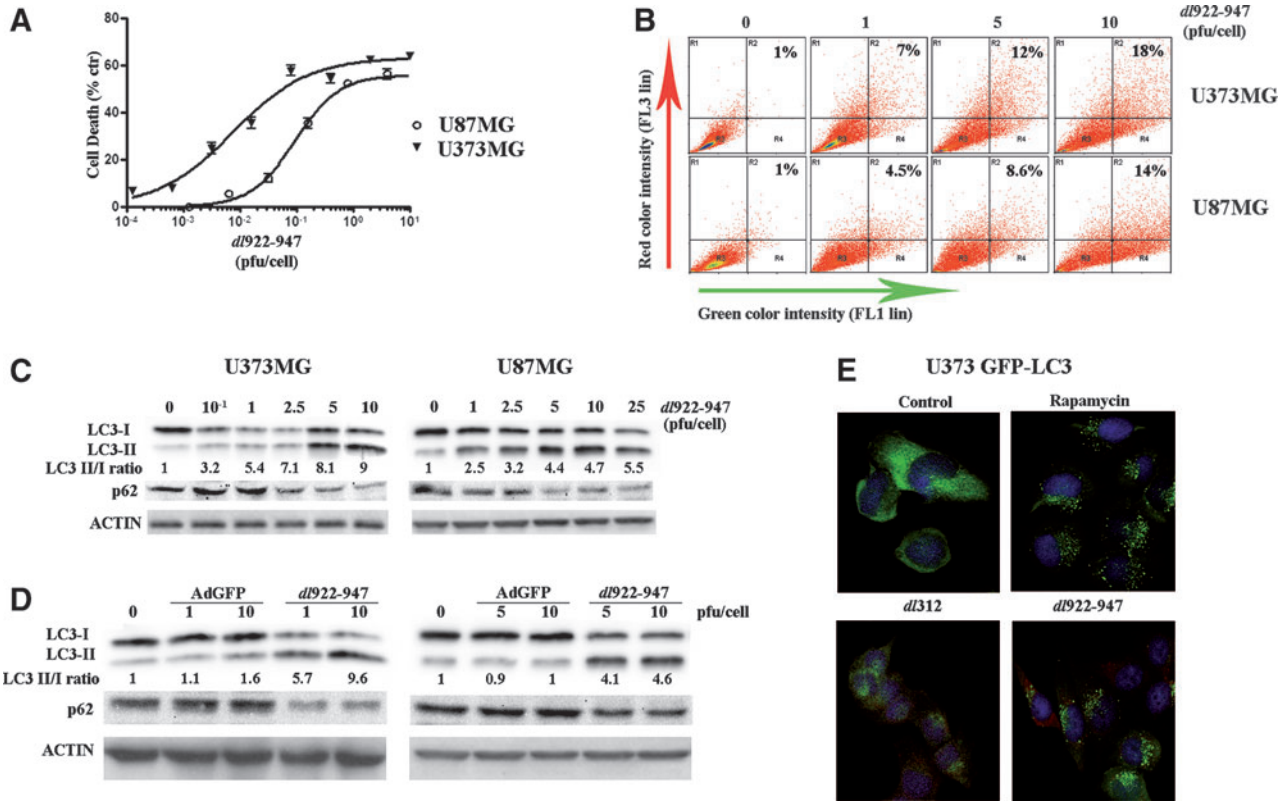

FIG. 1. *dl*922–947 induces cell death and autophagy in malignant glioma cells. **(A)** U373MG and U87MG cells were infected at the indicated MOIs and cell survival was analyzed 7 days postinfection. The percent survival rates of cells exposed to the virus were calculated by assuming the survival rate of untreated cells to be 100%. **(B)** U373MG and U87MG cells were infected with *dl*922–947 for 72 hr, stained with acridine orange for 15 min, and then subjected to flow cytometric analysis. Red-positive cells in upper quadrants were considered to be acidic vesicular organelles (AVOs) and the calculated percentages are shown. **(C** and **D)** Cells were infected with *dl*922–947 **(C** and **D)** or with AdGFP **(D)** and LC3-I→LC3-II conversion and p62 expression were analyzed after 72 hr. Numbers represent the ratio of the values obtained by densitometric analysis of LC3-II and LC3-I immunoblots. β-Actin was used as a loading control. **(E)** Immunofluorescence assay of stable clones of U373MG cells expressing fusion protein GFP-LC3 (U373 LC3-GFP) with anti-hexon antibody (red). Cells were infected with *dl*922–947 (0.1 PFU/cell) or *dl*312 (0.1 PFU/cell), or were treated with rapamycin (500 n*M*) for 72 hr, and green and red fluorescence was analyzed by confocal microscope. Data shown are representative of three independent experiments.

On autophagy activation, LC3-II is recruited to autophagosome membranes; therefore we decided to monitor LC3 localization during *dl*922–947 infection. U373MG clones expressing LC3 fused to green fluorescent protein were generated (U373 GFP-LC3) by stable transfection and GFP-LC3 tracked by immunofluorescence.

In untreated U373 GFP-LC3 cells or in cells infected with the nonreplicating adenoviral mutant *dl*312, a diffuse and mostly cytosolic distribution of fluorescence was observed (Fig. 1E). A less diffuse and more punctate pattern was observed 72 hr after infection with 0.1 PFU of *dl*922–947, indicating that LC3-II is recruited to the autophagosomal membranes; cells were costained with anti-hexon antibody as a control for viral infection. As a positive control, U373 GFP-LC3 cells were treated with the autophagy inducer rapamycin, showing the typical LC3-II localization pattern.

The accumulation of LC3-II could be due to autophagy flux or to interference with autophagosomal/lysosomal function. To discriminate between the two options, we evaluated the levels of the specific autophagy substrate p62/SQSTM1. During autophagy, p62 levels are reduced whereas, in the absence of autophagy, p62 levels are unmodified (Komatsu and Ichimura, 2010). As shown in Fig 1C, a clear decrease in p62 levels was observed, demonstrating that in *dl*922–947-infected cells the autophagic flux is enhanced.

Glioma cells were infected with a nonreplicating adenovirus expressing green fluorescence protein (AdGFP). AdGFP infection did not induce changes in LC3-II/LC3-I ratio or in p62 levels (Fig. 1D). This observation confirms that autophagy is a specific a feature occurring in infected cells in response to *dl*922–947 replication.

Taken together, these data demonstrate that glioma cells infected with the *dl*922–947 virus activate autophagic processes.

dl922–947 infection modulates autophagic signaling pathways and its effects are modified by specific pharmacological inhibitors

We evaluated the effects of *dl*922–947 infection on the Akt/mTOR/p70s6k and ERK1/2 pathways, which are,

respectively, negative and positive regulatory pathways of autophagy.

U373MG and U87MG cells were infected with *dl*922–947 in a dose–response experiment. Phosphorylation of p70s6k and Akt increased in a dose-dependent manner (Fig. 2A) in both cell lines, indicating activation of the negative regulatory pathway. Conversely, ERK1/2 phosphorylation was reduced on infection with *dl*922–947 in a dose-dependent manner (Fig. 2A), indicating inhibition of the positive regulatory pathway. AdGFP infection did not induce any of these effects (Fig. 2B). To better evaluate the role of ERK1/2 phosphorylation, a time-course experiment was performed, confirming a dose- and time-dependent reduction of ERK1/2 phosphorylation (Fig. 2C).

These data suggested to us that *dl*922–947 acts on autophagic pathways with compensatory mechanisms to counterbalance the cellular response. To clarify the role of the ERK1/2 pathway on the autophagic cellular response in infection, glioma cells were infected with *dl*922–947 in the presence of MEK-1 (MAPK [mitogen-activated protein kinase]/ERK kinase-1) inhibitor PD98059. An inhibitory dose of 25 μM was used for all the experiments. PD98059 enhanced *dl*922–947-induced cytotoxicity, leading to a significant reduction of LD_{50} values in both cell lines: from 0.008 to 0.001 PFU/cell in U373MG cells, and from 0.14 to 0.05 PFU/cell in U87MG cells (Fig. 3A). This observation confirms that blockage of the autophagic positive regulatory pathway favors viral cell-killing activity. Moreover, the combined treatment led to a further reduction of ERK-1/2 phosphorylation (Fig. 3B), along with a reduction on LC3-I→LC3-II conversion; conversely, in uninfected cells, the drug did not modify the LC3-II/LC3-I ratio (Fig. 3B).

To investigate the role of the Akt/mTOR/p70s6k pathway in *dl*922–947 infection, glioma cells were treated with the mTOR inhibitor rapamycin, a well-known autophagy inducer (Meijer and Codogno, 2004), and then infected with

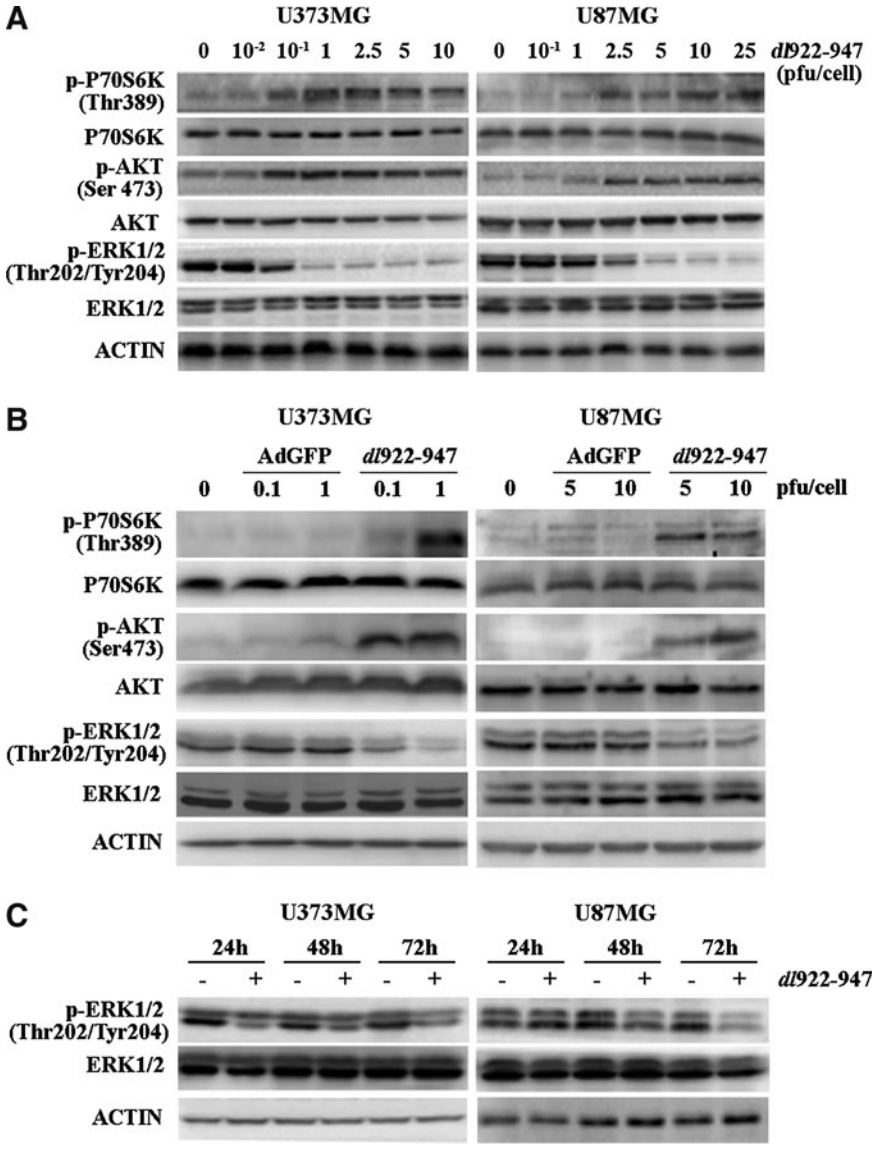

FIG. 2. Autophagy signaling pathways are modulated in response to *dl*922–947 infection in glioma cells. **(A)** U373MG and U87MG cells were infected with *dl*922–947 at the indicated MOIs for 72 hr. **(B)** Cells were infected with *dl*922–947 or AdGFP at the indicated MOIs for 72 hr. Expression of total and phosphorylated (p-) p70s6k, Akt, and ERK1/2 was analyzed by Western blot, using β-actin as a loading control. **(C)** U373MG and U87MG cells were infected with *dl*922–947 (1 PFU/cell for U373MG and 5 PFU/cell for U87MG). Levels of phosphorylated (p-) and total ERK1/2 was analyzed in a time course by Western blot. Results shown are representative of three independent experiments.

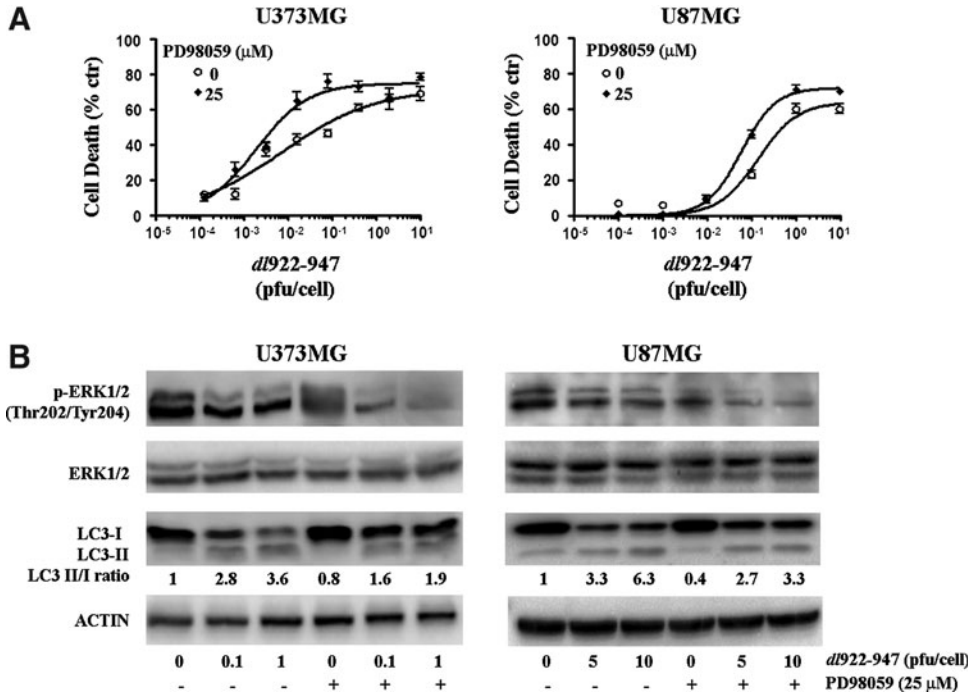

FIG. 3. Inhibition of the ERK1/2 pathway inhibits autophagy and enhances *dl*922–947-induced cytotoxicity. **(A)** Cells were treated with PD98059 (25 μM) and after 2 hr were infected with *dl*922–947 at the indicated MOIs. Cell survival was evaluated after 7 days. **(B)** U373MG and U87MG cells were treated with PD98059 (25 μM) for 2 hr and then infected with *dl*922–947 at the indicated MOIs. Expression of total and phosphorylated (p)-ERK1/2, and of LC3-I and LC3-II, were analyzed by Western blot after 72 hr. Numbers represent the ratio of the values obtained by densitometric analysis of LC3-II and LC3-I immunoblots. Results shown are representative of three independent experiments.

*dl*922–947. Treatment with rapamycin led to a reversion of p70s6k phosphorylation induced by the virus, paralleled by an increase in the LC3-II/LC3-I ratio (Fig. 4A). In both cell lines, rapamycin treatment led to a significant reduction of viral cytotoxicity, with an increase in LD_{50}, 42-fold for U373MG and 23-fold for U87MG (Fig. 4B). These results demonstrate that autophagy acts as a survival mechanism in glioma cells infected with *dl*922–947 and that the attenuation of autophagic response could increase viral cytotoxicity.

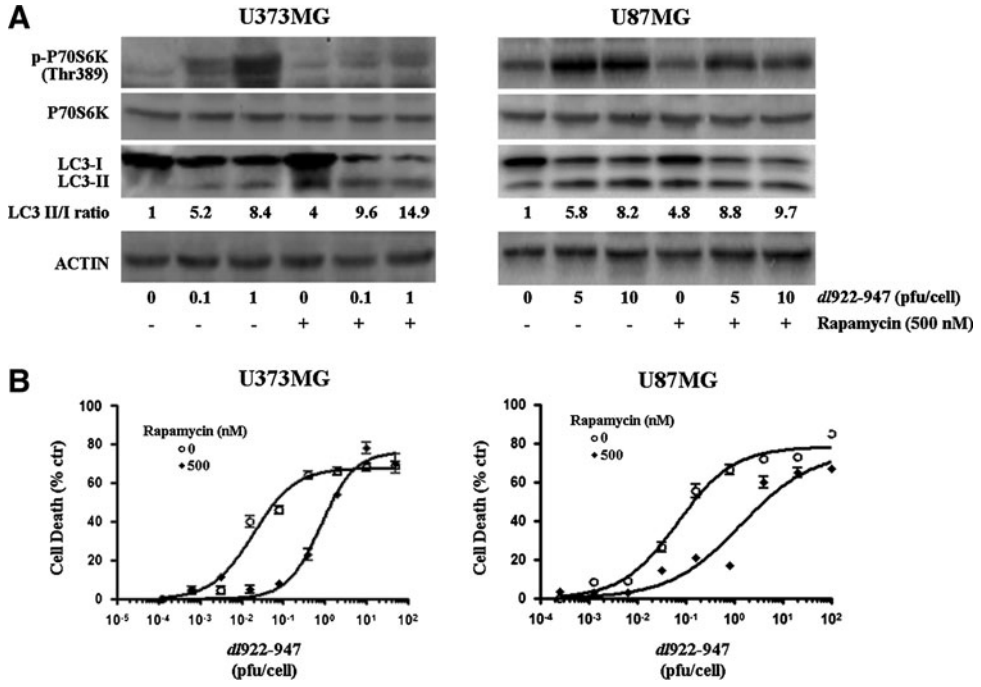

FIG. 4. Inhibition of the mammalian target of rapamycin (mTOR) pathway induces autophagy and decreases *dl*922–947-induced cytotoxicity. **(A)** U373MG and U87MG cells were treated with rapamycin (500 nM) for 2 hr and infected with *dl*922–947 at the indicated MOIs. Expression of total and phosphorylated (p-) p70s6K, and of LC3-I/II, was analyzed by Western blot after 72 hr. Numbers represent the ratio of the values obtained by densitometric analysis of LC3-II and LC3-I immunoblots. **(B)** Cells were treated with rapamycin (500 nM) and infected with *dl*922–947 after 2 hr at the indicated MOIs. Cell survival was evaluated after 7 days. A significant increase in LD_{50} values was obtained in both cell lines in the presence of rapamycin: from 0.019 to 0.802 in U373MG cells, and from 0.068 to 1.383 in U87MG cells. Results shown are representative of three independent experiments.

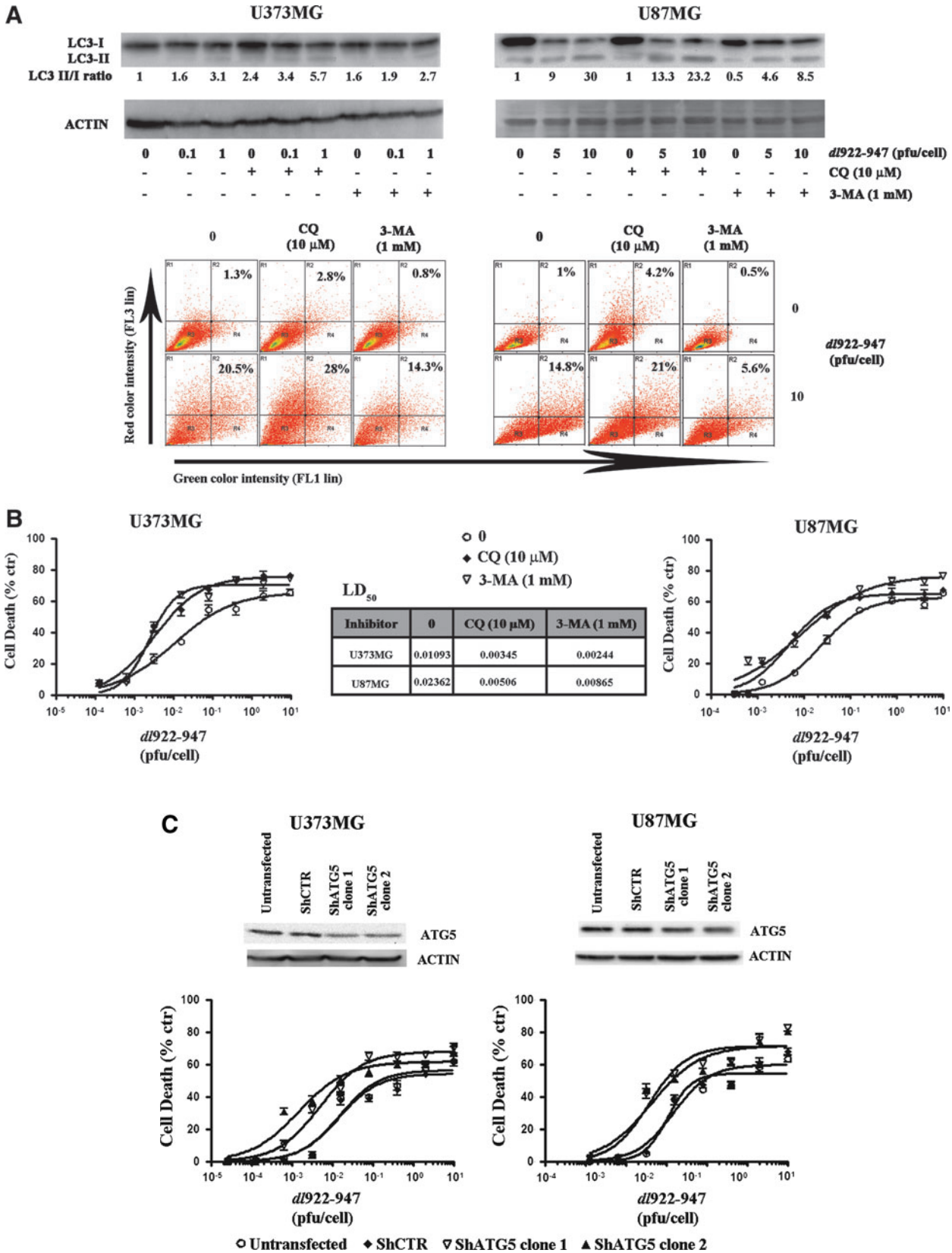

FIG. 5. Pharmacological autophagy inhibitors enhance *dl*922–947-induced cytotoxicity. **(A)** U373MG cells (*left*) and U87MG cells (*right*) were treated with chloroquine (CQ, 10 μM) or 3-methyladenine (3-MA, 1 m*M*) for 2 hr and infected with various MOIs of *dl*922–947 for 72 hr. LC3-I/II levels and AVO formation were analyzed by Western blot (*top*) and FACS analysis (*bottom*), respectively. Numbers represent the ratio of the values obtained by densitometric analysis of LC3-II and LC3-I immunoblots. **(B)** Cells were treated with CQ or 3-MA for 2 hr and then infected with various MOIs of *dl*922–947. Cell survival was evaluated after 7 days. **(C)** U373MG and U87MG clones stably expressing a scrambled control shRNA (shCTR) or a specific shRNA for Atg5 (shAtg5) were infected with various MOIs of *dl*922–947 and cell survival was evaluated after 7 days. Results shown are representative of three independent experiments. Color images available online at www.liebertonline.com/hum

Inhibition of autophagy increases dl922–947 cytotoxicity in glioma cells

Next, we evaluated the effect of pharmacological inhibition of autophagy on *dl*922–947 infection. To this end, we used two well-known inhibitors of autophagy: 3-methyladenine (3-MA) and hydroxychloroquine (CQ), acting at early and late stages of autophagy, respectively. CQ blocks the formation of autolysosomes, where LC3-II degradation occurs, thus inducing LC3-II accumulation (Amaravadi *et al.*, 2007), whereas 3-MA, an inhibitor of class III phosphatidylinositol-3 kinase (PI3KIII), blocks early autophagic signaling, preventing LC3-I→LC3-II conversion (Kondo *et al.*, 2005).

Accordingly, *dl*922–947-mediated LC3-I→LC3-II conversion induction and AVO formation were further increased by CQ, whereas they were partially reverted by treatment with 3-MA (Fig. 5A).

Treatment with a single dose of CQ (10 μM) or 3-MA (1 m*M*) increased *dl*922–947-induced cytotoxicity, with a reduction of LD_{50} values ranging from 2- to 5-fold (Fig. 5B). At the concentrations used, CQ or 3-MA treatment alone did not induce any toxic effect (data not shown).

Because CQ and 3-MA have a wide range of effects, not only specifically linked to autophagy, we have evaluated the effects of autophagy inhibition by generating stable glioma cells clones expressing Atg5 shRNA. We chose Atg5 because this gene is involved in both canonical and non-canonical autophagy (Scarlatti *et al.*, 2008). Although we did not obtain complete gene silencing, in all transfected clones a strong increase in virus-induced cell death was observed (Fig. 5C).

Our data confirm that inhibition of autophagy sensitizes glioma cells to the oncolytic effects of *dl*922–947.

Viral replication is not increased by autophagy modulation

It has been proposed that the results of oncolytic virotherapy are correlated with the efficacy of viral replication within cancer cells. Therefore, we evaluated viral replication in glioma cells treated with rapamycin, PD98059, and CQ. A slight, albeit not statistically significant, decrease in genome copies number on treatment was observed (Fig. 6A). It has been already demonstrated that inhibition of autophagy with 3-methyladenine (3-MA) resulted in decreased synthesis of adenoviral structural proteins, and thereby poor viral replication (Rodriguez-Rocha *et al.*, 2011).

We have previously demonstrated that Aurora B inhibitor AZD1152 enhanced caspase-3-dependent cell death of thyroid carcinoma cells infected with *dl*922–947, without an increase in viral replication (Libertini *et al.*, 2011). Moreover, several studies have shown that apoptosis and autophagy can be connected by a double switch (Díaz-Troya *et al.*, 2008; Tyler *et al.*, 2009) and that the inhibition of autophagy increased apoptotic cell death in cancer cells (Cardenas *et al.*, 1999; Shigemitsu *et al.*, 1999; Kondo *et al.*, 2005). Analysis of

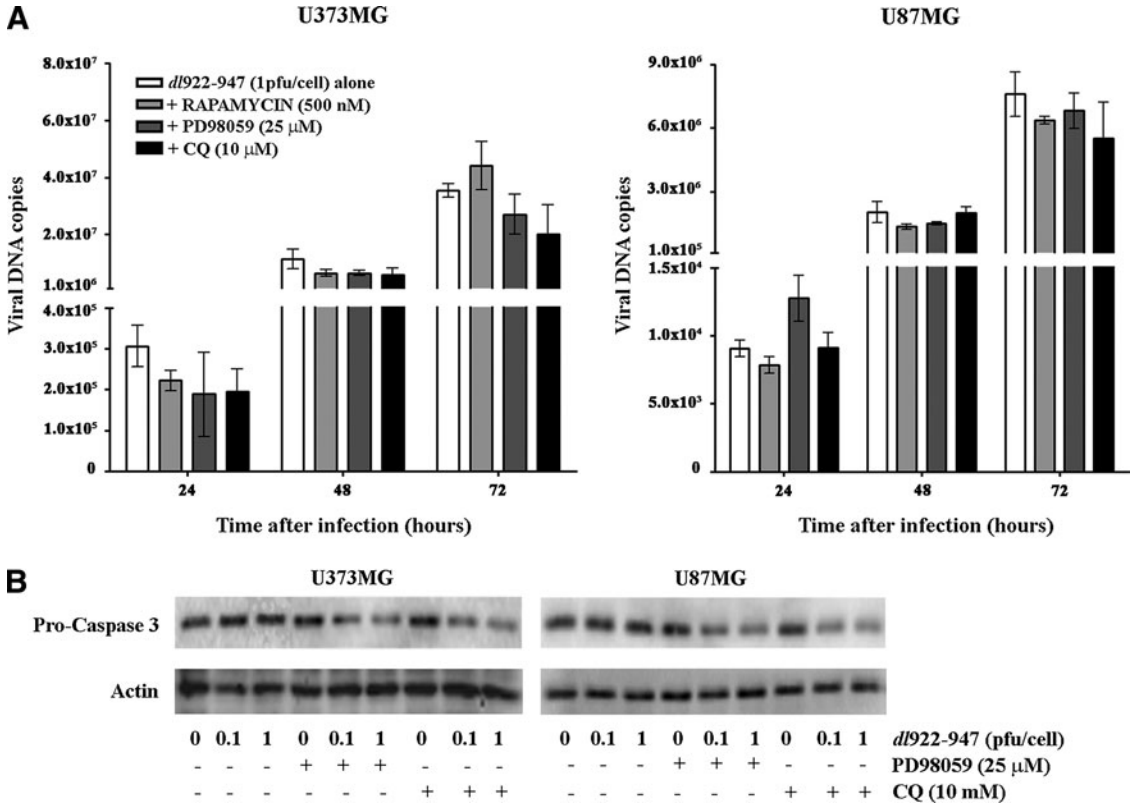

FIG. 6. **(A)** U373MG and U87MG cells were treated with rapamycin (500 n*M*), PD98059 (25 μM), or CQ (10 μM) and then infected with *dl*922–947 (1 PFU/cell). The number of viral copies was evaluated over time by real-time PCR. **(B)** Cells were treated with PD98059 or CQ for 2 hr and then infected with *dl*922–947 at the indicated MOIs. After 72 hr, caspase-3 levels were analyzed by Western blot, using β-actin as a loading control.

caspase-3 activation in glioma cells infected with *dl*922–947 showed that the inhibition of autophagy with PD98059 or CQ leads to a reduction of procaspase-3 levels, suggestive of caspase-3 cleavage (Fig. 6B). These results indicate that the increase in viral cytotoxicity in the presence of autophagy inhibitors might be due to the activation of apoptosis, rather than increased viral replication.

Chloroquine enhances dl922–947 oncolytic activity in vivo

To validate the potential therapeutic use of antiautophagic drugs in association with *dl*922–947, we analyzed the effects of the virus combined with CQ in U87MG xenograft tumors. Athymic mice were injected with U87MG cells and after 20 days the animals were randomized into four groups ($T = 0$ days).

In mice receiving the single treatments (*dl*922–947 or CQ), a nonsignificant reduction of tumor growth was observed, whereas CQ and *dl*922–947 combination treatment resulted in highly significant tumor growth inhibition (Fig. 7A). Starting from $T = 11$ days, the differences in tumor volume among the untreated group, the groups receiving the single treatments, and the group receiving the combined treatment were significant ($^*p < 0.05$), and became highly significant ($^{**}p < 0.01$) at $T = 23$ days.

CQ treatment and *dl*922–947 treatment were both able to increase the LC3-II/LC3-I ratio, and this effect was further increased by the combined treatment (Fig. 7B).

Studies have demonstrated that apoptosis-mediated cell death is increased by inhibition of autophagy in cancer cells (Kanzawa *et al*., 2004; Boya *et al*., 2005; Dalby *et al*., 2010; Platini *et al*., 2010). By analyzing caspase-3 activation in treated tumors, we showed that cleaved caspase-3 levels were undetectable in control tumors and barely detectable in *dl*922–947-infected tumors. In contrast, in CQ-treated tumors *dl*922–947 led to a more intense caspase-3 activation, compared with the tumors undergoing the CQ single treatment (Fig. 7B), thus indicating that chloroquine is effective in increasing the antitumor activity of *dl*922–947 and in inducing apoptosis in experimental glioma *in vivo*.

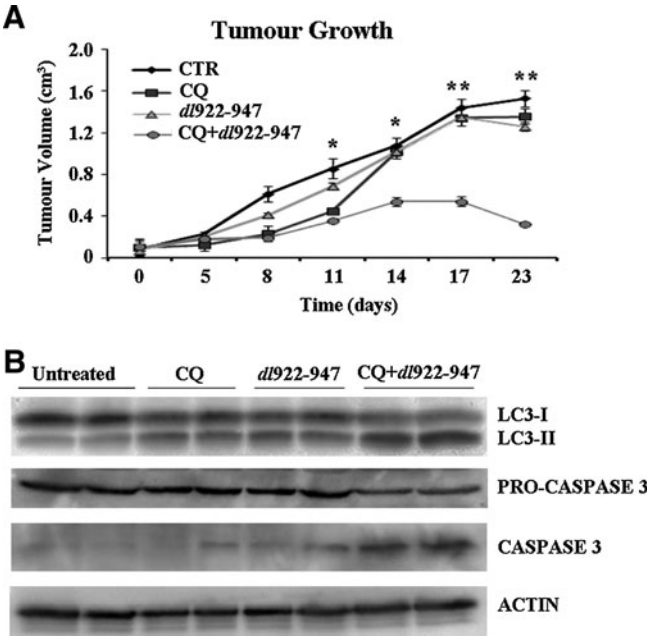

FIG. 7. Chloroquine enhances the activity of *dl*922–947 and delays the growth of glioma tumor xenografts. **(A)** Animals bearing U87MG tumor xenografts were randomized into four groups. Two groups received CQ (45 mg/kg) intraperitoneally every third day. *dl*922–947 (1×10^7 PFU, in a volume of 200 μl) was injected three times per week into one CQ-treated group and one untreated group. The difference between the untreated group and the group receiving the combined treatment become statistically significant ($^*p < 0.05$) from day 11. From day 17, until the end of the treatment, the difference became highly significant ($^{**}p < 0.01$). A statistically significant difference was also observed between the group receiving the combined treatment and the single-treatment groups ($^*p < 0.05$) from day 11 and from day 17 ($^{**}p < 0.01$). No statistically significant difference was observed between the groups receiving the single treatments and the untreated control group. **(B)** Animals bearing U87MG xenograft were treated or not with CQ (45 mg/kg) and intratumorally injected with *dl*922–947 (1×10^7 PFU) after 24 hr. Tumor tissue samples from two different animals from each treatment group were homogenized after 48 hr and LC3-I/II or caspase-3 levels were analyzed by Western blot. β-Actin was used as loading control.

Discussion

Glioblastoma multiforme (GBM) is one of the deadliest human cancers (Furnari *et al*., 2007). The therapy for GBM, which includes surgical resection, radiotherapy, and chemotherapy, has shown limited success. Consequently, the development of novel therapeutic approaches to improve patient survival is urgently required. A number of promising oncolytic viruses have demonstrated antiglioma activity in both preclinical and clinical settings (Brandes *et al*., 2008).

In the present study, we have analyzed the effects of E1A-mutated adenovirus *dl*922–947 against glioma cells, confirming its efficacy and showing that glioma cells undergo autophagy in response to *dl*922–947 infection, as confirmed by the dose-dependent development of acidic vesicular organelles, the increase in LC3-II levels, and the reduction of p62 levels. These effects were not observed on infection with control nonreplicating adenovirus (AdGFP or *dl*312), indicating that the activation of autophagy is dependent on viral replication.

In contrast to the induction of autophagy observed in infected cells, we show that *dl*922–947 infection activates the Akt/mTOR/p70s6k pathway, which is considered the main negative regulatory mechanism for autophagy (Blommaart *et al*., 1995; Yang *et al*., 2005), and simultaneously inhibits the ERK1/2 pathway, which is known to promote it (Pattingre *et al*., 2003). The nonreplicating control adenovirus AdGFP did not induce these effects. This apparent discrepancy could be due to compensatory mechanisms selectively operated by glioma cells to escape *dl*922–947 killing, although it is not possible to exclude that other pathways contribute to the cellular autophagic response to *dl*922–947 infection.

To address the role of these modulatory pathways in *dl*922–947-infected cells, we have used pharmacological inhibitors. The MEK-1 inhibitor PD98059 induced a block of autophagy, as shown by a reduction of LC3 conversion. Interestingly, this block was paralleled by an increase in

*dl*922–947 cytotoxicity. Conversely, treatment of infected cells with rapamycin, a well-known autophagy inducer, sharply increased cell survival. All together, our data suggest that autophagy plays a defensive/survival role during the infection with *dl*922–947, the autophagic machinery probably being involved in the destruction of viral structures. On the other hand, the effects exerted by *dl*922–947 infection on intracellular signals could likely represent an attempt of the virus to overcome the cellular autophagic response. Indeed, adenoviral infection can trigger an indirect cellular autophagy defense response and specific viral mechanisms have developed to prevent this response. Our data are in agreement with a study showing activation of mTOR and p70s6k pathway on adenoviral infection to ensure translation initiation of viral mRNAs (O'Shea *et al.*, 2005). Moreover, the early-expressed viral E3 gene product RID-α can insert into the autophagosomal membrane and arrest maturation by preventing fusion to the lysosome, thereby decreasing basal autophagy levels (Cianciola and Carlin, 2009). This latter mechanism can be excluded since *dl922-947* lacks the E3 gene.

It is known that autophagy and viral infections have complex interconnections. It has been suggested that some viruses could use autophagosomes as sites for replication, and therefore autophagy can support viral replication and assembly (Lin *et al*., 2010). Moreover, it has been observed that hepatitis C virus (Dreux *et al*., 2009; Tanida *et al*., 2009), polio virus (Suhy *et al*., 2000), and dengue virus serotypes 2 and 3 (Panyasrivanit *et al*., 2009) are able to sustain their replication by creating membrane alterations through subverting or inducing autophagy. On the other hand, it has been suggested that autophagy can act as a host defense against intracellular pathogens (xenophagy) (Lin *et al*., 2010), because viral replication may be confined within autophagic vesicles. An antiviral effect of autophagy has been confirmed during neurotropic Sindbis virus infection and in herpes simplex virus (HSV)-1 encephalitis (Lin *et al*., 2010).

Oncolytic viruses can modulate autophagy in target cells, including glioma cells. Δ24-RGD oncolytic adenovirus has been shown to induce autophagic cell death in brain tumor stem cells (Jiang *et al*., 2007, 2011). Autophagosome-mediated cell death was also observed in glioma cells infected with an oncolytic adenovirus driven by the survivin promoter (Ulasov *et al*., 2009). Furthermore, hTERT-Ad, an oncolytic adenovirus regulated by the human telomerase reverse transcriptase promoter, induced autophagic cell death in human malignant glioma through inactivation of the Akt/TOR pathway (Ito *et al*., 2006), and the inhibition of autophagy reduced viral cytotoxicity (Yokoyama *et al*., 2008). These results have suggested a role for autophagy as the main pathway of cell death in cells infected with replicating adenoviral vectors (Ito *et al*., 2006). In line with this hypothesis, *in vitro* studies showed that autophagy inhibition can decrease the oncolytic activity of Δ24-RGD in glioma cell lines (Jiang *et al*., 2011) and of the E1B-deleted adenovirus Adhz60 in lung carcinoma cell lines (Rodriguez-Rocha *et al*., 2011).

Here, we show *in vitro* and *in vivo* that inhibition of autophagic pathways increases the activity of the E1A-deleted oncolytic virus *dl*922–947, indicating that autophagy acts as a cell survival response. Our observation is consistent with Baird and colleagues (2008), who have already shown that 3-MA and chloroquine enhance the effects of *dl*922–947 in ovarian carcinoma cells, but are in contrast with those of the above-mentioned studies from Jiang and colleagues (2011) and Rodriguez-Rocha and colleagues (2011). The discrepancies could be due to the different oncolytic adenoviruses analyzed. It is also conceivable that different viruses elicit different cellular responses depending on the cancer cell type. In this regard, in anaplastic thyroid carcinoma cells, we did not observe autophagy after *dl*922–947 infection (Libertini *et al*., 2011), suggesting that the activation of the autophagic process and the subsequent cellular fate are most likely virus and cell type dependent. Further studies are required to better understand how adenoviruses interact with host cells.

Autophagy inhibition is receiving attention as a novel strategy for cancer treatment. New autophagy inhibitors have been reported to act as potent anticancer drugs and/or to sensitize cancer cells to the activity of anticancer agents (Amaravadi *et al*., 2007; Carew *et al*., 2007; Rubinsztein *et al*., 2007; Shingu *et al*., 2009). Chloroquine itself is emerging as a potential anticancer agent against various cancers, including gliomas (Degtyarev *et al*., 2008; Solomon and Lee, 2009). Here, we show that chloroquine strongly enhances the oncolytic effects of *dl*922–947 both *in vitro* and *in vivo*, encouraging the use of antiautophagic drugs for the development of therapies based on the use of *dl*922–947 oncolytic virus for the treatment of gliomas.

Acknowledgments

The authors thank Dr. Tamotsu Yoshimori (Osaka University) and Prof. Noboru Mizushima (Tokyo Medical and Dental University) for kindly providing the plasmid containing LC3 cDNA. The authors thank Salvatore Sequino for excellent technical assistance and Joanne Smith for proofreading this manuscript. Silvana Libertini was the recipient of an FIRC fellowship and is now the recipient of a Marie Curie fellowship. This study was supported by the Associazione Italiana per la Ricerca sul Cancro (AIRC).

Author Disclosure Statement

No competing financial interests exist.

References

Ahmadi, R., Dictus, C., Hartmann, C., *et al.* (2009). Long-term outcome and survival of surgically treated supratentorial low-grade glioma in adult patients. Acta Neurochir. (Wien) 151, 1359–1365.

Amaravadi, R.K., Yu, D., Lum, J.J., *et al.* (2007). Autophagy inhibition enhances therapy-induced apoptosis in a Myc-induced model of lymphoma. J. Clin. Invest. 117, 326–336.

Baehrecke, E.H. (2005). Autophagy: Dual roles in life and death? Nat. Rev. Mol. Cell. Biol. 6, 505–510.

Baird, S.K., Aerts, J.L., Eddaoudi, A., *et al.* (2008). Oncolytic adenoviral mutants induce a novel mode of programmed cell death in ovarian cancer. Oncogene 27, 3081–3090.

Blommaart, E.F., Luiken, J.J., Blommaart, P.J., *et al.* (1995). Phosphorylation of ribosomal protein S6 is inhibitory for autophagy in isolated rat hepatocytes. J. Biol. Chem. 270, 2320–2326.

Botta, G., Perruolo, G., Libertini, S., *et al.* (2010). PED/PEA-15 modulates coxsackievirus–adenovirus receptor expression

and adenoviral infectivity via ERK-mediated signals in glioma cells. Hum. Gene Ther. 21, 1067–1076.

Boya, P., González-Polo, R.A., Casares, N., *et al.* (2005). Inhibition of macroautophagy triggers apoptosis. Mol. Cell. Biol. 25, 1025–1040.

Brandes, A.A., Tosoni, A., Franceschi, E., *et al.* (2008). Glioblastoma in adults [review]. Crit. Rev. Oncol. Hematol. 67, 139–152.

Cardenas, M.E., Cutler, N.S., Lorenz, M.C., *et al.* (1999). The TOR signaling cascade regulates gene expression in response to nutrients. Genes Dev. 13, 3271–3279.

Carew, J.S., Nawrocki, S.T., Kahue, C.N., *et al.* (2007). Targeting autophagy augments the anticancer activity of the histone deacetylase inhibitor SAHA to overcome Bcr-Abl-mediated drug resistance. Blood 110, 313–322.

Cheong, S.C., Wang, Y., Meng, J.H., *et al.* (2008). E1A-expressing adenoviral E3B mutants act synergistically with chemotherapeutics in immunocompetent tumor models. Cancer Gene Ther. 15, 40–50.

Cianciola, N.L., and Carlin, C.R. (2009). Adenovirus RID-α activates an autonomous cholesterol regulatory mechanism that rescues defects linked to Niemann-Pick disease type C. J. Cell Biol. 187, 537–552.

Dalby, K.N., Tekedereli, I., Lopez-Berestein, G., and Ozpolat, B. (2010). Targeting the prodeath and prosurvival functions of autophagy as novel therapeutic strategies in cancer. Autophagy 6, 322–329.

Degtyarev, M., De Mazière, A., Orr, C., *et al.* (2008). Akt inhibition promotes autophagy and sensitizes PTEN-null tumors to lysosomotropic agents. J. Cell Biol. 183, 101–116.

Díaz-Troya, S., Pérez-Pérez, M.E., Florencio, F.J., and Crespo, J.L. (2008). The role of TOR in autophagy regulation from yeast to plants and mammals. Autophagy 4, 851–865.

Dreux, M., Gastaminza, P., Wieland, S.F., and Chisari, F.V. (2009). The autophagy machinery is required to initiate hepatitis C virus replication. Proc. Natl. Acad. Sci. U.S.A. 106, 14046–14051

Fueyo, J., Gomez-Manzano, C., Alemany, R., *et al.* (2000). A mutant oncolytic adenovirus targeting the Rb pathway produces anti-glioma effect *in vivo*. Oncogene. 19, 2–12.

Furnari, F.B., Fenton, T., Bachoo, R.M., *et al.* (2007). Malignant astrocytic glioma: Genetics, biology, and paths to treatment [review]. Genes Dev. 21, 2683–2710.

Haseley, A., Alvarez-Breckenridge, C., Chaudhury, A.R., and Kaur, B. (2009). Advances in oncolytic virus therapy for glioma. Recent Pat. CNS Drug Discov. 4, 1–13

Heise, C., Hermiston, T., Johnson, L., *et al.* (2000). An adenovirus E1A mutant that demonstrates potent and selective systemic anti-tumoral efficacy. Nat. Med. 6, 1134–1139.

Ito, H., Aoki, H., Kühnel, F., *et al.* (2006). Autophagic cell death of malignant glioma cells induced by a conditionally replicating adenovirus. J. Natl. Cancer Inst. 98, 625–636.

Jiang, H., Gomez-Manzano, C., Aoki, H., *et al.* (2007). Examination of the therapeutic potential of Delta-24-RGD in brain tumor stem cells: Role of autophagic cell death. J. Natl. Cancer Inst. 99, 1410–1414.

Jiang, H., White, E.J., Ríos-Vicil, C.I., *et al.* (2011). Human adenovirus type 5 induces cell lysis through autophagy and autophagy-triggered caspase activity. J. Virol. 85, 4720–4729.

Kabeya, Y., Mizushima, N., Ueno, T., *et al.* (2000). LC3, a mammalian homologue of yeast Apg8p, is localized in autophagosome membranes after processing. EMBO J. 19, 5720–5728.

Kanzawa, T., Germano, I.M., Komata, T., *et al.* (2004). Role of autophagy in temozolomide-induced cytotoxicity for malignant glioma cells. Cell Death Differ. 11, 448–457.

Komatsu, M., and Ichimura, Y. (2010). Physiological significance of selective degradation of p62 by autophagy. FEBS Lett. 584, 1374–1378 [review]. FEBS Lett. 584, 1374–1378.

Kondo, Y., Kanzawa, T., Sawaya, R., and Kondo, S. (2005). The role of autophagy in cancer development and response to therapy. Nat. Rev. Cancer 5, 726–734.

Libertini, S., Iacuzzo, I., Ferraro, A., *et al.* (2007). Lovastatin enhances the replication of the oncolytic adenovirus *dl*1520 and its antineoplastic activity against anaplastic thyroid carcinoma cells. Endocrinology 148, 5186–5194.

Libertini, S., Iacuzzo, I., Perruolo, G., *et al.* (2008). Bevacizumab increases viral distribution in human anaplastic thyroid carcinoma xenografts and enhances the effects of E1A-defective adenovirus *dl*922–947. Clin. Cancer Res. 14, 6505–6514.

Libertini, S., Abagnale, A., Passaro, C., *et al.* (2011). AZD1152 negatively affects the growth of anaplastic thyroid carcinoma cells and enhances the effects of oncolytic virus *dl*922–947. Endocr. Relat. Cancer 18, 129–141.

Lin, L.T., Dawson, P.W., and Richardson, C.D. (2010). Viral interactions with macroautophagy: A double-edged sword. Virology 402, 1–10.

Loos, B., and Engelbrecht, A.M. (2009). Cell death: A dynamic response concept. Autophagy 5, 590–603.

Meijer, A.J., and Codogno, P. (2004). Regulation and role of autophagy in mammalian cells. Int. J. Biochem. Cell Biol. 36, 2445–2462.

Mizushima, N. (2007). Autophagy: Process and function. Genes Dev. 21, 2861–2873.

Oriente, F., Iovino, S., Cabaro, S., *et al.* (2011). Prep1 controls insulin glucoregulatory function in liver by transcriptional targeting of SHP1 tyrosine phosphatase. Diabetes 60, 138–147.

O'Shea, C.C., Choi, S., McCormick, F., and Stokoe, D. (2005). Adenovirus overrides cellular checkpoints for protein translation. Cell Cycle 4, 883–888.

Paglin, S., Hollister, T., Delohery, T., *et al.* (2001). A novel response of cancer cells to radiation involves autophagy and formation of acidic vesicles. Cancer Res. 61, 439–444.

Panyasrivanit, M., Khakpoor, A., Wikan, N., and Smith, D.R. (2009). Linking dengue virus entry and translation/replication through amphisomes. Autophagy 5, 434–435.

Pattingre, S., Bauvy, C., and Codogno, P. (2003). Amino acids interfere with the ERK1/2-dependent control of macroautophagy by controlling the activation of Raf-1 in human colon cancer HT-29 cells. J. Biol. Chem. 278, 16667–16674.

Platini, F., Pérez-Tomás, R., Ambrosio, S., and Tessitore, L. (2010). Understanding autophagy in cell death control. Curr. Pharm. Des. 16, 101–113.

Rodriguez-Rocha, H., Gomez-Gutierrez, J.G., Garcia-Garcia, A., *et al.* (2011). Adenoviruses induce autophagy to promote virus replication and oncolysis. Virology 416, 9–15.

Rubinsztein, D.C., Gestwicki, J.E., Murphy, L.O., and Klionsky, D.J. (2007). Potential therapeutic applications of autophagy. Nat. Rev. Drug Discov. 6, 304–312.

Scarlatti, F., Maffei, R., Beau, I., *et al.* (2008). Non-canonical autophagy: An exception or an underestimated form of autophagy? Autophagy 4, 1083–1085.

Shigemitsu, K., Tsujishita, Y., Hara, K., *et al.* (1999). Regulation of translational effectors by amino acid and mammalian target of rapamycin signalling pathways: Possible involvement of autophagy in cultured hepatoma cells. J. Biol. Chem. 274, 1058–1065.

Shingu, T., Fujiwara, K., Bögler, O., *et al.* (2009). Inhibition of autophagy at a late stage enhances imatinib-induced cytotoxicity in human malignant glioma cells. Int. J. Cancer 124, 1060–1071.

Solomon, V.R., and Lee, H. (2009). Chloroquine and its analogs: A new promise of an old drug for effective and safe cancer therapies [review]. Eur. J. Pharmacol. 625, 220–233.

Suhy, D.A., Giddings, T.H., Jr., and Kirkegaard, K. (2000). Remodeling the endoplasmic reticulum by poliovirus infection and by individual viral proteins: An autophagy-like origin for virus-induced vesicles. J. Virol. 74, 8953–8965.

Tanida, I., Fukasawa, M., Ueno, T., *et al.* (2009). Knockdown of autophagy-related gene decreases the production of infectious hepatitis C virus particles. Autophagy 5, 937–945.

Tyler, M.A., Ulasov, I.V., and Lesniak, M.S. (2009). Cancer cell death by design: Apoptosis, autophagy and glioma virotherapy. Autophagy 5, 856–857.

Ulasov, I.V., Tyler, M.A., Zhu, Z.B., *et al.* (2009). Oncolytic adenoviral vectors which employ the survivin promoter induce glioma oncolysis via a process of beclin-dependent autophagy. Int. J. Oncol. 34, 729–742.

Yang, Y.P., Liang, Z.Q., Gu, Z.L., and Qin, Z.H. (2005). Molecular mechanism and regulation of autophagy. Acta Pharmacol. Sin. 26, 1421–1434.

Yokoyama, T., Iwado, E., Kondo, Y., *et al.* (2008). Autophagy-inducing agents augment the antitumor effect of telerase-selve oncolytic adenovirus OBP-405 on glioblastoma cells. Gene Ther. 15, 1233–1239.

Address correspondence to:
Dr. Giuseppe Portella
Dipartimento di Biologia e Patologia Cellulare e Molecolare
Facoltà di Medicina e Chirurgia
Università di Napoli Federico II
via S. Pansini 5
80131 Naples
Italy

E-mail: portella@unina.it

Received for publication July 6, 2011;
accepted after revision February 8, 2012.

Published online: April 4, 2012.

Endocrine-Related Cancer (2011) **18** 129–141

AZD1152 negatively affects the growth of anaplastic thyroid carcinoma cells and enhances the effects of oncolytic virus *dl922-947*

Silvana Libertini, Antonella Abagnale, Carmela Passaro, Ginevra Botta, Sara Barbato, Paolo Chieffi[1] and Giuseppe Portella*

Dipartimento di Biologia e Patologia Cellulare e Molecolare, Facoltà di Medicina e Chirurgia, Università di Napoli Federico II, Via S. Pansini 5, 80131 Napoli, Italy
[1]Dipartimento di Medicina Sperimentale, II Università di Napoli, Via Costantinopoli 16, 80138 Napoli, Italy

(Correspondence should be addressed to G Portella; Email: portella@unina.it)

*(S Libertini is now at The Beatson Institute for Cancer Research, Switchback Road, Bearsden, Glasgow G61 1BD, UK)

Abstract

Novel therapeutic approaches are required for the treatment of anaplastic thyroid carcinoma (ATC), an incurable disease resistant to current available therapies. Aurora B is an important mitotic kinase involved in chromosome segregation and cytokinesis. It is overexpressed in many cancers including ATC and represents a potential target for chemotherapy. The effects of AZD1152, a specific Aurora B kinase inhibitor, have been evaluated against ATC, showing G_2/M accumulation, polyploidy and subsequent cell death by mitotic catastrophe upon drug treatment. Only three administrations of AZD1152 significantly reduced the growth of ATC tumour xenogratfs. Oncolytic viruses in association with other forms of treatment have proven highly promising in preclinical and clinical reports. The oncolytic adenovirus *dl922-947* is active against ATC cells, and we have evaluated the effects of the association between AZD1152 and *dl922-947*. In cells treated with virus and drug, we report additive/synergistic killing effects. Interestingly, the phosphorylation of histone H3 (Ser10), the main Aurora B substrate, is inhibited by *dl922-947* in a dose-dependent manner, and completely abolished in association with AZD1152. The combined treatment significantly inhibited the growth of ATC tumour xenografts with respect to single treatments. Our data demonstrate that the Aurora B inhibitor AZD1152, alone or in combination with oncolytic virus *dl922-947*, could represent a novel therapeutic option for the treatment of ATC.

Endocrine-Related Cancer (2011) **18** 129–141

Introduction

Anaplastic thyroid carcinoma (ATC) is one of the most aggressive human malignancies, responsible for up to 40% of mortality from thyroid cancer. Although multimodality treatments are successfully applied for well-differentiated thyroid carcinomas, ATC survival rates have not been improved for decades: after diagnosis, patients have a median survival time of 4–6 months (Smallridge *et al*. 2009). Development and evaluation of novel therapeutic strategies are, therefore, desperately required.

Several approaches of gene therapy have been studied for ATC, such as differentiating therapy to restore radioiodine uptake, suicide therapy and oncolytic viruses. The latter are viral mutants able to replicate selectively in, and destroy tumour cells. The most common approach to achieve selectivity is the deletion of viral genes whose product is necessary for replication in normal cells, but expendable in cancer cells (Mullen & Tanabe 2002).

dl922-947 is an oncolytic adenovirus, which bears a deletion of 24 bp in E1A-conserved region 2 (CR2)

DOI: 10.1677/ERC-10-0234

Online version via http://www.endocrinology-journals.org

(Heise *et al*. 2000). This region normally binds to, and inactivates, host cell Rb, thus causing the release of E2F, followed by S-phase entry and subsequent viral DNA replication. Lacking a functional E1A-CR2 region, *dl922-947* mutant is unable to trigger S-phase entry of quiescent normal cells, but can actively replicate in cells with an aberrant G_1–S checkpoint. This checkpoint is lost in almost all cancer cells, and several *in vitro* and *in vivo* studies demonstrate the efficacy of *dl922-947* in a range of cancer cell lines (Heise *et al*. 2000). Its killing activity exceeds that of adenovirus 5 wild type (Ad5wt) and of the first generation virus *dl1520* (Heise *et al*. 2000); a phase I trial of *dl922-947* in women with relapsed ovarian cancer is under way (Baird *et al*. 2008).

We have shown that *dl922-947* is active against ATC cell lines and tumour xenografts (Libertini *et al*. 2008). However, data accumulated so far suggest that the oncolytic activity of viruses, although impressive, requires assistance in order to reach full efficacy. Using viruses in association with other forms of treatment has proven highly promising in preclinical and clinical reports. The association of viruses with specific drugs, not only able to directly kill tumour cells but also to increase viral oncolytic activity, would represent a powerful therapeutic tool.

The mitotic serine–threonine kinase Aurora B is a chromosomal passenger protein (Keen & Taylor 2009). Together with INCENP, Borealin and survivin, it exerts essential functions during mitosis, such as modifying histones at the chromatin, correcting misattachments while at the centromere, and regulating cytokinesis at the central spindle and later midbody (Keen & Taylor 2009). Aurora B is overexpressed in several human cancers, and its expression directly correlates with malignancy (Katayama *et al*. 1999, Araki *et al*. 2004, Chieffi *et al*. 2004, 2006, Kurai *et al*. 2005, Smith *et al*. 2005, Sorrentino *et al*. 2005, López-Ríos *et al*. 2006, Vischioni *et al*. 2006, Qi *et al*. 2007, Tanaka *et al*. 2008). Upon Aurora B depletion or inhibition, the cells with intact checkpoint function arrest with 4N DNA content, while those with compromised p53-dependent pathway undergo endoreduplication and apoptosis (Keen & Taylor 2004).

Cells lacking a p53-mediated post-mitotic checkpoint are highly responsive to Aurora B inhibition, thus suggesting a wide therapeutic window between normal and tumour cells (Keen & Taylor 2004). In human ATC, alterations of the p53 tumour suppressor gene are a constant feature (Smallridge *et al*. 2009), and we have previously shown that Aurora B is overexpressed in ATC (Sorrentino *et al*. 2005). All these data indicate that the treatment of ATC could benefit from the use of an Aurora B inhibitor.

It has been reported that the block in G_2/M phase improves viral entry and replication (Seidman *et al*. 2001); therefore, we have hypothesized that Aurora B inhibition could enhance the oncolytic effects of *dl922-947* adenovirus. We selected AZD1152 as an Aurora B inhibitor due to its high selectivity for Aurora B and its good solubility, which makes it appropriate for clinical use (Wilkinson *et al*. 2007). Recent studies showed that AZD1152 significantly reduces tumour growth in a panel of solid human cancer xenograft models (Wilkinson *et al*. 2007).

In this report, we show that AZD1152 is active against ATC cells, inducing cell death through mitotic catastrophe. We also demonstrate that the drug is able to enhance the anti-neoplastic effects of *dl922-947* oncolytic virus in both *in vitro* and *in vivo* models of ATC. Our data hint towards a mechanism of how AZD1152 and *dl922-947* can synergistically kill ATC cells.

Materials and methods

Cells, adenoviruses and drugs

Human ATC cell lines such as BHT101-5, Cal62, FRO and 8505C have been authenticated as shown previously (Schweppe *et al*. 2008). All ATC cell lines used have a non-functional *p53* gene: in BHT101-5 cells, a 251 Ile→Thr substitution has been reported, 8505C cells present an Arg→Gly in position 248, Cal62 cells are characterized by A161D mutation while FRO cells are p53 null (Schweppe *et al*. 2008).

dl922-947 has a 24-bp deletion in E1A-CR2 (Heise *et al*. 2000). AdGFP is a non-replicating E1-deleted adenovirus encoding green fluorescent protein (GFP; Libertini *et al*. 2007). Viral stocks were expanded, purified, stored and quantified as previously reported (Libertini *et al*. 2007).

AZD1152-HQPA was dissolved in DMSO to a final concentration of 10 mM and stored at −20 °C. AZD1152 was dissolved in 0.3 M Tris–HCl (pH 9) to a final concentration of 10 mg/ml, each mouse received 300 µl of suspension i.p., i.e. 3 mg of prodrug, corresponding to 2.5 mg of active drug.

Viability assay

BHT101-5, Cal62, FRO and 8505C cell lines have been treated with a different range of drug concentrations since their sensitivity to AZD1152 treatment varies. Treated cells were fixed with 50% TCA and stained with 0.4% sulforhodamine B in 1% acetic

acid as already described (Libertini *et al*. 2008). The percentages of surviving cells after treatment were calculated by assuming that the number of surviving untreated cells is 100%.

FACS analysis

PH3 and cell cycle

Cells treated with AZD1152, virus or both were harvested by trypsinization, fixed in 70% cold ethanol and prepared as already described (Esposito *et al*. 2009) using antibodies anti-phospho-histone H3 (Ser10) and anti-histone H3 (Upstate, Biotechnology Inc, Waltham, MA, USA).

AdGFP infection

FRO cells were treated for 24 h with AZD1152 25 nM, washed and then infected with AdGFP (0, 25 or 50 pfu/cell). Forty-eight hours post infection, cells were trypsinized, washed, resuspended in 300 µl of PBS and analysed for the emission in FITC channel.

Samples were acquired with a CYAN flow cytometer (DAKO Corporation, San Jose, CA, USA) and analysed using SUMMIT software.

Micronuclei counting

Cells grown on cover slips and treated as described were fixed 15′ in 3% paraformaldehyde, permeabilized with 0.2% Triton X-100 10′ and then stained 5′ with Hoechst 33258 (1 µg/ml, Sigma–Aldrich). The washes were followed by mounting the cover slips onto glass slides with glycerol:PBS 1:1.

Synchronization

Cells were treated for 12 h with thymidine (2 mM), released for 10 h in fresh media and retreated for further 12 h with thymidine. Cells were washed twice in fresh media, then treated and harvested as indicated.

Antibodies for western blot

Procaspase-3 (sc-56053; 1:100, Santa Cruz Biotechnology Inc, Santa Cruz, CA, USA), caspase-3 (ab13585, 1:500, Abcam, Cambridge, MA, USA), phospho-histone H3 (Ser10) (06570, 1:500, Upstate Biotechnology Inc, Waltham, MA, USA), histone H3 rabbit polyclonal IgG (31949; 1:1000, Upstate) and actin (sc-10731, 1:500, Santa Cruz) are the antibodies used for western blot.

Tumourigenicity assay, viral replication and distribution

Experiments were performed in 6-week-old female athymic mice (Charles River Laboratories International Inc, MA, USA). Mice were maintained at the Dipartimento di Biologia e Patologia Animal Facility. Animal experiments were conducted in accordance with accepted standards of animal care and in accordance with the Italian regulations for the welfare of animals used in the studies of experimental neoplasia. The study was approved by our institutional committee on animal care.

To evaluate the effects of *dl922-947* in combination with AZD1152, FRO cells (1×10^7) were injected into the right flank of 80 athymic mice. After 40 days, tumour volume was evaluated, and the animals were divided into four groups (20 animals/group) with similar average tumour size. Tumour diameters were measured with callipers, and tumour volumes (V) were calculated by the formula of rotational ellipsoid: $V=A\times B^2/2$ (A is the axial diameter and B is the rotational diameter).

Viral replication and distribution were evaluated as previously described (Libertini *et al*. 2008).

Statistical analysis

The analysis of the cell killing effect *in vitro* was made by isobolograms generated to calculate the concentration of each agent killing 50% of cells (EC_{50}) using untreated cells or cells treated with one agent only as controls, as previously described (Cheong *et al*. 2008).

Comparisons among different treatment groups in the experiments *in vivo* were made by the ANOVA method and the Bonferroni *post hoc* test using commercial software (GraphPad Prism 4, GraphPad Software Inc, La Jolla, CA, USA). Differences in the rate of tumour growth in mice were assessed for each time point of the observation period.

Results

AZD1152 treatment induces cell death in ATC cells

Aurora B kinase is overexpressed in ATC, and blocking its expression or activity reduces ATC cell growth (Sorrentino *et al*. 2005). To confirm Aurora B as a therapeutic target, we have evaluated the effects of Aurora B inhibitor AZD1152 on the survival of human ATC cell lines FRO, BHT101-5, 8505C and Cal62.

All cell lines are highly sensitive to AZD1152, with an IC_{50} ranging from 8 to 50 nM for Cal62 and

FRO cells respectively (Fig. 1A). Aurora B inhibition induces endoreduplication thus increasing cell diameter; this could underestimate drug effects when standard proliferation assays are used. Therefore, the anti-proliferative effect of AZD1152 was also determined by cell counting. As shown in Fig. 1B, the inhibitor significantly reduces cell number after 1 day of treatment, further confirming the high efficacy of the drug.

AZD1152 blocks Ser10 H3 phosphorylation and induces mitotic catastrophe

Aurora B phosphorylates histone H3 on serine 10 during mitosis (Prigent & Dimitrov 2003). To confirm AZD1152 effects on Aurora B activity, we treated FRO and BHT101-5 cells for 24 h and performed a FACS analysis by using a specific anti-phospho-Ser10 histone H3 antibody (Fig. 1C).

To analyse the effects of Aurora B inhibition on cell cycle, cells were stained with propidium iodide. Cell cycle profiles were also analysed after 48 h to monitor the effects of a prolonged exposure.

As shown in Fig. 2A and B, a dose- and time-dependent increase in polyploid cells was observed; this increase was paralleled by the reduction in Ser10 H3 phosphorylation levels (Fig. 1C). After 24 h of treatment, a subG$_1$ fraction and G$_2$/M accumulation were observed in both cell lines. Immunofluorescence analysis shows that the inhibition of Ser10 H3 phosphorylation caused by AZD1152 treatment does not affect chromosome condensation (Fig. 1D).

The increase of cells with $\geq$4N DNA content and a subsequent subG$_1$ suggest that AZD1152-treated cells die through mitotic catastrophe, a form of programmed cell death resulting from aberrant mitosis. Such mitosis does not produce proper

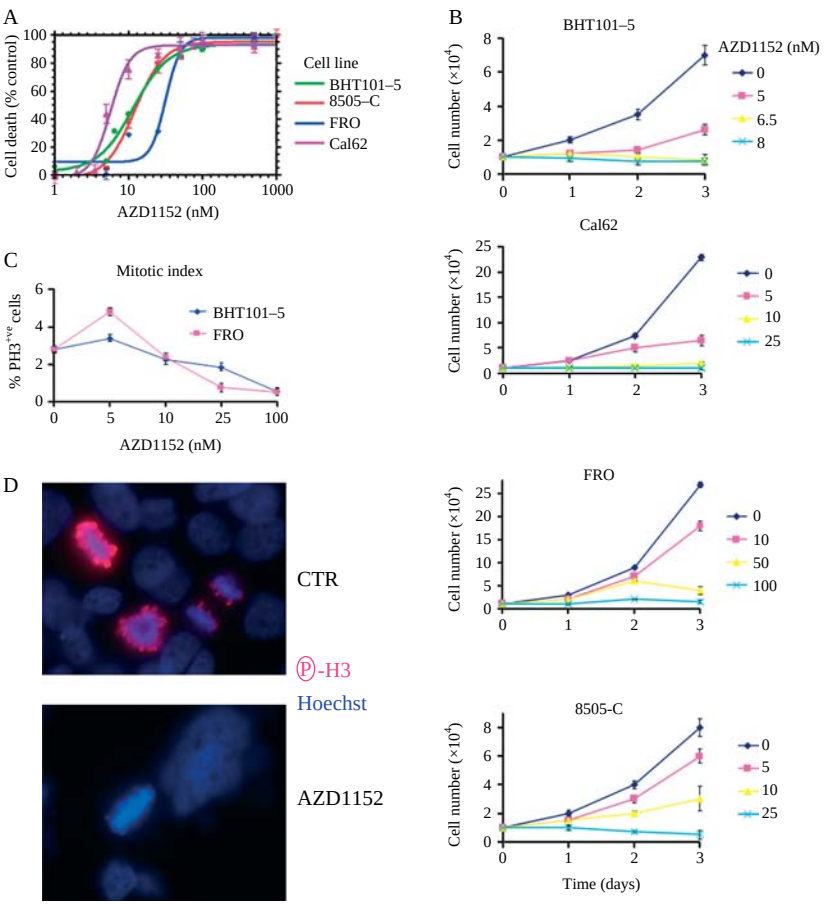

Figure 1 AZD1152 kills ATC cells. (A) ATC cells were treated with AZD1152, and survival was evaluated after 7 days by sulforhodamine B method. (B) Cells were plated in 12-well plates, treated with different amount of AZD1152 and counted at the indicated time points. (C) FRO and BHT101-5 cells were treated for 24 h, and phospho-Ser10 H3 levels were evaluated by FACS analysis. The bars in (A), (B) and (C) indicate the S.D. The data are the mean of three different experiments. (D) FRO cells were treated or not for 16 h with 100 nM AZD1152 and phospho-Ser10 H3 visualized by immunofluorescence.

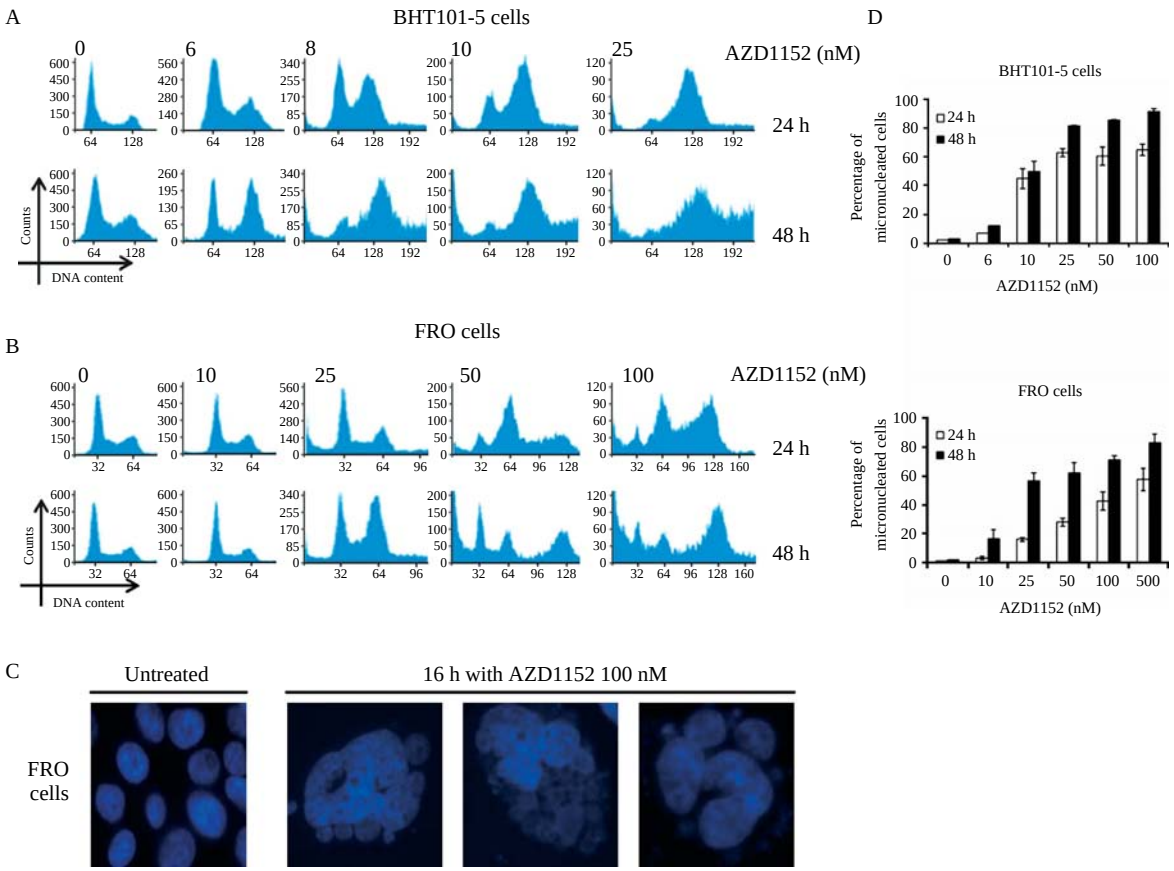

Figure 2 AZD1152 induces mitotic catastrophe. Cell cycle of BHT101-5 (A) and FRO (B) cells was analysed 24 (upper panel) or 48 h (lower panel) after AZD1152 treatment. (C) Hoechst staining of FRO cells treated or not with AZD1152. The same magnification (40×) was used in the images. (D) Quantification of data obtained by Hoechst staining. The cells with ≥3 micronuclei were counted as positive.

chromosome segregation and cell division, and leads to the formation of large non-viable cells characterized by micronuclei (Castedo *et al*. 2004*a*). Micronuclei are nuclear envelopes around clusters of missegregated chromosomes (examples in Fig. 2C). By immunofluorescence, we have quantified the number of FRO- and BHT101-5-micronucleated cells after AZD1152 treatment (Fig. 2D). A clear dose- and time-dependent increase in the number of micronucleated cells was observed.

AZD1152 and *dl922-947* show synergistic effects on ATC cells

It has been proposed that drugs interfering with mitosis and cytokinesis could potentiate viral oncolysis (Seidman *et al*. 2001). Therefore, we hypothesized that the association with AZD1152 could positively affect the activity of the oncolytic adenovirus *dl922-947*.

FRO and BHT101-5 cells were treated with AZD1152 and simultaneously infected with *dl922-947*; cell survival was evaluated after 7 days, showing additive/synergistic effects (Fig. 3A, Table 1). In order to understand whether AZD1152 sensitizes cells to viral action, we have treated FRO and BHT101-5 cells with AZD1152 for 24 h and then infected with *dl922-947*. The effects were evaluated after 6 days: the data obtained show that 24 h pre-treatment is sufficient to significantly increase the killing activity of *dl922-947* (Fig. 3B, Table 2), confirming that the inhibitor sensitizes cells to viral action. It is also worth noting that 24 h treatment with AZD1152 alone significantly affects cell survival.

AZD1152 does not affect cellular infectivity

It has been proposed that drugs can enhance viral oncolytic activity by increasing viral entry in target cells (Anders *et al*. 2003). To monitor this step, FRO

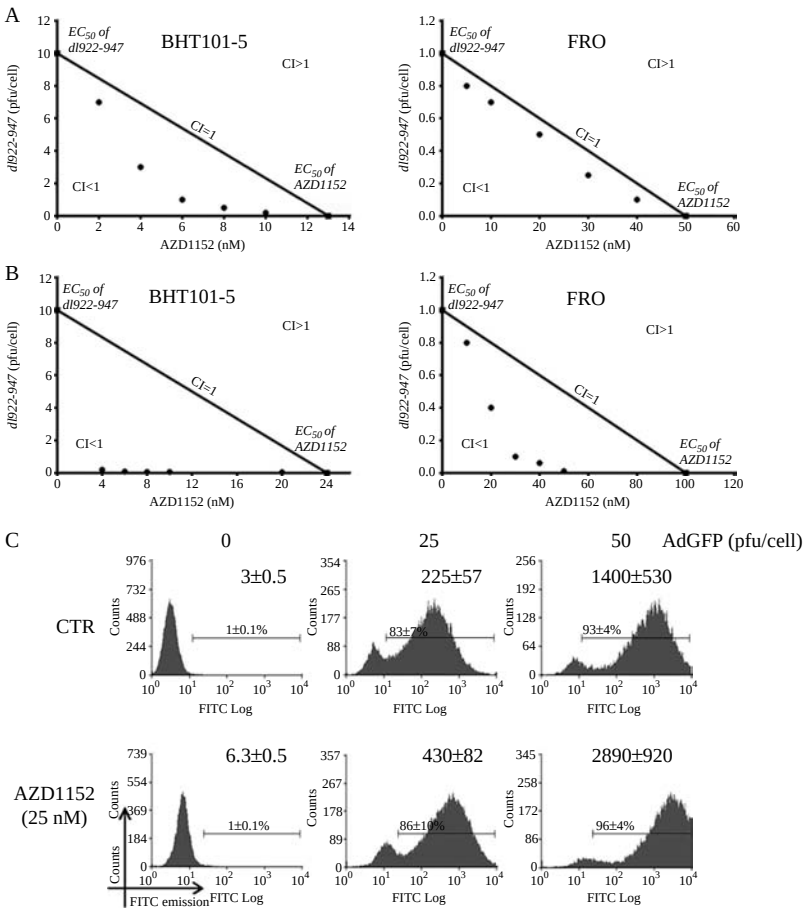

Figure 3 AZD enhances the oncolytic activity of *dl922-947* but does not increase cellular infectivity. (A) FRO and BHT101-5 cells were treated with five fixed combination ratios of *dl922-947* and AZD1152, and cell viability was determined by sulforhodamine B assay 7 days post infection. Dose–response curve and EC_{50} values were used to construct isobolograms and calculate combination indexes (CI) for each ratio. Ratios are expressed as virus (pfu/cell) to drug (nM). A line is drawn connecting the EC_{50} values of the virus and drug as a single agent. A ratio producing a $CI \leq 0.8$ is considered synergistic, a ratio producing CIs between 0.8 and 1.2 is considered additive and a ratio producing $CI \geq 1.2$ is considered antagonistic. (B) Cells were treated for 24 h with the drug; then, the media were replaced with media containing the virus alone. Survival was evaluated after 6 days with isobolograms obtained as above. (C) FRO cells were treated for 24 h with AZD1152, and then infected with AdGFP. Viral entry was quantified by monitoring the percentage of GFP-positive cells (numbers on the bars) and the average expression in FITC channel (numbers on top right) after 24 h. The percentage of GFP-positive cells does not significantly change upon AZD1152 pre-treatment, being ~85% for 25 pfu/cell and ~95% for 50 pfu/cell, regardless of drug pre-treatment. The FITC ratio in infected and uninfected cells upon drug treatment showed no significant change (75±31-fold increase versus 68±19 for 25 pfu/cell and 466±246-fold increase versus 458±182 for 50 pfu/cell).

cells were pre-treated for 24 h with AZD1152 at a low concentration (able to induce G_2/M block but not death after 48 h) and then infected with a non-replicating reporter adenovirus transducing GFP (AdGFP). After additional 24 h, GFP emission was evaluated by cytofluorimetric analysis. The percentage of GFP cells was not modified by AZD1152 pre-treatment, although a positive shift in FITC channel was observed (Fig. 3C). This increase is apparent, since AZD1152 treatment enlarges the cells thus enhancing basal fluorescence. Indeed, analysis of the FITC ratio in infected and uninfected cells treated or not with AZD1152 showed no significant difference. Similar results were obtained with BHT101-5 cells (data not shown).

dl922-947 and AZD1152 induce subG$_1$ phase population in treated cells

Next, cell cycle profiles in infected cells, treated or not with AZD1152, were evaluated. To better discriminate differences in cell cycle phases, timing and cell death, a double thymidine block was performed to synchronize cells in G_1. As shown in Fig. 4, in untreated cells, 10 h

Table 1 Simultaneous treatment with AZD1152 and *dl922-947*

Cell line	Ratio ((pfu/cell)/(nM))	EC_{50} *dl922-947* (pfu/cell)	EC_{50} AZD1152 (nM)	CI
BHT101-5	AZD1152 alone	0	13	
	dl922-947 alone	10	0	
	1:50	0.2	10	0.79
	1:16	0.5	8	0.67
	1:6	1	6	0.56
	1:1	5	4	0.8
	4:1	8	2	0.95
FRO	AZD1152 alone	0	50	
	dl922-947 alone	1	0	
	1:400	0.1	40	0.9
	1:120	0.25	30	0.85
	1:40	0.5	20	0.9
	1:14	0.7	10	0.9
	1:6	0.8	5	0.9

after thymidine release, about 30% of the population re-entered G_1 phase; a similar profile was observed in infected cells. Conversely, after 10 h, AZD1152 induced a G_2/M accumulation that was not modified by the association with *dl922-947*. Starting from 20 h, a significant increase in $subG_1$ phase was observed in both AZD1152- and *dl922-947*-treated cells. Interestingly, the combination between drug and virus increased the percentage of cells in $subG_1$ fraction compared with single treatments. It is also worth noting that, in the combined treatment, the increase in $subG_1$ fraction at later time points is associated with a decrease in polyploidy fractions, suggesting that dying cells ($subG_1$ fraction) are the ones that escaped G_2/M block.

Caspase-3 activation has been observed in some models of mitotic catastrophe (Castedo *et al*. 2004*a*,*b*), and *dl922-947* induces $subG_1$ accumulation and caspase-3 cleavage in ovarian cancer cells (Baird *et al*. 2008). Therefore, we analysed caspase-3 activation in treated ATC cells. As shown in Fig. 5A, while *dl922-947* induces caspase-3 cleavage, AZD1152 does not. Interestingly, in the combined treatment, an earlier decrease of procaspase-3 with respect to virus treatment alone was observed. This observation suggests that the inhibitor could enhance viral-induced cell death by accelerating the activation of caspase-3 pathway.

dl922-947 reduces H3 phosphorylation

FRO cells infected with *dl922-947* show G_2/M accumulation and tetraploidy (Fig. 4), suggestive of a mitotic block. During a normal mitosis, histone H3 is phosphorylated on Ser 10 (28–29); the viral effects on cell cycle prompted us to analyse whether *dl922-947* acted on this substrate.

We treated FRO cells for 24 h with different amounts of virus and drug, alone or in combination. Cells were stained with propidium iodide and with anti-phospho-Ser10 H3 histone antibody to monitor the percentage of PH3-positive cells during the cell cycle (Fig. 5B). *dl922-947* alone is able to decrease the percentage of PH3-positive cells and, together with AZD1152, Ser10 H3 phosphorylation is almost completely abolished: FACS data were confirmed by western blot analysis of PH3 levels (Fig. 5C).

AZD1152 increases *dl922-947* oncolytic activity *in vivo*

To further validate the potential therapeutic use of AZD1152 in association with *dl922-947*, we analysed the effects of the combined treatment on xenograft tumours. To study the effect of the association in the worst possible scenario, FRO cells were chosen, being the least sensitive to AZD1152 effect (Fig. 1) and viral infection (Libertini *et al*. 2008). A low viral dose (1×10^6 pfu) was used to better evaluate the effects of the combined treatment; virus was administered by i.t. injection to avoid first pass effect.

Animals were divided into four groups: untreated, treated with AZD1152, *dl922-947* or both. As shown in Fig. 6A, AZD1152 and *dl922-947* in combination have a stronger anti-tumour activity than when used alone. As already described, no toxicities were observed in virus-treated animals (Libertini *et al*. 2008). Drug-treated animals showed slight weight loss and dehydration on the third day of treatment, but

Table 2 AZD1152 pre-treatment on *dl922-947*-infected cells

Cell line	Ratio ((pfu/cell)/(nM))	EC_{50} *dl922-947* (pfu/cell)	EC_{50} AZD1152 (nM)	CI
BHT101-5	AZD1152 alone	0	24	
	dl922-947 alone	10	0	
	1:500	0.04	20	0.84
	1:167	0.06	10	0.42
	1:114	0.07	8	0.34
	1:62	0.08	5	0.21
	1:20	0.2	4	0.19
FRO	AZD1152 alone	0	100	
	dl922-947 alone	1	0	
	1:5000	0.01	50	0.51
	1:667	0.06	40	0.46
	1:300	0.1	30	0.4
	1:50	0.4	20	0.6
	1:12	0.8	10	0.9

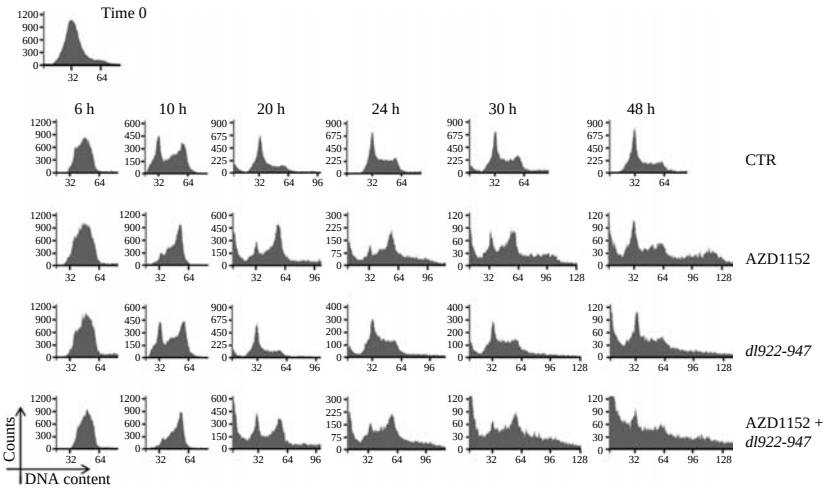

Figure 4 AZD1152 and *dl922-947* induce tetraploidy and cell death. FRO cells were synchronized in G_1 phase and treated with AZD1152 10 nM, *dl922-947* (25 pfu/cell) or both. FACS analysis was performed to analyse the cell cycle.

recovered after 2–3 days. In the combined treatment group, animals took longer to recover (4–5 days), but no other symptoms were observed.

Viral replication analysis in animals pre-treated with AZD1152 showed an increase of genome copies (Fig. 6B). However, this effect was not observed *in vitro* (data not shown). It has been hypothesized that the pre-treatment with anti-neoplastic drugs could improve intratumoural viral diffusion by reducing the number of neoplastic cells (Vähä-Koskela *et al.* 2007). To address this point, FRO xenografts animals, pre-treated or not with AZD1152, were injected intratumourally with AdGFP. GFP expression was evaluated by fluorescence microscopy analysis (Fig. 6C). In control tumours, a faint fluorescence signal was observed, whereas in AZD1152-treated tumours, a more intense fluorescence signal was detected. It is worth noting that both viral replication and distribution were increased three times upon drug treatment (Fig. 6B and C).

Discussion

ATC is one of the most lethal neoplasia and leads to death in a short time. Active therapies are not available, making the development of novel therapeutic strategies imperative (Smallridge *et al.* 2009).

AZD1152 is a reversible ATP-competitive Aurora inhibitor, which is 1000-fold more selective for Aurora kinase B than for Aurora kinase A (Wilkinson *et al.* 2007). The effects of AZD1152 have been already assessed in *in vivo* models of human leukaemia (Wilkinson *et al.* 2007, Yang *et al.* 2007, Walsby *et al.* 2008, Oke *et al.* 2009), breast cancer (Gully *et al.* 2010),

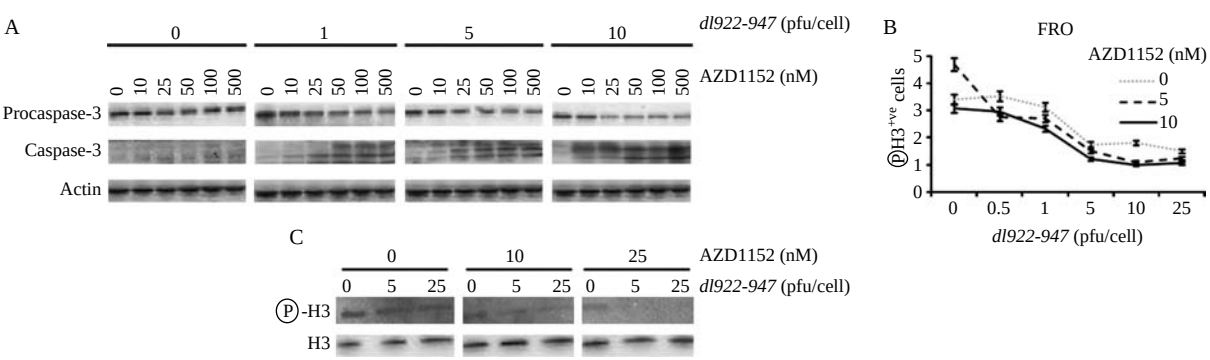

Figure 5 *dl922-947* induces caspase-3 activation and decreases PH3 levels. (A) FRO cells were synchronized in G_1 phase and treated with different combinations of *dl922-947* and AZD1152. Attached and detached cells were harvested, and western blot analysis was performed to quantify procaspase- and activated caspase-3 levels. Fifty micrograms of lysate were loaded in each well. FRO cells were treated for 24 h with different amounts of AZD1152 and *dl922-947*, alone or in combination. Ser10 PH3 levels were evaluated by FACS (B) and western blot analysis (C).

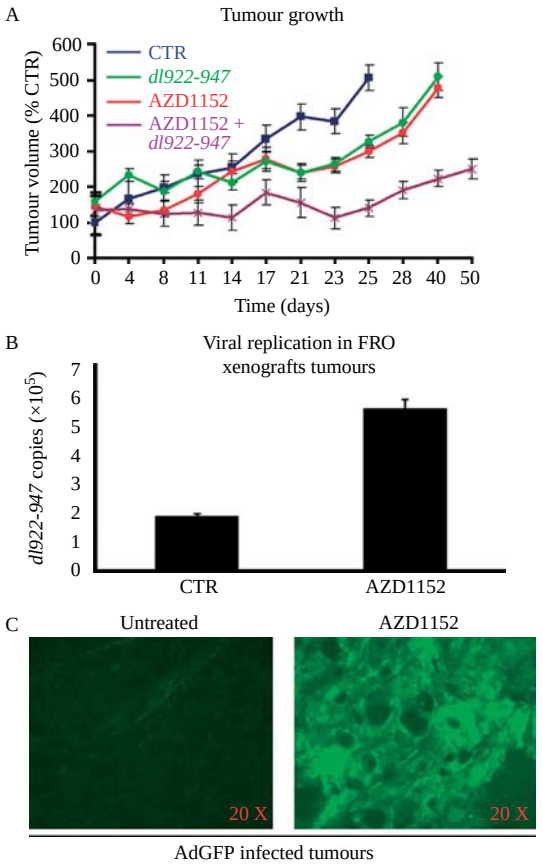

Figure 6 AZD1152 delays tumour growth and facilitates *dl922-947* replication and distribution. (A) Tumour bearing mice were randomized into four groups. Two groups received AZD1152 (100 mg/kg per day) i.p. from T1 to T3 and from T15 to T17. *dl922-947* (1×10^6 pfu, in a volume of 300 μl) was injected at T4, T8, T11 and T15 into one AZD1152-treated group and one untreated group. The control group was injected with saline solution. Tumour volume is expressed as a percentage of the volume observed at day 0 in the control group. The difference between treated and untreated groups becomes statistically significant ($P<0.05$) from day 17 for virus versus control and drug versus control, and from day 8 for combined treatment versus control. At day 21, a significant difference ($P<0.05$) was observed between the combined treatment group and single treatment groups. From day 23 till the end of the treatment, the difference became highly significant ($P<0.01$). (B) FRO cells (1×10^7 cells) were injected intratumourally within ten athymic mice. Forty days later, when tumours were detectable, animals were divided into two groups, which received respectively AZD1152 (2.5 mg/mouse) or saline solution i.p. After 24 h, *dl922-947* (1×10^6 pfu, in a volume of 300 μl) was injected intratumourally in both groups. Two days later, animals were killed. DNA was extracted from 100 mg of tumour tissue, and the number of viral copies was evaluated by real-time PCR. The data are the mean of three different experiments. (C) Ten FRO-induced xenograft tumours were injected i.p with AZD1152 (100 mg/kg per day) or saline solution for 3 consecutive days and, after 2 days, AdGFP (1×10^7 pfu, in a volume of 300 μl) was injected intratumourally in both groups. Two days later, animals were killed, tumours were excised and GFP distribution was evaluated by confocal microscopy. The quantification of the digitized signal showed a threefold increase upon AZD1152 treatment.

hepatocellular carcinoma (Aihara *et al.* 2010), and colon and lung cancers (Wilkinson *et al.* 2007). AZD1152 and other Aurora inhibitors are currently in early clinical evaluation, showing reversible neutropenia as a major side effect (Keen & Taylor 2009).

In the present study, we have demonstrated that AZD1152 is active against ATC cells and that the effects are observed within 24 h. These data are consistent with the high levels of Aurora B expression (Sorrentino *et al.* 2005), the lack of a functional p53 pathway (Schweppe *et al.* 2008) and the short doubling time (10 h) of ATC cells. In the present study, we have also shown that just three doses of AZD1152 significantly delay the growth of ATC tumour xenografts.

Another Aurora inhibitor, VX-680, has been previously evaluated on ATC cell lines showing inhibition of cell proliferation and cell death; however, the drug was not evaluated *in vivo* (Arlot-Bonnemains *et al.* 2008). Cells treated with VX-680 showed an increase in DNA content (>4N), reduction of Ser10 H3 phosphorylation, subG$_1$ accumulation and activation of caspase-3 (Arlot-Bonnemains *et al.* 2008). The authors concluded that VX-680 activated the apoptotic cascade in ATC cells, and suggested that the effects reported were due to the inhibition of Aurora A rather than Aurora B. VX-680 inhibits Aurora kinases with comparable inhibition constants, ranging from 0.6 nM for Aurora A to 18 nM for Aurora B; hence, it is plausible that the effects exerted by VX-680 on ATC cells are due to the inhibition of both Aurora kinases. In addition, it has been previously reported in other cell models that effects seen with VX-680 closely resemble those described for Aurora B inhibition (Keen & Taylor 2004) and mirror the effects described here with AZD1152 on ATC cells. Moreover, the IC$_{50}$ of VX-680 on ATC cells ranged from 25 to 150 nM: these concentrations are also sufficient to inhibit the kinase FLT3 (Harrington *et al.* 2004, Arlot-Bonnemains *et al.* 2008). On the other hand, the IC$_{50}$ of AZD1152 in this study ranges from 5 to 30 nM, indicating that AZD1152 could achieve a therapeutic effect at lower and less toxic concentrations. Therefore, our results clearly indicate using both *in vitro* and *in vivo* models that selective inhibition of Aurora B could represent a therapeutic option for the treatment of ATC.

Oncolytic viruses are emerging as new therapeutic tools for the treatment of cancer, and we previously demonstrated that the mutants *dl1520* and *dl922-947* are active against ATC *in vitro* and *in vivo* (Libertini *et al.* 2007, 2008). It has been reported that drugs able to block cells in G$_2$/M or inhibit cytokinesis could enhance the effects of oncolytic viruses

(Seidman *et al*. 2001). Since AZD1152 has a clear effect on cell division, we wondered whether it could positively affect *dl922-947* activity. The data presented in this manuscript demonstrate the efficacy of this combination both *in vitro* and *in vivo*.

To understand how AZD1152 enhances oncolytic activity, we first monitored viral entry upon drug treatment. Our data show that AZD1152 does not affect viral entry. The synchronization in G_2/M phase leads to modest, but significant, translocation of CAR receptor to the cell surface of A549 lung carcinoma cells (Seidman *et al*. 2001). Although AZD1152-treated cells accumulate in G_2/M phase, membrane levels of CAR and its co-receptors integrins $\alpha_v\beta_3$, $\alpha_v\beta_5$ and $\alpha_v\beta_1$ do not increase after AZD1152 treatment (data not shown). By using AdGFP, we did not observe any difference in viral entry during each cell cycle phase (data not shown). Our observation is not in agreement with Seidman *et al*. (2001); this discrepancy could be due to the different cellular system used or to a very slight increase in receptor levels hidden by the increase in cellular size.

Secondly, we analysed cell death mechanisms induced by virus and drug, alone or in combination. AZD1152 induces a G_2/M block and tetraploidy in ATC cells. This aberrant mitotic phenotype, the presence of micronuclei and the appearance of subG_1 population demonstrate that AZD1152-treated cells die through mitotic catastrophe. According to the literature, mitotic catastrophe could share biochemical hallmarks with apoptosis, such as mitochondrial membrane permeabilization (MMP) and caspase cleavage (Castedo *et al*. 2004*a*,*b*). In our study, despite the clear induction of mitotic catastrophe, AZD1152 did not induce caspase-3 activation (Fig. 5) and MMP (data not shown). Like AZD1152-treated cells, ATC-infected cells show enlargement and polyploidy. However, it is possible to exclude death by mitotic catastrophe since, upon infection, cells detach, a feature not observed in mitotic catastrophe. Moreover, in the few adhering cells, we have not observed the presence of micronuclei (data not shown). We have also excluded autophagic cell death, since neither beclin 1 activation nor LC3I–II conversion were induced, and accumulation of autophagic vesicular organelles was not observed by FACS analysis in acridine orange-stained cells (data not shown). Our data extend to ATC cells the observation of Baird *et al*. (2008) that infection with mutant oncolytic adenovirus leads to programmed cell death lacking the features of classical apoptosis, but showing some apoptotic markers, such as subG_1 accumulation and caspase-3 activation. Interestingly, the association with AZD1152 accelerates the appearance of cleaved caspase-3 and increases the percentage of cells in subG_1 phase. Our results indicate that AZD1152 enhances the cytotoxic effects of oncolytic viruses, although the cell death mechanisms are not yet defined.

During mitosis, Aurora B is involved in phosphorylation of histone H3 on Ser10 (Ditchfield *et al*. 2003, Hauf *et al*. 2003). Accordingly, AZD1152 strongly reduces H3 phosphorylation. It has been reported that the oncolytic herpes virus G47D decreases phospho-Ser10 H3 levels (Passer *et al*. 2009), and we observed that the oncolytic adenovirus *dl922-947* (Fig. 5B) and Ad5wt (personal observation) have a similar effect. These data suggest that modulation of PH3 levels is a common feature of viral infections; it is conceivable that viruses prematurely end mitosis in order to switch cell machinery to viral replication.

The first oncolytic adenovirus described, *dl1520* (Heise *et al*. 1997), has shown improved effects in clinical trials in combinations with chemotherapy (Kumar *et al*. 2008). In 2005, China approved the world's first oncolytic virus therapy for cancer treatment, with modified adenovirus H101, similar to *dl1520* (Yu & Fang 2007). In a phase III trial, a 79% response rate for H101 plus chemotherapy, compared with 40% for chemotherapy alone, was observed (Yu & Fang 2007). Other oncolytic viruses have entered into clinical trials: their efficacy and safety, and synergistic effects in association with other drugs have been demonstrated, confirming virotherapy as a promising direction for the treatment of cancer (Liu *et al*. 2007). Oncolytic viruses target neoplastic cells using a mechanism different from that of anti-neoplastic drug; therefore, the combination treatment could contribute to avoid the development of resistant cancer cells, thus increasing the cure rate.

Data presented here demonstrate that the selective inhibitor of Aurora B kinase AZD1152 is highly effective against ATC cell lines and tumour xenografts, and could represent a novel therapeutic option for the treatment of this dismal disease. We have also shown that AZD1152 enhances the effects of *dl922-947* against ATC; similar combined approaches could be used for the treatment of ATC and other aggressive and incurable human cancers.

Declaration of interest

The authors declare that there is no conflict of interest that could be perceived as prejudicing the impartiality of the research reported.

Funding

This study was supported by the Associazione Italiana per la Ricerca sul Cancro (AIRC). S Libertini was recipient of FIRC fellowship.

Acknowledgements

We thank Dr Elizabeth Anderson and Odedra Rajesh, AstraZeneca UK, for their help in the preparation of this article. We also thank AstraZeneca for kindly providing us with AZD1152 and AZD1152-HQPA. We thank Salvatore Sequino for his excellent technical assistance and Joanne Smith for proofreading this manuscript.

References

Aihara A, Tanaka S, Yasen M, Matsumura S, Mitsunori Y, Murakata A, Noguchi N, Kudo A, Nakamura N, Ito K *et al.* 2010 The selective Aurora B kinase inhibitor AZD1152 as a novel treatment for hepatocellular carcinoma. *Journal of Hepatology* **52** 63–71. (doi:10.1016/j.jhep.2009.10.013)

Anders M, Christian C, McMahon M, McCormick F & Korn WM 2003 Inhibition of the Raf/MEK/ERK pathway up-regulates expression of the coxsackievirus and adenovirus receptor in cancer cells. *Cancer Research* **63** 2088–2095.

Araki K, Nozaki K, Ueba T, Tatsuka M & Hashimoto N 2004 High expression of Aurora-B/Aurora and Ipll-like midbody-associated protein (AIM-1) in astrocytomas. *Journal of Neuro-Oncology* **67** 53–64. (doi:10.1023/B:NEON.0000021784.33421.05)

Arlot-Bonnemains Y, Baldini E, Martin B, Delcros JG, Toller M, Curcio F, Ambesi-Impiombato FS, D'Armiento M & Ulisse S 2008 Effects of the Aurora kinase inhibitor VX-680 on anaplastic thyroid cancer-derived cell lines. *Endocrine-Related Cancer* **15** 559–568. (doi:10.1677/ERC-08-0021)

Baird SK, Aerts JL, Eddaoudi A, Lockley M, Lemoine NR & McNeish IA 2008 Oncolytic adenoviral mutants induce a novel mode of programmed cell death in ovarian cancer. *Oncogene* **27** 3081–3090. (doi:10.1038/sj.onc.1210977)

Castedo M, Perfettini JL, Roumier T, Valent A, Raslova H, Yakushijin K, Horne D, Feunteun J, Lenoir G, Medema R *et al.* 2004*a* Mitotic catastrophe constitutes a special case of apoptosis whose suppression entails aneuploidy. *Oncogene* **23** 4362–4370. (doi:10.1038/sj.onc.1207572)

Castedo M, Perfettini JL, Roumier T, Andreau K, Medema R & Kroemer G 2004*b* Cell death by mitotic catastrophe: a molecular definition. *Oncogene* **23** 2825–2837. (doi:10.1038/sj.onc.1207528)

Cheong SC, Wang Y, Meng JH, Hill R, Sweeney K, Kirn D, Lemoine NR & Halldén G 2008 E1A-expressing adenoviral E3B mutants act synergistically with chemotherapeutics in immunocompetent tumor models. *Cancer Gene Therapy* **15** 40–50. (doi:10.1038/sj.cgt.7701099)

Chieffi P, Troncone G, Caleo A, Libertini S, Linardopoulos S, Tramontano D & Portella G 2004 Aurora B expression in normal testis and seminomas. *Journal of Endocrinology* **181** 263–270. (doi:10.1677/joe.0.1810263)

Chieffi P, Cozzolino L, Kisslinger A, Libertini S, Staibano S, Mansueto G, De Rosa G, Villacci A, Vitale M, Linardopoulos S *et al.* 2006 Aurora B expression directly correlates with prostate cancer malignancy and influence prostate cell proliferation. *Prostate* **66** 326–333. (doi:10.1002/pros.20345)

Ditchfield C, Johnson VL, Tighe A, Ellston R, Haworth C, Johnson T, Mortlock A, Keen N & Taylor SS 2003 Aurora B couples chromosome alignment with anaphase by targeting BubR1, Mad2, and Cenp-E to kinetochores. *Journal of Cell Biology* **161** 267–280. (doi:10.1083/jcb.200208091)

Esposito F, Libertini S, Franco R, Abagnale A, Marra L, Portella G & Chieffi P 2009 Aurora B expression in post-puberal testicular germ cell tumours. *Journal of Cellular Physiology* **221** 435–439. (doi:10.1002/jcp.21875)

Gully CP, Zhang F, Chen J, Yeung JA, Velazquez-Torres G, Wang E, Yeung SC & Lee MH 2010 Antineoplastic effects of an Aurora B kinase inhibitor in breast cancer. *Molecular Cancer* **9** 42. (doi:10.1186/1476-4598-9-42)

Harrington EA, Bebbington D, Moore J, Rasmussen RK, Ajose-Adeogun AO, Nakayama T, Graham JA, Demur C, Hercend T, Diu-Hercend A *et al.* 2004 VX-680, a potent and selective small-molecule inhibitor of the Aurora kinases, suppresses tumor growth *in vivo*. *Nature Medicine* **10** 262–267. (doi:10.1038/nm1003)

Hauf S, Cole RW, LaTerra S, Zimmer C, Schnapp G, Walter R, Heckel A, van Meel J, Rieder CL & Peters JM 2003 The small molecule Hesperadin reveals a role for Aurora B in correcting kinetochore-microtubule attachment and in maintaining the spindle assembly checkpoint. *Journal of Cell Biology* **161** 281–294. (doi:10.1083/jcb.200208092)

Heise C, Sampson-Johannes A, Williams A, McCormick F, Von Hoff DD & Kirn DH 1997 ONYX-015, an E1B gene-attenuated adenovirus, causes tumor-specific cytolysis and antitumoral efficacy that can be augmented by standard chemotherapeutic agents. *Nature Medicine* **3** 639–645. (doi:10.1038/nm0697-639)

Heise C, Hermiston T, Johnson L, Brooks G, Sampson-Johannes A, Williams A, Hawkins L & Kirn D 2000 An adenovirus E1A mutant that demonstrates potent and selective systemic anti-tumoral efficacy. *Nature Medicine* **6** 1134–1139. (doi:10.1038/80474)

Katayama H, Ota T, Jisaki F, Ueda Y, Tanaka T, Odashima S, Suzuki F, Terada Y & Tatsuka M 1999 Mitotic kinase expression and colorectal cancer progression. *Journal of the National Cancer Institute* **91** 1160–1162. (doi:10.1093/jnci/91.13.1160)

Keen N & Taylor S 2004 Aurora-kinase inhibitors as anticancer agents. *Nature Reviews. Cancer* **4** 927–936. (doi:10.1038/nrc1502)

Keen N & Taylor S 2009 Mitotic drivers – inhibitors of the Aurora B kinase. *Cancer Metastasis Reviews* **28** 185–195. (doi:10.1007/s10555-009-9184-9)

Kumar S, Gao L, Yeagy B & Reid T 2008 Virus combinations and chemotherapy for the treatment of human cancers. *Current Opinion in Molecular Therapeutics* **10** 371–379.

Kurai M, Shiozawa T, Shih HC, Miyamoto T, Feng YZ, Kashima H, Suzuki A & Konishi I 2005 Expression of Aurora kinases A and B in normal, hyperplastic, and malignant human endometrium: Aurora B as a predictor for poor prognosis in endometrial carcinoma. *Human Pathology* **36** 1281–1288. (doi:10.1016/j.humpath.2005.09.014)

Libertini S, Iacuzzo I, Ferraro A, Vitale M, Bifulco M, Fusco A & Portella G 2007 Lovastatin enhances the replication of the oncolytic adenovirus *dl1520* and its antineoplastic activity against anaplastic thyroid carcinoma cells. *Endocrinology* **148** 5186–5194. (doi:10.1210/en.2007-0752)

Libertini S, Iacuzzo I, Perruolo G, Scala S, Ieranò C, Franco R, Hallden G & Portella G 2008 Bevacizumab increases viral distribution in human anaplastic thyroid carcinoma xenografts and enhances the effects of E1A-defective adenovirus *dl922-947*. *Clinical Cancer Research* **14** 6505–6514. (doi:10.1158/1078-0432.CCR-08-0200)

Liu TC, Galanis E & Kirn D 2007 Clinical trial results with oncolytic virotherapy: a century of promise, a decade of progress. *Nature Clinical Practice. Oncology* **4** 101–117. (doi:10.1038/ncponc0736)

López-Ríos F, Chuai S, Flores R, Shimizu S, Ohno T, Wakahara K, Illei PB, Hussain S, Krug L, Zakowski MF *et al.* 2006 Global gene expression profiling of pleural mesotheliomas: overexpression of aurora kinases and P16/CDKN2A deletion as prognostic factors and critical evaluation of microarray-based prognostic prediction. *Cancer Research* **66** 2970–2979. (doi:10.1158/0008-5472.CAN-05-3907)

Mullen JT & Tanabe KK 2002 Viral oncolysis. *Oncologist* **7** 106–119. (doi:10.1634/theoncologist.7-2-106)

Oke A, Pearce D, Wilkinson RW, Crafter C, Odedra R, Cavenagh J, Fitzgibbon J, Lister AT, Joel S & Bonnet D 2009 AZD1152 rapidly and negatively affects the growth and survival of human acute myeloid leukemia cells *in vitro* and *in vivo*. *Cancer Research* **69** 4150–4158. (doi:10.1158/0008-5472.CAN-08-3203)

Passer BJ, Castelo-Branco P, Buhrman JS, Varghese S, Rabkin SD & Martuza RL 2009 Oncolytic herpes simplex virus vectors and taxanes synergize to promote killing of prostate cancer cells. *Cancer Gene Therapy* **16** 551–560. (doi:10.1038/cgt.2009.10)

Prigent C & Dimitrov S 2003 Phosphorylation of serine 10 in histone H3, what for? *Journal of Cell Science* **116** 3677–3685. (doi:10.1242/jcs.00735)

Qi G, Ogawa I, Kudo Y, Miyauchi M, Siriwardena BS, Shimamoto F, Tatsuka M & Takata T 2007 Aurora-B expression and its correlation with cell proliferation and metastasis in oral cancer. *Virchows Archiv* **450** 297–302. (doi:10.1007/s00428-006-0360-9)

Schweppe RE, Klopper JP, Korch C, Pugazhenthi U, Benezra M, Knauf JA, Fagin JA, Marlow LA, Copland JA, Smallridge RC *et al.* 2008 Deoxyribonucleic acid profiling analysis of 40 human thyroid cancer cell lines reveals cross-contamination resulting in cell line redundancy and misidentification. *Journal of Clinical Endocrinology and Metabolism* **93** 4331–4341. (doi:10.1210/jc.2008-1102)

Seidman MA, Hogan SM, Wendland RL, Worgall S, Crystal RG & Leopold PL 2001 Variation in adenovirus receptor expression and adenovirus vector-mediated transgene expression at defined stages of the cell cycle. *Molecular Therapy* **4** 13–21. (doi:10.1006/mthe.2001.0414)

Smallridge RC, Marlow LA & Copland JA 2009 Anaplastic thyroid cancer: molecular pathogenesis and emerging therapies. *Endocrine-Related Cancer* **16** 17–44. (doi:10.1677/ERC-08-0154)

Smith SL, Bowers NL, Betticher DC, Gautschi O, Ratschiller D, Hoban PR, Booton R, Santibáñez-Koref MF & Heighway J 2005 Overexpression of aurora B kinase (AURKB) in primary non-small cell lung carcinoma is frequent, generally driven from one allele, and correlates with the level of genetic instability. *British Journal of Cancer* **93** 719–729. (doi:10.1038/sj.bjc.6602779)

Sorrentino R, Libertini S, Pallante PL, Troncone G, Palombini L, Bavetsias V, Spalletti-Cernia D, Laccetti P, Linardopoulos S, Chieffi P *et al.* 2005 Aurora B overexpression associates with the thyroid carcinoma undifferentiated phenotype and is required for thyroid carcinoma cell proliferation. *Journal of Clinical Endocrinology and Metabolism* **90** 928–935. (doi:10.1210/jc.2004-1518)

Tanaka S, Arii S, Yasen M, Mogushi K, Su NT, Zhao C, Imoto I, Eishi Y, Inazawa J, Miki Y *et al.* 2008 Aurora kinase B is a predictive factor for the aggressive recurrence of hepatocellular carcinoma after curative hepatectomy. *British Journal of Surgery* **95** 611–619. (doi:10.1002/bjs.6011)

Vähä-Koskela MJ, Heikkilä JE & Hinkkanen AE 2007 Oncolytic viruses in cancer therapy. *Cancer Letters* **254** 178–216. (doi:10.1016/j.canlet.2007.02.002)

Vischioni B, Oudejans JJ, Vos W, Rodriguez JA & Giaccone G 2006 Frequent overexpression of aurora B kinase, a novel drug target, in non-small cell lung carcinoma patients. *Molecular Cancer Therapeutics* **5** 2905–2913. (doi:10.1158/1535-7163.MCT-06-0301)

Walsby E, Walsh V, Pepper C, Burnett A & Mills K 2008 Effects of the aurora kinase inhibitors AZD1152-HQPA and ZM447439 on growth arrest and polyploidy in acute myeloid leukemia cell lines and primary blasts. *Haematologica* **93** 662–669. (doi:10.3324/haematol.12148)

Wilkinson RW, Odedra R, Heaton SP, Wedge SR, Keen NJ, Crafter C, Foster JR, Brady MC, Bigley A, Brown E *et al.* 2007 AZD1152, a selective inhibitor of Aurora B kinase, inhibits human tumor xenograft growth by inducing apoptosis. *Clinical Cancer Research* **13** 3682–3688. (doi:10.1158/1078-0432.CCR-06-2979)

Yang J, Ikezoe T, Nishioka C, Tasaka T, Taniguchi A, Kuwayama Y, Komatsu N, Bandobashi K, Togitani K, Koeffler HP *et al.* 2007 AZD1152, a novel and selective aurora B kinase inhibitor, induces growth arrest, apoptosis, and sensitization for tubulin depolymerizing agent or topoisomerase II inhibitor in human acute leukemia cells *in vitro* and *in vivo*. *Blood* **110** 2034–2040. (doi:10.1182/blood-2007-02-073700)

Yu W & Fang H 2007 Clinical trials with oncolytic adenovirus in China. *Current Cancer Drug Targets* **7** 141–148. (doi:10.2174/156800907780058817)